Synthesis and Rheological Characterization of Polyhydroxybutyrate with Different Topologies and Microstructures

by

Tannaz Ebrahimi

M.Sc., Amirkabir University of Technology (Tehran Polytechnic), 2010

A THESIS SUBMITTED IN PARTIAL FULFILLMENT OF

THE REQUIREMENTS FOR THE DEGREE OF

DOCTOR OF PHILOSOPHY

in

THE FACULTY OF GRADUATE AND POSTDOCTORAL STUDIES

(Chemical and Biological Engineering)

THE UNIVERSITY OF BRITISH COLUMBIA

(Vancouver)

December 2017

Abstract

Series of monodispersed linear and star-shaped polyhydroxybutyrate (PHB)s were synthesized using controlled indium and zinc based complexes through immortal ring opening polymerization of β-butyrolactone (BBL) in the presence of benzyl alcohol, tris(hydroxymethyl)benzene, and dipentaerythritol chain transfer agents. The topologies of the prepared PHBs of various molecular weights were investigated using solution and melt rheological characterizations. The powerlaw relationship between the radius of gyration and hydrodynamic radii of the linear and star PHBs with the molecular weight confirmed that the molecules are self-similar. Reduced values of compactness factor relative to that of linear counterparts and exponential scalling of the zero-shear viscosity of the stars with span molecular weight confirmed the presence of branching on the PHB backbone.

A series of racemic and enantiopure zinc complexes were synthesized and fully characterized for the polymerization of BBL to form high molecular weight syndiotactic PHBs (P_r up to 75%). Complex (±)-[($NNHO_{tBu}$)ZnOBn]$_2$ (**9**) showed unprecedented reactivity and control towards the polymerization of up to 20000 equivalents of BBL in the presence of 5000 equivalents of benzyl alcohol. Isothermal time sweep tests at temperatures above the melting point of the syndio-rich PHBs showed thermally stable behavior of these polymers at temperatures below 140 ^oC. The zero-shear viscosity of the syndio-riched PHBs was higher than their atactic counterparts and showed a power-law relationship with the molecular weight confirming the linear microstructure and the absence of cyclic or branched species in the melt. The extensional rheometry revealed high melt strength in a range of strain rates as a result of flow induced crystallization.

Easy to make, indium-salan complexes were reported for the polymerization of as-received lactide. The solution state characterization of these polymers showed narrow molecular weight distributions with molecular weights closely matching the theoretical molecular weight as an indication of a robust catalytic system. These complexes are capable of polymerizing impure lactide isomers in the melt state under ambient atmospheric conditions to form high molecular weight symmetric star shaped multi-block PLAs with high melting points, up to 197 ^{o}C. This catalytic system can also be used for the formation of star-shaped PHB-PLA copolymers in inert atmosphere.

Lay Summary

The environmental concerns associated with the accumulation of plastic wastes in the environment, has raised great interest in the development of biodegradable polymers. Polyhydroxybutyrate (PHB) and polylactide (PLA) are two of the most important biodegradable and biocompatible polyesters, with a wide range of potential applications in commodity products and pharmaceutics. The main focus of this interdisciplinary PhD thesis is to explore the effect of different topologies and microstructures of PHB on its physical and processing properties. To this end, new catalytic systems will be reported and fully characterized and their performance during the polymerization will be investigated. Also it is shown that multiblock copolymers of PLA with star-shaped topologies can be made under facile fume-hood conditions using a newly developed catalyst.

Preface

The work reported in chapter 3 is based on the following publications in *Macromolecules* and *Dalton Transactions*:

1. **T. Ebrahimi**, P. Mehrkhodavandi, S. G. Hatzikiriakos, "Synthesis and Rheological Characterization of Star-Shaped and Linear Poly (hydroxybutyrate)", ***Macromolecules***, 2015, 48, 6672
2. I. Yu, **T. Ebrahimi**, P. Mehrkhodavandi, S. G. Hatzikiriakos, "Star-shaped PHB–PLA block copolymers: immortal polymerization with dinuclear indium catalysts" ***Dalton Trans.***, 2015, 44, 14248

In this chapter, X-ray crystallography of complex (**2**) was performed by our former PhD student, Dr. Insun Yu. The preparation of complexes (**1**), (**2**), and (**3**) for the polymerizations were carried out by myself. I performed all the polymerizations along with polymers solution, and rheological characterizations. The polymerization section of the *Dalton* paper and the complete manuscript submitted to *Macromolecules* were written by myself and edited/modified by Professor Hatzikiriakos and Professor Mehrkhodavandi.

Part of the polymerization results presented in this chapter is published in *Macromolecules* as a collaborative work with Professor Evelyne van Rymbeke:

3. **T. Ebrahimi**, H. Taghipour, D. Grießl, P. Mehrkhodavandi, S. G. Hatzikiriakos, and E. van Ruymbeke, "Binary Blends Entangled Star and Linear Poly(hydroxybutyrate): Effect of Constraint Release and Dynamic Tube Dilation", ***Macromolecules***, 2017, 50, 2535

This chapter has been presented in the following international conferences:

- **T. Ebrahimi*[1]**, I. Yu, P. Mehrkhodavandi, S. G. Hatzikiriakos, "Linear and star shaped polyhydroxybutyrate using immortal ring opening polymerization of β-butyrolactone" ICBMC'14, May 13-16, 2014, Montreal, Canada.

[1] * refers to the presenter at the conference

- **T. Ebrahimi**, P. Mehrkhodavandi, S. G. Hatzikiriakos*, "Solution and Melt Rheology of Symmetric Star-Shaped Poly (hydroxybutyrate) Generated from Immortal Ring Opening Polymerization of β-Butyrolactone", Society of Rheology Meeting : SOR 87th Annual Meeting, October 11-15, 2015, Baltimore, USA.

The materials covered in chapter 4 are based on the following publications in *Macromolecules* and *Inorganic Chemistry*:

4. **T. Ebrahimi**, D.C. Aluthge, S. G. Hatzikiriakos and P. Mehrkhodavandi**,** "Highly Active Chiral Zinc Catalysts for Immortal Polymerization of β-Butyrlactone Form Melt Processable Syndio-rich Poly (hydroxybutyrate)", ***Macromolecules***, 2016, 49, 8812
5. **T. Ebrahimi**, E. Mamleeva, I.Yu, S. G. Hatzikiriakos and P. Mehrkhodavandi, "The role of nitrogen donors in zinc catalysts for lactide ring opening polymerization", ***Inorganic Chemistry***, 2016, 55, 9445

In this chapter racemic and enantiopure cumyl, adamantyl, and triphenylsilyl substituted ligands were provided by our former PhD student, Dr. Kim Osten. Catalyst preparation, characterization, and X-ray crystallographic measurements were conducted by myself. X-ray crystallographic measurements and refinements of complex (±)-**6** was performed by Dr. Dinesh C. Aluthge. I also performed all the polymer characterizations and rheological measurements. The original version of the *Macromolecules* manuscripts was written by myself and edited/modified by Professor Hatzikiriakos and Professor Mehrkhodavandi. The *Inorg. Chem* manuscript was written in collaboration with the coauthors and edited/modified by Professor Mehrkhodavandi.

This chapter has also been presented in the following international conferences:

- **T. Ebrahimi***, S. G. Hatzikiriakos, P. Mehrkhodavandi, "Processable Poly (Hydroxybutyrate): Synthesis and Rheological Characterizations", 100th CSC, May 28-June 1, 2017, Toronto, ON, Canada.
- **T. Ebrahimi***, S. G. Hatzikiriakos, P. Mehrkhodavandi, "Highly active and syndioselective zinc complexes for the immortal ring-opening polymerization of β-butyrolactone", 251st ACS National Meeting & Exposition March 13-17, 2016, San Diego, USA.

Chapter 5 is published in *ACS Catalysis* and its intellectual property is protected under a patent application:

6. **T. Ebrahimi**, D.C. Aluthge, B. O. Patrick S. G. Hatzikiriakos, P. Mehrkhodavandi, "Air Stable and Moisture Resistant Indium Salan Catalysts for Living Multi-block PLA Formation", ***ACS Catalysis***, 2017, 7, 6413

7. P. Mehrkhodavandi and **T. Ebrahimi**, "Salan indium catalysts and methods of manufacture and use thereof", US 62/469,699, March 2017

In this chapter, enantiopure salan ligands where prepared in collaboration with Brian Tam, our undergraduate summer student. I performed catalyst preparations, characterization and X-ray crystallographies. Dr. Brian O. Patrick performed further refinements on the X-ray results of complexes (**17**) and (**18**) to improve their quality for publication. All the polymerizations and polymer characterizations were carried out by myself. The original version of the manuscript was written by myself and edited/modified by Professor Mehrkhodavandi.

This chapter has also been presented in the following international conference:

- **T. Ebrahimi**, S G. Hatzikiriakos, P. Mehrkhodavandi, "Moisture resistant indium complexes for ring opening polymerization of lactide", 251st ACS National Meeting & Exposition March 13-17, 2016, San Diego, USA.

Table of Contents

List of Tables

List of Figures

List of Abbreviations

Ad	adamantyl
a_T	horizontal shift factor
BBL	β-butyrolactone
BnOH	Benzyl alcohol
BSW	Baumgaertel-Schausberger-Winter
b_T	vertical shift factor
$^{13}C\{^1H\}$	Proton decoupled carbon NMR
C_6D_6	deuterated benzene
calc.	calculated
CD_2Cl_2	deuterated dichloromethane
$CDCl_3$	deuterated chloroform
Cm	cumyl
conv.	conversion
CTA	chain transfer agent
d	days
Da	Dalton (gram per mole)
DCM	dichloromethane
d*n*/d*c*	refractive index increment
Đ	dispersity index
DPET	dipentaerythritol

E_a	activation energy of flow, kJ/mol
EA	elemental analysis
equiv.	equivalence
et al.	and others
EtOH	ethanol
G’	storage modulus, Pa
G”	loss modulus, Pa
G*	complex modulus, Pa
G(t)	stress relaxation modulus, Pa
gi	generalized Maxwell model parameter, relaxation modulus, Pa
G^0_N	plateau modulus, MPa
GPC	gel permeation chromatography
^1H	proton
$^1H\{^1H\}$	homonuclear decoupled proton
h	hours
h(γ)	damping function
in situ	in a chemical reaction
in vacuo	under vacuum
iROP	immortal ring opening polymerization
K-BKZ	Kaye-Bernstein, Kearsley and Zapas
KO*t*Bu	potassium *tert*-butoxide
LA	lactide

LVE	linear viscoelastic envelope
M	molar (moles per liter)
MALDI-TOF	matrix-assisted laser desorption time of flight
M_{BnOH}	molar mass of benzyl and hydroxy end group (108.14 g/mol)
M_{THMP}	molar mass of THMB end group (168.19 g/mol)
M_{EtOH}	molar mass of ethoxy end group (46.07 g/mol)
mg	milligram
MHz	megahertz
min.	minutes
mL	milliliters
M_{BBL}	molar mass of BBL (86.09 g/mol)
M_{LA}	molar mass of lactide (144.13 g/mol)
mM	milimolars
mmol	milimoles
M_n	number average molecular weight
mol	moles
M_W	weight average molecular weight
NaOEt	sodium ethoxide
n_e	slope of entanglement zone
n_g	slope of glass transition zone
NMR	nuclear magnetic resonance
OBn	benzoxide

OEt	ethoxide
PCL	poly(ε-caprolactone)
PDLA	poly(D-lactic acid)
PGSE	pulsed gradient spin-echo
PHA	polyhydroxyalkanoate
PHB	polyhydroxybutyrate
PLA	poly(lactide) or poly(lactic acid)
PLLA	poly(L-lactic acid)
PM	parsimonious relaxation spectrum
P_m	probability of *meso* linkages within a polymer chain
ppm	part per millions
P_r	probability of *racemic* linkages within a polymer chain
R.T.	room temperature
rac-LA	racemic mixture of lactide
Rg	radius of gyration
Rh	hydrodynamic radii
ROP	ring opening polymerization
SER	Sentmanat Extensional Rheometer
$SiPh_3$	triphenylsilyl
T	temperature
t	time
t-Bu	*tert*-butyl

temp.	temperature
Tg	glass transition temperature (^{o}C)
THMB	1, 3, 5-tris(hydroxymethyl)benzene
theo.	theoretical
THF	tetrahydrofuran
Tm	melting temperature (^{o}C)
Tol.	toluene
Tref	reference temperature
WLF	Williams-Landel-Ferry
WXRD	Wide angle X-ray diffraction
(±)	racemic
^{o}C	degrees Celsius

List of Symbols

η^*	complex viscosity, Pa.s
ω_c	crossover frequency, 1/s
ω_{max}	frequency at which loss modulus reaches the maximum value in rubbery region
η'	dynamic viscosity, Pa.s
ω	frequency rad/s
λi	generalized Maxwell model parameter, relaxation time, s
$\dot{\varepsilon}$	Hencky strain rate, s^{-1}
$[\eta]$	intrinsic viscosity, Pa.s
η''	out-of-phase component of complex viscosity, Pa.s
δ	phase shift
τ_d, λ_{max}	longest relaxation time (disentanglement relaxation time), s
τ_R	arm retraction relaxation time, s
$\dot{\gamma}$	shear rate, s^{-1}
γ	shear strain
σ	shear stress, Pa.s
η^+	steady shear stress growth coefficient, Pa.s
σ_0	stress amplitude in oscillatory shear, Pa
η_E^+	tensile stress growth coefficient, Pa.s
η_0	zero-shear viscosity, Pa.s

Acknowledgements

First and foremost, I would like to express my gratitude to my supervisors, Professor Savvas G. Hatzikiriakos and Professor Parisa Mehrkhodavandi for their constant guidance, scientific insights, and encouragements throughout my PhD studies. I am greatly indebted to them for their support, understanding and commitment in all the steps of my research. Their drive and enthusiasm have always motivated me in my studies and my life.

I would also like to thank the members of my supervisory and examining committee, Professor Kevin Smith and Professor Laurel Schafer for their valuable feedback and suggestions during my PhD. Also special thanks to Professor Brian O. Patrick for his time and effort in training me in X-Ray Crystallography.

My best wishes go to my previous and present colleagues in the Rheology and the Chemistry labs for giving me help in all stages of my studies. I appreciate them for their helpful guidance and discussions and making lab a pleasant and memorable place to work in. I would like to specially thank Dr. Mahmoud Ansari and Dr. Insun Yu for their guidance and mentorship at the first stages of my PhD studies. Thank you to Love Ese Chile, as a supportive colleague and a caring friend, for her constructive discussions and feedback.

I would like to express my sincere gratitude to my wonderful parents, Maryam and Habib, for their unconditional love, constant support, and encouragement throughout my PhD studies. Thank you to my brother, Dariush, and his wife, Elham, for always being there for me.

Special thanks to my better half, Ehsan, for his endless love and patience, without him this thesis would not have been possible. He has been the source of strength and motivation all during my studies and his guidance has always illuminated my professional pathway.

to my family,

Chapter 1: Introduction

The ever growing desire for a more convenient lifestyle in the past decades has increased the demand for more versatile and advanced polymeric products with new properties and functionalities. The production of this category of materials has shown profound progress, due to the recent advances in science and technology. Nowadays, polymeric materials can be found in a wide range of applications from electronics and packaging, all the way through to medical and pharmaceutical appliances. Although polymers are playing an important role to advance our daily life, mass production and accumulation of over 290 million tons of biostable plastics per year has caused serious environmental issues (e.g. Ingestion of plastic waste and exposure to chemicals within plastics (plasticizers, thermal/UV stabilizers, pigments and etc.) has affected the marine animals and living organisms through interruptions in their biological functions. Humans are also affected by plastic pollution through exposure to toxic chemicals leached by plastics in the water that, can enter the food chain, and threaten their health). In addition, most of the synthetic polymers are produced from petroleum resources, which increases the annual consumption of oil. [1-5] Biodegradable polymers have been therefore proposed as a solution.[6] These materials undergo degradation and decomposition in the presence of microorganisms to form water, CO_2, and biomass. Biodegradable polymers are divided into three main categories of polysaccharides, naturally occurring polyhydroxyalkanoates (PHAs), and synthetic aliphatic polyesters (e.g. polylactic acid (PLA), poly (ε-caprolactone) (PCL), and poly (β-hydroxybutyrates) (PHB)) or ester containing polymers such as poly(ester amide)s, poly(ester carbonate)s, poly(ester urethane)s and poly(ester urea)s.

One of the most important members of the family of biodegradable and biocompatible polymers is poly (β-hydroxybutyrates) (PHB), an aliphatic polyester, with a wide range of potential applications from commodity products to medical devices. This polymer can be produced from bacterial fermentation techniques, however, the product is highly isotactic and crystalline with a broad molecular weight distribution. As a result, due to the low melt strength and highly brittle nature, melt processing and applications of this polymer is limited.[2,7,8] In order to overcome these shortcomings, chemical synthetic routes such as metal-catalyzed ring opening polymerization (ROP) of strained cyclic ester, β-butyrolactone (BBL), have been developed to control the molecular weight, molecular weight distribution, and microstructure of the resulting polymer. This system provides the only way to have stereocontrol during the polymerization, to form isotactic (stereogenic centers attain same configuration), syndiotactic (chiral centers have alternating configuration), and atactic (chiral centers distributed in a random fashion) PHBs.[2,9]

To minimize metallic contamination and increase catalyst productivity, immortal ROP has been considered as a solution, in which a protic source, like an alcohol, will act as a chain transfer agent (CTA). In this technique much lower catalyst concentration is required and by using functionalized alcohols, functionalized polymers can be synthesized (e.g. star-shaped polymers can be formed by using polyols as chain transfer agents).[10]

Star-shaped polymers exhibit interesting properties compared to their linear counterparts, owing to their specific topology.[11,12] These materials possess lower hydrodynamic radii, enhanced melt viscosity, and higher concentration of end groups, to tailor their properties for specific applications. Owing to this exclusive structure, biodegradable star polymers are established as a technologically important class of nanomaterials with a broad range of applications in life sciences

and nanotechnologies. Star shaped biodegradable polymers, including polylactic acid (PLA) and poly(ε-caprolactone)(PCL), with different numbers of arms and molecular weights have been synthesized widely through the ROP of lactide[13-21] and ε-caprolactone[13,22-28] in the presence of appropriate catalysts and co-catalysts. However, due to the presence of a limited number of active complexes that stay robust in the presence of high loadings of CTA and BBL, there are no synthetic reports on the preparation of well-defined star shaped PHBs.

In addition to topology, control of polymers microstructure and morphology is a key tool to tailor their properties for specific applications. In developing organometallic complexes for the polymerization of BBL, the emphasis is mostly on designing systems that reach the highest stereoselectivity. For instance, landmark yttrium[29] and chromium[30,31] based catalysts are reported for the formation of highly syndiotactic (up to 95%) and isotactic (up to 80%) PHBs, however with either low molecular weights, or broad molecular weight distributions. Although stereoregularity is an important parameter in the design of mechanically strong materials, for thermally susceptible polymers, such as PHB, other parameters including a low degree of crystallinity, high density of entanglements, and melt strength must be taken into consideration. To this end, highly robust catalysts to form high molecular weight monodisperse PHBs, with moderate levels of stereoselectivity are required.

One of the ultimate goals of polymer science, is to develop new polymeric materials that can be used as commodity products. These product are usually being produced through plastic processing techniques, including extrusion, injection molding, blow molding, film blowing, fiber spinning, and several other methods. In order to optimize the processing conditions, rheological studies have to be conducted. Rheology is important in investigating and evaluating bulk properties

of polymers in melt state and their performance under common plastic processing conditions. Subtle changes in polymer topologies and microstructures will readily affect their viscoelastic properties in both linear and non-linear regions. Rheology is a strong and facile technique that can also be used to characterize polymers with high sensitivity and can predict their physical properties after melt processing. Although there is interest in developing processable PHBs, there exist no comprehensive studies in the literature on the effect of PHB topology and microstructure on its rheological properties.

A wide range of biodegradable polymers including polylactic acid (PLA), have been synthesized in the presence of well-explored organocatalytic,[32,33] as well as main group and transition metal-based catalysts.[9,10,34-48] However, despite these concentrated efforts in catalyst development, tin octanoate, ($Sn(Oct)_2$) remains the most common catalyst used for ring opening polymerization (ROP) of lactide in industrial plants. $Sn(Oct)_2$ allows the ROP of lactide in the melt without the use of inert atmosphere; however, $Sn(Oct)_2$ has poor control over the polymerization due to extensive transesterification reactions. [1,6,48-55] In addition, this catalyst is not active for the polymerization of many other cyclic esters, including BBL.

Although the development of catalysts for the polymerization of cyclic esters such as lactide and BBL has been the subject of intense research for the past two decades, most catalytic studies focus either on catalyst performance or its stereoselectivity. While these properties are important, most studies neglect the fact that other aspects are often of greater importance in an industrial setting, e.g. catalyst air/moisture stability, tolerance against unpurified monomer, and the possibility to perform the polymerization in the melt state. Thus, PLA is still being produced using $Sn(Oct)_2$ rather than any of the more active and better performing catalysts.

The main goal of this interdisciplinary thesis is to form star-shaped and processable PHBs through bridging catalysis to polymer engineering. To this end, star-shaped PHB homopolymers and block copolymers (PLA-PHB) are made using a newly developed catalytic system. The synthesized stars are highly symmetric with well-defined structures based on melt rheological and solution viscometric results. New zinc based catalysts to form thermorheologically stable, and processable PHBs are also reported for the first time. Based on isothermal time sweep tests and extensional rheometeric results, it has been shown that these polymers are actually processable with potential to be used in the fabrication of plastic bags and fibers. Also, a surprisingly active and controlled catalyst for homo- and co-polymerization of cyclic esters, including lactide, is reported to form symmetric star block copolymers under ambient atmospheric conditions for the first time.

1.1 Polyhydroxyalkanoates (PHA)

Polyhydroxyalkanoates (PHAs) are a family of aliphatic polyesters synthesized through bacterial fermentation technique as carbon and energy storage granules. Natural PHAs are strictly isotactic, with (*R*)-configuration at chiral centers throughout the backbone. The fact that these polymers have plastic behavior and are biodegradable, makes them potential replacements for biostable conventional polymers such as polyethylene and polypropylene. [2,56]

Microbial fermentation of natural hydrocarbons including sugar, starch, and wood has been used to prepare PHAs in large scale. Commercialization of PHAs including poly (β-hydroxybutyrate) (PHB) and poly((*R*)-3-hydroxybutyrate-*co*-(*R*)-3-hydroxyvalerate) (PHBV) took place in 1980 and 1990 by ICI (UK) and Chemie Linz (Austria) in the scale of 20-300 tons per year.[54,56] These materials were mainly used in packaging and drug delivery applications.

Imperial Chemical Industries then followed by developing different types of PHAs under the commercial name of 'Biopol' which was distributed in the U.S. by Monsanto and later by Metabolix. Currently different types of PHAs under commercial names of Biomer, Biogreen, Biocycle, and Metabolix are produced by Biomer Biotechnology Co. (Germany), Mitsubishi Gas Chemical (Japan), PHA Industrials (Brazil), Tianan Biologic Material (USA), and Telles (USA). Recently, up to 10,000 tons/year of PHAs under the commercial name of Ecogen are produced by Tianjin Green Bio-Science in China.[57-59] In the meantime, the global production of high density polyethylene reached over 40 million tons/year in 2016, and the global demand for polyethylene resins including HDPE, LLDPE and LDPE is expected to increase to up to 99.6 million tons/year in 2018.[57]

The cost of carbon source, small scale production, costly fermentation, and purification processes of PHAs, are the main causes of the insignificant production of these materials compared to conventional polyolefines, as in 2006, PHAs were sold at 10-12 €/kg. Current research will result in the cost reduction of carbon sources, which constitutes almost 50% of the whole cost of the production. The savings will be realized through using alternative crude carbon sources such as potatoes, sugarcane, and non-edible agricultural residues.[60,61]

PHB, as the most commonly found member of PHAs, was isolated and discovered from bacteria for the first time in 1925 by a French microbiologist, Maurice Lemoigne.[62] Natural PHB has a fully isotactic microstructure and as a result its molecules arrange in a double axis right-handed helix. Due to this highly ordered microstructure, naturally occurring PHB is highly crystalline (55–80%). PHB crystallites melt down at 175-185 ^{o}C depending on the molecular weight of the polymer. Importantly this temperature is very close to its thermal degradation temperature which is about 180 ^{o}C.[2,63] Although PHB has comparable mechanical properties such

as Young's modulus, tensile, and impact strength to that of isotactic Polypropylene (Table 1.1), it suffers from very low extensibility due to the presence of large spherolites and continuous in-situ crystallization after melt processing. Naturally occurring PHB has high oxygen impermeability and UV resistance which makes it a good candidate for food packaging applications, however, intensive thermal degradation due to ester bond pyrolysis at common plastic processing temperatures, reduces its thermal stability and processing window.[2] Furthermore, PHB suffers from very low melt strength which prohibits its processing under high extensional stresses. [2,56,58]

Table 1.1 Physical and thermal properties of PHB and other similar materials[2]

Polymer	Melting point (°C)	Glass transition (°C)	Young's Modulus (MPa)	Strain (%)	Tensile strength (MPa)
PHB	1750-183	-4	3.5-4.0	3.0-8.0	43
i-PP	170-176	-10	1.0-1.7	500-900	34
PET	250-256	75	2.2-2.9	100-7300	70
Nylon-6,6	265	70	2.8	60	83

Production of derivatives based on PHB via the biosynthesis of copolyesters containing PHB units with other 3-hydroxyalkanoate units,[64] such as PHBV[65] and poly (3-hydroxybutyrate-co-3-hydroxyhexanoate) (PHBHH), has been considered to enhance the mechanical and processing properties of PHB.[66,67] Also, blends with other biodegradable polymers and addition of bio-based fillers such as starch and cellulose, plasticizers, and nucleating agents have been attempted to enhance the mechanical properties and reduce the melting point of PHB through formation of numerous, small, and imperfect crystallites.[6,68-70]

1.2 Polylactic acid (PLA)

Although naturally occurring PHAs have shown extensive potential to be used in place of biostable plastics, synthetic biodegradable polymers are much more versatile and tunable to have properties and functions suitable for individual purposes. These polymers are also adaptable for mass production.[6] The most important category of synthetic biodegradable polymers belongs to aliphatic polyesters including PCL, PHB, and PLA.

PLA, is the leading thermoplastic amongst biodegradable polymers, due to its availability and low cost production. PLA can be produced from 100% renewable resources, such as corn and sugar beets.[57] PLA is a rigid polymer with mechanical properties close to that of polystyrene (PS) and poly(ethylene terephthalate) (PET).[71] PLA has applications in several fields, including flexible and rigid packaging, cutleries, bottles, drink cups and biomedical applications such as sutures and bone implants.[50] PLA can be produced through polycondensation polymerization of lactic acid, prepared from the fermentation of sugars from different carbohydrate sources such as corn. However, this technique is limited to the production of low molecular weight PLA (6500 Da) due to the difficulties associated with the removal of trace water in the late stages of polymerization. Techniques such as azeotropic removal of water can relatively increase the final product molecular weight, however the required vacuum facilities and the high amounts of impurities in the final product will still be a challenge.[1] Alternatively, ring opening polymerization of cyclic diester lactide (LA) using organometallic initiators will result in efficient large scale production of PLAs with high molecular weights and low molecular weight distributions, under mild conditions.[41]

Lactide monomer is produced from depolymerization of PLA oligomers prepared from the polycondensation reaction, in the presence of Sn^{II}-carboxylate or alkoxide. L-lactic acid is the naturally occurring isomer of lactic acid. Therefore, the major product of the depolymerization of

the oligomers is L-LA. However, some side reactions including racemization during the production of LA causes formation of other isomers, D-LA and *meso*-LA, in lower extent. Purification steps, including recrystallization or distillation removes *meso*-LA from the product, resulting typically in a product composed of 98-99% L-LA contaminated with 1-2% D-LA.[58]

Industrial production of PLA is through ROP of lactide in the presence of homoleptic complexes such as Tin (II) octanoate ($Sn(Oct)_2$) or aluminum(III) isopropoxide ($Al(Oi\text{-}pr)_3$. These complexes can produce high molecular weight PLA, however, they suffer from the lack of control over polymerization, which usually results in broad molecular weight distributions.

Polymerization of pure L-LA using $Sn(Oct)_2$ forms crystalline isotactic PLA without any epimerization. However, these complexes are only capable of forming atactic PLA from a racemic mixture of L- and D-LA.

Currently, NatureWorks is the largest producer of PLA, with a capacity of over 150,000 ton/year in its US manufacturing facility (in Blair, Nebraska).[72,73]

1.3 Microstructures of poly (hydroxybutyrate) (PHB)

The PHB repeating unit contains a stereogenic center that leads to the formation of different microstructures. The microstructure of PHB is related to its tacticity which is defined by the relative stereochemistry of each neighboring stereogenic center along the polymer chain.[43] If the chiral centers are randomly arranged throughout the polymer chain, it produces atactic PHB. Alternating enchainment of opposite stereogenic centers along the polymer chain results in a syndiotactic microstructure. And, if the chiral centers attain similar configurations, the resulting PHB will be isotactic.

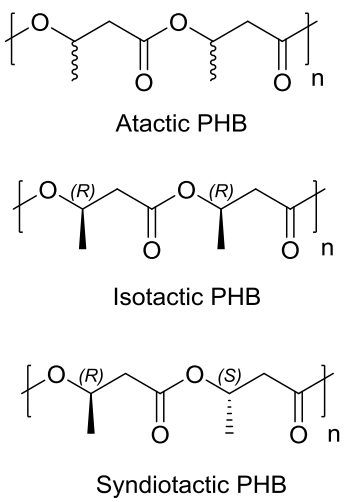

Figure 1.1 Representation of possible PHB microstructures

To determine the tacticity of PHB, carbonyl and methylene carbons are studied using inverse gated $^{13}C\{^{1}H\}$ NMR spectroscopy. Figure 1.2, shows a schematic of $^{13}C\{^{1}H\}$ NMR spectrum of PHB. In the carbonyl region, the upfield (~169.0 ppm) and downfield (~169.2 ppm) signals correspond to the *meso* (*m*) diad sequences (two adjacent stereocenters have the same configuration) and the *racemic* (*r*) diad sequences (two adjacent stereocenters have opposite configuration) respectively, also in the methylene region (40.5 ppm - 41.0 ppm), triad sensitivity has been observed. The P_r and P_m values which are the probability of racemic-linkages and meso-linkages can be calculated from the ratio of the integration of (*r*) diad and (*m*) diad sequences in the carbonyl region to the total integration of the carbonyl region ((*m*) + (*r*)).[29,74-76]

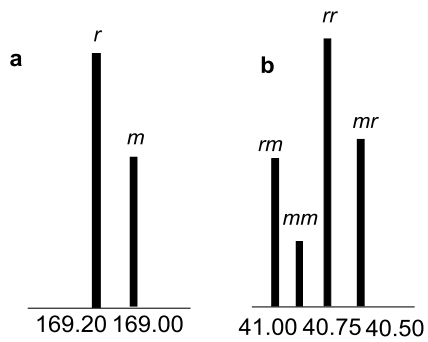

Figure 1.2 Schematic representation of inverse gated $^{13}C\{^{1}H\}$ NMR spectrum of PHB at **(a)** carbonyl region, and **(b)** methylene region

The tacticity of the chains directly influences polymer physical and mechanical properties. Atactic PHB is amorphous and has elastomeric properties with potential applications in food packaging, and soft-tissue engineering, where the mechanical properties of the polymer scaffold should match those of the tissue to be grown.[77] The completely isotactic synthetic PHB shows an excessively crystalline microstructure and a high melting point, very close to its bacterial based counterparts. Based on the results reported by Doi and coworkers, 70–80% isotactic PHB is ideal in terms of lower melting point and crystallinity.[78]

Although isotactic PHBs can be produced through fermentation and synthetic routes, syndiotactic PHB is not naturally occurring. This polymer was first synthesized by Kricheldorf and coworkers in 1990 with 62% and 70% syndiotacticity. The prepared polymers showed Young's modulus values of 9.5 MPa and 13.4 MPa with 450–500% extensibility.[79] Highly crystalline PHBs of 94% syndiotactic bias show high melting points of 183 ^{o}C, close to that of pure isotactic PHB.[29]

PHB's stereoregularity affects its enzymatic degradation as well as other parameters including backbone composition, molecular weight, crystallinity, and glass transition temperature. With

depolymerases, highly crystalline (*R*)-PHB can readily undergo hydrolysis. Atactic PHB degrades more slowly than (*R*)-PHB.[80]

PHB depolymerase has an affinity towards the complete (*R*)-configuration of the PHB side chains and hence naturally occurring PHBs readily undergo enzymatic degradations. In contrast to natural PHB, syndiotactic and atactic PHB consist of a mixture of (*R*)- and (*S*)-stereocenters which results in slower enzymatic degradation compared to isotactic PHB.[81,82]

According to the crystalline-induced biodegradation process, proposed by Scandola et al.[83], atactic segments of PHB undergo quick enzymatic degradation when it is in physical blends with, or di-block copolymerized with crystalline PHAs.[84]

It has been reported that biodegradation of atactic PHB improves in binary blends with naturally occurring poly(3-hydroxybutyrate-*co*-3-hydroxyvalerate) (PHBV),[85] poly(ε-caprolactone) (PCL), and poly(*L*-lactic acid) (PLLA).[86] Abe et al. related this phenomenon to the disfavored bonding of PHB depolymerase to the mobile amorphous PHB chains in rubbery state at temperatures well above the glass transition temperature. In blends of atactic PHB with crystalline PHAs, the depolymerase is readily absorbed on the surfaces where enzyme's substrate-binding domain can be provided by the crystalline PHB segments and then, the hydrolysis of atactic PHB component will occur.[8]

1.4 Microstructures of poly (lactic acid) (PLA)

Lactide (LA) has three different isomers including L-LA and D-LA and *meso*-LA due to the presence of two stereogenic centers. These monomers along with the racemate mixture are commercially available and formation of different microstructures is possible through stereocontrolled polymerization of LA.

Polymerization of any of the pure lactide isomers forms isotactic PLA featuring all stereocenters along the polymer chain having the same configuration. Isotactic PLA can be in the form of stereoblock, stereogradient, stereocomplex, and multiblock PLA.

Unlike the polymerization of enantiopure lactide, *rac*-lactide can form different microstructures including heterotactic and atactic PLA. Heterotactic PLA forms from alternating incorporation of D- and L- configured monomers of *rac*-lactide in the backbone as a result of which chiral centers along the polymer chain doubly alternate. Atactic PLA in which stereocenters are distributed along the chain in a random fashion can be produced from non-selective systems. Polymerization of *meso*-lactide can potentially form either syndiotactic (stereocenters alternate along the polymer chain) or heterotactic PLA (Figure 1.3).

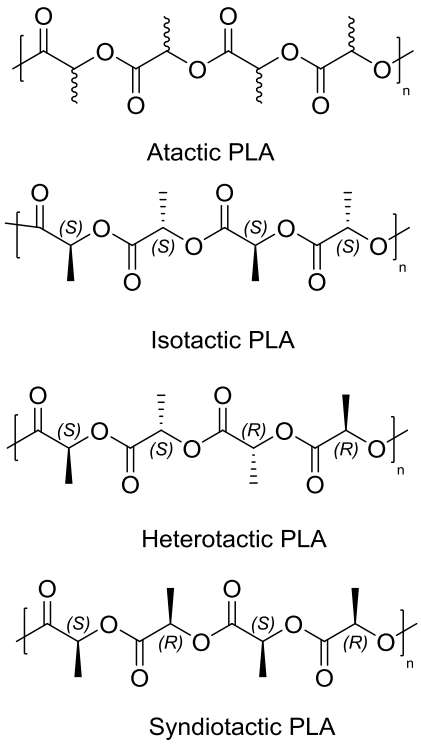

Figure 1.3 Representation of possible PLA microstructures

Tacticity of PLA also affects its melting (T_m) and glass transition temperature (T_g). For instance, isotactic PLA is crystalline with melting point reaching 180 ^oC and a T_g of about of 50 ^oC. Stereoblock PLA has a melting point of 210 ^oC with the same range of glass transition temperatures. Blending the macromolecular isomers of D- and L-PLAs forms higher order supramolecular assembly with considerable crystalline morphology through stereocomplex formation. These materials exhibit a substantially higher T_m (ca. 230 ^oC) compared to the homochiral crystals of each individual component. Atactic and heterotactic PLA are mostly reported as amorphous with T_g of 50 ^oC. [87,88]

PLA tacticity can be obtained by homonuclear decoupled ^{1}HNMR ($^1H\{^1H\}$ NMR) analysis of tetrad sequences (it provides better resolution of the tetrads and is easier to quantify than ^{13}CNMR spectroscopy).[89] Tetrad is a unit of four adjacent stereogenic centers which can be expressed by the three different linkages present, either *m* or *r*. In the absence of any side reactions like epimerization or transesterification, ROP of lactide monomers results in well-defined possible tetrad sequences and each tetrad sequence corresponds to a unique chemical shift in the ($^1H\{^1H\}$ NMR) spectrum of the polymer.[89,90]

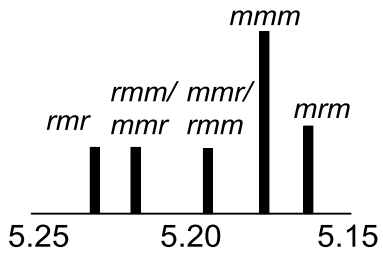

Figure 1.4 Homonuclear decoupled ^{1}H NMR of PLA from *rac*-lactide

The characteristic signals in the $^{1}H\{^{1}H\}$ NMR spectrum of PLA are the methine protons (5.15-5.25 ppm region), which decouple from the neighboring methyl groups (~1.6 ppm) in order to simplify the spectrum into a series of singlets (Figure 1.4). There exists five tetrad sequences of PLA according to Bernoullian statistics, which include *mmm*, *mmr*, *rmm*, *rmr*, and *mrm*, however the *rmm* and *mmr* tetrads are not distinguishable. With the application of Bernoullian statistics, the probability of *racemic* and *meso* linkages can be determined using the integration of *rmr* tetrad (x) as 1, and the relative integral values of *rmm*/*mmr* (y) and *mmr*/*rmm*, *mmm*, and *mrm* as (z). Summation of x, y, and z results in the total integration value, ε. Hence, [*rmr*] = $P_r^2/2 = 1/\varepsilon$ and $P_r = (2/\varepsilon)^{1/2}$. [*mmr*/*rmm*] = $y/\varepsilon = P_r P_m/2$ and $P_m = 2y/\varepsilon P_r$. [89] A fully heterotactic PLA has a P_r = 1, and a fully isotactic PLA attains a P_m = 1, and atactic PLA is being described by $P_r = P_m = 0.5$.

1.5 Synthesis of PLA and PHB through ring-opening polymerization (ROP)

1.5.1 ROP of β-butyrolactone

In addition to the bacterial fermentation technique, PHB can be synthesized from alternating copolymerization of propylene oxide and carbon monoxide, and through metal-mediated ROP of β-butyrolactone (BBL).

The limited access to high molecular weight PHBs and relatively low yields of alternating copolymerization of propylene oxide and carbon monoxide[91,92], has left the ROP of BBL through metal-mediated coordination-insertion mechanism as the most promising technique to form PHBs of different tacticities and microstructures. BBL, along with other functionalized β-lactones can be prepared from epoxide carbonylation in the presence of $[(salph)Al(THF)_2][Co(CO)_4]$ complexes.[93,94]

Metal-mediated complexes are in the form of LnMR , in which Ln = is the ancillary ligand, M, is the electropositive metal, and R represents the initiator, typically alkoxide, alkyl, or amide groups.

Dittrich and Schulz reported the first mechanistic studies on the coordination-insertion ROP. This mechanism starts with monomer coordination to the metal center through the carbonyl oxygen, followed by the nucleophilic attack of the alkoxide initiator to the carbonyl carbon (Figure 1.5). Acyl-oxygen bond cleavage results in the ring opening of the monomer and the formation of new metal-alkoxide initiator. The newly formed metal-alkoxide will now act as the initiator to ring open the upcoming monomer and the propagation of the polymer chain. ROP can potentially proceed through a living polymerization with no transfer and/or termination reactions until monomer depletion. As a result, this system is high yielding and forms polymers with narrow molecular weight distribution.[41,95-97]

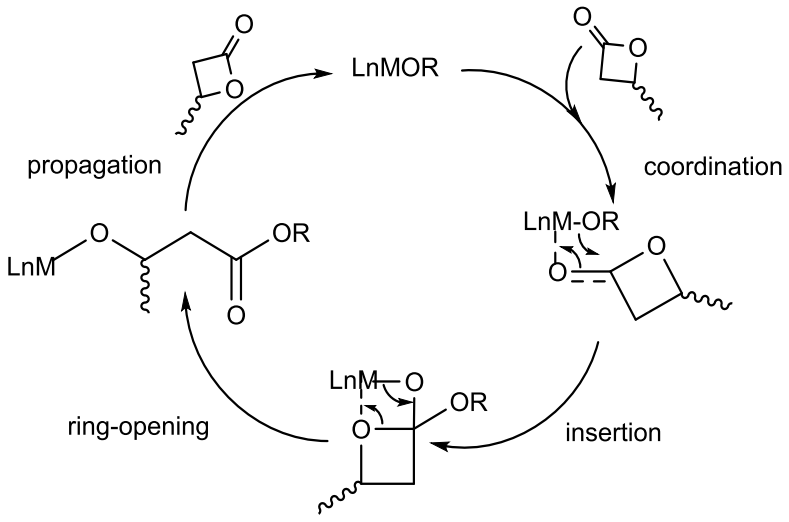

Figure 1.5 Coordination-insertion mechanism for the ROP of BBL by metal catalysts.

Stereoselectivity in the polymerization can proceed through two mechanisms, chain-end control (CEC) and enantiomorphic site control (ESC). In the CEC, which is more dominant in achiral systems, the stereochemistry of the last inserted monomer dictates the stereochemistry of the incoming monomer. Whereas in ESC the ancillary ligand determines which monomer to be enchained. This mechanism is usually more dominant in complexes with chiral ligands, however, these two mechanisms may combine depending on the system.[41]

Transesterification in ROP is the major side reaction and it occurs through two possible mechanisms of intramolecular and/or intermolecular transesterification (Figure 1.6). In case of intramolecular transesterification, back biting happens and as a result, oligomers and macrocycles will form. The absence of the chain end is a sign of this mechanism. Intermolecular transesterification takes place between two neighboring polymer chains resulting in chain redistribution. These side reactions increase the molecular weight distribution of the final product, and as a continuous mechanism may cause molecular weight reduction. This results in irreproducible polymerization.[48]

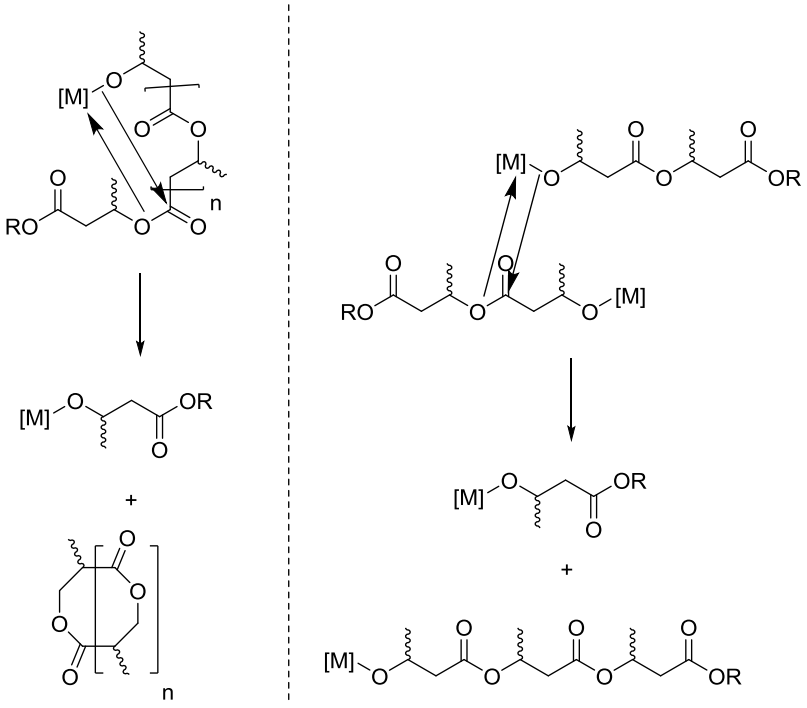

Figure 1.6 Intramolecular (left) and intermolecular (right) transesterification side reactions.

ROP of BBL using metal catalysts including Mg and Zn[98-107] Al,[108-111] In,[100,112-117] Sn,[95,118,119], rare earth, [74,75,120-126] and transition metals[30,109,127-129] as well as organocatalysts [130-135] has emerged as a pathway to access PHBs with more varied microstructures and properties.[9,45,87] Some examples are listed in Figure 1.7.

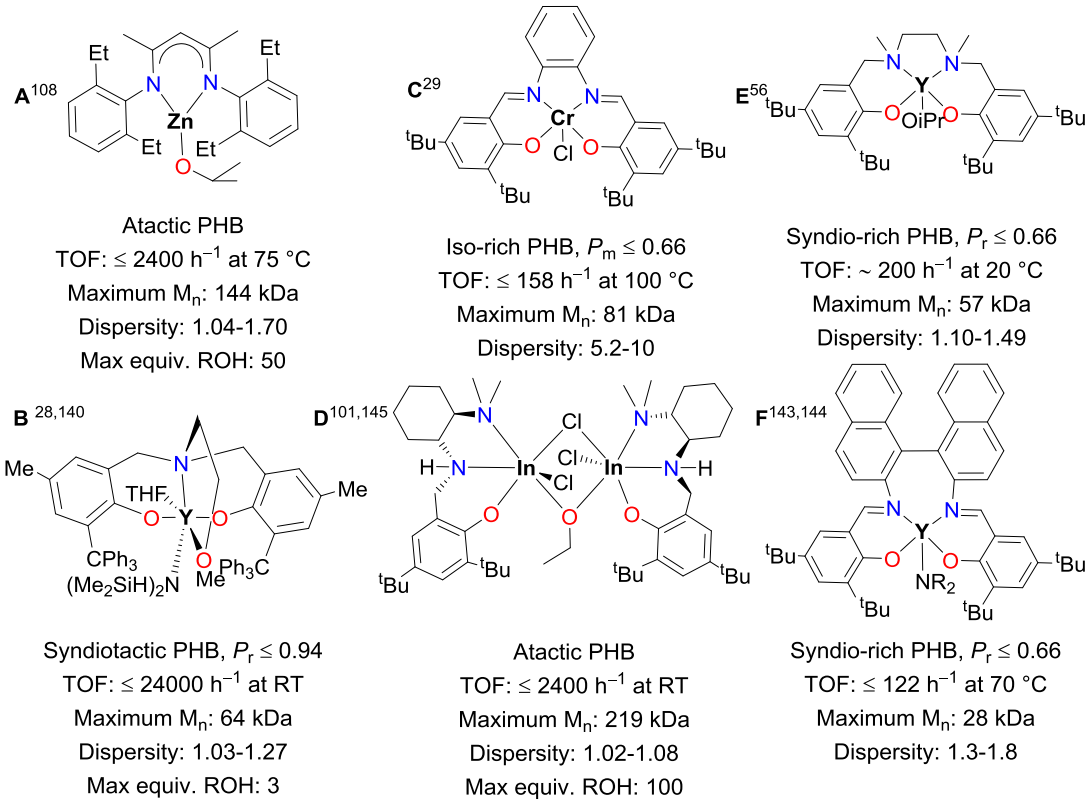

Figure 1.7 Landmark catalysts for the living and immortal polymerization of BBL.

Despite some promising early works[79,95,136-138] in metal-catalyzed polymerization of BBL, a breakthrough in the field came in 2002 when Coates *et al.* introduced (**A**) [107] as the first organometallic complexes to polymerize *rac*-BBL in a living manner to yield atactic PHB with molecular weights of more than 100 kgmol^{-1}and low polydispersity (~1.1).

Following this, Carpentier *et al.* reported a highly active alkoxy-amino-bisphenolate yttrium initiator (**B**) to form highly syndiotactic PHB (P_r up to 0.94) from *rac*-BBL; however with the highest reachable molecular weight of 60 kgmol^{-1}.[29,139]

Achiral chromium(III) salophen complexes (**C**) were introduced by Rieger *et al.* in 2008 to polymerize BBL to isotactically enriched high molecular weight PHBs with very broad molecular

weight distributions ($Đ$ ~ 5-10). Mass transfer problems due to very high viscosities of the resulted polymers have been reported as the reason for this observation. Polymers showed multiple melting points (116-149 °C) with the highest molecular weights of 250 $kgmol^{-1}$.[30]

A series of tin complexes were reported to afford low molecular weight (2.5-84 $kgmol^{-1}$), moderately syndiotactic PHB (P_r > 0.7).[95,119,137,140,141] Salan- and Salen-supported yttrium complexes have been reported to form syndiorich PHB with a range of melting temperatures (**E**, **F**).[142-144]

We have reported the dinuclear indium complex (**D**) as an excellent initiator for the living ring opening polymerization of *rac*- BBL to form atactic PHB with great control over molecular weight.[112] It is worth noting that this catalyst produces highest molecular weights of PHB (314 $kgmol^{-1}$) with lowest dispersities, among the synthesized PHBs that have been reported so far.[100,145]

Among the catalysts mentioned above, some are capable of proceeding the polymerization in a living manner where the initiation is faster than the propagation and as a result all chains will grow at the same time producing narrow molecular weight distribution. A shortcoming of this system is that to grow each polymer chain, one molecule of the catalyst is required leading to high catalyst residues and potential health problems associated with the toxicity of the metal-based species in medical applications of the polymer.

Due to concerns associated with the presence of metallic contaminations, immortal ROP of cyclic esters, first introduced by Inoue, has been considered as a solution to this problem.[146] In immortal ROP, a metallic complex will act as the initiator and a protic source, like an alcohol, will act as a chain transfer agent. Rapid and reversible transfer reaction between the growing chain and the alcohol molecules renders formation of monodisperse polymers. Therefore, only a very low initiator concentration is required and the number of the polymer chains will be equal to the sum

of the number of initiator and co-initiator molecules (Figure 1.8 shows a simplified schematic of this reaction).

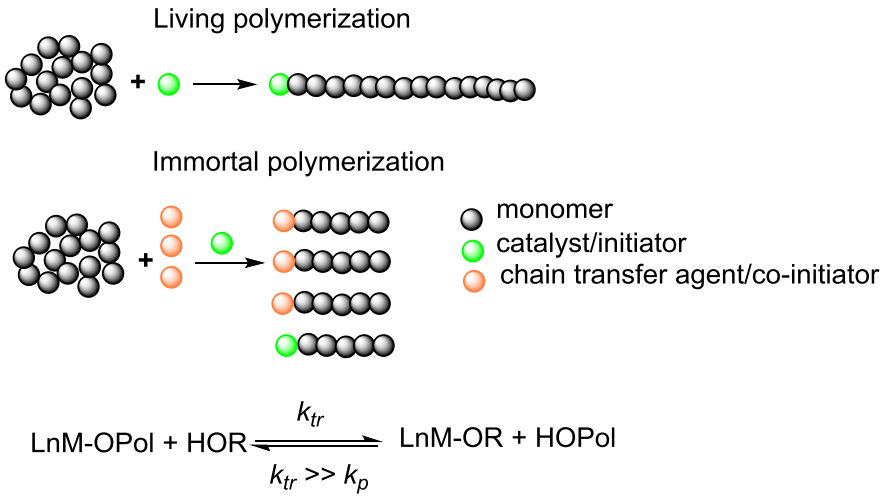

Figure 1.8 Representation of immortal ring opening polymerizations

An example of this, comes from Carpentier *et al.* whose amino-alkoxy-bis(phenolate)yttrium complexes (**B**) are active in the presence of 3 equivalents of isopropanol to polymerize 800 equivalents of BBL within 5 min to form syndiotactic PHBs (P_r ~ 0.9, M_n = 21.9 kgmol^{-1}, $Đ$ = 1.17). In 2008, a lanthanide alkoxide complex was reported capable of immortal ROP of BBL in the presence of 1 equivalent of *i*PrOH to produce syndiotactic PHBs (P_r ~ 0.8), however, the molecular weights were low and reaction rates were slow. [75] In 2009, Carpentier *et al.* reported that complex (**A**) stays active in the presence of up to 50 equivalence of isopropyl alcohol or benzyl alcohol for both solution and bulk polymerization of BBL. [10,139,147-150]

In 2012, we reported that dinuclear indium complex (**D**) is also an active catalyst for immortal ROP of BBL.[112,114] It is a remarkably active initiator for the highly controlled immortal ROP of BBL in the presence of high loadings of ethanol and monomethylated poly(ethylene glycol)[112].

1.5.2 ROP of lactide

ROP can proceed through different mechanisms, however the metal-mediated route through coordination-insertion ring opening polymerization has by far received more attention due to its better control over the polymerization and better selectivity towards the backbone microstructure.

First generation of metal based coordination-insertion catalysts for the ROP of lactide, were mainly homoleptic complexes including $Sn(Oct)_2$, zinc(II) lactate, and Al ($OiPr)_3$. As mentioned above, $Sn(Oct)_2$ is the most widely established precatalyst to produce high molecular weight PLA in large scales in the presence of protic reagents such as alcohols as co-initiators. [151,152]

However, the presence of extensive intra- and intermolecular transesterifications in these systems results in the very broad molecular weight distribution and unpredictable molecular weights. Importantly, homoleptic metal complexes are non-selective towards the polymerization of *rac*-LA.

Consequently, well-defined single site complexes with various sets of ligands, have been developed to enhance control over molecular weight, its distribution, and stereoselectivity. Some of the landmark highly selective catalysts introduced for the polymerization of lactide are shown in Figure 1.9.[68,79,95,141,153-158]

Highly isoselective Aluminum salen ((*R*)-SalBinap Al(OR)) catalyst (**G**) was introduced by Spassky to form crystalline PLA from the polymerization of *rac*-LA in solution state.[155] Importantly D-isomer of lactide predominately enchained until about 50% while L-lactide remained in the solution. The kinetic studies revealed that the rate of polymerization towards D-LA is almost 20 times faster than that of the L-LA, highlighting the site selective character of the catalyst which results in the formation of stereoblock PLA. However, this system suffers from

extensive transesterifications and causes broad molecular weight distribution. The melting temperature of the polymers were reported to reach up to 187 °C.

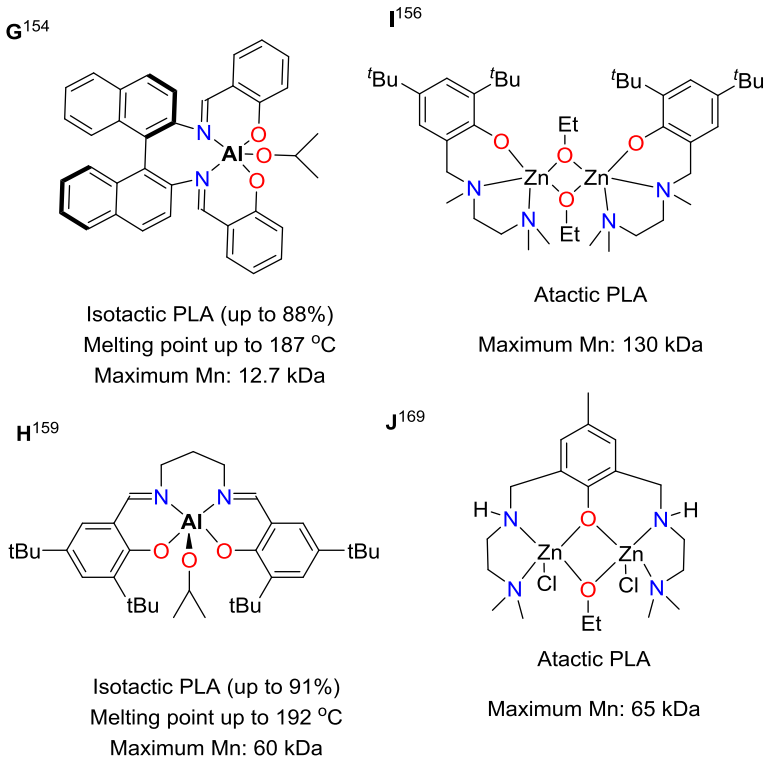

Figure 1.9 Representative catalysts for the polymerization of lactide.

Followed by this in 2002, Feijen *et al.* reported an enantiopure salen aluminum isopropoxide complex bearing the Jacobsen ligand. This catalyst is convenient to prepare and preferentially polymerizes L-LA over D-LA with a rate 14 times faster. Although this system forms highly crystalline stereoblock PLA, it is only capable of formation of low molecular weight PLA.[159]

An aluminium based complex (**H**) was reported afterwards by Nomura *et al.* to form highly isotacic stereoblock PLA with P_m = 0.98 and T_m = 207 °C. So far this complex is by far the most isoselective catalyst to form stereoblock PLA from the ROP of *rac*-lactide by an achiral system.[160]

In 2008, we reported complex (**D**) as an exceptionally active and controlled catalyst toward the living polymerization of lactide. Polymerization of 200 equivalents of lactide using this complex reaches over 90% conversion in 30 min, at 25 °C in dichloromethane. Furthermore, sequential addition of monomer increased the molecular weight systematically without any changes in the rate of the polymerization or increase in the dispersity parameter. This catalyst favors the polymerization of L-LA and forms moderately isotactic PLA from the polymerization of *rac*-LA. Using this system the molecular weight of PLA could reach to 350 $kgmol^{-1}$, which is exceptional. Mechanistic investigations indicated that the complex remains dinuclear during the polymerization.[161-165]

The first chiral indium salen catalyst was reported by our group in 2012. Unlike chiral aluminum salen complexes, this catalyst displayed a combination of high activity and isoselectivity. Mechanistic studies revealed that the complex isoselectivity follows an enantiomorphic site control mechanism. Catalyst preference for the polymerization of L-LA over D-LA formed stereoblock PLLA-b-PDLA, however with no significant crystallinity, which was assigned to the presence of transesterification reactions.[166,167]

Despite the limited isoselective catalysts, heterotactic PLA is more accessible with a wider range of metal centers and ligand sets. Zinc alkoxide complex (**A**) is among the most heteroselective catalysts for the polymerization of lactide (P_r = 0.94). This catalyst is highly reactive and 97% conversion of lactide is reachable in 2 h at 0 °C. [154]

Group 3 metal complexes based on lanthanum, neodymium, and yttrium bearing achiral aminobisphenolate ligands were prepared for the first time by Carpentier *et al.* in 2004 to form highly heterotactic PLA (P_r = 0.81 to 0.92).[168] This group showed that alcoholysis of this

complexes in the presence of isopropanol forms yttrium-alkoxide complexes with which higher reactivity and productivity would be attained. [169]

Zinc ethoxide catalyst bearing a tridentate diamino-phenoxy ligand (**I**) the dizinc-monoalkoxide complex (**J**) were reported by Hillmyer and Tolman as highly active catalysts for the polymerization of lactide. Polymerization results with (**I**) showed molecular weights lower than expected which was linked to the presence of impurities. Polymerization of *rac*-LA initiated by (**J**) was rapid (90% conversion within 30 min) at room temperature with good molecular weight control and narrow molecular weight distribution. Both complexes form atactic PLA, however with no significant epimerization over the polymerization of L-LA resulting in the formation of isotactic PLA.[157,170]

1.6 Thermorheological characterization of polymers

Viscosity of Newtonian fluids, such as water, do not change by applying shear or strain forces. However, most of the existing fluids are not categorized as Newtonian fluids as their viscosity is a function of applied stress, and in some cases duration of the applied stress. Non-Newtonian fluids are generally divided into Bingham plastics, pseudoplastics, dilatants, thixotropics and rheopectics.

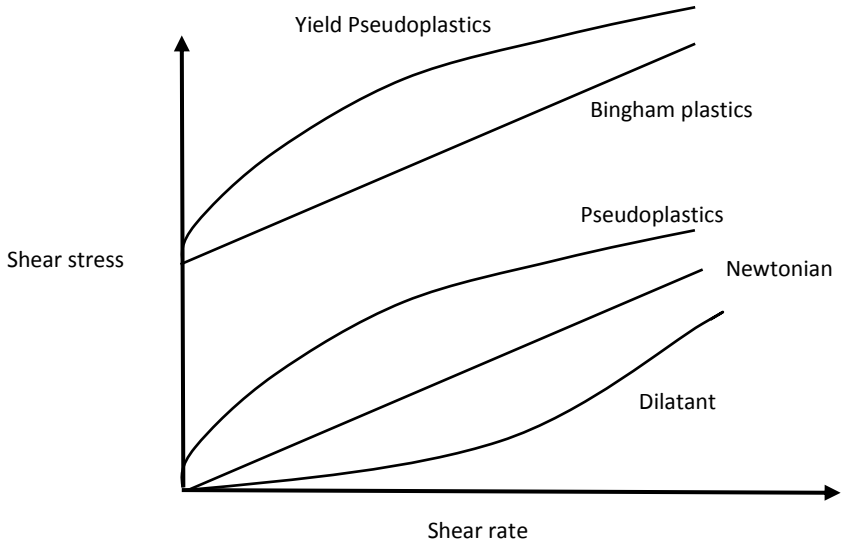

Figure 1.10 Shear dependent behavior of common non-Newtonian fluids

Bingham plastics require an initial yield stress to flow, such as toothpaste, mayonnaise, and mustard. Pseudoplastics, also known as shear thinning fluids, undergo structural destructions under shear fields and as a result, their viscosity decreases by applying shear rates. This behavior is mostly reported in suspensions such as ketchup, blood, paint, etc. In dilatants fluids, however, the viscosity increases upon application of shear forces. These materials are mostly known as shear thickening fluids, with examples including concentrated corn starch suspensions (Figure 1.10). Thixotropics and rheopectics are basically pseudoplastics and dilatants fluids respectively, however their viscosity is also a function of the duration of applied stress. Examples of thixotropics and rheopectic fluids includes yogurt and egg white respectively.[171]

Unlike simple fluids, polymeric materials are known as viscoelastic fluids. The term *visco*, comes after their potential fluid-like behavior (dissipation of applied energy). The term *elastic* comes after their potential solid-like behavior (energy storage) upon application of external forces.[172]

Rheology is the science of studying the relationship between the applied stress and the resulted deformation in non-Newtonian and viscoelastic materials in forms of mathematical constitutive equations. Polymer melt-processing involves a combination of complex shear and strain fields that causes formation of homogeneous polymeric melts and mixtures. Rheological studies of polymer melt helps us predict the processing properties of polymers through measuring important material functions such as shear viscosity and dynamic moduli. Rotational and extensional rheometers are commonly used to investigate polymer viscoelastic behaviors.[172,173]

1.6.1 Rotational rheometery

Shear dependent viscoelastic properties of polymers are mostly studied using rotational rheometers. Simplest geometries of rotational rheometers are parallel plates and cone-plates (Figure 1.11). In both cases, the sample will be subjected to shear forces while it is being squeezed between two plates, one stationary, and the other rotating at a specified angular velocity. Parallel plates are more popular for linear-viscoelastic measurements (e.g. small-amplitude oscillatory shear. Not suitable for non-linear measurements as the shear rate varies with height and radii at different location between the gaps: $\dot{\gamma} = \Omega r/h$, where Ω is the angular velocity (rad/s), h is the sample gap height, and r is the radii). Cone-plate geometry, however, provides nearly uniform shear rates throughout the sample (Shear Rate: $\dot{\gamma} = \Omega/\theta_0$, where Ω is the angular velocity (rad/s) and θ_0 is the cone angle) at higher shear rates, which makes it a suitable rheometer for non-linear measurements (e.g. large-strain stress relaxation and start-up of shear flow).[172]

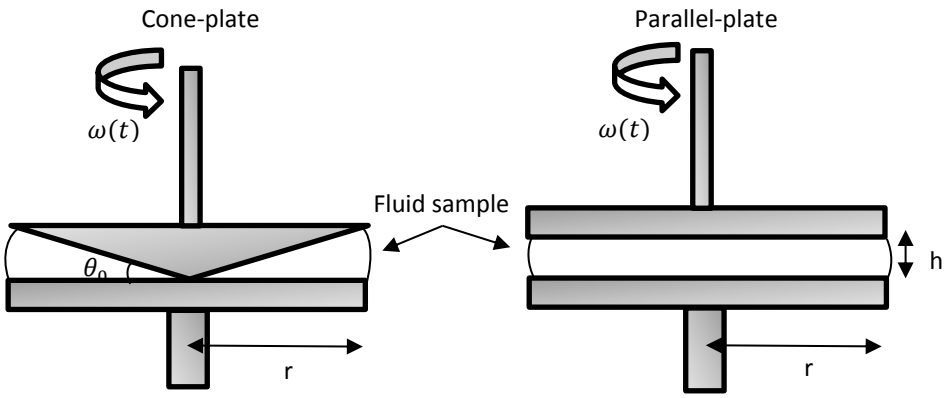

Figure 1.11 Representation of parallel-plate and cone-plate rotational rheometers[174]

One of the most applied rheological measurements suitable for polymer characterization is small amplitude oscillatory shear. In this test, sample will be subjected to a sinusoidal displacement of the upper plate, which causes oscillatory shear deformation:

$$\gamma\,(t) = \gamma_0 \sin\,(\omega t)$$

where γ_0 represents the strain amplitude and ω is the angular frequency. The periodic applied stress ($\sigma(t)$) can then be measured using the equation below in the linear viscoelastic region (small strain amplitudes), where σ_0 is the stress amplitude and δ represents the phase shift or loss angle:

$$\sigma\,(t) = \sigma_0 \sin(\omega t + \delta)$$

By means of trigonometric identities, the above equation may be written as:

$$\sigma\,(t) = \gamma_0\,[G'(\omega) \sin(\omega t) + G''(\omega) \cos(\omega t)]$$

In this equation, the first term relates to the in-phase response to the applied strain which, also is known as storage or elastic modulus (*G'*). The second term corresponds to the out-of-phase response to the applied strain, which is known as loss or viscous modulus (*G''*). It is also suggested to consider *G'* and *G''* as real and imaginary parts of complex modulus, G*, which can be quantified as:

$$|G^*| = \sqrt{G'^2 + G''^2}$$

The complex viscosity can then be estimated using the complex modulus, with the absolute value of: $|\eta^*| = |G^*|/\omega$.

In plastic processing, wide range of deformation rates are applied to the specimen, however, not all of them can be simulated using conventional oscillatory rheometers. Hence, in order to expand the range of deformation rates (frequencies), which represents expanded time frame of experiment, rheological data measured at different temperatures can be brought together on a single master curve using the "time-Temperature superposition" principle. This concept can only be applied to thermo-rheologically simple materials in the linear viscoelastic region. Thermo-rheological simplicity means that the sample does not undergo any structural changes in the considered temperature range. Using this technique, the master curve (showing materials parameters such as *G*', *G*'', η^*, or *G**), represents an 'extension' to the operating time, or frequency scale of the rheometer.

Master curves can be obtained by plotting the multiplication of the materials parameters, including storage and loss moduli by a vertical shift factor (b_T), versus the multiplication result of quantities with time units (such as frequency or shear rate) with horizontal shift factor a_T.

b_T usually is temperature independent, and hence can be considered as unity. a_T, however, can be obtained from the amount of horizontal shift required to bring the data corresponding to a specific temperature T onto the same curve obtained at another temperature or T_{ref}.

The amount of a_T can be measured using the Williams, Landel, and Ferry (WLF) equation:[11,172,173]

$$log(a_T) = -C_1(T - T_{ref})/(C_2 + T - T_{ref}),$$

where C_1 and C_2 are materials constants determined at T_{ref}. This equation is valid at temperatures close to the glass transition temperature, T_g. At temperatures higher than T_g + 100 K horizontal shift factor can be obtained using an empirical relationship, the Arrhenius equation, (Dealy and Wissbrun, 1999), where E_a is the flow activation energy, R is the gas constant, and T_{ref} is the reference temperature.

$$a_T = exp[-E_a/R(\frac{1}{T} - \frac{1}{T_r})]$$

It is worth noting that flow activation energy provides insight on the molecular structure of polymers, for instance the presence of long-chain branching increases the E_a compared to their linear counterparts.[172,173]

1.6.2 Extensional rheometery

Extensional deformation exists in most of the common plastic processing techniques and it plays an important role specifically in dies and molds at the diverging and converging areas. Many products including plastic bags and fibers, form outside of the die in melt state, in which case the sample experiences large extensional flows.

Simple extensional flow, also known as uniaxial extension, is a very well-known standard rheological procedure to measure polymers extensional rheological properties under certain extensional rates. Hencky strain is the logarithmic change of sample length, *L(t)*, over time as follows:

$$\varepsilon_H(t) = \ln(L(t)/L_0)$$

In this equation L_0 is the initial length of the sample, and ε_H is the Hencky strain. Derivative of the above equation results in Hencky strain rate that is:

$$\dot{\varepsilon}_H = (dL/dt)/L_0$$

The amount of tensile stress required to stretch the sample ($\sigma_E(t, \dot{\varepsilon}_H)$) is proportional to $\dot{\varepsilon}_H$, and the proportionality constant is the tensile stress growth coefficient defined as:

$$\eta_E^+(t, \dot{\varepsilon}_H) = \sigma_E(t, \dot{\varepsilon}_H)/\dot{\varepsilon}_H$$

At sufficiently small strain rates, the tensile stress growth coefficient is three times the zero-shear viscosity ($\eta_E^+ = 3\eta_0$).

Different devices based on stretching samples in melt state exists, however, the Sentmanat Extensional Rheometer (SER) is the most easy-to-use. This simple system comes as a detachable fixture for commercially available rotational rheometers, which fits inside regular oven systems to investigate materials extensional behavior at different temperatures.[175,176]

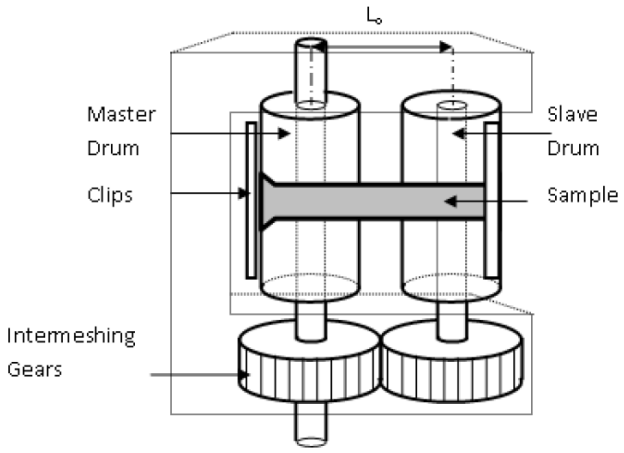

Figure 1.12 Schematic illustration of a Sentmanat extensional fixture[177]

In this test, a sample strip is placed between two counter-rotating drums (master and slave windup drums) and is subjected to different Hencky strains, which can be calculated from constant drive shaft rotation rate, ω, as follows:

$$\dot{\varepsilon}_H = 2R\Omega/L_0$$

In this expression R and L_o represent the radius of the windup drums, and length of the sample in between the drums (centerline distance between the master and slave drums). The applied torque can be measured from the applied force as T = 2FR.[176]

Due to application of tensile force, the cross sectional area of the sample undergoes changes while the test is being ran, and it can be measured from $A(t) = A_0 \exp(-\dot{\varepsilon}_H t)$. Based on the aforementioned definition of the stress growth coefficient, it can be measured by:

$$\eta_E^+(t) = F(t)/\dot{\varepsilon}_H A(t)$$

and the time dependent amount of force, F(t), will then be measured by the machine from the torque signal.[172,173]

1.7 Star shaped (sparsely branched) PLA and PHB

Star (sparsely branched) polymers exhibit interesting properties compared to their linear counterparts. The presence of several arms radiating from a central core causes lower solution viscosity, lower hydrodynamic radii, and lower glass transition temperature compared to the linear analogue of the same molecular weight. In addition, the presence of branch points contributes to melting point reduction and increase in melt viscosity/strength. Importantly due to the presence of multiple branch tips and increased concentration of end groups, functionalization of these polymers to tailor their properties for specific applications is possible.[178,179]

Two methods have been introduced to synthesize star-shaped polymers a core-first method, and arm-first method. In the core first method, the polymerization is initiated from a multi-functional initiator, and polymer propagation will proceed directly from the active core. In the

arm first method, monofunctional living chains are used as the initiators to react with an appropriately reactive multifunctional polymer core. [21]

The core first method has been extensively employed for the ROP of lactide,[21,180,181] caprolactone, glycolide, [21, 203] and trimethylene carbonate[182] to form star-shaped biodegradable polymers. These polymers are mainly synthesized using a multifunctional alcohol and a metal based catalyst making an active metal-alkoxide initiator, following monomer ROP through the coordination-insertion mechanism.[21,181]

The field of metal based or organic catalyzed ROP of various types of cyclic esters and carbonates has been extensively reviewed in the literature.[21,181,183] Herein, only a brief overview of the reports on the preparation of star shaped PLA and PHB will be discussed.

$Sn(Oct)_2$, is one of the most widely used catalysts for the preparation of star shaped PLA with various architectures in the presence of discrete, miktoarm and dendritic/ hyperbranched cores. Discrete cores or polyols, have widely been used in order to form PLA stars with different number of arms. A series of 3-armed star PLA is made using trimethylolpropane (TMP) as the chain transfer agent.[184-189] diTMP and erythritol have been used to form 4-arm star PLAs.[19,185] 5-arm stars are reported using xylitol. Dipentaerythritol (DPET) and tripentaerythritol (TPE) have been used to make 6 and 8 armed star PLAs, respectively. [185]

In 2010, Shaver, et al. investigated the effect of rigid and flexible star cores on the thermal and physical properties of PLA with three and six armed star topologies, utilizing $Sn(Oct)_2$. Based on their results, high catalyst loadings up to one catalyst unit per chain transfer agent hydroxyl group renders bimodal molecular weight distributions due to either self-initiation behavior of the catalyst or the presence of impurities. This will increase the transesterification reactions and hence decreases the molecular weight of the stars in long reaction periods. Rigid aromatic cores, elongate

initiation, and hence causes an increase in molecular weight distribution. [21,190] Although many of the multi-armed PLA stars have been synthesized using $Sn(Oct)_2$, it should be noted that this catalyst is a strong transesterification agent, which, as mentioned before, is one of the major shortcomings of tin in ROP of cyclic esters. Furthermore this catalyst suffers from the lack of stereocontrol over the PLA backbone microstructure.

Aluminum complexes bearing salan and salen ligands were used by Cameron and Shaver to form heterotactic, and isotactic PLAs using *rac*-lactide and DPET as the co-initiator. Based on their results, an increase in isotacticity, increase of T_g and degradation temperatures of the resulting polymers. Additionally they showed that to enhance hydrolysis resistance, higher isotacticity bias (>70%) was required. Profound differences were also reported in the crystallite size and d-spacing from powder-XRD results.[190]

Wei *et al.* (2010) reported the preparation of heterotactic symmetric 3-arm star PLAs in the presence of triethanolamine as a triol using an yttrium alkyl complex bearing salan ligand. The prepared polymers showed high molecular weights with narrow molecular weight distributions ($Đ$ = 1.02-1.09).

Synthesis of an array of symmetric and asymmetric stereo-miktoarm star-shaped PLAs made of PLLA and PDLA arms has been recently reported by Satoh et al.[191] Click coupling reaction of azide functionalized PDLAs and ethynyl-functionalized PLLAs having one, two or three initiating sites, formed linear stereoblock and stereo-miktoarm star PLAs. Using WXRD and DSC results, the formation of stereocomplex crystals in the linear stereoblock and stereo-miktoarm star PLAs in the absence of any homochiral crystallization was confirmed. As expected, the increased number of arms in the stereo-miktoarm star PLAs reduced the melting point as well as the crystallinity of

the stereocomplex crystals. Importantly, symmetric stereo-miktoarm star PLAs exhibited higher crystallinity compare to the asymmetric counterparts.

Stimuli-responsive, luminescent 3-arm PLA suitable for drug delivery and imaging purposes were formed recently using discrete transition metal complexes. These metalloinitiator were iron based with hydroxyl functionalized dibenzoylmethane (dbm) ligands $Fe(dbmOH)_3$. $Fe(dbmOH)_3$-mediated polymerization of LA was fast and highly efficient, with no significant transesterification. The presence of $Fe(dbm)_3$ complex as a pH-responsive and luminescent core, and biocompatible/biodegradable PLA arms makes this system a potential agent for imaging and cancer therapy.[192]

New luminescent, biocompatible and biodegradable 4-armed star polymers with aggregation-induced emission (AIE) characteristics were recently reported by Zhao et al. [193] Various functional four-arm star polymers were synthesized via ROPs of LA, among other cyclic monomers including propargylfunctionalized trimethylene carbonates in the presence of tetrahydroxyl-functionalized tetraphenylethene (TPE) as the chain transfer agent and salan lutetium complex as the catalyst. The authors showed that the presence of polyester/polycarbonate arms attached to TPE, with excellent AIE properties, enhances its solubility and significantly improves its processability. For example, while small AIE molecules require costly vacuum sublimation and vapor deposition processes for the fabrication of luminescent films, the AIE functionalized polymer solutions can easily be casted to form thin photoluminescent films to be used in medical imaging and electronic materials.

Knauss et al. used glycidol as a chain transfer agent for immortal polymerization of lactide to form glycidol end-capped linear PLAs in solution state at 80 ^{o}C. However, the polymerization results at melt state at high temperatures 130^{o}C and formed high molecular weight PLA in the

presence of same amount of glycidol. Solution viscometric measurements confirmed the formation of hyperbranched PLA architectures due to the *in-situ* ROP of glycidol molecules. Polymerization of glycidol, forms multiple hydroxyl sites along the chain to initiate ROP of lactide monomer. As a result, PLA branches grow in dendritic structure.[194]

Although there exist so many examples of star shaped PLA along with other types of polyesters, due to the lack of appropriate catalysts for the polymerization of BBL in the presence of protic groups, reports on PHB star polymers are very limited. For instance, 4-arm star PHBs have been synthesized through ring-opening polymerization of BBL in the presence of ethoxylated pentaerythritols and Sn[195] and Lu[196] based catalysts; however, due to the prevalence of extensive transesterification reactions and lack of catalyst reactivity, the resulting polymers showed broad dispersities and/or low molecular weights.

1.7.1 Rheological studies on star-shaped PLA

Linear rheological measurements can be used to study the effect of branching on polymer processing. Immobile branch points of the star polymers hinders the curvilinear/reptational motion of the linear chains and as a result, the rheology of stars is quite different from that of linear polymers. Star polymers relax mainly through a combination of arm-retraction (also known as contour-length fluctuations, primitive path fluctuation) and constraint release (dynamic dilation).[197] Since in star polymers, reptation is prohibited because of the presence of branch points, their relaxation is strongly dependent on the molecular weight of the arms and is independent of the number of arms for slightly branched stars (number of arms < 30).[178,198-200]

Early models based on linear polymers suggested that for high molecular weight star polymers, η_0 (zero-shear viscosity) scales exponentially with molecular weight for star polymers

compared to its power-law growth in linear polymers. [201,202] Distinctively different shapes of the dynamic frequency sweep test results of the star polymers versus the linear polymers have been reported by Fetters, et al.[178] They showed that the frequency (ω_c) at which G'(ω) crosses G"(ω) is approximately the reciprocal of the longest relaxation time (disentanglement relaxation time), τ_d. At frequencies higher than ω_c, the value of G" decreases for linear polymers, while it increases for stars, and finally reaches a maximum at ω_{max}, which is the reciprocal of the arm retraction relaxation time, τ_R. Since, ω_{max} (or ${\tau_R}^{-1}$) has a power law relationship with the arm molecular weight, and ω_c (or ${\tau_d}^{-1}$) scales exponentially with the arm molecular weight, the region between ω_{max} and ω_c, increases upon increasing arm molecular weight, representing a broader relaxation time spectrum.[203] Snijkers, et al. have reported the rheological investigation of well-defined symmetric entangled polyisoprene stars with four and eight arms and different molar masses of the arms (ranging from 56 $kgmol^{-1}$to 103 $kgmol^{-1}$). Based on non-linear viscoelastic measurements, they proposed that during steady shear, star shaped samples tend to orient in the flow direction rather than stretch. Similar results have also been reported by previous research groups.[204-206]

Although the viscoelastic properties of polyolefinic star shaped polymers has a rich history and has been extensively reviewed in common textbooks, and there is a considerable interest on the synthesis of star-branched biodegradable aliphatic polyesters, studies on the melt rheological properties of these category of materials are quite rare.

One of the landmark papers on the rheological properties of PLA star polymers has been published by Dorgan, *et al*.[207] The authors prepared linear, four and six armed star PLAs using Sn $(Oct)_2$ as the catalyst and multifunctional alcohols as the chain transfer agents. Based on their rheological measurements, they reported enhanced zero-shear viscosity and more shear-thinning

behavior in star PLA compare to the linear counterparts. The authors noted, however, that there were some difficulties in drawing a precise perspective about the rheological properties of the samples because of relatively high dispersities ($Đ \sim 2$) and thermorheologically complex behavior of crystalline PLA.

Preparation of star-shaped and comb-like poly(L-Lactic acid) (PLLA), was reported by Nouri *et al.* through employing multifunctional initiators. Hyperbranched PLLA was also prepared using glycidol as initiator/co-monomer. In a melt state polymerization (T = 130 ^{o}C), simultaneous ring opening and incorporation of glycidol and L-LA into the polymer backbone resulted in the formation of hyperbranched architectures. Formation of desired structures were confirmed using FTIR, size exclusion chromatography, and ^{1}H NMR techniques. DSC and optical microscopy showed a profound improvement in PLA crystallization due to the presence of branch points that can act as nucleating sites. Extensional rheometery (SER) revealed a significant difference in the extensional viscosity of linear and branched polymers. While commercial linear PLA, did not show any significant strain hardening, the branched analogues revealed a pronounced strain hardening behavior after the plateau region. Based on these results, they concluded that branching can be considered as a practical tool to improve the crystallization and rheological properties of polylactide.[194,208]

1.7.2 Rheological studies on PHB

Rheological characterization of pure bacterial based PHB was first reported by Arakawa *et al.* in 2006.[209] The homopolymer was obtained from Industrial S/A, and samples suitable for rheological measurements were prepared through compression molding at 180 ^{o}C for 3 min. Oscillatory shear modulus and capillary extrusion were used to investigate the rheological and

thermal degradation at the processing temperature of 180 ^{o}C. It was found that the oscillatory shear moduli and the steady-state shear stress decreased extensively during isothermal measurements at the melting point. Based on the GPC results, the molecular weight of the sample decreased from 250 $kgmol^{-1}$ to 100 $kgmol^{-1}$ after 10 minutes residence time in the rheometer at 180 ^{o}C. Importantly, the reduction of molecular weight during isothermal measurements, diminishes the melt elasticity and the onset of gross, chaotic melt fracture, which caused extensive surface roughness on the extrudates surface during capillary extrusion. Based on these results, the authors mentioned that the residence time during injection-molding or extrusion of PHB has to be seriously taken into account as the molecular weight reduction and loss of melt strength is almost inevitable.

In order to enlarge the processing window of PHB, the addition of phenol-based compounds have been investigated as it decreases the polymer melting point. Yu *et al.* reported the addition of 4,4-dihydroxydiphenylpropane (DOH_2) to PHB to decrease its melting point from 176 to 113 ^{o} C upon addition of 50% of DOH_2. The presence of intermolecular hydrogen bonds between the carbonyl groups of PHB and the hydroxyl groups of DOH_2 was confirmed by FTIR. Due to the presence of hydrogen bonding, chain mobility of PHB was limited after blending with DOH_2 molecules, resulting in an increase in the glass transition temperature from 1.2 to 7.3 ^{o} C, indicating miscibility of PHB with DOH_2. Based on TGA results, although the presence of DOH_2 decreased the melting point, the existence of it decreased the thermal decomposition temperature of PHB. This is due to the fact that DOH_2 molecules are dihydroxy phenols bearing proton donors with acidic properties which at high temperatures can cause extended chain scissioning.[210]

Feng *et al.* demonstrated that grafting maleic anhydride (MA) onto PHB chains interferes with the random chain scission of the polyester and decreases the thermal decomposition temperature

of PHB-g-MA. However, the presence of the grafting did not affect the melting point and processability of PHB.[211]

In 2010, Mousavioun *et al.* reported that the presence of intermolecular interactions due to hydrogen bonding between the reactive functional groups of soda lignin and the carbonyl groups of PHB decreases the thermal decomposition of PHB, however high loading of additives, up to 40%, will be required.[212]

More recently, Santagata *et al*. used pomace extract (EP), from the bio-waste of winery industry, as thermal and processing stabilizer for PHB. While isothermal annealing of high molecular weight Biomer PHB (M_w = 840 kgmol^{-1}) at 190 ^oC causes two orders of magnitudes reduction of the complex viscosity over 10 minutes, the presence of 5 and 15% EP in the blends resulted in an enhancement in the thermal stability of the product, with stable rheological properties at 120 ^oC, for 100 seconds. The presence of EP, also increased the terminal viscosity by 2 fold. Importantly, EP maintained molecular weight of PHB to some exten after processing (M_w after processing without Ep = 134 kgmol^{-1}, with Ep = 540 kgmol^{-1}). Dynamic mechanical and tensile tests showed that EP slightly improved the polymer ductility.[213]

Thermal degradation of PHB during melt mixing is due to random chain scission forming shorter polymer chains with crotonic and carboxyl end groups as a consequence of the β-elimination reaction. One of the proposed strategies to control the chain scission, is to incorporate chemicals that react with at least one of the newly generated end groups. For instance, polymerization of the crotonyl moieties bearing unsaturated bonds, have been attempted by employing free radical initiators along with multifunctional unsaturated compounds;[214] however, no improvement was observed. Also, the addition of free radical initiators caused an acceleration in thermal degradation of PHB. In other attempts, the addition of epoxide containing chemicals

such as poly (methyl methacrylateco- glycidyl methacrylate) (PGMA) with pendant epoxide groups was used to improve the thermal stability of PHB. In this strategy, carboxyl end groups may participate in crosslinking reactions with epoxide moieties. GPC and TGA results showed an increase in the molecular weight of PHB due to crosslinking, and slight improvement in thermal stability of the blends.[215]

In 2014 Maurer *et al.* suggested that the presence of metal ion contaminants and other impurities in as-received PHB may accelerate the polymer degradation process. Therefore they purified high molar mass PHB obtained from Biomer (M_w = 620 $kgmol^{-1}$), and studied its thermal stability using isothermal frequency sweep tests, in the presence of a series of commercially available additives known to react with carboxylic acid groups. These additives include: bis(3,4-epoxycyclohexylmethyl) adipate (BECMA), 2,2'-bis(2-oxazoline) (BOX), trimethylolpropane tris(2-methyl-1-aziridinepropionate) (PETAP), triphenyl phosphate (TPP), tris(nonylphenyl) phosphate (TNPP), polycarbodiimide (PCDI), and poly(methyl metharylate-co-glycidyl methacrylate) (GMA.MMA).

Their rheological measurements and the GPC results after the tests, revealed that PCDI and GMA.MMA have a minor impact on the thermal stability of PHB. While, TPP and TNPP did not affect the thermal stability of PHB. The presence of BECMA, BOX, and PETAP resulted in a strong decrease of the dynamic modulus (Figure 1.13).[216]

Although addition of PCDI and GMA.MMA showed improvement on the thermal stability, the presence of these low molecular weight polymers in the blend, caused plasticization effect and as a result (more profoundly for GMA.MMA containing system), the complex modulus of the blend decreased significantly at concentrations above 5 wt% (Figure 1.13).[216]

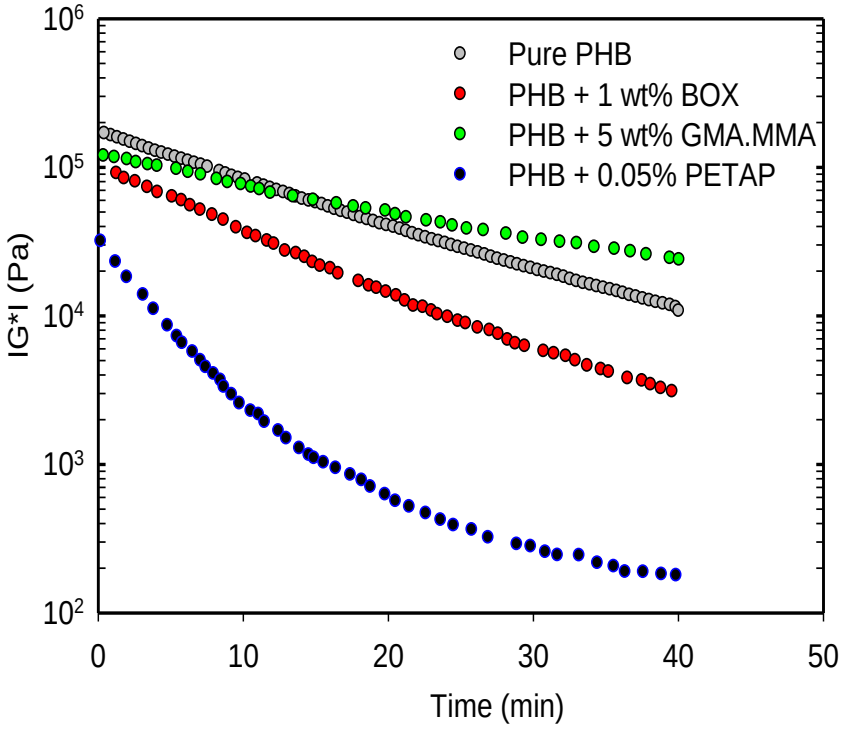

Figure 1.13 Dynamic shear modulus of pure PHB and PHB containing BOX , GMA.MMA, and PETAP as a function of time, at 180°C and at $\boldsymbol{\omega} = 62.8$ rad/s. [216]

1.8 Thesis objectives

The ultimate goal of this interdisciplinary PhD thesis is to synthesize and thoroughly characterize the rheological and physical behavior of a series of controlled topology and microstructure poly(hydroxybutyrate) (PHB) as a function of molecular weight, degree of branching, and stereoregularity. We will suggest a new approach towards the design of catalysts suitable for the formation of truly processable PHBs with potential applications in commodity products. New catalysts are also being introduced with potential industrial applications for the preparation of star-shaped multiblock copolyesters under facile fume hood conditions.

The particular objectives can be summarized as follows:

1. Synthesis and rheological characterization of star-shaped PHBs: To this end, monodisperse linear and three armed star-shaped poly(hydroxybutyrates) (PHBs) using dinuclear indium complex, $[(NNO_{tBu})InCl]_2(\mu\text{-}Cl)(\mu\text{-}OTHMB)$ will be prepared. Preparation of structurally well-defined 6-armed star PHBs using the recently developed mononuclear ethyl zinc complex $(NNO_{tBu})Zn(CH_2CH_3)$ and a hexol (dipentaerythritol (DPET)) as co-initiator will be discussed. The solution and melt rheological properties of the prepared well defined star PHBs along with their linear analogues will thoroughly be investigated.

2. Preparation of processable PHBs without any need for thermal stabilizers or processing aids: zinc based dinuclear complexes will be prepared and used for the immortal polymerization of gram scale BBL to form high molecular weight monodispersed syndio-enriched PHBs. Thermorheological characterization of the polymers in both rotational and extensional modes, along with the tensile test results will be used to investigate the melt and solid state behavior of the prepared polymers.

3. Development of new easy-to-prepare indium based catalysts for the preparation of star polymers in ambient atmospheric conditions: Dinuclear indium salan complexes will be introduced as an exceptionally tolerant and stable catalyst in moist air. Importantly, this catalyst possesses unprecedented activity in melt-state for the polymerization of different isomers of lactide in open air to form stereo-triblock copolymers.

1.9 Thesis organization

This thesis is organized as follows: Chapter 1 provided an introduction to clarify the motivations of the current thesis along with a comprehensive literature review on polyhdroxybutyrate and polylactic acid microstructures, synthetic routs and rheology. Chapter 2 will present the materials, methodologies, catalysts synthesis, and representative polymerization set-ups used for the development of this thesis. In chapter 3, the synthesis of 3-arm and 6-arm star PHBs will be described using indium and zinc based complexes in the solution state to afford symmetric model materials. A complete investigation on solution viscometric properties of the polymers is provided along with their frequency and shear dependent melt-viscoelastic behavior. The structure-property relationships for these polymers will also be represented. In chapter 4, a modified version of the zinc complex studied in chapter 2, will be used and developed to form high molecular weight syndio-enriched PHBs with stable isothermal frequency-sweep tests results at high temperatures. Detailed extesional rhemetric results will be obtained as a proof of processability of these polymers. In chapter 5, polymerization of high loadings of enantiopure lactide in air using newly developed salan-indium catalyst will be discussed. Finally, chapter 6 will summarize the results and conclusions and provide suggestions for future work.

Chapter 2: Materials and methodologies

2.1 Materials purifications

Diethy ether (Et_2O), hexane, and toluene were degassed and dried using activated alumina in a Solvent Purification System from Innovation Technology, Inc. Deuterium-labelled NMR solvents were purchased from Sigma Aldrich and Cambridge Isotope Laboratory. Tetrahydrofuran (THF) was purchased from Sigma-Aldrich and further dried over Na/benzophenone and vacuum-transferred to a Strauss flask and then degassed through a series of freeze-pump-thaw cycles. CH_2Cl_2, $CDCl_3$, C_6D_6, BBL, and pyridin-2-ylmethanol were dried over CaH_2 and vacuum-transferred to a Strauss flask and then degassed through a series of freeze-pump-thaw cycles. Racemic and enantiopure lactide was obtained from PURAC America Inc. and recrystallized from hot toluene three times then dried under vacuum before use. Other chemicals and solvents were purchased from Sigma-Aldrich, Fisher, Alfa Aesar, or STREM and were used without further purification. Chiral diaminoaryloxy ligands, $H(N_RNO_R)$ were synthesized according to literature procedures.[163,217] Bacterial based highly Isotactic PHB (iPHB) was provided from Biomer corporations. All the air and moisture sensitive operations were done in an MBraun glove box or using a standard Schlenk line.

2.2 Gel Permeation Chromatography (GPC)

Average molar mass (M_n), dispersity ($Đ$), radius of gyration (R_g), hydrodynamic radii (R_h), and intrinsic viscosity [η] values were determined by a triple detection GPC-MALS-viscometer using an Agilent liquid chromatograph equipped with an Agilant 1200 series pump and autosampler, three Phenogel 5 μm Narrow Bore columns (4.6 × 300 mm with 500 Å, 103 Å and 104 Å pore

size), a Wyatt Optilab differential refractometer, Wyatt miniDAWN TREOS (multi-angle laser light scattering detector), and a Wyatt ViscoStar viscometer. The column temperature was 40°C. A flow rate of 0.5 mL/min was used and samples were prepared in THF (ca. 1 mg/mL). The refractive index increment dn/dc of linear and star PHB samples were measured separately off-line by an Optilab rEX refractive index detector (λ = 658 nm) using a series of different concentration solutions. The operating temperature was 25 °C. Data were processed by ASTRA software (Wyatt Technology). The dn/dc values for PLA were collected from literature.

R_h was also measured using a DynaPro-99-E50 dynamic light scattering module (R_h detection range from 0.18 nm - 2500 nm) with a GaAs laser (658 nm) at 25 ^oC. The instrument was equipped with a temperature-controlled microsampler (MSXTC-12). Sample concentration was the same as that of the GPC measurements in THF (ca. 1 mg/mL). Intrinsic viscosities of dilute solutions (1-5 mg/mL) of linear and star PHBs were also measured using a Cannon-Fenske viscometer in THF.

2.3 MALDI-TOF mass spectrometry

Mass spectra were recorded on a Bruker Autoflex MALDI-TOF (time-of-flight mass (TOF) spectrometer equipped with MALDI ion source) operated in either linear or reflection mode. For MALDI-TOF measurement, the sample was dissolved in dichloromethane (0.6 mg/μL); 2,5-dihydroxybenzoic acid (DHB) (0.02 mg/μL) was used as the matrix (10:1) and 1 μL of sodium trifluoroacetate (100 mM) was added as the cation source.

2.4 Differential scanning calorimetery (DSC)

DSC measurements were performed to detect the melting and glass transition temperatures of the polymers using a TA Instruments-Q1000. Experiments were carried out under nitrogen

atmosphere with ~3 mg of the samples sealed in an aluminum pan. Starting from room temperature, syndio enriched samples were heated to 100 °C with a 10 °C /min heating rate, followed by cooling to room temperature at a 5 °C /min rate, and heated to 100 °C with a 10 °C /min heating rate. Since no considerable crystalizations were observed during the cooling ramp, T_m values were determined using the first heating ramp. Highly syndiotactic and isotactic samples were heated to 200 °C with 10 °C /min heating ramp and cooled to room temperature with 5 °C /min cooling rate. Tm values reported are extracted from the second heating ramp.

DSC measurements for atactic PHBs were also performed on a TA Instruments – Q1000. Experiments were carried out under nitrogen atmosphere with ~4 mg of the samples sealed in an aluminum pan. After cooling down the samples to the low temperature of -20°C, they were heated from -20°C to 80 °C with a 10 °C /min heating rate, followed by cooling to -20°C at a 5 °C /min rate, and heated to 80 °C with a 10 °C /min heating rate. The glass transition temperature T_g was determined using the second heating ramp.

2.5 Thermogravimetric analysis

Duplicated thermal decomposition results were obtained using a thermogravimetric analysis Shimadzu TGA-50 at a heating rate of 20°C/min from 30 to 600 °C under an inert atmosphere of nitrogen.

2.6 Rheological measurements

All the rheological measurements were performed under a nitrogen atmosphere to minimize degradation of the polymer samples during testing. The linear viscoelastic properties of the

samples were determined by a rotational rheometer (Anton-Paar, MCR 501/502) equipped with parallel plate geometry (diameter of 8 mm). Gaps of 0.3–0.6 mm were set to minimize edge effects and ensure a reasonable aspect ratio of plate radius and gap. Dynamic time sweep measurements were carried out at an angular frequency of 1 rad/s at different temperatures for crystalline and semi- crystalline samples to examine the thermal stability of the samples. Small amplitude frequency sweep tests were performed at frequencies in the range of 0.01 to 100 1/s, with a strain of 1% and temperatures ranging from 25-100 °C for amorphous samples and above melting point for the crystalline ones.

Start-up of shear flow tests were performed using a cone and plate geometry with 25mm diameter and angle of 1°. The steady state shear viscosity versus time curves were generated for all samples for shear rates in the range from 0.01 to 0.5 1/s. Also step shear strain tests were carried out to investigate the relaxation modulus and damping function over a range of strains. The damping functions were used to model the rheological behavior of the samples using Wagner model.

Uniaxial extensional flow measurements were conducted using the Sentmanat Extensional Rheometer (SER-2) which is a fixture to the MCR 502 (Anton-Paar) rheometer. Samples were prepared by hot press at temperature above melting points. For syndio enriched PHBs the extensional stress growth coefficients were measured at 80°C, which is well above the melting point. Measurements were carried out at different Hencky strain rates ranging from 0.1 to 20 s^{-1}. All measurements were done under a nitrogen atmosphere to avoid degradation.

2.7 Tensile Measurements

COM-TEN 95 series tensile testing equipment was used for the tests at ambient temperature. Samples were cut from the center of the hot-pressed sheets to minimize edge imperfections. For the tests, crosshead speed was adjusted at 25mm/min using a 40 mm gage length and 178 N capacity load cell. Each test was repeated 3 time per sample and the average values of the tensile Young's modulus and elongation at break were reported.

2.8 NMR spectroscopy

Bruker Avance 400dir MHz spectrometer, Bruker Avance 400inv MHz spectrometer and Bruker Avance 600 MHz spectrometer were used to record the ^{1}H NMR, $^{13}C\{^{1}H\}$ NMR, and homonuclear decoupled ^{1}H NMR ($^{1}H\{^{1}H\}$NMR) experiments. ^{1}H NMR chemical shifts are given in ppm versus residual protons in deuterated solvents as follows: δ 1.73 and 3.58 for $CDCl_3$. $^{13}C\{^{1}H\}$ NMR chemical shifts are given in ppm versus residual ^{13}C in solvents as follows: δ 77.23 for $CDCl_3$.

2.9 X-ray crystallography

Diffraction measurements for X-ray crystallography were made on a Bruker DUO diffraction with graphite monchromated Mo-Kα radiation. The structure was solved by direct methods and refined by full-matrix least-squares using the SHELXL crystallographic software of the Bruker-AXS.

2.10 Elemental analysis

Unless specified, all non-hydrogen were refined with anisotropic displacement parameters. EA CHN analysis was performed using a Carlo Erba EA1108 elemental analyzer.

2.11 Synthesis of complexes 1-19

Synthesis of complex (±)-(1). A suspension of KOBn (26 mg, 0.18 mmol) in toluene (1.5 mL) was added dropwise to a stirring suspension of (NNO_{tBu})$InCl_2$ (195 mg, 0.34 mmol) in toluene (3 mL) at room temperature. The reaction mixture was stirred for 2 h. The resulting white precipitate was filtered through Celite to yield a colorless filtrate. All volatiles were removed in *vacuo*, and hexane (3 mL) was added to the residue to precipitate a white solid. The clear supernatant was decanted off of the white solid. The product was dried in *vacuo* for few hours (132 mg, 64%). ^{1}H NMR ($CDCl_3$, 600MHz) δ 7.64 (2H, d, $^3J_{H\text{-}H}$ = 7.3 Hz, *ortho-H* of benzyl alkoxide), 7.21 (2H, d, $^4J_{H\text{-}H}$ = 2.4 Hz, Ar *H*), 6.94 (1H, t, $^3J_{H\text{-}H}$ = 7.3 Hz, *para-H* of benzyl alkoxide), 6.87 (2H, t, $^3J_{H\text{-}H}$ = 7.5 Hz, *meta-H* of benzyl alkoxide), 6.55 (2H, d, $^4J_{H\text{-}H}$ = 2.3 Hz, Ar *H*), 5.79 (1H, d, $^2J_{H\text{-}H}$ = 11.7 Hz, -O-C*H*$_2$- of benzyl alkoxide), 5.03 (1H, d, $^2J_{H\text{-}H}$ = 11.8 Hz, -O-C*H*$_2$- of benzyl alkoxide), 4.20 (2H, d, $^2J_{H\text{-}H}$ = 13.5 Hz, -NH-C*H*$_2$-Ar), 3.38 (2H, d, $^2J_{H\text{-}H}$ = 13.5 Hz, -NH-C*H*$_2$-Ar), 2.87 – 2.78 (4H, m, -N*H*- and -C*H*- of DACH), 2.69 (6H, s, -N(C*H*$_3$)$_2$), 2.51 (2H, dq, $^3J_{H\text{-}H}$ = 3.9 Hz, 10.9 Hz, -C*H*- of DACH), 2.40 (2H, br. d, $^3J_{H\text{-}H}$ = 12.3 Hz, -C*H*$_2$- of DACH), 2.02 (6H, s, -N(C*H*$_3$)$_2$), 1.94 – 1.87 (2H, m, -C*H*$_2$- of DACH), 1.82 (4H, t, $^3J_{H\text{-}H}$ = 14.5 Hz, -C*H*$_2$- of DACH), 1.48 (18H, s, Ar-C(C*H*$_3$)$_3$), 1.31 – 1.20 (20H, m, -C*H*$_2$- of DACH and Ar-C(C*H*$_3$)$_3$), 1.20 – 1.14 (2H, m, -C*H*$_2$- of DACH), 1.07 – 0.97 (2H, m, -C*H*$_2$- of DACH); ^{13}C{^{1}H} NMR ($CDCl_3$, 151MHz) δ 162.3 (Ar *C*), 142.3 (Ar *C*), 138.8 (Ar *C*), 136.7 (Ar *C*), 130.4 (Ar *C*-H), 127.2 (Ar *C*-H), 126.5 (Ar *C*-H), 126.3 (Ar *C*-H), 119.6 (Ar *C*), 69.1 (-O-*C*H$_2$-C$_6$H$_5$), 64.8 (-*C*H- of DACH), 53.0 (-*C*H- of DACH), 50.5 (-HN-*C*H$_2$-Ar), 44.4 (-N(*C*H$_3$)$_2$), 38.3 (-N(*C*H$_3$)$_2$), 35.6 (Ar-*C*(CH$_3$)$_3$), 34.1 (Ar-*C*(CH$_3$)$_3$), 32.0 (Ar-C(*C*H$_3$)$_3$), 30.9 (-*C*H$_2$- of DACH), 30.5 (Ar-C(*C*H$_3$)$_3$), 25.0 (-*C*H$_2$- of DACH), 24.9 (-*C*H$_2$- of DACH), 22.0 (-*C*H$_2$- of DACH). Anal. Calcd. For $C_{53}H_{85}Cl_3In_2N_4O_3$: C 54.77; H 7.37; N 4.82. Found: C 54.67; H 7.22; N 4.79.

Synthesis of complex (±)-(2). A suspension of 1,3,5-tris(hydroxymethyl)benzene (11 mg, 0.065 mmol) in toluene (1.5 mL) was added dropwise to a solution of complex **1** (71 mg, 0.064 mmol) in toluene (3 mL). The reaction mixture was stirred at room temperature or 70 °C for 16 h. After removal of the solvent *in vacuo* a white solid of complex **2** was collected and washed with hexane (3 × 5 mL). The collected white solid **2** was dried *in vacuo* at least for a few hours. (63 mg, 81%) X-ray quality colorless crystals of complex **2** were grown in toluene at 25 °C. ^{1}H NMR ($CDCl_3$, 600MHz) δ 7.71 (2H, br. s., $^{3}J_{H\text{-}H}$ = 7.3 Hz, *ortho-H* of THMB), 7.28 (2H, d, $^{4}J_{H\text{-}H}$ = 2.2 Hz, Ar *H*), 6.97 (1H, br. s., *para-H* of THMB), 6.63 (2H, br. s., Ar *H*), 5.80 (1H, d, $^{2}J_{H\text{-}H}$ = 11.4 Hz, -O-C*H*$_2$- of THMB), 5.08 (1H, d, $^{2}J_{H\text{-}H}$ = 11.5 Hz, -O-C*H*$_2$- of THMB), 4.40 (2H, dd, $^{3}J_{H\text{-}H}$ = 5.6 Hz, $^{2}J_{H\text{-}H}$ = 12.9 Hz, HO-C*H*$_2$- of THMB), 4.26 (2H, dd, $^{3}J_{H\text{-}H}$ = 7.9 Hz, $^{2}J_{H\text{-}H}$ = 12.8 Hz, HO-C*H*$_2$- of THMB), 4.03(2H, br. s., -NH-C*H*$_2$-Ar), 3.38 (2H, d, $^{2}J_{H\text{-}H}$ = 12.7 Hz, -NH-C*H*$_2$-Ar), 2.91 – 2.80 (2H, m, -C*H*- of DACH), 2.75 (2H, br. s., -NH-), 2.68 (6H, s, -N(C*H*$_3$)$_2$), 2.50 – 2.39 (2H, m, -C*H*- of DACH), 2.38 (2H, br. s., -C*H*$_2$- of DACH), 1.99 (6H, s, -N(C*H*$_3$)$_2$), 1.94 – 1.86 (2H, m, -C*H*$_2$- of DACH), 1.82 (4H, br. t., $^{3}J_{H\text{-}H}$ = 11.8 Hz, -C*H*$_2$- of DACH), 1.58 – 1.46 (20H, s, -C*H*$_2$- of DACH and Ar-C(C*H*$_3$)$_3$), 1.39 (4H, br. s., *H*O- of THMB), 1.27 (18H, s, Ar-C(C*H*$_3$)$_3$), 1.21 – 1.12 (2H, m, -C*H*$_2$- of DACH), 1.12 – 0.93 (4H, m, -C*H*$_2$- of DACH); ^{13}C{^{1}H} NMR ($CDCl_3$, 151MHz) δ 162.2 (Ar *C*), 143.1 (Ar *C*), 140.7 (Ar *C*), 139.0 (Ar *C*), 137.0 (Ar *C*), 128.5 (Ar *C*-H), 126.3 (Ar *C*-H), 124.5 (Ar *C*-H), 124.1 (Ar *C*-H), 119.9 (Ar *C*), 68.5 (-O-*C*H$_2$-Ar of TMB), 65.4 (HO-*C*H$_2$-Ar of TMB), 64.6 (-*C*H- of DACH), 53.1 (-*C*H- of DACH), 50.1 (-HN-*C*H$_2$-Ar), 44.4 (-N(*C*H$_3$)$_2$), 38.2 (-N(*C*H$_3$)$_2$), 35.6 (Ar-*C*(CH$_3$)$_3$), 34.0 (Ar-*C*(CH$_3$)$_3$), 31.9 (Ar-C(*C*H$_3$)$_3$), 30.9 (-*C*H$_2$- of DACH), 30.4 (Ar-C(*C*H$_3$)$_3$), 24.9 (-*C*H$_2$- of DACH), 24.9 (-*C*H$_2$- of DACH), 22.0 (-*C*H$_2$- of DACH). Anal. Calcd. For $C_{55}H_{89}Cl_3In_2N_4O_5$: C 54.04; H 7.34; N 4.58. Found: C 54.12; H 7.30; N 4.68.

Synthesis of complex (±)-4. This complex was made based on previously reported procedure.[218]

Synthesis of complex (±)-6. A solution of (±)-H(NN_HO_{Cm}) proligand (200 mg, 0.415 mmol) and $Zn(CH_2CH_3)_2$ (0.0480 mL, 0.415 mmol) in Et_2O (5 mL) was stirred at room temperature for 30 min. The solvent was removed *in vacuo* to dryness. The desired product was isolated as a white solid without further purification. Yield 180 mg 90%. ^{1}H NMR ($CDCl_3$, 600MHz): δ 7.48 (1H, d, $^4J_{H-H}$ = 2.7 Hz, Ar H), 7.46-7.02 (10H, overlapping m, C(CH2)Ph), 6.53 (1H, d, $^4J_{H-H}$ = 2.7 Hz, Ar H), 4.20 (1H, dd, $^3J_{H-H}$ = 12.3 Hz, $^2J_{H-H}$ = 2.2 Hz, -HN-CH_2-Ar), 3.43 (1H, dd, $^3J_{H-H}$ = 12.4 Hz, $^2J_{H-H}$ = 2.26 Hz, -HN-CH_2-Ar), 2.21-2.5 (1H, td, $^3J_{H-H}$ = 4.4 Hz, 10.9 Hz, -CH- of DACH), 2.02 (3H, s, -N(CH_3)$_2$), 1.96 (3H, s, -N(CH_3)$_2$), 1.91 (1H, m, DACH), 1.75 – 1.50 (12H, m, -CH- of DACH and Ar-C(CH_3)$_2$Ph), 1.25 (3H, m, -CH_3- of ethyl), 1.10 – 0.80 (2H, m, -CH_2- of DACH), 0.66 (3H, s, Ar-C(CH_3)$_2$Ph), 0.02 (2H, m, -CH_2- of ethyl); ^{13}C{^{1}H} NMR ($CDCl_3$, 151MHz): δ165.12,152.79, 150.61, 136.16, 133.16, 128.79, 127.57, 127.51, 126.73, 125.18, 124.93, 124.18, 121.11, 68.02, 53.53, 49.80, 44.59, 42.09, 35.63, 31.94, 31.02, 26.19, 24.70, 20.83, 13.39. Anal. Calcd. For $C_{35}H_{47}N_2OZn$: C, 72.84; H, 8.21; N, 4.85. Found: C 71.85; H 7.89; N 4.45.

Synthesis of complex (*R*,*R*)-6. A solution of (*R*,*R*)-H(NN_HO_{Cm}) proligand (300 mg, 0.618 mmol) and $Zn(CH_2CH_3)_2$ (0.0700 mL, 0.618 mmol) in Et_2O (5 mL) was stirred at room temperature for 30 min The solvent was removed in vacuo to dryness. The desired product was isolated as a white solid without further purification. Yield 285 mg 95%. ^{1}H NMR (CD_2Cl_2, 600MHz): δ 7.48 (1H, d, $^4J_{H-H}$ = 2.7 Hz, Ar H), 7.46-7.02 (10H, overlapping m, C(CH_2)Ph), 6.53 (1H, d, $^4J_{H-H}$ = 2.7 Hz, Ar H), 4.20 (1H, dd, $^3J_{H-H}$ = 12.3 Hz, $^2J_{H-H}$ = 2.2 Hz, -HN-CH_2-Ar), 3.43 (1H, dd, $^3J_{H-H}$ = 12.4 Hz, $^2J_{H-H}$ = 2.26 Hz, -HN-CH_2-Ar), 2.21-2.5 (1H, td, $^3J_{H-H}$ = 4.4 Hz, 10.9 Hz, -CH- of DACH), 2.02 (3H, s, -N(CH_3)$_2$), 1.96 (3H, s, -N(CH_3)$_2$), 1.91 (1H, m, DACH), 1.75 – 1.50 (12H, m, -CH- of DACH and Ar-C(CH_3)$_2$Ph), 1.25 (3H, m, -CH_3- of ethyl), 1.10 – 0.80 (2H, m, -CH_2- of DACH),

0.66 (3H, s, Ar-C(CH_3)$_2$Ph), 0.02 (2H, m, -CH_2- of ethyl); $^{13}C\{^1H\}$ NMR ($CDCl_3$, 151MHz): δ 165.13, 152.81, 150.63, 136.18, 133.17, 128.8, 127.58, 127.51, 126.9, 124.93, 124.18, 121.11, 60.04, 53.54, 49.82, 44.60, 41.85, 35.64, 31.95, 30.95, 26.20, 24.80, 24.59, 20.84, 13.39. Anal. Calcd. For $C_{35}H_{47}N_2OZn$: C, 72.84; H, 8.21; N, 4.85. Found: C 72.55; H 8.11; N 4.65.

Synthesis of complex (±)-7. A solution of (±)-H(NN_HO_{Ad}) proligand (300 mg, 0.564 mmol) and Zn(CH_2CH_3)$_2$ (0.0650 mL, 0.564 mmol) in Et_2O (5 mL) was stirred at room temperature for 30 min The solvent was removed in vacuo to dryness. The desired product was isolated as a white solid without further purification. Yield 246 mg 82%.^{1}H NMR (CD_2Cl_2, 600MHz): δ 7.10 (1H, d, $^4J_{H-H}$ = 2.7 Hz, -Ar H), 6.74 (1H, d, $^4J_{H-H}$ = 2.7 Hz, -Ar H), 4.32 (1H, d, $^2J_{H-H}$ = 11.9 Hz, -HN-CH_2-Ar), 3.59 (1H, d, $^2J_{H-H}$ = 10.3 Hz, -HN-CH_2-Ar), 2.44 (1H, m, NCH), 2.39 (3H, s, N(CH3)2), 2.56 (1H, m, DACH), 2.05 (1H, m, NH), 2.29 (3H, m, Ad), 2.19 (3H, m, Ad), 2.03 (3H, m, Ad), 1.56 (3H, s, N(CH3)2), 1.22 (3H, m, -CH_3- of ethyl), 1.27 (9H, s, C(CH_3)^3), 1.86 (2H, m, DACH), 1.82 (3H, m, Ad), 1.73 (3H, m, Ad), 1.32 (1.5H, t, 3JHH = 6 Hz, –OCH2CH3), 1.28 (9H, s, C(CH3)3), 1.25 (2H, m, DACH), 1.13 (1H, m, DACH), 1.03 (1H,m, DACH), 0.13 (2H, m, -CH_2- of ethyl); $^{13}C\{^1H\}$ NMR ($CDCl_3$, 151MHz): δ165.33, 137.08, 134.03, 125.8, 123.77, 120.94, 63.82, 59.94, 56.50, 46.02, 44.83, 38.98, 38.17, 35.32, 31.91, 29.90, 24.54, 22.46, 21.68, 13.39.Anal. Calcd. For $C_{31}H_{49}N_2OZn$: C, 70.10; H, 9.30; N, 5.27. Found: C 69.78; H 9.57; N 5.45.

Synthesis of complex (*R,R*)-8. A solution of (*R,R*)-H($NNHO_{SiPh3}$) proligand (250 mg, 0.407 mmol) and Zn(CH_2CH_3)$_2$ (0.0460 mL, 0.407 mmol) in Et_2O (5 mL) was stirred at room temperature for 30 min The solvent was removed in vacuo to dryness. The desired product was isolated as a light yellow solid without further purification. Yield 220 mg 88%. ^{1}H NMR (CD_2Cl_2, 600MHz): δ 7.68 (6H, m, $SiPh_3$), 7.32 (9H, m, $SiPh_3$), 7.24 (1H, m, ArH), 6.79 (1H, m, ArH), 4.33

(1H, d, $^{2}J_{H\text{-}H}$ = 12 Hz, -HN-CH_2-Ar), 3.63 (1H, m, -HN-CH_2-Ar), 2.38 (1H, m, NH), 2.16 (3H, s, NCH_3), 1.97 (1H, m, CHN), 1.93 (3H, s, NCH_3)1.76 (2H, m, CHN + DACH), 1.19 (3H, m, -CH_3- of ethyl), 1.11 (3H, m, DACH), 0.94 (3H, s, Ar–CH3), 0.95 (4H, m, DACH), 0.04 (2H, m, -CH_2- of ethyl); $^{13}C\{^{1}H\}$ NMR ($CDCl_3$, 151MHz): δ 139.36, 134.65, 128.43, 127.19, 68.45, 67.97, 53.49, 49.45, 44.57, 36.46, 31.98, 25.60, 24.69, 24.59, 20.87, 20.52, 13.54. Anal. Calcd. For $C_{36}H_{44}N_2OSiZn$: C, 70.40; H, 7.22; N, 4.56. Found: C 69.85; H 7.00; N 4.53. Same procedure was used to form the (±)-5 complex using (±)-H($NNHO_{SiPh3}$) as the proligand with 70% yield. The ^{1}H NMR and $^{13}C\{^{1}H\}$ NMR of the racemic complex is similar to that of the enantiopure one.

Synthesis of complex (±)-9. This complex was made based on a previously reported procedure.[219]

Synthesis of complex (±)-10. To a solution of complex **5** (250 mg, 0.523 mmol) in cold pentane (−30 °C, 5 mL) equimolar amount of benzyl alcohol (0.0550 ml, 0.532 mmol) was added at room temperature. The reaction mixture was stirred for 4 h, and a white sticky solid was collected after several wash with cold pentane. The solvent was removed in vacuo to dryness. Yield 150 mg 60%. ^{1}H NMR (600 MHz, $CDCl_3$): 7.47-7.33 (overlapping m, Ar-H), 4.78 (2H, sh. s., -CH_2- of benzyl alkoxide), 4.08 (1H, d, $^{2}J_{H\text{-}H}$ = 11.9 Hz, -HN-CH2-Ar), 3.31 (1H, d, $^{2}J_{H\text{-}H}$ = 10.3 Hz, -HN-CH_2-Ar), 2.74-2.31(3H, m, -CH- of DACH), 2.42 (6H, s, -N(CH_3)$_2$), 1.76 (3H, s, -N(CH_3)), 1.45 (6H, s, -ArC(CH_3)$_2$Ph), 1.27 (6H, s, -ArC(CH_3)$_2$Ph), 1.86 – 1.00 (8H, m, -CH_2- of DACH); $^{13}C\{^{1}H\}$ NMR ($CDCl_3$, 151MHz): δ 164.12, 137.69, 135.13, 128.22, 125.96, 124.22, 120.13, 64.25, 60.13, 56.59, 45.58, 38.72, 37.85, 35.38, 33.77, 31.83, 29.77, 24.45, 24.32, 21.84, 14.04. Anal. Calcd. For $C_{31}H_{48}N_2O_2Zn$: C, 68.18; H, 8.86; N, 5.13. Found: C 68.35; H 8.53; N 5.10.

Synthesis of complex (±)-11. To a solution of complex (±)-**6** (100 mg, 0.172 mmol) in toluene (5 mL) an equimolar amount of benzyl alcohol (0.0170 ml, 0.172 mmol) in toluene (0.5 mL) was added at room temperature. The reaction mixture was stirred for 4 h, and a white solid was precipitated and washed with cold hexanes. The solvent was removed in vacuo to dryness. Yield 78 mg 80%. ^{1}H NMR (600 MHz, $CDCl_3$): 7.47-6.96 (15H, overlapping m, -C(CH_2)Ph and -CH_2-Ph), δ 7.19 (1H, d, $^{4}J_{H\text{-}H}$ = 2.7 Hz, -Ar H), 6.47 (1H, d, $^{4}J_{H\text{-}H}$ = 2.7 Hz, -Ar H), 4.71 (2H, s., -CH_2- of benzyl alkoxide), 4.06 (1H, d, $^{2}J_{H\text{-}H}$ = 11.9 Hz, -HN-CH_2-Ar), 3.18 (1H, d, $^{2}J_{H\text{-}H}$ = 10.3 Hz, -HN-CH_2-Ar), 2.25 – 2.01 (1H, NH), 2.01 – 1.94 (2H, m, -CH- of DACH), 1.75 (3H, s, -N(CH_3)$_2$), 1.65 (6H, s, -ArC(CH_3)$_2$Ph), 1.57 (3H, s, -N(CH_3)$_2$), 1.26 – 0.87 (8H, m, -CH_2- of DACH); ^{13}C{^{1}H} NMR ($CDCl_3$, 151MHz): δ164.24, 152.69, 136.18, 128.34, 127.51, 127.07, 126.76, 124.91, 123.99, 120.15, 68.41, 68.03, 67.20, 49.03, 42.38, 42.01, 31.96, 31.54, 31.19, 30.95, 24.72, 24.45, 21.27. Anal. Calcd. For $C_{80}H_{100}N_4O_4Zn_2$: C, 73.21; H, 7.68; N, 4.27. Found: C 72.15; H 7.61; N 4.25.

Synthesis of complex (*R,R*)-11. To a solution of complex (*R,R*)-**6** (160 mg, 0.276 mmol) in toluene (5 mL) equimolar amount of benzyl alcohol (0.0290 ml, 0.276 mmol) in toluene (0.5 mL) was added at room temperature. The reaction mixture was stirred for 4 h, and a white solid was precipitated and washed with cold hexanes. The solvent was removed in vacuo to dryness. Yield 125 mg 78%. ^{1}H NMR (600 MHz, $CDCl_3$): 7.47-6.95 (15H, overlapping m, -C(CH_2)Ph and -CH_2-Ph), δ 7.05 (1H, d, $^{4}J_{H\text{-}H}$ = 2.7 Hz, -Ar H), 6.50 (1H, d, $^{4}J_{H\text{-}H}$ = 2.7 Hz, -Ar H), 4.75 (2H, br. s., -CH_2- of benzyl alkoxide), 4.05 (1H, d, $^{2}J_{H\text{-}H}$ = 11.9 Hz, -HN-CH_2-Ar), 3.20 (1H, d, $^{2}J_{H\text{-}H}$ = 10.3 Hz, -HN-CH_2-Ar), 2.69 (3H, s, -N(CH_3)$_2$), 2.01 – 1.56 (3H, m, -CH- of DACH), 1.78 (6H, s, -ArC(CH_3)$_2$Ph), 1.76 (6H, s, -ArC(CH_3)$_2$Ph), 1.28 (3H, s, -N(CH_3)$_2$), 1.26 – 0.87 (8H, m, -CH_2- of

DACH); $^{13}C\{^{1}H\}$ NMR ($CDCl_3$, 151MHz): δ 164.31,152.91, 136.71, 136.52, 131.65, 128.3, 127.49, 126.79, 124.87, 124.10, 76.17, 50.53, 48.94, 42.66, 42.01, 32.40, 31.21, 30.96, 29.93, 27.75, 24.68, 24.18, 21.42. Anal. Calcd. For $C_{80}H_{100}N_4O_4Zn_2$: C, 73.21; H, 7.68; N, 4.27. Found: C 70.15; H 7.17; N 4.29.

Synthesis of complex (±)-12. To a solution of complex (±)-**7** (200 mg, 0.376 mmol) in toluene (5 mL) an equimolar amount of benzyl alcohol (0.0380 ml, 0.376 mmol) in toluene (0.5 mL) was added at room temperature. The reaction mixture was stirred for 4 h, and a light yellow solid was precipitated and washed with cold hexanes. The solvent was removed in vacuo to dryness. Yield 136 mg 68%. ^{1}H NMR (600 MHz, CDCl3): 7.85-7.63 (7H, overlapping m, Ar-H), 5.15 (1H, d, -CH_2- of benzyl alkoxide), 4.98 (1H, s, -CH2- of benzyl alkoxide), 4.35 (1H, d, $^{2}J_{H\text{-}H}$ = 10.1 Hz, -HN-CH_2-Ar), 3.39 (1H, d, $^{2}J_{H\text{-}H}$ = 10.3 Hz, -HN-CH_2-Ar), 2.57 (3H, s, -N(CH_3)$_2$), 2.49 (1H, m, DACH), 2.33 (1H, m, NH), 2.31 (3H, m, Ad), 2.24 (3H, m, Ad), 2.07 (3H, s, Ad), 1.98 (1H, m, DACH), 1.86 (3H, s, N(CH_3)$_2$), 1.78 (8H, s, Ad, DACH), 1.22 (9H, s, C(CH_3)$_3$), 0.96 (2H, m, DACH), 0.73 (2H, m, DACH); $^{13}C\{^{1}H\}$ NMR ($CDCl_3$, 151MHz) δ 163.41, 137.92, 129.21, 128.19, 126.11, 123.83, 120.87, 70.59, 68.22, 49.50, 44.98, 40.75, 37.42, 37..27, 34.64, 33.82, 31.77, 29.27, 29.04, 25.26, 24.48, 21.53, 20.68. Anal. Calcd. For $C_{72}H_{104}N_4O_4Zn_2$: C, 70.86; H, 8.59; N, 4.59. Found: C 69.66; H 8.36; N 5.34.

Synthesis of complex (*R,R*)-13. To a solution of complex (*R,R*)-**8** (80 mg, 0.116 mmol) in toluene (5 mL) equimolar amount of benzyl alcohol (0.0120 ml, 0. 0.116 mmol) in toluene (0.5 mL) was added at room temperature. The reaction mixture was stirred for 4 h, and a white solid was precipitated and washed with cold hexanes. The solvent was removed in vacuo to dryness. Yield 65 mg 81%. ^{1}H NMR (600 MHz, $CDCl_3$): δ 8.19 (6H, m, $SiPh_3$), 7.33 (9H, m, $SiPh_3$),8.09-7.02

(7H, overlapping s, Ar-H), 4.73 (1H, d, $^{2}J_{H\text{-}H}$ = 10.6 Hz ,-CH_2- of benzyl alkoxide), 4.43 (1H, d, $^{2}J_{H\text{-}H}$ = 10.6 Hz, -CH_2- of benzyl alkoxide), 4.41 (1H, d, $^{2}J_{H\text{-}H}$ = 11.9 Hz, -HN-CH_2-Ar), 3.35 (1H, d, $^{2}J_{H\text{-}H}$ = 10.3 Hz, -HN-CH_2-Ar), 2.34 (6H, s, -N(CH_3)$_2$), 2.18 (1H, m, -CH- of DACH), 1.98 (1H, d, $^{2}J_{H\text{-}H}$ = 10.3 Hz, -CH- of DACH), 1.66 (1H, s, -CH- of DACH), , 1.63 (3H, s, -Ar-CH_3), 1.31 – 0.45 (8H, m, -CH_2- of DACH); $^{13}C\{^{1}H\}$ NMR ($CDCl_3$, 151MHz) δ 171.79, 139.56, 136.91, 136.74, 134.41, 128.57, 128.20, 127.02, 126.44, 119.81, 67.59, 48.90, 44.82,37.33, 31.58, 30.10, 29.69, 24.71, 21.14, 20.45. Anal. Calcd. For $C_{80}H_{92}N_2O_2Si_2Zn_2$: C, 71.13; H, 6.70; N, 4.05. Found: C 70.90; H 6.71; N 4.16.

Synthesis of complex (±)-14. To a solution of complex (±)-**4** (200 mg, 0.440 mmol) in toluene (5 mL) equimolar amount of pyridin-2-ylmethanol (0.0430 ml, 0. 0.440 mmol) in toluene (0.5 mL) was added at room temperature. The reaction mixture was stirred for 4 h, and a white solid was precipitated and washed with cold hexanes. The solvent was removed in vacuo to dryness. Yield 150 mg 75 %. ^{1}H NMR (600 MHz, CDCl3): δ 8.96 (1H, s, ArH(pyr)), 7.72 (1H, t, $^{3}J_{H\text{-}H}$ = 10.2 Hz, ArH(pyr)), 7.30 (1H, t, $^{3}J_{H\text{-}H}$ = 10.2 Hz, ArH(pyr)), 7.20 (1H, s, Ar *H*), 6.77 (1H, s, Ar *H*), 5.17 (2H, s , -C*H*$_2$- of Zn-CH2-Pyr), 4.57 (1H, d, $^{2}J_{H\text{-}H}$ = 10.1 Hz, -HN-CH_2-Ar), 3.75 (1H, d, $^{2}J_{H\text{-}H}$ = 10.2 Hz, -HN-CH_2-Ar), 2.07 (6H, s, -N(CH_3)$_2$), 1.84-1.76 (3H, m, -C*H2*- of DACH and -NH-), 1.52 (9H, s, Ar-C(C*H*$_3$)$_3$), 1.28 (9H, s, Ar-C(C*H*$_3$)$_3$), 1.26 (2H, m, -C*H*$_2$- of DACH), 1.22 (2H, m, , -C*H*$_2$- of DACH), 1.19 (2H, m, , -C*H*$_2$- of DACH); $^{13}C\{^{1}H\}$ NMR ($CDCl_3$, 151MHz): δ 164.46, 147.28, 137.22, 136.75, 133.38, 128.19, 125.74, 123.31, 121.77, 121.10, 120.83, 67.23, 66.54, 51.97,50.02, 49.90, 44.31, 38.66, 35.32, 33.70, 31.90, 29.89, 29.62, 24.79, 24.69, 21.34. Anal. Calcd. $C_{29}H_{45}N_3O_2Zn$: C, 65.34; H, 8.51; N, 7.88. Found: C 65.79; H 8.48; N 7.67.

Synthesis of complex complex (±)-15. To a solution of complex (±)-**7** (150 mg, 0.282 mmol) in toluene (5 mL) equimolar amount of pyridin-2-ylmethanol (0.0270 ml, 0. 0.282 mmol) in toluene

(0.5 mL) was added at room temperature. The reaction mixture was stirred for 4 h, and a white solid was precipitated and washed with cold hexanes. The solvent was removed in vacuo to dryness. Yield 136 mg 68%. ^{1}H NMR (600 MHz, CDCl3): δ 8.96 (1H, s, ArH(pyr)), 7.72 (1H, t, $^{3}J_{H\text{-}H}$ = 10.2 Hz, ArH(pyr)), 7.30 (1H, t, $^{3}J_{H\text{-}H}$ = 10.2 Hz, ArH(pyr)), 7.20 (1H, s, Ar *H*), 6.77 (1H, s, Ar *H*), 5.17 (2H, s , -C*H*$_2$- of Zn-CH$_2$-Pyr), 4.55 (1H, d, $^{2}J_{H\text{-}H}$ = 10.2 Hz, -HN-CH$_2$-Ar), 3.71 (1H, d, $^{2}J_{H\text{-}H}$ = 10.1 Hz, -HN-CH$_2$-Ar), 2.07 (6H, s, -N(CH$_3$)$_2$), 2.43 (2H, m, -C*H*- of DACH), 2.38 (3H, m, Ad), 2.26 (3H, m, Ad and -NH-), 2.05 (6H, s, N(CH$_3$)$_2$), 2.03 (3H, s, Ad), 1.77 (8H, m, Ad and –CH$_2$- of DACH), 1.24 (2H, m, -CH$_2$- of DACH), 1.07 (2H, m, -CH$_2$- of DACH); ^{13}C{^{1}H} NMR (CDCl$_3$, 151MHz): δ164.83, 147.12, 137.4, 137.23, 133.71, 129.01, 128.19, 125.68, 123.14, 121.70, 121.31, 67.57, 52.01, 51.91, 49.94, 49.82, 44.35, 40.44, 38.39, 37.38, 37.22, 33.76, 31.9, 29.38, 29.2, 24.80, 21.28. Anal. Calcd. For $C_{35}H_{51}N_3O_2Zn$: C, 68.78; H, 8.41; N, 6.88. Found: C 70.45; H 8.07; N 6.35.

Synthesis of complex (±)-16. To a solution of complex (±)-**8** (90 mg, 0.146 mmol) in toluene (5 mL) an equimolar amount of pyridin-2-ylmethanol (0.0140 ml, 0.146 mmol) in toluene (0.5 mL) was added at room temperature. The reaction mixture was stirred for 4 h, and a white solid was precipitated and washed with cold hexanes. The solvent was removed in vacuo to dryness. Yield 65 mg 81%. ^{1}H NMR (600 MHz, CDCl3): δ 7.66 (6H, m, SiPh3), δ 7.53 (1H, s, ArH(pyr)), 7.18 (9H, m, SiPh3), 7.16 (1H, s, Ar *H*), 7.08 (1H, t, $^{3}J_{H\text{-}H}$ = 10.2 Hz, ArH(pyr)), 6.83 (1H, s, Ar *H*), 6.51 (1H, t, $^{3}J_{H\text{-}H}$ = 10.2 Hz, ArH(pyr)), 5.03 (2H, m , -C*H*$_2$- of Zn-CH$_2$-Pyr), 4.66 (1H, d, $^{2}J_{H\text{-}H}$ = 10.1 Hz, -HN-CH$_2$-Ar), 3.82 (1H, d, $^{2}J_{H\text{-}H}$ = 10.1 Hz, -HN-CH$_2$-Ar), 2.51 (2H, m, -C*H*- of DACH), 2.35 (1H, s, -NH-), 2.09 (3H, Ar-CH$_3$), 1.88 (3H, s, N-CH$_3$), 1.76 (2H, m,–CH$_2$- of DACH), 1.43 (3H, s, N-CH$_3$)1.19-1.04 (8H, m, -CH$_2$- of DACH); ^{13}C{^{1}H} NMR (CDCl$_3$, 151MHz): δ 172.21, 148.16, 139.67, 137.35, 136.79, 134.74, 128.34, 126.98, 121.67, 120.30, 119.85, 67.24, 51.73,

49.34, 43.75, 37.83, 30.54, 24.74, 24.43, 21.41, 20.35. Anal. Calcd. For $C_{40}H_{44}N_3O_2SiZn$: C, 69.40; H, 6.41; N, 6.07. Found: C 69.49; H 6.69; N 5.87.

Synthesis of complex (*RR*/*RR*) and (±)- (**17**). A suspension of KOtBu (100 mg, 0.91 mmol) in 2.5 mL of THF was added dropwise to a suspension of $H_2(ON_HN_HO)$ (260 mg, 0.47 mmol) in THF (2.5 mL). After stirring the reaction mixture for 12 h at room temperature, salt formation was observed. The resulting off-white solid ($K_2(ON_HN_HO)$) was isolated by vacuum filtration, and dried under high vacuum for approximately 1 h. The $K_2(ON_HN_HO)$ (100 mg; 0.16 mmol) was further reacted with $InCl_3$ (74 mg; 0.33 mmol) in 5 ml of THF. The mixture was stirred at room temperature for a further 16 h. The mixture was vacuum filtered through a Celite plug to generate "$(ON_HN_HO)InCl$" which was not isolated and used in the subsequent step without further purification. 100 mg (0.14 mmol) of the formed $(ON_HN_HO)InCl$ was dissolved in Toluene and slurry of NaOEt (22mg, 0.33 mmol) was added to the solution and stirred for a few hours until full conversion achieved. After filtration and solvent removal, an off white solid was isolated and dried under high vacuum for 2 hours. Complex **17** was isolated as a white powder without further purification (55%). ^{1}H NMR ($CDCl_3$, 600MHz) δ 7.30 (2H, d, $^4J_{H\text{-}H}$ = 2.2 Hz, Ar *H*), 6.75 (2H, d, Ar *H*), 5.06 (1H, d, $^2J_{H\text{-}H}$ = 11.5 Hz, NH-CH_2-Ar), 4.68 (1H, m, O-C*H*$_2$- of ethoxide), 4.46 (1H, t., $^3J_{H\text{-}H}$ = 7.9 Hz, NH-C*H*$_2$- Ar), 3.73(1H, d., $^2J_{H\text{-}H}$ = 12.7 Hz, -NH-C*H*$_2$-Ar), 3.63 (1H, d, $^2J_{H\text{-}H}$ = 12.7 Hz, -NH-C*H*$_2$-Ar), 3.23 (1H, m, -C*H*- of DACH), 2.65 (1H, m, -NH-), 2.46 (1H, d, -C*H*- of DACH), 2.25 (2H, m, -C*H*- of DACH), 1.84 (2H, br. s., -C*H*$_2$- of DACH), 1.47– 1.21 (2H, m, -C*H*$_2$- of DACH), 1.62 – 1.49 (9H, s, -C*H*$_2$- of DACH and Ar-C(C*H*$_3$)$_3$), 1.27 (21H, s, -C*H*$_2$- of DACH and Ar-C(C*H*$_3$)$_3$), 1.04 (9H, s, Ar-C(C*H*$_3$)$_3$), 1.21 – 1.12 (2H, m, -C*H*$_2$- of DACH), 1.12 – 0.93 (4H, m, -C*H*$_2$- of DACH); ^{13}C{^{1}H NMR ($CDCl_3$, 151MHz) δ162.82, 161.04, 139.85, 138.67, 137.23, 136.38, 129.03, 128.23, 126.62, 124.6, 124.45, 124.17, 122.15, 120.18, 64.28, 57.32, 56.71,

51.7, 49.77, 35.43, 35.14, 33.87, 31.8, 31.70, 30.27, 28.99, 24.98, 24.8, 20.38 Anal. Calcd. For $C_{74}H_{117}ClIn_2N_4O_5$: C 63.1; H 8.38; N 3.98. Found: C 62.12; H 9.10; N 3.85.

Single crystals of (*RR*/*RR*)-**17** suitable for X-ray crystallography where grown from slow evaporation of a saturated solution in Toluene.

Synthesis of complexes (*RR*/*RR*) and (±)-(18). Compound **17** (racemic or enantiopure) was removed from an inert atmosphere and dissolved in wet DCM (~22.4 ppm water) for 48 h to yield the air and moisture stable compound **2** as an off white solid (95%). ^{1}H NMR ($CDCl_3$, 600MHz) δ 7.28 (2H, d, $^4J_{H\text{-}H}$ = 2.2 Hz, Ar *H*), 6.74 (2H, d, Ar *H*), 4.99 (1H, d, $^2J_{H\text{-}H}$ = 11.5 Hz, NH-CH2-Ar), 4.46 (1H, t., $^3J_{H\text{-}H}$ = 7.9 Hz, NH-C*H*$_2$- Ar), 3.74(1H, d., $^2J_{H\text{-}H}$ = 12.7 Hz, -NH-C*H*$_2$-Ar), 3.67 (1H, d, $^2J_{H\text{-}H}$ = 12.7 Hz, -NH-C*H*$_2$-Ar), 3.27 (1H, m, -C*H*- of DACH), 2.77 (1H, m, -NH-), 2.46 (1H, d, -C*H*- of DACH), 2.28 (2H, m, -C*H*- of DACH), 1.80 (2H, br. s., -C*H*$_2$- of DACH), 1.60– 1.21 (2H, m, -C*H*$_2$- of DACH), 1.59 – 1.43 (9H, s, -C*H*$_2$- of DACH and Ar-C(C*H*$_3$)$_3$), 1.25 (21H, s, -C*H*$_2$- of DACH and Ar-C(C*H*$_3$)$_3$), 0.99 (9H, s, Ar-C(C*H*$_3$)$_3$), 1.21 – 1.12 (2H, m, -C*H*$_2$- of DACH), 1.19 – 0.9 (4H, m, -C*H*$_2$- of DACH); ^{13}C{^{1}H NMR ($CDCl_3$, 151MHz) δ162.82, 162.04, 139.83, 139.67, 137.53, 136.75,137.52, 136.38,128.22, 126.67, 124.6, 124.45, 124.57, 122.16, 120.67, 120.18, 57.73, 56.50, 51.7, 51.19, 49.82, 35.42, 35.91, 31.75, 31.70, 29.99, 28.94, 24.93, 24.76, 20.38 Anal. Calcd. For $C_{60}H_{92}Cl_2In_2N_4O_3$: C 58.4; H 7.52; N 4.54. Found: C 58.43; H 7.44; N 4.49.

Single crystals of (*RR*/*RR*)-**18** suitable for X-ray crystallography where grown from slow evaporation of a saturated solution in Toluene.

Synthesis of complex (*RR*/*RR*) (19). A sample of (ON_HN_HO)InCl (100 mg, 0.143 mmol) generated in situ (see above) was dissolved in toluene and a slurry of NaOH (13.16 mg, 1.33 mmol) was added to the solution and stirred for 24 h. After filtration and solvent removal, an off white solid was isolated and dried under high vacuum for 2 h. After washing with hexanes complex **19**

was yielded as a white powder (55%). ^{1}H NMR ($CDCl_3$, 600MHz) δ 7.28 (2H, d, $^{4}J_{H\text{-}H}$ = 2.2 Hz, Ar *H*), 6.74 (2H, d, Ar *H*), 4.99 (1H, d, $^{2}J_{H\text{-}H}$ = 11.5 Hz, NH-CH2-Ar), 4.43 (1H, t., $^{3}J_{H\text{-}H}$ = 7.9 Hz, NH-CH_2- Ar), 3.37(1H, d., $^{2}J_{H\text{-}H}$ = 12.7 Hz, -NH-CH_2-Ar), 3.67 (1H, d, $^{2}J_{H\text{-}H}$ = 12.7 Hz, -NH-CH_2-Ar), 3.23 (1H, m, -C*H*- of DACH), 2.77 (1H, m, -NH-), 2.26 (1H, d, -C*H*- of DACH), 2.25 (2H, m, -C*H*- of DACH), 1.84 (2H, br. s., -CH_2- of DACH), 1.47– 1.21 (2H, m, -CH_2- of DACH), 1.62 – 1.49 (9H, s, -CH_2- of DACH and Ar-C(CH_3)$_3$), 1.27 (21H, s, -CH_2- of DACH and Ar-C(CH_3)$_3$), 1.04 (9H, s, Ar-C(CH_3)$_3$), 1.21 – 1.12 (2H, m, -CH_2- of DACH), 1.12 – 0.93 (4H, m, -CH_2- of DACH); ^{13}C{^{1}H NMR ($CDCl_3$, 151MHz) δ162.82, 161.04, 139.85, 138.67, 137.23, 136.38, 129.03, 128.23, 126.62, 124.6, 124.45, 124.17, 122.15, 120.18, 64.28, 57.32, 56.71, 51.7, 49.77, 35.43, 35.14, 33.87, 31.8, 31.70, 30.27, 28.99, 24.98, 24.8, 20.38 Anal. Calcd. For C,63.52; H, 8.44; N, 4.12; Found: C 63.12; H 8.90; N 3.95.

Single crystals of (*RR*/*RR*)-**19** suitable for X-ray crystallography where grown from slow evaporation of a saturated solution in Toluene.

2.12 Representative polymerization setups

In situ preparation of complex 1 and representative large-scale immortal polymerization of BBL with complex (1) in the presence of BnOH. A 20 ml scintillation vial was charged with 1.34 mL of stock solution of [(NNO$_{tBu}$)InCl]$_2$(μ-Cl)(μ-OEt) in THF (0.0027 M, 0.0037 mmol). A 1.5 ml stock solution of BnOH in THF (0.097 M, 0.146 mmol) was added to the catalyst solution and stirred for 1 h and then dried under vacuum for a few hours to remove resulted ethanol and all the solvent and generate complex **1** as a white powder. The white powder, used without further purification, was dissolved in 2 ml THF and BBL (1.50 mL, 18.3 mmol) was added dropwise to the stirring solution. The reaction mixture was stirred overnight and then quenched with 0.5 ml of

HCl (1.5 M in Et_2O). A sample of the mixture was dissolved in wet $CDCl_3$ to be analyzed by ^1H NMR spectroscopy to determine conversion. The residue was quenched in cold methanol (0 °C), the precipitated polymer was frozen by immersing the vial in liquid nitrogen, and subsequently the supernatant was decanted off. To remove the trace amounts of the catalyst, the last three steps were repeated three times and the isolated polymer was dried under high vacuum overnight prior to analysis.

In situ preparation of complex (2) and representative large-scale immortal polymerization of BBL with 2 in the presence of tris(hydroxymethyl)benzene (THMB). In a 20 ml scintillation vial 1.34 ml stock solution of (**1**) in THF (0.0027 M, 0.0037 mmol) was added. THMB (25 mg) was dissolved in 2 ml of THF (0.072 M, 0.146 mmol) and added to the catalyst solution, stirred for 1 h and then dried under vacuum for a few hours to remove resulted ethanol and all the solvent and generate complex **2** as a white powder. The white powder, used without further purification, was dissolved in 2 ml THF and BBL (1.50 mL, 18.3 mmol) was added dropwise to the stirring solution. The reaction mixture was stirred overnight and then quenched with 0.5 ml of HCl (1.5 M HCl in Et_2O). A sample of the mixture was dissolved in wet $CDCl_3$ to be analyzed by ^1H NMR spectroscopy to determine conversion. The residue was quenched in cold methanol (0 °C) and the precipitated polymer was solidified by immersing the vial in liquid nitrogen and subsequently, the supernatant was decanted off. To remove the trace amounts of the catalyst, the last three steps were repeated three times and the isolated polymer was dried under high vacuum for overnight prior to analysis.

Large-scale immortal polymerization of BBL with complex (3) in the presence of DPET. A solution of DPET (2.0 mg, 0.0078 mmol) in CH_2Cl_2 (0.5 mL) was added to a 20 ml scintillation vial of (NNO_{tBu})Zn(CH_2CH_3) (**3**) (2.0 mg, 0.0044 mmol) and stirred over 30 min at room

temperature just prior to the addition of a solution of BBL (1.00 ml, 11.7 mmol) in CH_2Cl_2 (2 mL). The reaction mixture was then stirred for 16 h at room temperature. A sample of the reaction mixture (*ca.* 0.02 mL) was dissolved in $CDCl_3$ to be analyzed by ^1H NMR spectroscopy to determine conversion. The resulting mixture was concentrated under vacuum and quenched by the addition of cold wet methanol. The polymer precipitated from solution and quickly solidified in liquid N_2. The supernatant was decanted off and the polymer was dried under vacuum. To remove the trace amount of the catalyst, the last three steps were repeated three times and the isolated polymer was dried under high vacuum for overnight prior to analysis.

Large-scale immortal polymerization of BBL with complex (±)-9 in the presence of BnOH. A solution of BnOH (0.24 ml, 2.35 mmol) in CH_2Cl_2 (0.50 mL) was added to a 20 ml scintillation vial which was charged with 0.50 ml of **(±)-6** standard solution in CH_2Cl_2 (0.50 mg, 0.00047 mmol) and stirred over 30 min at room temperature just prior to the addition of a solution of BBL (0.76 ml, 9.20 mmol) in CH_2Cl_2 (2 mL). The reaction mixture was then stirred for 8 h at room temperature. A sample of the reaction mixture was dissolved in $CDCl_3$ to measure the conversion by ^1H NMR spectroscopy. The resulting mixture was concentrated under vacuum and quenched by the addition of cold wet methanol. The polymer precipitated from solution and quickly solidified in liquid N_2. The supernatant was decanted off and the polymer was dried under vacuum. To remove the trace amount of the catalyst, the last three steps were repeated three times and the isolated polymer was dried under high vacuum for overnight prior to analysis.

NMR scale polymerization of BBL with (±)-9. A Teflonsealed NMR tube was charged with a 0.25 mL solution of a catalyst stock solution in (0.25 mL, 0.0022 mmol) and frozen in glovebox using a liquid N2 cold wall (–90 °C). 0.25 mL of pure CD_2Cl_2 was then added and frozen on top of the catalyst layer using the same procedure. A 0.5 mL stock solution of BBL (0.5 mL, 0.88

mmol) in CD_2Cl_2, containing an internal standard 1,3,5-trimethoxybenzene (2.5 mg, 0.02 mmol), was added to the frozen solutions and frozen again to form a trilayer. The NMR tube was sealed and quickly evacuated by vacuum to remove N_2 gas from the NMR tube. Solutions were thawed and quickly mixed before the NMR tube was loaded into the NMR spectrometer (400MHz Avance Bruker Spectrometer). Polymerizations were very quick and exothermic and first scans were recorded at above 40% conversion of monomer. The polymerization was monitored to > 90% conversion.

NMR scale polymerization of *rac*-lactide with (*RR*/*RR*)-17. In a teflon sealed NMR tube, 0.50 mL of **1** in CD_2Cl_2 (0.0048 M, 0.0024 mmol) was added to a solution of *rac*-lactide (66 mg; 0.47 mmol) and an internal standard 1,3,5-trimethoxybenzene (5mg; 0.03mmol,) in 0.48mL of CD_2Cl_2. This mixture was immediately cooled in liquid nitrogen. The NMR tube was warmed to room temperature before it was inserted into the instrument (400 MHz Avance Bruker Spectrometer). The polymerization was monitored to ca. 95% conversion.

Large-scale polymerization of *rac*-lactide using (*RR*/*RR*)-17. Racemic lactide (129.3 mg, 0.92mmol) was dissolved in 6 mL of CD_2Cl_2 in a vial and stirred using a magnetic stir bar. To this solution 1mL of a stock solution of (**17**) in CD_2Cl_2 was added (0.0046 M; 0.0046 mmol). The reaction was allowed to proceed for 16 h and then concentrated to dryness. The resulting polymeric material was dissolved in a minimum amount of CD_2Cl_2 and added to cold wet methanol (0 ºC, 7 mL). The polymer crashed out of solution, and was isolated by centrifugation. The supernatant was decanted off and the polymer was dried under high vacuum for 2 h.

Large-scale immortal polymerization of *rac*-Lactide and *rac*-BBL with (*RR*/*RR*)-17 in the presence of 1,3,5-tris (hydroxymethyl)benzene (THMB). Two parallel reactions were set up in two different 20 ml scintillation vials which were both charged with equal amounts of the reagents

in order to check the conversions before addition of the second monomer. Each of the scintillation vial were first charged with 0.15 ml stock solution of (**17**) in THF (0.007 M, 0.00106 mmol) was added. 0.32 ml of THMB solution in THF (0.044 M, 0.014 mmol) was also added to the catalyst solution, stirred for 2 h and then dried under vacuum for a few hours to remove resulted ethanol and all the solvent. The white powder then was dissolved in 2.5 ml THF and while stirring, a solution of LA in THF (0.32 g, 0.88 M, 2.22 mmol) was added. The mixture was allowed to stir overnight and a ^{1}H NMR spectrum was obtained to determine the monomer conversion and then a solution of the second monomer BBL (0.15 ml, 0.75 M, 1.87 mmol) in THF was added to the reaction. The polymerization was allowed to stir overnight and then quenched with acidic Et_2O (0.5 ml of 1.5 M HCl in Et_2O). A few drops of the mixture were removed to check conversion and the remaining mixture was quenched in cold methanol (0 °C). The precipitated polymer was solidified by immersing the vial in liquid nitrogen. Then, the supernatant was decanted off. The resulting polymer was washed with cold methanol (1 × 3 ml) with the same procedure and then dried under vacuum overnight.

Large-scale block-copolymerization of lactide using (*RR*/*RR*)-18 in Air. Calculated amounts of (*RR*/*RR*) -**18** and THMB were added in to a flask outside the N_2 box followed by addition of L-LA. The reaction started by immersing the flask in oil bath at 130 °C. After specified amount of time (full conversion in 1 h), due to increased viscosity, temperature raised to 155 °C and few drops of Toluene and D-LA was added. The conversion was measured after 2hrs followed by the addition of L-LA to form tri-block copolymers after stirring for another 2 h.

Chapter 3: Synthesis and rheological characterization of star-shaped and linear poly(hydroxybutyrate)

In this chapter monodisperse linear, three-armed and six-armed star-shaped PHBs were prepared using indium and zinc based catalysts. Viscometric results confirmed the presence of symmetric well-defined star PHBs in solution state. Melt rheological behavior of these materials was also compared to investigate the effect of the different PHB architectures on its properties and to understand the relationship between PHBs topologies and its rheological behavior. The shear dependent non-linear rheological behavior of these polymers is also reported along with the modeling that resulted from the K-BKZ Wagner constitutive equation.

3.1 Introduction

Recent advances in biodegradable polymer synthesis, such as poly (lactic acid) (PLA) and poly(hydroxyalkanoates) (PHAs), have focused on the custom design and synthesis of polymers with tailored properties for use in biomedical applications.[181,220-222] In particular, poly(β-hydroxybutyrate) (PHB), generated through ring opening polymerization of β-butyrolactone (BBL), is an important biocompatible polymer that has not been studied to the same extent as other polyesters such as PLA.[223-225] Despite its high ring strain,[226] rapid and highly controlled polymerization of BBL to produce high molecular weight PHB is rare due to the low activity of most catalysts towards β-lactones, and the high prevalence of chain termination events with this monomer.[9,30,74-76,126,134,142,147,148,227,228] These side reactions limit the possibilities for expanding PHB polymer architecture through forming branch points or block copolymers.[229 230]

Immortal ring opening polymerization of lactide (LA) in the presence of linear or branched chain transfer agents such as alcohols is a promising route towards reducing metal and ligand contamination and has produced an array of end-functionalized polymers with various architectures.[181,220,231,232] In particular, star-shaped PLAs, which can be synthesized through immortal polymerization with multidentate alcohols, have smaller hydrodynamic radii, lower viscosities, and higher functional group concentration than their linear counterparts and have found applications in drug delivery among other fields.[21] In contrast, immortal polymerization of BBL is difficult due to a paucity of compatible catalytic systems.[10,107,125,149,150] Reports of star-shaped PHB are rare.[233-235]

We have reported that dinuclear indium complex, [(NNOtBu)InCl]2(μ -Cl)(μ-OEt) (**D**),[236] is a highly active and controlled catalyst for the living polymerization of LA and is capable of immortal ring opening polymerization of BBL in the presence of up to 100 equivalents of added alcohol such as ethanol and monomethylated poly(ethylene glycol).[112] In addition to unprecedented stability in the presence of alcohols and the high rate of reactivity with BBL, catalyst D is also able to form PLA-PHB-PLA triblock polymers through simple sequential addition.[114] Our work in this area has shown that the dinuclear nature of (**D**) is essential in controlling polymer micro- and macrostructure in lactide polymerization.[162-165,237,238]

Here in this chapter, the first example of a one-component precursor to star-shaped polyesters, $[(NNO_{tBu})InCl]_2(\mu\text{-Cl})(\mu\text{-OTHMB})$ (**2**) ([OTHMB] = 3,5-bis(hydroxymethyl)phenyl)methoxide), and its utilization in the synthesis of previously unknown 3-armed star-shaped PHB and PLLA-PHB block copolymers will be reported. We have reported zinc complexes with the same ligand

framework[218] and have expanded work to imine analogues (±) (NN_iO_{tBu})ZnEt (**3**). This complex will be used for the formation of 6-armed star PHBs in the presence of hexols.

3.2 Results and discussion

3.2.1 Preparation of active indium and zinc based catalysts for the polymerization of BBL

Dinuclear indium complex $[(NNO_{tBu})InCl]_2(\mu\text{-}Cl)(\mu\text{-}OEt)$ (**D**) is prepared according to the literature procedures.[162-165,236] Reaction of (**D**) with excess benzyl alcohol in THF for 1 hour followed by the removal of solvent and unreacted benzyl alcohol affords formation of benzyl alkoxy bridged complex (**1**) ($[(NNO_{tBu})InCl]_2(\mu\text{-}Cl)(\mu\text{-}OBn)$) (Figure A1-2) (Scheme1). Likewise, the reaction of excess 1,3,5-tris(hydroxymethyl)benzene (THMB) with complex **D** in THF at room temperature or in the presence of 1 equivalents of THMB in toluene at 70 °C, forms an OTHMB-bridged complex, $[(NNO_{tBu})InCl](\mu\text{-}Cl)(\mu\text{-}OTHMB)$ **2** (Scheme 1). The solution structure of (**2**) is also confirmed by proton and carbon NMR spectroscopies (Figure A3-4). The ^1H NMR spectrum ($CDCl_3$, 25 °C) of complex **2** shows two AB doublets at 5.08 and 5.80 ppm belonging to the In-O-CH_2-$C_6H_3(CH_2OH)_2$ protons immediately coordinated to the indium centers and two AB doublets at 4.26 and 4.40 ppm assigned to the distal In-O-CH_2-$C_6H_3(CH_2OH)_2$ protons. The presence of excess THMB does not form a bis-alkoxy bridged complex and there is no evidence of THMB bridged between multiple indium centers. Crystals of complex **2** suitable for single crystal X-ray structural determination can be obtained from a toluene solution at room temperature. Complex **2** is dinuclear with two octahedral indium centers asymmetrically bridged by chloride and (3,5-bis(hydroxymethyl)phenyl)methoxide, -OTHMB, ligands (Figure A5). The bond lengths and angles for homochiral (*SS*/*SS*)-**5** are similar to those for previously reported asymmetrically-

bridged homochiral dimers in the series.[162-165,237,238] Ethyl zinc complex (**3**) (±) (NN_iO_{tBu})ZnEt was prepared according to our previously reported procedure through ethane elimination of diethyl zinc ($ZnEt_2$) in the presence of proligand in diethylether for 1 hour (Scheme 1).[239]

Scheme 1. Synthesis of complexes **1-3**

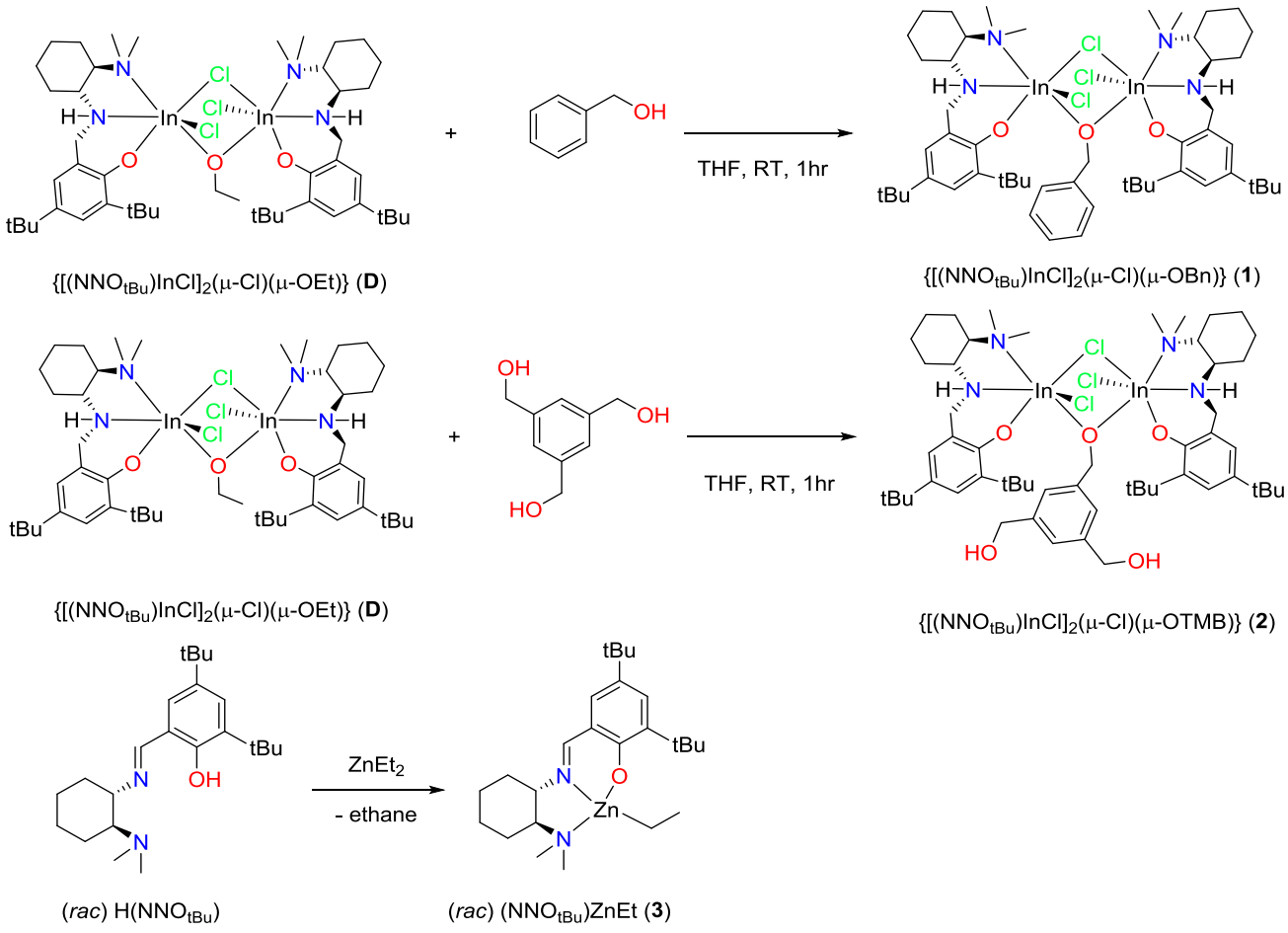

3.2.2 Immortal ROP of BBL with complexes 1 and 2 in the presence of BnOH and THMB

Catalysts **1** and **2** can be used to polymerize up to 20000 equivalents of BBL in the presence of high loadings of BnOH and THMB to form linear and star shaped poly(hydroxybutyrate) (Table 3.1). The resulting polymers show narrow dispersities ($Đ$ = 1.01-1.08) with good agreement between calculated and experimental molecular weights (Figure 3.1 (a), (b)). In particular, this system forms highly controlled star-shaped polymers in the presence of a wide range of monomers: a THMB:**2** ratio of 590 can be used to generate well-controlled star-shaped oligomers (Table 3.1, entry 9), while with a ratio of 4:1 star shaped polymers with molecular weights as high as 220 $kgmol^{-1}$ can be obtained. All PHBs generated with the indium catalysts are atactic.[112]

Table 3.1. Polymerization of BBL in the presence of BnOH and THMB.

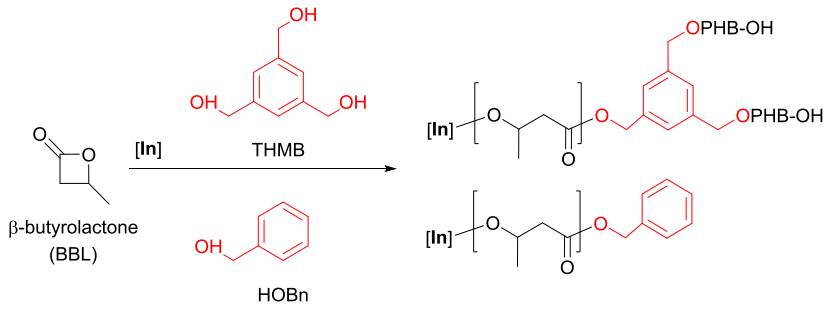

	ROH	[M]:[ROH]:[I]	Conv.[a] (%)	$M_{n,theo}$[b] gmol^{-1}	$M_{n,GPC}$[c] gmol^{-1}	$M_{w,GPC}$[c] gmol^{-1}	$Đ$[c]	Tg °C
1	BnOH	5000/190/1	>99	2433	2370[d]	-	-	-
2	BnOH	5000/40/1	>98	10714	12320	12800	1.04	-
3	BnOH	5000/20/1	>98	21260	22560	23010	1.02	-
4	BnOH	5000/10/1	>98	42352	48090	49050	1.02	0.5
5	BnOH	5000/5/1	>99	83258	89100	91770	1.03	1.1
6	BnOH	5000/2.7/1	>98	156342	121360	143200	1.17	2.3
7	BnOH	5000/1.66/1	>99	256823	157380	162100	1.03	1.5
8	BnOH	5000/1.25/1	>99	341024	222790	225020	1.03	2.1
9	THMB	7400/590/1	>87	1107	1250[d]	-	-	-
10	THMB	5000/300/1	>97	1560	1695[d]	-	-	-
11[e]	THMB	5000/40/1	>99	10822	9820	10507	1.07	-
12[e]	THMB	5000/20/1	96	20830	23200	23660	1.02	-
13	THMB	5000/10/1	95	41061	44490	44930	1.01	0.5
14	THMB	5000/5/1	>99	85397	77200	83380	1.08	1.0
15	THMB	5000/4/1	>99	106704	111010	116020	1.04	1.5
16	THMB	10000/4/1	>96	206782	138030	146280	1.06	0.5
17	THMB	20000/4/1	>90	387573	219600	223300	1.02	1.5

For entries 1-8, initiator [I] is **1**, for entries 9-17 [I] is **2**. [a] Monomer conversion, determined by ^{1}H NMR spectroscopy. [b] Calculated from ($[BBL]_o/([ROH]/[I])$ × monomer conversion × M_{BBL}) + M_{ROH} (M_{BBL} = 86.09 gmol^{-1}, M_{BnOH} = 108.14 gmol^{-1}, M_{THMB} = 168.19 gmol^{-1}).[c], determined by GPC-LLS using dn/dc = 0.068 for PHB in THF, $Đ$ = Dispersity index. [d] ^{1}H NMR molecular weight. [e] Reference ([113]).

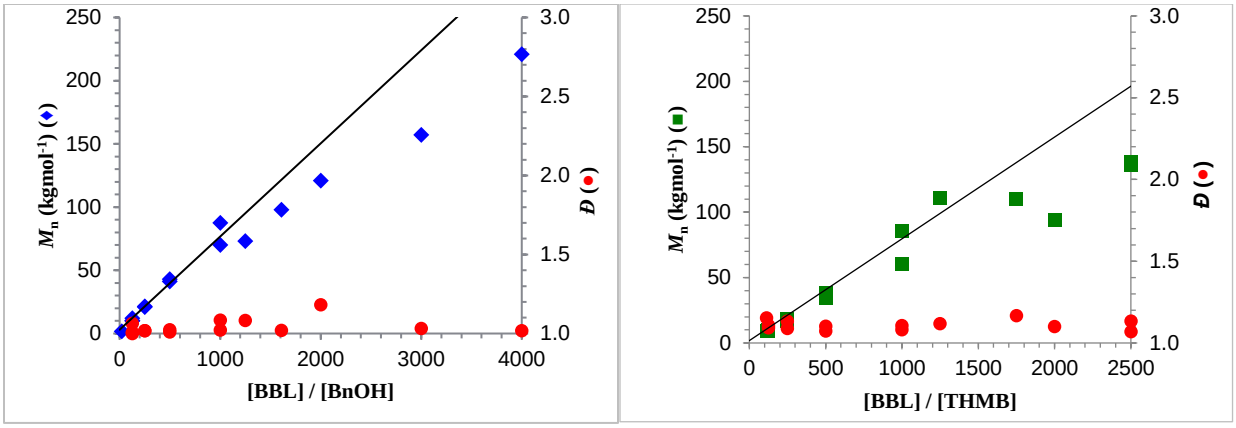

Figure 3.1 a) Plots of observed PHB M_n and dispersity (●) as functions [BBL]:[initiator] for a) left, (♦) BnOH + catalyst **1** and **b)** right, (■) THMB + catalyst 2. The line indicates calculated M_n values based on the BBL:initiator ratio. All reactions were carried out at room temperature in THF and polymer samples were obtained at >98% conversion.

Figure 3.2(a) shows the ^{1}H NMR spectrum of the oligomers obtained from the polymerization of [BBL]/[THMB]/[**2**] 7400:590:1, which was quenched at 87% conversion and the unreacted monomer removed *in vacuo*. The spectrum shows diagnostic chain end PHB(CH_3)-C*H*-OH methine protons at 4.2 ppm (peak g) and the core aryl protons at 7.3 ppm (peak a), which confirms the presence of THMB as the polymer core. The integral ratio of the PHB methine protons (peaks e+g) to peak a is ~ 4. This value corresponds to the expected number of repeat units per arm of the star (7400/590*0.87/3 = 3.63). These results are also confirmed by the MALDI-TOF mass spectrum (Figure 3.2(b)).

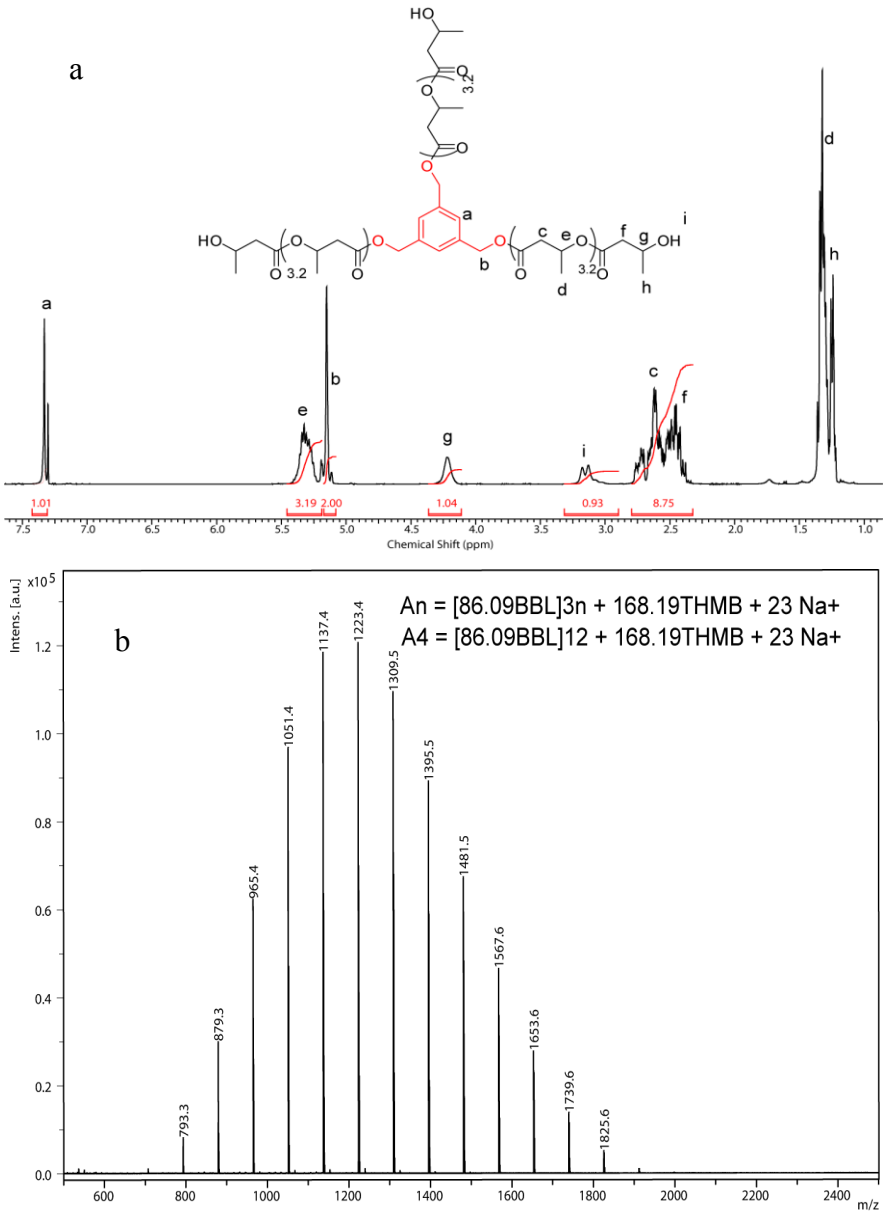

Figure 3.2 (a) ^{1}H NMR spectrum ($CDCl_3$, 25 °C) and **(b)** MALDI-TOF spectrum of 3-arm star PHB isolated from polymerization of [BBL]:[THMB]:[**2**] ratios of 7400:590:1 (Table 3.1, entry 9). Reaction stopped after 87% conversion and the monomer left overs where removed under high vacuum overnight.

A unique ability of this system is the immortal block-copolymerization of BBL and LA, regardless of the sequence of addition. Sequential addition of BBL followed by L-LA, or vice versa, to catalyst **2** (prepared in situ with complex (**D**) and 5 equiv THMB) forms star block copolymers PHB-PLLA or PLLA-PHB, respectively (Table 3.2). For example, the first addition

of 625 equiv BBL yields 3-arm star PHB homopolymer with M_n value (46 kgmol^{-1}) close to the calculated value (53 kgmol^{-1}) (Figure 3.3. (a) dashed line). Monomer conversion can be determined by ^{1}H NMR spectroscopy. Next, the addition of 373 equiv L-LA to the reaction mixture containing the 3-arm star PHB forms 3-arm star copolymer PHB-PLLA with M_n corresponding to 625 BBL and 373 L-LA enchained units (Figure 3.3. (a) solid line). Reversing the order of addition also yields a star-shaped block copolymer (Figure 3.3. (b)). This acceptable agreement between experimental and theoretical molecular weights of the resulting block copolymers, along with very narrow molecular weight distributions, implies that no matter the monomer addition sequence, there is good control in block copolymerization of BBL and LA.

Table 3.2. Block copolymerization of BBL and L-LA using *in-situ* formed complex **2** in the presence of THMB as chain transfer agent in THF at room temperature.

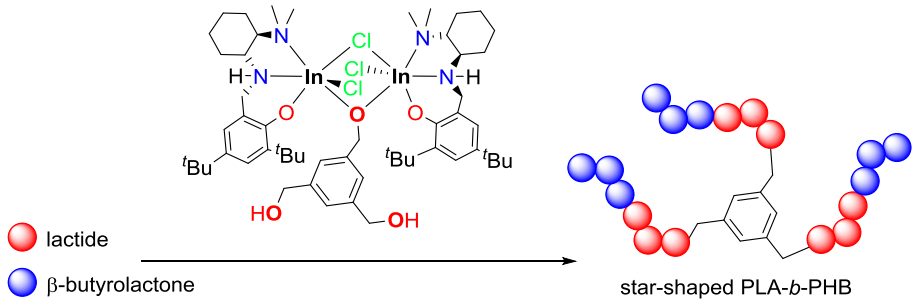

	M1(M2)	ROH	[M1+M2]: [ROH]:[I]	$M_{n,theo}$[c]/ gmol^{-1}	$M_{n,GPC}$[d] gmol^{-1}	$Đ$[d]
1[a,e]	BBL (L-LA)	THMB	3125 + 1865/5/1	103433	103000	1.01
2[b,e]	L-LA (BBL)	THMB	1865 + 3125/5/1	98052	96277	1.01

Unless otherwise state, all reaction carried out in THF at 25 °C over 16h to >95% conversion. [a]Order of monomer BBL followed by L-LA, conversion BBL:L-LA 99 : 93. [b]Order of monomer L-LA followed by BBL, conversion L-LA:BBL 96 : 86. Monomer conversion determined by 1H NMR spectroscopy. [c] Calculated from ($[M1]_o$/([ROH]/[I]) × monomer conversion × M_{M1}) + ($[M_2]_o$/([ROH]/[I]) × monomer conversion × M_{M2}) + M_{ROH} (M_{BBL} = 86.09 gmol^{-1}, $M_{L\text{-}LA}$ = 144.13 gmol^{-1}, M_{BnOH} = 108.14 gmol^{-1}, M_{THMB} = 168.19 gmol^{-1}). [d] Determined by GPC-MALS in THF using dn/dc = 0.068 for PHB. [e] Block copolymers

are not soluble in THF so $CHCl_3$ is used as the GPC solvent (dn/dc = 0.034 for PHB and dn/dc = 0.029 for PLLA).

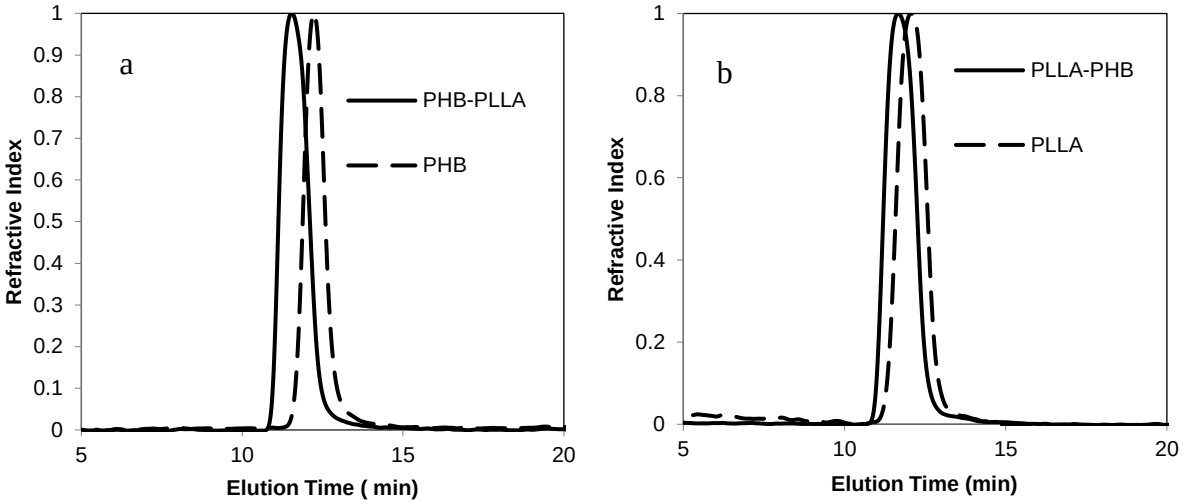

Figure 3.3 Overlaid GPC traces of 3 arm star block copolymers produced by consecutive additions of **(a)** 625 equiv. of [BBL]:[THMB] and 373 equiv. of [L-LA]:[THMB] and **(b)** 373 equiv. of [L-LA]:[THMB] and 625 equiv. of [BBL]:[THMB] (bottom) with complex **2** in THF at 25 °C. (a) 1st addition, dashed line (M_n = 49 kgmol^{-1}, $Đ$ =1.01) for BBL; 2nd addition, solid line (M_n = 103 kgmol^{-1}, $Đ$ = 1.01) for PHB-*b*-PLLA (Table 3.2. entry 1). (b) right, 1st addition, dashed line (M_n = 43 kgmol^{-1}, $Đ$ =1.01) for L-LA; 2nd addition, solid line (M_n = 96 kgmol^{-1}, $Đ$ =1.01 for PLLA-PHB (Table 3.2. entry 2).

3.2.3 Immortal ROP of BBL with complex 3 in the presence of dipentaerythritol (DPET)

In order to synthesize multi-branched star PHBs, dipentaerythritol (DPET) can be used as the chain transfer agent.[190] However, attempts to prepare star polymers with indium catalysts were unsuccessful; attempts to generate macroinitiators through reacting $[(NNO_{tBu})InCl]_2(\mu\text{-Cl})(\mu\text{-OEt})$, with DPET prior to monomer addition failed due to insolubility of DPET in various organic solvents. Polymerization of BBL in the presence of DPET and complex (**D**) at room temperature formed a mixture of linear and star shaped polymers, indicating that the rate of propagation is higher than alcoholysis under these reaction conditions. Reactions at higher temperatures in the

presence of catalysts are not controlled. Indeed, the reaction of DPET and neat BBL at 120 °C without added catalyst, results in uncontrolled BBL oligomerization with broad molecular weight distribution, with a side reaction that forms crotonate end groups (Figure A.10).

Alternatively, we can use zinc alkyl complex **3**, which itself is not a reactive initiator for BBL polymerization in the absence of a nucleophile, to generate high molecular weight star PHBs (Table 3.3). Ring opening polymerization of BBL with **3** and DPET forms moderately syndiotactic PHB with P_r values ranging around 0.55 to 0.62. DSC thermograms of this set of polymers show a broad melting range from 50 °C to 62 °C with low melting enthalpies of 2.3 to 3.5 J/g, which shows that the samples are mainly amorphous (Figure A.12). The dispersities of the resulting polymers are ~1.2 and as the monomer to catalyst ratio increases, the molecular weight does not increase proportionally due to transesterification reactions; the maximum accessible molecular weight using this catalytic system is ~100 $kgmol^{-1}$ (Table 3.3 and Figure 3.4).[107]

Table 3.3. Polymerization of high equivalents of BBL by complex 2 in the presence of DPET.

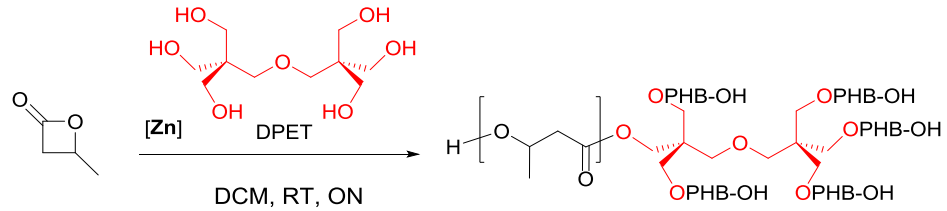

Entry	[M]:[ROH]:[I]	Conv.[a] (%)	$M_{n,theo}$[b] gmol^{-1}	$M_{n,GPC}$[c] gmol^{-1}	$M_{w,GPC}$[c] gmol^{-1}	$Đ$[c]	P_r[e]	T_g (°C)	T_m (°C)
1	294/1/1	98	25538	26120 (25796[d])	27950	1.07	0.54	-[g]	-[g]
2	670/1/1	89	51589	43190	51390	1.20	0.55	1.2	-[g]
3	822/1/1	88	60358	48200	61700	1.30	0.54	1.5	48.2
4	940/1/1	90	70086	67840	76660	1.13	0.58	0.8	52.1
5	1200/1/1	86	89099	79200	82360	1.04	0.60	0.2	50.9[f]
6	1300/1/1	85	95383	85860	96160	1.12	0.55	2.0	49.3[f]
7	2050/1/1	80	141441	101300	115900	1.14	0.62	2.5	62.3[f]

All reactions were carried out at room temperature in CH_2Cl_2. ROH = DPET, I = complex **3**. [a] Monomer conversion, determined by ^{1}H NMR spectroscopy. [b] Calculated from ([BBL]$_o$/([ROH]/[I]) × monomer conversion × M_{BBL}) + M_{ROH} (M_{BBL} = 86.09 gmol^{-1}, M_{DPET} = 254.28 gmol^{-1}).[c] Determined by GPC-LLS using dn/dc = 0.060 for 6armed star PHBs in THF. [d] ^{1}H NMR molecular weight. [e] P_r is the probability of racemic linkages between monomer units and is determined by methane region of invers gated ^{13}C{^{1}H} NMR spectra. [f] DSC thermograms are presented in Figure A.12. [g] Not determined.

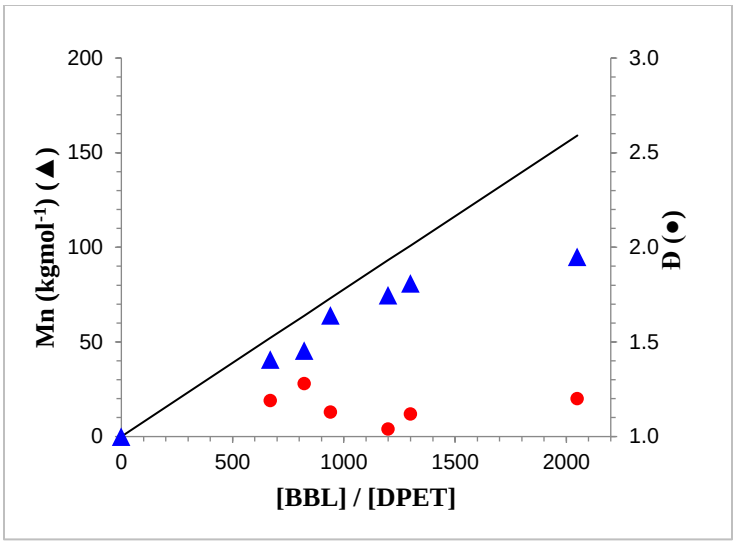

Figure 3.4 Plots of observed PHB M_n (▲) and dispersity (•) as functions [BBL]:[DPET] for catalyst **3**. The line indicates calculated M_n values based on the (BBL:initiator ratio)x90%conversion. All reactions were carried out at room temperature in CH_2Cl_2 and polymer samples were obtained at >85% conversion.

Chain end analysis of a representative sample (BBL/DPET/**3** : 294/1/1) using ^{1}H NMR spectroscopy reveals the absence of DPET alcohol resonances at 0.44 and 3.59 ppm and the presence of a broad resonance at 4.14 ppm corresponding to the polyol core, which confirms activation of all six alcohol functionalities for each catalyst (Figure 3.5). The presence of the DPET core is also confirmed by MALDI-TOF (Figure 3.6) and ^{13}C DEPT results (Figure A.11).

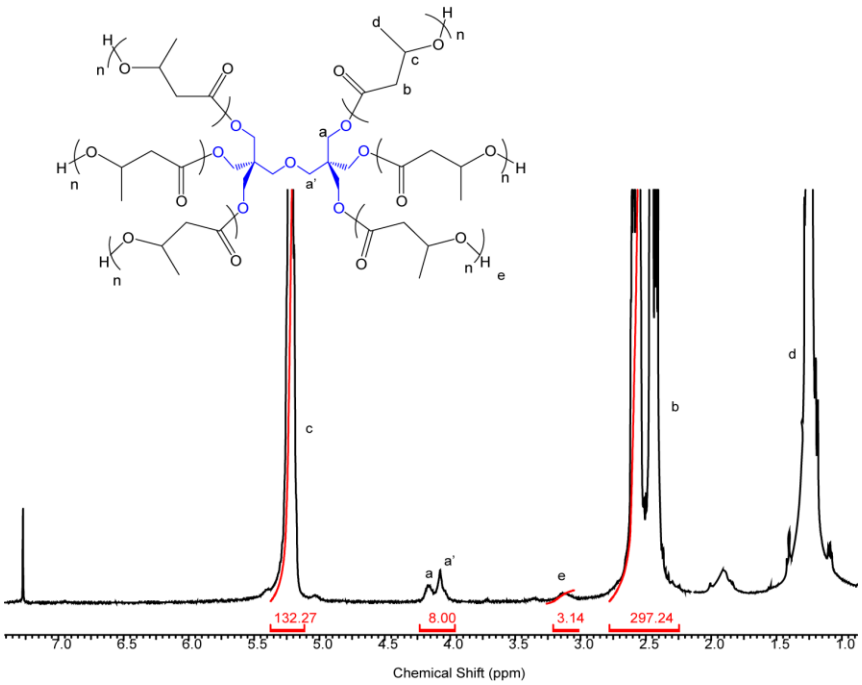

Figure 3.5 ^{1}H NMR ($CDCl_3$, 25 °C) spectrum of the isolated star PHB [BBL]:[DPET]:[**3**] ratios of 294:1:1(Table 3.3, entry 1).

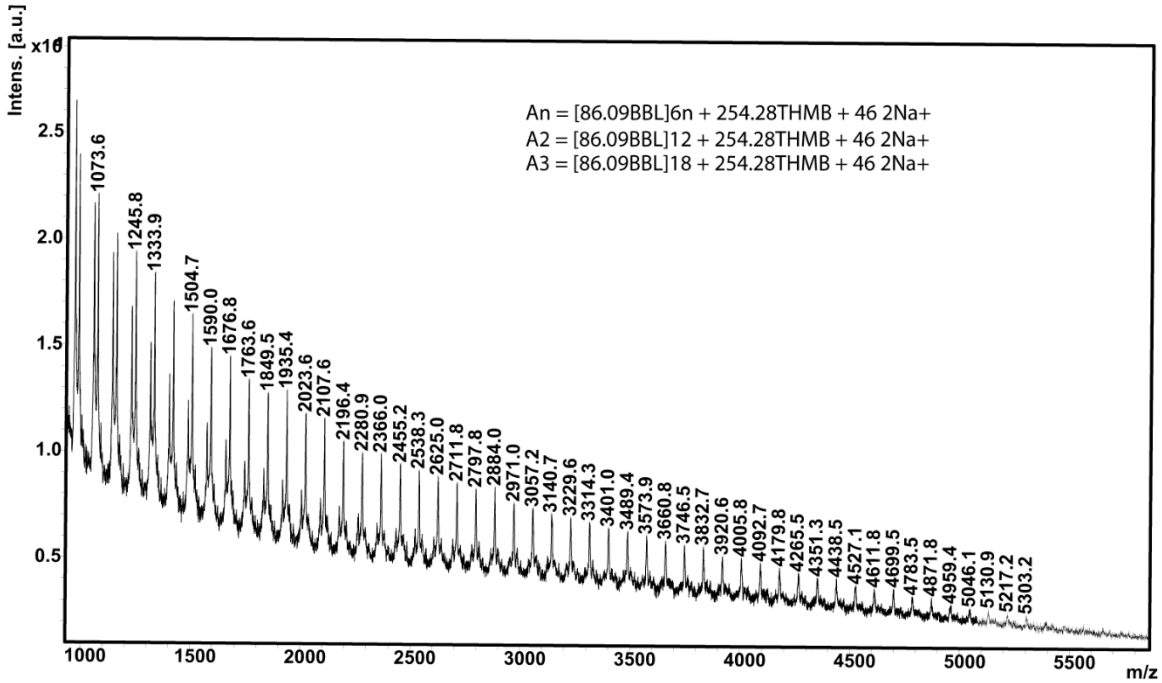

Figure 3.6 MALDI-TOF spectrum the isolated star PHB [BBL]:[DPET]:[**3**] ratios of 294:1:1(Table 3.3, entry 1).

3.2.4 Solution Viscometery

Star-shaped PHB homopolymers, and their rheology, are unexplored. We studied the solution and melt rheological properties of the synthesized polymers to characterize their topology and bulk properties.

Plots of molecular weight dependence of intrinsic viscosities of linear and star-shaped PHBs are shown in Figure 3.7. These values are consistent with the results obtained from Cannon-Fenske viscometer in THF (Figure A.16 (a-d)). It is apparent that at a given molecular weight, [η] decreases for both sets of star polymers, and more significantly for 6-armed star PHBs compared to their linear counterparts. Using the power law Mark-Houwink equation, the following values of the parameters were determined for the three classes of PHB polymers : $[\eta]_{linear} = 0.019\, M_{w,LS}^{0.74}$, $[\eta]_{3armed-star} = 0.013\, M_{w,LS}^{0.76}$, $[\eta]_{6armed-star} = 0.008\, M_{w,LS}^{0.79}$. The Mark Houwink exponent is between 0.74 and 0.79. This exponent is 0.5 in poor solvent, such as Hexanes and 0.8 in good solvent, such as THF, conditions. These results show that THF is a good solvent for linear and branched PHBs and the polymers possess random coil conformation in this solvent.

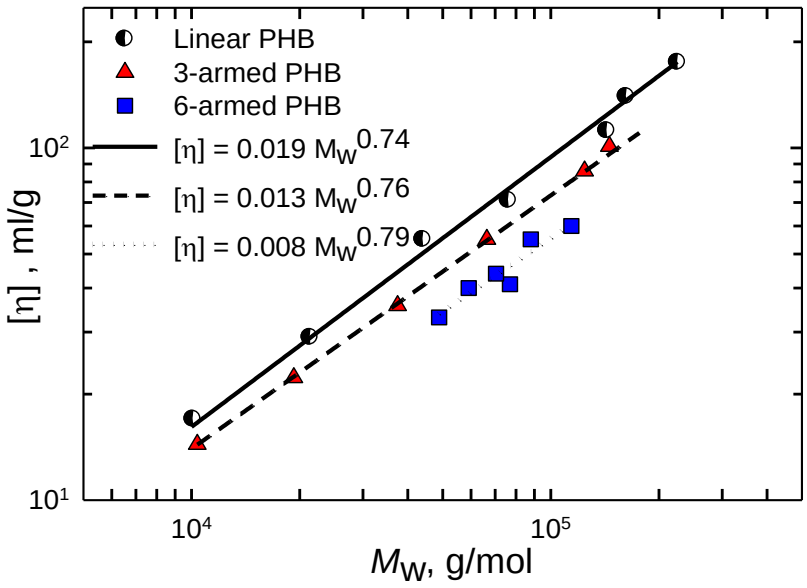

Figure 3.7 The intrinsic viscosities of PHBs of different architecture versus weight average molecular weight (M_w) at 25 °C . The slope of the straight lines (Mark-Houwink exponents) are 0.74 for linear, 0.76 for 3-armed, and 0.79 for 6-armed samples implying good-solvent conditions.

The measured values of the hydrodynamic radii, R_h, the radius of gyration, R_g, and their ratio (R_g/R_h) are depicted in Figure 3.8 and Figures 3.9 (a) and (b) for the linear, 3-armed and 6-armed star series as a function of M_W. The power-low relationship of R_h and R_g with M_w of the samples indicated that the molecules are highly self-similar. The compactness factor, R_g/R_h, is 0.78 for a hard sphere, while for a linear polymer chain the value is 1.86. For self-similar structures, the ratio is constant and as the ratio of R_g/R_h decreases, the intramolecular crowding increases, which indicates enhanced packing of segments within a molecule. For the present materials, the range is very narrow (1.78 <R_g/R_h< 2) for linear PHBs (Figures 3.8), thereby implying that the molecules are monodispersed; this ratio is 1.35 <Rg/Rh< 1.4 for the 3-armed-PHBs and 1.2 <Rg/Rh< 1.25 for the 6-armed samples. The constant values of the compactness factor and the fact that increasing

the branching number reduces the R_g/R_h demonstrates that the branching is structurally well-defined, regular, and compact for both sets of star polymers (Figures 3.9 (a), (b)).

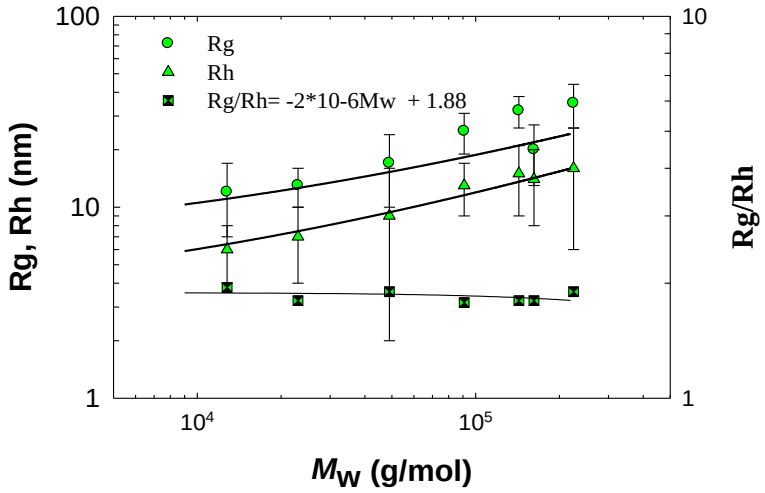

Figure 3.8 Measured radii of gyrations, hydrodynamic radii and R_g/R_h vs. weight-averaged molecular weight in a series of linear PHBs.

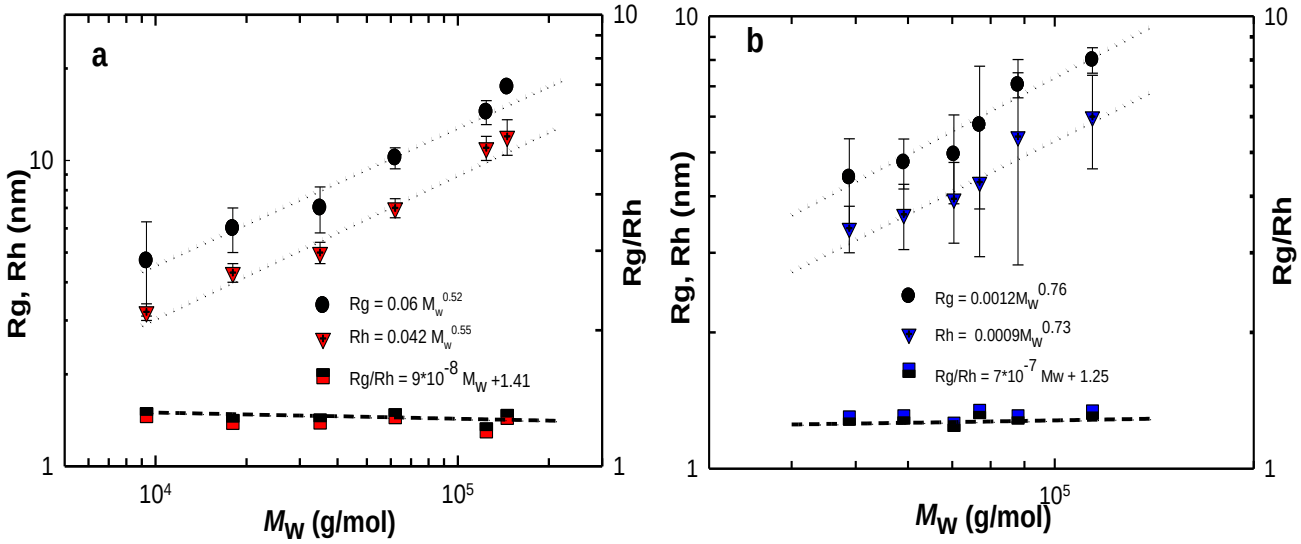

Figure 3.9 Measured radii of gyrations and hydrodynamic radii vs. weight-averaged molecular weight in a series of **(a)** 3-armed and **(b)** 6-armed star polymers. Errors reported are based on multiple measurements made with different batches of solutions.

3.2.5 Melt viscoelastic properties

3.2.5.1 Dynamic frequency sweep tests

Figure 3.10 shows representative master curves of the viscoelastic moduli of linear, 3-armed, and 6-armed star polymers of high molecular weights. The master curves were obtained by superposing the isothermal linear frequency sweep test results of the polymers measured from 25 °C to 70 °C. The various curves were shifted by means of applying the time-temperature superposition (tTS) principle in order to generate the master curves at the reference temperature of T_{ref} = 50 °C. In order to produce smooth master curves, both horizontal a_T and vertical shift factors b_T, which were close to 1, were used. a_T values versus temperature obey the Arrhenius equation, $a_T = exp[-E_a/R(\frac{1}{T} - \frac{1}{T_r})]$, where E_a is the activation energy of flow, R is the universal gas constant, and T_r is the reference temperature. Straight line fitting of the data results in an average activation energy of 129.1 kJ/mol for the linear, 135.8 kJ/mol for the 3-armed, and 155.4 kJ/mol for 6-armed star PHBs, respectively. Increased flow activation energies of the star polymers indicates the influence of the presence of branches on the viscoelastic properties of the polymers. Also using the WLF equation, $log(a_T) = -C_1(T - T_r)/(C_2 + T - T_r)$, the following parameters were obtained: C_1= 7.2 K^{-1}, C_2 = 110.1 K for linear polymer and 6.7 K^{-1}, 103.1 K for 3-armed and 7.5 K^{-1} and 100.8 K, for 6-armed samples (Figure 3.11).

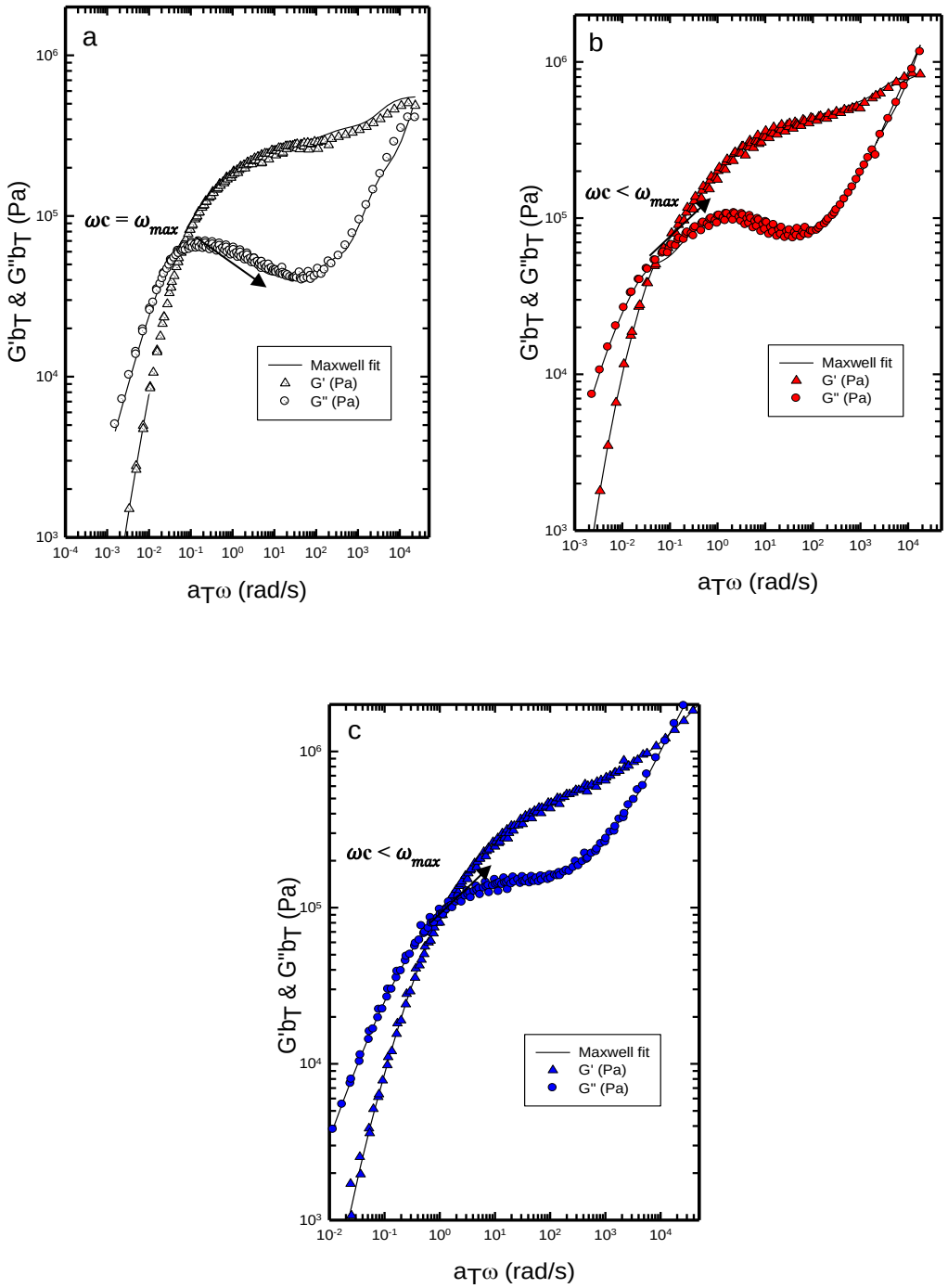

Figure 3.10 Master curves of the dynamic moduli G' and G″ as a function of angular frequency ω for the PHB melts at 50 °C **(a)** entry 7 in Table 3.1 (Linear PHB, M_w = 162 kgmol^{-1}, $Đ$ = 1.03), **(b)** entry 16 in Table 3.1 (3-armed star PHB, M_w = 146 kgmol^{-1}, $Đ$ = 1.06), **(c)** entry 7 in Table 3.3 (6-armed star PHB, M_w = 115 kgmol^{-1}, $Đ$ = 1.14). Continuous lines represent the fitting of the parsimonious relaxation spectrum (Equations A.1 and A.2, Figure A.14 (a-c)). (Molecular weight dependence of G' and G″ of linear, 3-armed, and 6-armed stars are presented in Figure A.13 (a-f)).

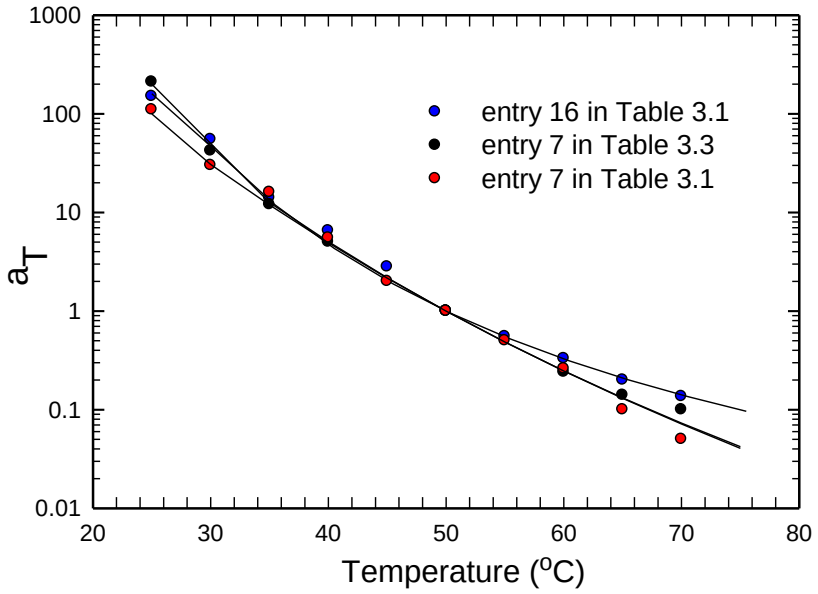

Figure 3.11 Horizontal time-Temperature superposition shift factors and the WLF fit as a function of temperature.

Applicability of the tTS principle and the WLF equation indicated that the samples in the measuring temperature window are all thermorheologically simple fluids. Similar plots to those depicted in Figure 3.10 were also prepared for a range of molecular weights of the linear and star polymers (Figure A.13). All the curves converged at very high frequencies in the transition to the glassy zone. The rubbery region was also clearly observed within the intermediate frequency zone, which is an indicator of the monodispersity of the polymers. Finally, the terminal zone was reached at very low frequencies, where the characteristic slopes G' $\propto \omega^2$ and G"$\propto \omega$ were obtained.

Comparing the LVE plots of Figure 3.10, it is apparent that the frequency dependence of the elastic and loss moduli of linear and star PHBs are different. In the case of linear PHBs, the crossover frequency, ω_c, ($G'=G''$) in the terminal region, coincides with ω_{max}, revealing an isolated band of relaxation times of a narrow molecular weight distributed polymer. Meanwhile

for the star PHB samples, the ω_c values are lower than the corresponding ω_{max}. This is due to the presence of a different relaxation mechanism, the "arm retraction (breathing mode)" relaxation, significantly different from the reptation mechanism of linear polymers.[178] Although the shape of G'' of entry 16 of Table 3.1 (Figure 3.10 (b)) follows the characteristic fingerprint of the breathing mode relaxation of the star branched polymers, the G''_{max} of the 6-armed polymers (Figure 3.10 (c)), is not as significant as that of the 3-armed polymer, which can be assigned to their lower entanglement density. Entanglement molecular weight of the polymers can be estimated from $M_e = \rho_0 RT/G_N^0$, where ρ_0 is the density, R is the gas constant, T is the measurement temperature, and G_N^0 is the plateau modulus.

In order to estimate the plateau modulus, Van-Gurp Palman plots (Loss-angle(δ) Vs. Complex modulus $|G^*|$) were used[240] (Figure 3.12). The obtained G_N^0 for linear, 3-armed, and six-armed star samples are 0.5 MPa, 0.45 MPa, and 0.55 MPa, which are in agreement with the results obtained from the Parsimonious relaxation spectrum (Figure A.14).

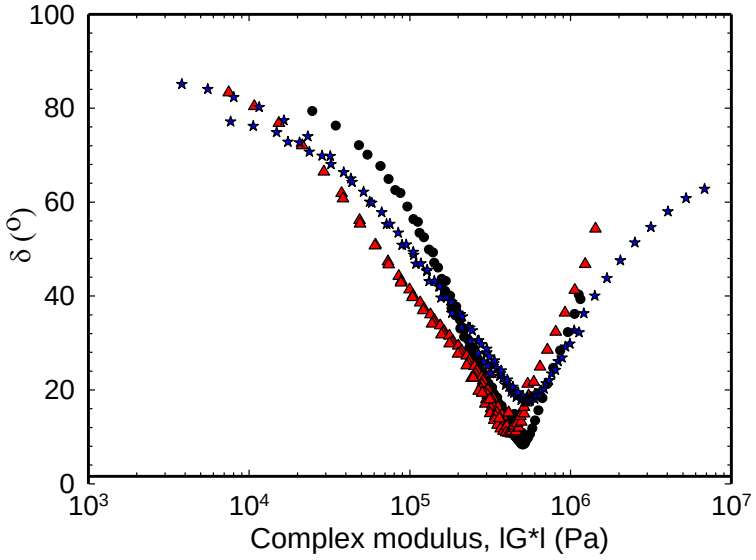

Figure 3.12 Van Gurp-Palmen plots of entry 7 of Table 3.1 (Linear PHB, M_w = 162 kgmol^{-1}, $Đ$ = 1.03) (filled circles), entry 16 of Table 3.1 (3-armed star PHB, M_w =146 kgmol^{-1}, $Đ$ = 1.06) (filled triangles), entry 7 of Table 3.3 (6-armed star PHB, M_w = 114 kgmol^{-1}, $Đ$ = 1.14) (filled stars).

The entanglements molecular weight of linear PHBs, M_e, is calculated from the plateau modulus using $M_e = \rho_0 RT/G_N^0$ assuming a density of 0.90 g/cm^3, at T = 323 K which results in M_e = 4833 gmol^{-1}. In order to obtain a precise estimation of the entanglement molecular weight of the stars, the McLeish-Milner equation was used.[199] Based on their theory, there is an exponential relationship between the zero-shear viscosity (η_0) and arms molecular weight (M_{arm}) as $\eta_0 = Aexp(\gamma \frac{M_{arm}}{M_e})$, where A is a constant and γ has the universal value of 0.48.[241] The Newtonian zero-shear viscosities were obtained in the low frequency region using $\lim_{\omega \to 0} G"(\omega)/\omega = \eta_0$. The results are plotted in Figure 3.13 for linear and star-shaped PHBs versus the molecular weight of the longest linear span in the molecule (twice the arm molecular weight of a star). The viscosity of the linear polymers follows the power law relationship $\eta_0 = 5 \times$

$10^{-12}M_w^{3.42}$. Meanwhile, η_0 for symmetric stars scales exponentially with the arm molecular weight.

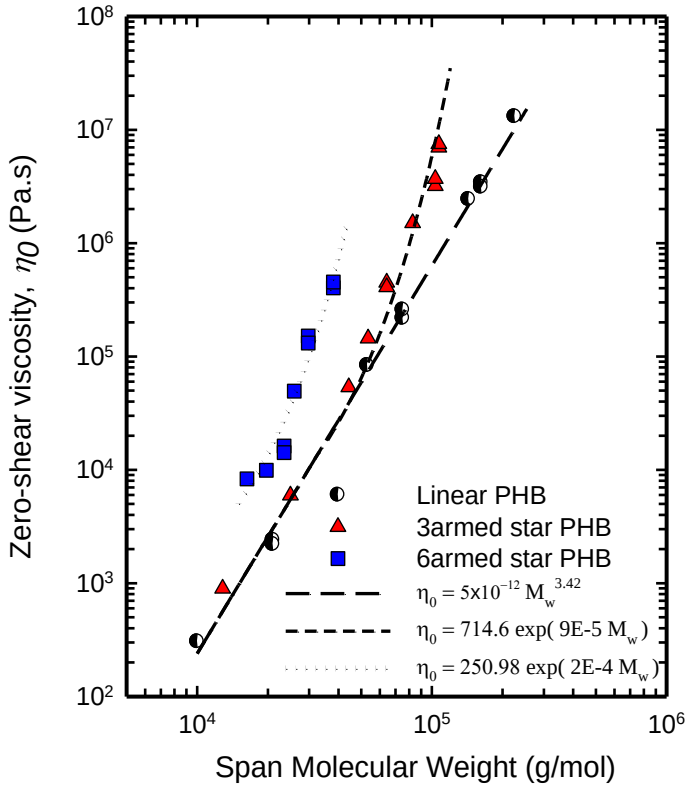

Figure 3.13 Scaling of the zero shear viscosity on the molecular weight of the series of linear, and star-shaped polymers

The exponential dependence of zero-shear viscosity on the molecular weight of star-branched polyisoprenes and other branched polymers such as polyglycerols has been also reported.[178,242,243] The entanglement molecular weight of the stars estimated from the McLeish-Milner relationship, results in M_e value of 5052 and 4800 gmol^{-1} for the 3-armed and the 6-armed star PHBs respectively. Considering the linear samples as a 2-amed star polymer, for the high molecular weight linear sample examined (entry 7 of Table 3.1), the branch entanglement number, $Z = M_a$ /

M_e, is 16, while this number is 9.5 and 4.02 for the 3-armed and the 6-armed star samples shown in Figure 3.10 (b-c). Hence, the absence of a distinct arm retraction relaxation mode in the dynamic frequency sweep tests results can be attributed to the lower entanglement density of the 6-armed star PHBs. Additionally, the broader molecular weight distribution of this sample (1.14) might be another factor affecting its viscoelastic properties, as broader molecular weight distributions eases relaxation through dynamic dilation. Nevertheless, arm retraction is still an activated process as it was shown by the exponential dependence of the viscosity of the 6-armed stars on the arm length.

As a universal plot (Figure 3.13), the zero-shear viscosity versus the span molecular weight should be independent of the number of arms. However, the zero-shear viscosity of 6-arm stars is higher than that of the 3-arms for comparable span molecular weights. Dorgan *et al.* have also reported the same non-universality in zero shear viscosity of the 4-armed and 6-armed star shaped poly (lactic acids) PLAs.[207] They assigned this lack of universality to several parameters, such as thermal degradation and relatively high molecular weight distributions ($Đ \sim 2$) of the star polymers, which directly affects the symmetry of the star molecules. The rheological measurements of the current work have been performed at relatively low temperatures and the dispersity of the polymers are all less than 1.2. Hence, this disparity is attributed to the different chain conformation of moderately syndiotactic microstructure of the 6-armed star PHBs. This observation is consistent with the results have been reported by Wang et al. on the effect of tacticity on viscoelastic properties of polystyrenes. [244]

3.2.5.2 Start-up of shear flow test results

To examine further the flow properties of PHB melts, startup of steady shear tests were performed at various shear rates to compare the behavior of the various architectures of the PHB

polymers (Figure 3.14). As the shear rate increases, the time dependent shear growth coefficient reaches an overshoot, followed by a decrease of the steady-state viscosity. The observed viscosity overshoot, or the yield stress is due to chain alignments and arm disentanglement,[206,245] the extent of which is less pronounced for six armed PHBs, possibly due to its broader molecular weight distribution. Strain hardening due to chain stretching was not observed for the linear and star-shaped PHB samples at the shear rates studied, which is known for monodisperse linear and sparsely branched polymers.

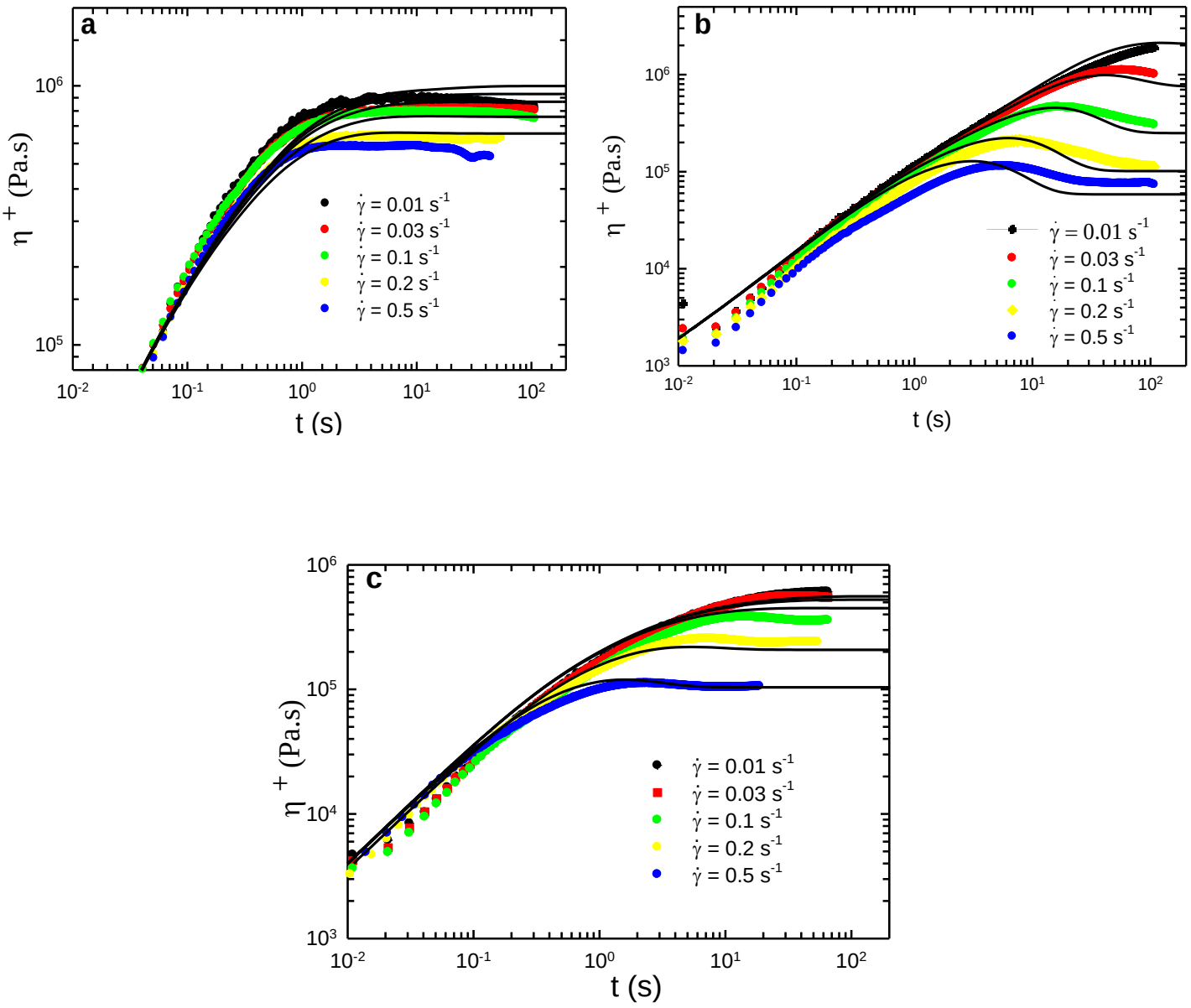

Figure 3.14 The shear stress growth coefficient of linear and star-shaped samples at different levels of shear rate, at 50°C **(a)** From Table 3.1 entry 7 (Linear PHB, *M*w = 160 kgmol^{-1}, *Đ* = 1.03), **(b)** From Table 3.1 entry 16 (3-armed star PHB, *M*w =146 kgmol^{-1}, *Đ* = 1.06), **(c)** From Table 3.2 entry 7 (6-armed star PHB, *M*w = 115 kgmol^{-1}, *Đ* = 1.14). The continuous lines represent the predictions of the K-BKZ model using Osaki damping functions.

One key observation in Figure 3.14 is the progressive reduction of transient viscosity with shear rate increase, which is more profound for star shaped PHBs. This higher degree of shear

thinning observed for the stars versus the linear PHBs is consistent with the previously reported results on stars-shaped polyisoprenes[242] and polylactides.[181,207,246] The lower entanglement density, and the presence of branch tips in the star polymer melts, are the reasons for the observed decreased viscosity at higher shear rates. However, at lower shear rates or in the linear viscoelastic region, the branch points enhance the viscosity due to imposing more constrain against molecular dynamics.

In an attempt to predict the start-up of shear flow results Wagner model was used.[172] This model is the simplified version of the K-BKZ as a popular constitutive equation to predict the non-linear viscoelastic behavior of the polymeric melts, which can be written as follows:

$$\boldsymbol{\sigma} = \int_{-\infty}^{t} \left(\sum_i \frac{gi}{\lambda i} \exp(-(t-t'))/\lambda i\right) h(\gamma)\, \boldsymbol{B}(t,t')dt' \qquad (1)$$

where $\boldsymbol{\sigma}$ and $\boldsymbol{B}$ are the stress and Finger strain tensors (representing the material strain history) and *h(γ)* represents the damping function. The damping function can be determined using experimental data, if the time-strain separability principle applies to the material. As a result, $h(\gamma) = G(t,\gamma)/G(t)$, which can be determined as a vertical shift factor of the stress relaxation modulus curves, $G(t,\gamma)$, (Figure A.15 (a) to (f)) that best superimpose to the liner relaxation modulus $G(t)$. Data points are finally fitted to the double-exponential Osaki function (Eqn. 2),

$$h(\gamma) = aexp(-m\gamma) + (1-a)\exp(-n\gamma) \qquad (2)$$

in which *a*, *n*, and *m* are fitting parameters. The Wagner model predictions are shown in (Figure 3.14) as solid lines. As it can be seen, the calculated viscosities can satisfactorily predict the viscosity overshoot and more shear thin behavior of the stars compared to the linear PHBs, which shows that the non-Newtonian feature of the star PHBs is predominantly influenced by their relaxation mechanisms under large strains.

3.3 Summary

High molecular weight symmetric star shaped poly(hydroxybutyrate) were synthesized via immortal ROP of BBL using indium and zinc catalysts $[(NNO_{tBu})InCl]_2(\mu\text{-}Cl)(\mu\text{-}OTHMB)$ (**2**) and $(NN_iO_{tBu})Zn(CH_2CH_3)$ (**3**) in the presence of a triol (THMB) and a hexol (DPET) as the chain transfer agents. The chain end analysis using ^1H NMR and MALDI-TOF revealed the presence of the CTAs as the star core. The indium catalyst **2** showed highly controlled living and immortal polymerization of BBL, with each catalyst molecule generating up to 590 macromolecules to afford hydroxyl-functionalized, star-shaped PHBs. Zinc catalyst **3** generates moderately syndiotactic PHBs with maximum molecular weights of ~100 $kgmol^{-1}$, however the presence of side reactions hinders access to higher molecular weights.

The solution and melt viscoelastic properties of the various molecular weight linear and star-shaped PHBs were also investigated. Power law relationships of the R_g and R_h with molecular weights, and lower amounts of the intrinsic viscosity and compactness factors of the stars compared to that of the linear PHBs indicated the self-similar and symmetric topology of the star PHBs. From melt rheology, the entanglement molecular weights of the linear and star shaped PHB homopolymers are estimated. The zero-shear viscosity of the linear PHBs has shown a scaling of $\eta_0 \propto M_w^{3.42}$ to be consistent with those reported for linear monodisperse polymers, while η_0 for symmetric stars scales exponentially with the arm molecular weight. Furthermore, transient shear viscosity growth of the samples indicates more shear thinning behavior of the stars compare to the linear PHBs due to the dynamic dilution effect of arm tips and lower entanglement densities of the stars, which eases the shear alignment of the chains. We hope to develop our insights into the rheology and synthesis of hydroxyl functionalized star-shaped PHBs to generate new families of biodegradable materials.

Chapter 4: Synthesis of syndioenriched polyhydroxybutyate using chiral zinc complexes and thermorheological characterization of it as a processable PHB

This chapter makes two major contributions to the formation of PHB with better processability. First, we report the formation of semicrystalline syndiotacticly enriched PHB from racemic BBL catalyzed by chiral zinc complexes. These systems display remarkably high protic group tolerance in the presence of up to 5000 equivalents of alcohol, by far surpassing any literature report on immortal polymerization of BBL. Second, we show for the first time that moderately syndiotactic PHBs are processable in the absence of additional processing aids, making it possible to study their viscoelastic and extensional rheological and mechanical properties for the first time.

4.1 Introduction

As mentioned in chapter 1, one of the challenges in the use of bacterial based PHB as a biodegradable plastic, is its limited processing window due to its high melting point and high entanglement molecular weight. The thermal degradation temperature of PHB is close to the processing temperature, as a result, PHB undergoes extensive thermal degradation during the melt processing. In addition, high entanglement molecular weight and hence, low melt strength limits processing under high shear/strain forces, such as film blowing and filament winding. [209,247,248] In order to improve the processability of PHB, several techniques including blending with other polymers,[249-251] addition of thermal stabilizers, cross-linking agents, nucleating agents,[248,252-254]and even block copolymerization with other PHAs through microbial synthetic routes,[8,255] have been attempted, however, with very limited success.

For this reason, in order to make PHB processable, "backbone engineering" can be the only solution. In this technique, using synthetic routes, such as ROP of BBL, and only by having a well-behaved catalytic system, we can control the backbone microstructure, and the crystallinity of PHB. Also, having a robust system, we can increase the molecular weight, and reduce the molecular weight distribution of the polymer to enhance its melt strength.

In catalyst design, in order to increase catalytic productivity and reduce metal contamination of the final product, immortal ROP in the presence of chain transfer agents may be considered; however there exists a limited number of catalysts that stay active in the presence of chain transfer agents.[10] Zinc as a non-toxic metal with high functional group tolerance has been considered as a suitable candidate for immortal polymerization.

Single site zinc(II) complexes bearing β-diiminate ligand framework ([(BDI-Zn(μ-O^{i}Pr)]$_2$) are known as highly active and selective catalysts for *rac*- and *meso*-lactide polymerization.[154,156] These complexes were also found to be active to polymerize high equivalents of *rac*-BBL under mild conditions, however, without stereoselectivity.[256] The same catalytic system was successfully used for immortal polymerization of *rac*-BBL with high loadings of isopropanol up to 50 equivalents to produce PHBs with controlled molecular weights.[257] Multidentate amino-ether phenolate ligands were used to form a series of zinc complexes by Sarazin and coworkers. Although these complexes showed a unique ability to polymerize 50000 equivalence of lactide in the presence of 1000 equivalents of CTA, immortal polymerization of 500 equivalence of BBL in the presence of 10 equivalents of isopropanol could reach full conversion in 3 hrs at high temperatures. [258,259]

Although zinc ethyl complexes bearing chiral diaminophenoxy proligands are very stable complexes,[218] in chapter 3 we showed that the imine backbone analogue allowed formation of 6-

armed star PHBs in the presence of DPET. However, polymerizations were not well-controlled and showed moderate reactivity and selectivity, nonetheless, the prepared star polymers were relatively symmetric and showed enhanced melt viscosity compare to their linear and 3 armed analogues.[100]

In this chapter, aimed at increasing the catalytic reactivity and selectivity of complex (**3**), its analogues with alkoxy initiators and different substituents on the ligand will be reported. The functional group tolerance of these complexes will be examined through setting up immortal polymerizations with high loadings of benzyl alcohol (BnOH). After determining the optimized system for large scale polymerization of BBL, up to 2 grams of controlled microstructure PHBs will be prepared and detailed thermorheological characterizations will be reported.

4.2 Results and Discussion

4.2.1 Synthesis and characterization of zinc complexes

Racemic and (*R,R*) 2,6-di-*t*-butyl-(((2(dimethylamino)cyclohexyl)amino)methyl)phenol with various substituents H($NN_{R2}O_{R1}$) (R_1 = *t*-Bu, Cm, $SiPh_3$, Ad; R_2 = H, Me) can be prepared according to previously published procedures.[165,260] Alkane elimination reaction of the proligands with one equivalent of $ZnEt_2$ forms the corresponding known[218] (±)-($NN_{Me}O_{tBu}$)ZnEt (**4**) and (±)-(NN_HO_{tBu})ZnEt (**5**) and newly synthesized (±)/(*R,R*)-(NN_HO_{Cm})ZnEt (**6**), (±)-(NN_HO_{Ad})ZnEt (**7**), and (±)/(*R,R*)-(NN_HO_{SiPh3})ZnEt (**8**) alkyl zinc complexes (Scheme 4.1). The ^{1}H NMR spectra ($CDCl_3$, 25 °C) of complexes **6**-**8** are similar to those of previously reported complexes **4** and **5** with two signals for the $N(CH_3)_2$ appear between 1.75 to 2.50 ppm as two separate singlets, suggesting that the terminal amine does not dissociate from the zinc center (Figure B.1-4).[218] This is in contrast to analogous zinc ethyl complexes bearing achiral diaminophenolate ligands which

show exchange between the two N(CH_3)$_2$ signals.[170] The molecular structure of complex **6**, analyzed by single-crystal X-ray diffraction, is similar to that of **5** and confirms the κ^3-coordination mode of the ligand in the solid state (Figure B.14).[218,261]

Alkoxy zinc complexes (±)-**10**, (±)/(*R,R*)-**11**, (±)-**12**, and (*R,R*)-**13** were prepared through the alcoholysis of alkyl zinc complexes **5-8** with one equiv. of benzyl alcohol in toluene at room temperature for 4 h (Scheme 4.1). Complex **10** was highly soluble in most organic solvents which complicates its purification process and led to low yield (60%). The racemic version of the bulkier substituted complex **13** was however insoluble in most organic solvents due to aggregation which inhibits its further characterization. Therefore the enantiopure version of it was prepared. Complexes (**11-13**) were isolated as off-white solids in >80% yields. Complexes (±)-**10** and (±)/(*R,R*)-**11** show a distinctive singlet for the (-CH_2-) protons of the benzyl alkoxy group at 4.75 ppm (Figure B.5-7). This observation infers fluxional behavior and the free rotation of the alkoxide bridge around the O-C bond in these complexes. However in (±)-**12** and (*R,R*)-**13** the methylene protons appear as multiplets due to possible hindered rotation (Figure B.8,9). The solution state structures of these complexes confirm the rigidity of the ancillary ligands for (±)-**10**, (±)/(*R,R*)-**11** and **12** as protons of the terminal amine represent two distinct and sharp singlets. While (*R,R*)-**13** is more labile as the -N(CH_3)$_2$ protons appear as one sharp singlet which is due to terminal amine dissociation and κ^2 coordination of the ligand in solution.

Scheme 4.1 Formation of alkyl and alkoxy zinc complexes

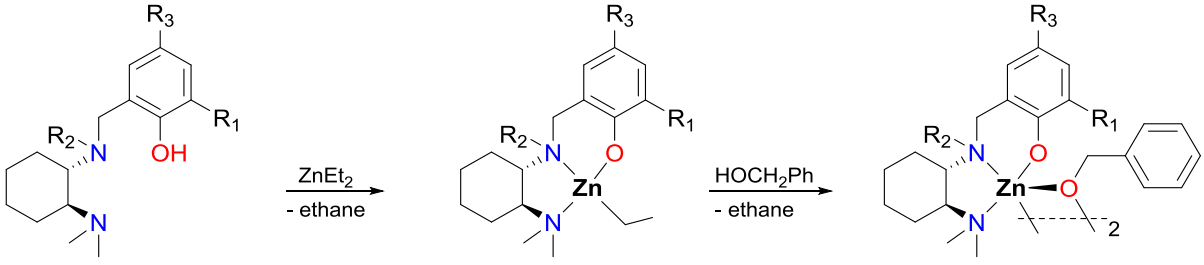

(±)-**H(NN$_{R2}$O$_{R1}$)**

R_1 = R_3 = *t*-Bu, R_2 = H	(±)-(NN$_H$O$_{tBu}$)ZnEt (**4**)	(±)-[(NN$_H$O$_{tBu}$)ZnOBn]$_2$ (**9**)
R_1 = R_3 = *t*-Bu, R_2 = Me	(±)-(NN$_{Me}$O$_{tBu}$)ZnEt (**5**)	(±)-[(NN$_{Me}$O$_{tBu}$)ZnOBn]$_2$ (**10**)
R_1 = R_3 = Cm, R_2 = H	(±)/(*R,R*)-(NN$_H$O$_{Cm}$)ZnEt (**6**)	(±)/(*R,R*)-[(NN$_H$O$_{Cm}$)ZnOBn]$_2$ (**11**)
R_1 = Ad, R_3 = *t*-Bu, R_2 = H	(±)-(NN$_H$O$_{Ad}$)ZnEt (**7**)	(±)-[(NN$_H$O$_{Ad}$)ZnOBn]$_2$ (**12**)
R_1 = SiPh2, R_3 = Me, R_2 = H	(±)/(*R,R*)-(NN$_H$O$_{SiPh3}$)ZnEt (**8**)	(*R,R*)-[(NN$_H$O$_{SiPh3}$)ZnOBn]$_2$ (**13**)

Single crystals of complexes (±)-**11** and (*R,R*)-**13** were isolated from a solution of toluene and ether at room temperature (Figures 4.1, Figure B. 16, 17, Table B.1). In the solid state (±)-**11** forms a heterochiral (*RR/SS*) dimer with an inversion center and distorted trigonal bipyramidal zinc centers bridged by benzyl alkoxy ligands. The molecular structure of complex (±)-**11** retains the κ^3-coordination mode of the (NN$_H$O$_{cm}$) ligands which is in accordance to its solution structure. Complex **13** crystalizes as a homo-chiral (*RR*/*RR*) dimer in the non-centrosymmetric monoclinic space group and also retains the κ^3-coordination mode.

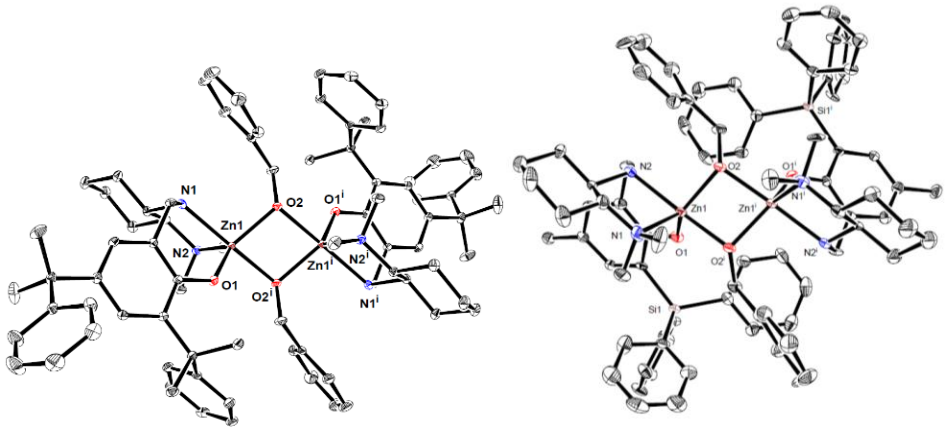

Figure 4.1 Molecular structures of complex (±)-**11 (a, left)** and (*R*,*R*)-**13 (b, right)** (depicted with thermal ellipsoids at 50% probability and H atoms as well as solvent molecules omitted for clarity).

X-ray quality single crystals of complex (±)-**10** were grown from a saturated solution in cold pentane. In stark contrast to aggregation behaviour observed in zinc alkoxide catalysts [170,262] as well as related systems,[263,264] complex **10** is monomeric in the solid state (Figure 4.2, Figure B.15). The solid state structure of **10** shows two mononuclear (*SS*)-**10** complexes in the unit cell. This complex crystalizes in a centrosymmetric triclinic space group, implying that both *SS*- and *RR*-enantiomers exist in the unit cell.

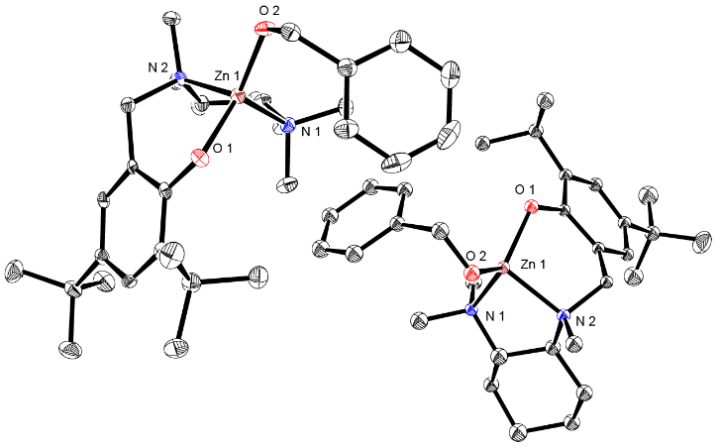

Figure 4.2 Molecular structure of complex (±)-**10** (depicted with thermal ellipsoids at 50% probability and most H atoms as well as solvent molecules omitted for clarity).

We have previously shown that alcoholysis of complex (±)-**5** with one equivalent of phenol forms ($NN_{Me}O_{tBu}$)Zn(O-Ph).[218] ($NN_{Me}O_{tBu}$)Zn(O-Ph) is mononuclear in the solid state and it was attributed to the presence of hydrogen bonding phenol in the crystal lattice. [218] This is not the case for **10**. A comparison of the solid state structures of half of (±)-**9** and (±)-**10** shows that in **9** the benzyl alkoxy group is pointing towards the central N-H while for **10** the presence of the N–CH_3 group forces the benzyl group towards the zinc center (Figure 4.3). This difference between the two complexes is most pronounced in the $N_{central}$-Zn1-O_{Benzyl} angles, which is significantly larger for **10** (96 vs 112°). This observation suggests that the zinc center is more crowded in the latter system.

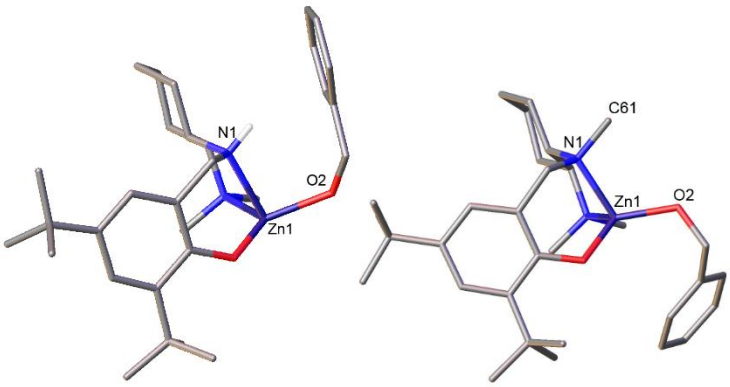

Figure 4.3 Structural comparison of (a, left) complex **9** (only one side of the dimer is shown) and (b, right) complex **10**.

In an attempt to hinder aggregation in solution, the benzyl alkoxide group was replaced with a coordinating pyridin-2-ylmethoxide in a strategy that was successful for related indium alkoxide complexes.[166] The alkyl elimination reaction of racemic complexes (±)-**4**, (±)-**7**, and (±)-**8**, with pyridin-2-ylmethanol forms the corresponding alkoxide complexes (±)-(NN_HO_{tBu})ZnOCH_2Pyr (**14**), (±)-(NN_HO_{Ad})ZnOCH_2Pyr (**15**), and (±)-(NN_HO_{SiPh3})ZnOCH_2Pyr (**16**) (Scheme 4.2).

Scheme 4.2. Synthesis of (±)-(NN_HO_{R1})$ZnOCH_2Pyr$ complexes

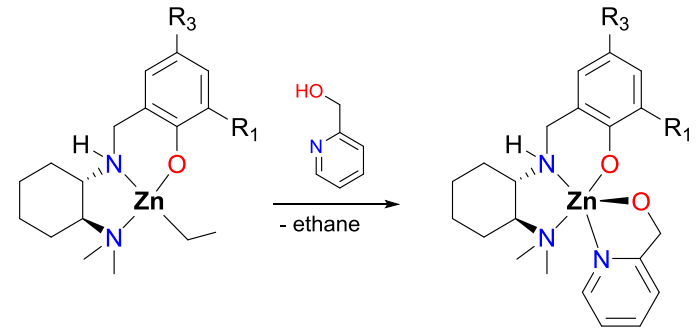

(±)-(NN_HO_{tBu})ZnEt (**4**)
(±)-(NN_HO_{Ad})ZnEt (**7**)
(±)-(NN_HO_{SiPh3})ZnEt (**8**)

(±)-(NN_HO_{tBu})$ZnOCH_2Pyr$ (**14**)
(±)-(NN_HO_{Ad})$ZnOCH_2Pyr$ (**15**)
(±)-(NN_HO_{SiPh3})$ZnOCH_2Pyr$ (**16**)

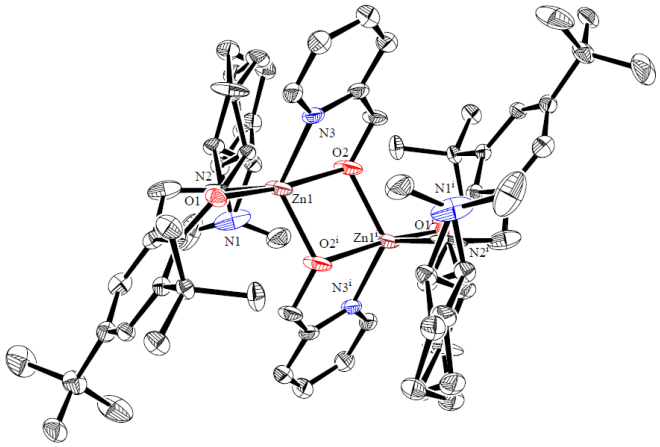

Figure 4.4 Molecular structure of complex (±)-**14** (depicted with thermal ellipsoids at 50% probability and most H atoms as well as solvent molecules omitted for clarity (Figure S16)).

Single crystals suitable for X-ray crystallography of (±)-**14** were obtained from a mixture of toluene and hexane. Complex (±)-**14** has a dimeric structure, with the pyridin-2-ylmethoxide moieties with both κ^2-O,N and μ-O chelating motifs. The two zinc centres are supported by κ^2-coordinated (NN_HO_{R1}) ligands, with the -$N(CH_3)_2$ groups no longer coordinated to the metal centres (Figure 4.4, Figure B.18).

The ^{1}H NMR spectrum of (±)-**14** shows a singlet corresponding to the methylene resonances of pyridin-2-ylmethoxide at 5.17 ppm, while for complexes (±)-**15** and (±)-**16** the methylene protons appear as multiplets at 5.15–5.23 and 4.99–5.13 ppm (Figures B.10-12). This suggests fluxional behavior for the pyridine moiety and greater lability for (±)-**14** in solution compared to its bulkier analogues.

To investigate the nuclearity of the complexes in solution, pulsed field-gradient spin echo (PGSE) ^{1}H NMR experiments can be carried out for complexes **9**-**16** to determine their diffusion coefficients (D_t) and their hydrodynamic radii (r_H) (Table 4.1, Figure B.13). The D_t values of adamantyl substituted (±)-**12** is similar to that of complex (±)-**9**, with values 20–30% smaller than those for the proligands,[162,265-267] suggesting that the major species for (±)-**9** and (±)-**12** is dinuclear in solution (Table 4.1, entries 4, and 6). Complex (*rac*)-**10** with tertiary central amine has D_t value similar to those of the proligand which indicates the mononuclear structure of the complex in solution state in accordance to its solid state structure. The diffusion coefficients of complexes **14**-**16** show a difference of only 10-15% from the corresponding proligands, suggesting that the major species are mononuclear in solution (Table 4.1, entries 8-10). Notably, (*R,R*)-**13** with bulky *ortho* substituents possess D_t value of 8.61 which is very close to its mononuclear analogue, (±)-**16**, in solution. This observation indicates that although **13** is dinuclear in the solid state, it dissociates in the solution state into mononuclear species due to the presence of bulky $SiPh_3$ substituents.[162,166]

Table 4.1 Diffusion coefficients and hydrodynamic radii

	Compound	D_t[a] ($\times 10^{-10}$ m^2s^{-1})	r_H[b](Å)	$r_{X\text{-}ray}$[c](Å)
1	(±)-H(NN_HO_{tBu}) [165]	12.0	5.2	…
2	(±)-H(NN_HO_{Ad}) [162]	10.2	6.0	…
3	(±)-H(NN_HO_{SiPh3}) [162]	9.1	6.3	…
4	(±)-**9** [261]	7.7(3)	7.5	6.9
5	(±)-**10**	9.82(9)	5.9(5)	5.64
6	(±)-**12**	7.2(2)	7.8	….
7	(*R*,*R*)-**13**	8.6(5)	6.6	7.8
8	(±)-**14**	9.9(5)	5.9	5.5
9	(±)-**15**	9.3(5)	6.2	….
10	(±)-**16**	8.7(2)	6.6	….

[a]Determined using PGSE NMR spectroscopy with tetrakis(trimethylsilyl)silane (TMSS) as an internal standard. [Compound] = 4.5 mM; samples were prepared in 0.94 mM TMSS solution in CD_2Cl_2. D_t is calculated from slopes of plots of $\ln(I/I_0)$ vs. $\gamma^2\delta^2G^2[\Delta-(\delta/3)]\times10^{-10}$ (m^2 s). [b]Calculated from D_t values using a modified Stokes-Einstein equation (see Appendix B). [c]Calculated, where solid-state data is available, from the crystal structure unit cell volume (V) as well as the number of the compound of interest (n) occupying the unit cell assuming spherical shape $(3V/4\pi n)^{1/3}$.

4.2.2 Living polymerization of BBL in the presence of complexes 9-16

Large scale polymerizations of BBL with complexes **9-16** were conducted in dichloromethane at room temperature (Table 4.2). Polymerization of BBL with complex **9** proceeds rapidly under mild conditions allowing full conversion of 400-3000 equivalents of BBL in less than five [268] to 30 minutes to form high molecular weight PHB ([BBL] = 3.5-4.5 mol·L^{-1}). Polymers generated with this catalyst have predictable M_n values and low dispersity ($Đ$), which is indicative of living polymerization (Table 4.2, entries 1-6).

Table 4.2 Living polymerization of BBL using complexes **9**-**16**. [a]

	Catalyst	$[BBL]_o$: [initiator]	Time (min)[c]	Conv. [b] (%)	TOF (h^{-1})	$M_{n,theo}$ [d] (g mol^{-1})	$M_{n,GPC}$ [e] (g mol^{-1})	$Đ$ [e]	P_r [f]
1	(±)-**9**	400	~1	>99	23760	34540	34900	1.27	0.71
2[g]	(±)-**9**	400	16 h	75	18	25930	21200	1.34	0.75
3	(±)-**9**	645	10	>99	3483	55640	75500	1.20	0.70
4	(±)-**9**	1000	10	>99	5940	86090	88000	1.33	0.67
5	(±)-**9**	2000	30	>99	3960	172290	120000	1.19	0.68
6	(±)-**9**	3000	30	62	3720	160230	140000	1.17	0.66
7	(±)-**10**	400	16 h	> 99	24	34544	25200	1.38	-
8	(±)-**11**	413	60	95	392	33880	15800	1.40	0.57
9	(±)-**12**	400	60	>99	396	34500	30300	1.17	0.65
10	(±)-**12**	1200	60	91	1080	84120	90400	1.05	0.63
11	(±)-**12**	1600	60	80	1280	110300	103500	1.04	0.61
12	(±)-**12**	4000	60	71	2800	244600	213300	1.02	0.60
13	(*R*,*R*)-**13**	200	240	>99	50	17310	12600	1.31	-
14	(*R*,*R*)-**13**	600	240	92	138	47630	43100	1.30	-
15	(*R*,*R*)-**13**	800	240	93	186	64160	60100	1.30	-
16	(*R*,*R*)-**13**	2000	240	95	475	163680	96000	1.21	-
17	(±)-**14**	400	10	>99	2376	34540	30400	1.04	0.67
18	(±)-**15**	400	10	>99	2376	34540	35800	1.12	0.61
19	(±)-**16**	400	60	>99	396	34540	32100	1.20	0.55

[a] All reaction carried out in CH_2Cl_2 at 25 °C. [b] Monomer conversion, determined by ^1H NMR spectroscopy. [c]Non-optimized reaction time. [d] Calculated from $[M]_o/[initiator] \times$ monomer conversion $\times M_M + M_{BnOH}$ (M_{BBL} = 86.09 g/mol, M_{BnOH} = 108.14 g/mol). [e] Determined by GPC-MLLS (gel permeation chromatography Multi-angle laser light scattering) to the polystyrene standard calibration via the Mark–Houwink equation in CH_2Cl_2 at 25 °C ($[\eta] = KM^a$ while $[\eta]$ = intrinsic viscosity, M = molecular weight, and K and a are Mark–Houwink parameters, $K = 1.832 \times 10^{-4}$ dl/g and $a = 0.69$; dn/dc = 0.067 mL/g for PHB in THF). [f] P_r is the probability of racemic linkages between monomer units and is determined by carbonyl region of inverse gated $^{13}C\{^1H\}$ NMR spectra (Figure S18).[165,236] [g] Carried out at −30 °C.

High turnover frequencies can be obtained; for example, Table 4.2, entry 1 we estimate a TOF of ≥ 23000 h^{-1}. Polymerization of 200 equivalents of BBL in CD_2Cl_2 monitored by *in situ* ^1H NMR spectroscopy at room temperature shows an observed rate of BBL polymerization with **9** ($k_{obs} = 4.3 \times 10^{-3}$ s^{-1}, Table 4.3 entry 1) which is two orders of magnitude faster than complex **D** ($k_{obs} = 3.3 \times 10^{-5}$ s^{-1}) (Figure B.19).[113]

Table 4.3 Polymerization of BBL with catalysts **9-16**

	Catalyst	k_{obs} ($\times 10^{-3}$ s^{-1}) [a]	P_r
1	(±)-**9**	4.3(1)[a]	0.71
2	(±)-**10**	0.20 (0.10)	0.52
3	(±)-**11**	2.3(2)	0.57
4	(*R,R*)-**11**	1.1(2)	0.53
5	(±)-**12**	2.7(3)	0.67
6	(*R,R*)-**13**	0.80(5)	0.55
7	(±)-**14**	3.8(1)	0.66
8	(±)-**15**	2.1(3)	0.60
9	(±)-**16**	1.2(2)	0.58

All the reaction carried out in an NMR tube in CD_2Cl_2 at 25 °C and followed to 98% conversion. [BBL] = 0.16 M. [catalyst] = 0.40 mM in CD_2Cl_2. 1,3,5-trimethoxybenzene (TMB) used as internal standard. k_{obs} determined from the slope of the plots of ln([BBL]/[TMB]) vs. time. [a] Due to the high reaction rates, polymerizations were monitored after ~ 30% conversion (Figure B.19).

The steric environment of the complexes with different substituents on the phenolate ring has an impact on the rates of propagation in these systems. Complexes with bulkier *ortho* substituents, cumyl (±)-**11**, adamantyl (±)-**12**, and triphenyl silyl (*R,R*)-**13**, show somewhat reduced activity (Table 4.2 entries 8-16). *In situ* ^1H NMR studies confirm the reduced rates of polymerization for (±)-**11** ($k_{obs} = 2.3 \times 10^{-3}$ s^{-1}) and (±)-**12** ($k_{obs} = 2.7 \times 10^{-3}$ s^{-1}) compared to the *t*-Bu substituted complex (±)-**9** under the same reaction conditions. The decrease in rate is more pronounced for

the enantiopure complexes: the rates for (*R,R*)-**13** ($k_{obs} = 0.8 \times 10^{-3}$ s^{-1}) and (*R,R*)-**11** ($k_{obs} = 1.1 \times 10^{-3}$ s^{-1}) are similar while those of the enantiopure and racemic **11** differ by a factor of two (Table 4.3).[165]

The rates of polymerization for the methoxy pyridyl adducts (±)-**14**, (±)-**15**, and (±)-**16** are essentially the same as the respective benzyl oxide adducts (Table 4.3, entries 7-9), which suggests that complexes (±)-**9** and (±)-**12**, similar to (*R,R*)-**13**, are also mainly monomeric during the polymerization.

Importantly, ROP of BBL catalyzed by complex (±)-**9** forms syndiotactically-enriched PHBs, as an indicative of chain end control mechanism,[2,10,29,74,75] with the probability of racemic linkages (P_r) in the range 0.66-0.75 (Table 4.2, Figure B.20). Chain end analysis of the polymerization of 50 equivalents of BBL with MALDI-TOF mass spectroscopy and ^{1}H NMR spectroscopy showed methoxy chain ends after quenching in methanol with no evidence of elimination reactions due to the absence of crotonate species (Figure B.21, 22). Larger loadings of BBL as well as polymerizations that are not quenched after full conversion immediately undergo depolymerization that results in polymers with lower molecular weights and syndiotacticity (Table B.2). Interestingly, aside from the reduced reactivity, bulkier complexes (±)-**11** and (*R,R*)-**13** show reduced syndioselectivity. In particular, (*R,R*)-**13** yields essentially atactic PHB (Table 4.2, entries 8 and 13-16). This suggests the effect of catalyst site selectivity and its interference with the chain-end control mechanism, however, drawing a solid conclusion on the mechanism of selectivity requires more in detailed studies which is not in the scope of this study.

Despite high reactivity and syndioselectivity of complex **9**, its analogue with central tertiary amine and more crowded zin center (complex **10**) enables the polymerization of 400 equivalents of BBL to full conversion overnight and it loses the selectivity as it only offers atactic PHBs (Table

4.2, entry 7 and Table 4.3, entry 2). We have previously shown that there is a profound difference between dinuclear indium complexes bearing the same ligand sets with secondary vs. tertiary central amines in catalyst reactivity towards *rac*-lactide polymerization due to the absence of hydrogen bonding between halide ligand and the tertiary central amine which led to catalyst dissociation during polymerization. This leads us to conclude that in these ligand series, the presence of tertiary amine donor results in dramatic reduction in the catalytic reactivity and selectivity of the complexes of different metal centers such as indium and zinc.

4.2.3 Immortal ring opening polymerization of BBL using complex 9 in the presence of benzyl alcohol (BnOH)

Polymerizations of 40000 equivalents of BBL in the presence of 100 equivalents of benzyl alcohol (BnOH) catalyzed by (±)-**9** forms syndio-rich PHB with narrow dispersity (Table 4.4, entry 1). We found that this catalytic system exhibits good reproducibility and high conversions with up to 5000 equivalents of BnOH to form PHBs with controlled molecular weights (Table 4.4, entry 7). The ^{1}H NMR spectra of this sample reveals characteristic resonance signals at 4.23 ppm corresponding to the α-hydroxyl methine proton and a sharp multiplet at 7.35 ppm assigned to aromatic protons of the chain end (Figure B.23). Additionally, chain-end analyses of the PHB oligomers by MALDI-TOF mass spectroscopy (Figure B.24) show good agreement between theoretical and experimental molecular weights, indicative of the controlled and immortal nature of the catalytic process with complex **9** in the presence of benzyl alcohol. The bulkier analogues behave similarly (Table 4.4 entries 8-9). To our knowledge, complex **9** is the first example of a catalyst that tolerates such high loadings of alcohol while maintaining its high catalytic reactivity and stereo control over the polymerization of BBL.

Table 4.4 Immortal polymerization of BBL using complexes **9-11** and benzyl alcohol as the chain transfer agent.

	Catalyst	[BBL]$_o$: [ROH]: [initiator]	Time (h) [e]	Conv. [a] (%)	$M_{n,theo}$ [b] (gmol^{-1})	$M_{n,GPC}$ [c] (gmol^{-1})	$M_{n,NMR}$ [d] (gmol^{-1})	$Đ$ [c]	P_r [f]
1	(±)-**9**	40000/100/1	8	63	20950	20100	21300	1.02	0.71
2	(±)-**9**	10000/100/1	8	90	7700	7280	7500	1.04	0.69
3	(±)-**9**	10000/250/1	8	87	3080	2880	2900	1.03	-
4	(±)-**9**	10000/500/1	8	86	1580	1440	1400	1.05	-
5	(±)-**9**	10000/1000/1	8	86	850	890	860	1.03	-
6	(±)-**9**	10000/2500/1	8	94	430	-	530	-	-
7	(±)-**9**	20000/5000/1	8	90	430	-	370	-	-
8	(±)-**10**	1000/100/1	1	98	960	-	960	-	-
9	(±)-**11**	1000/100/1	1	>99	960	-	930	-	-

All reaction carried out in CH_2Cl_2 at 25 °C. [a] Monomer conversion, determined by ^{1}H NMR spectroscopy. [b] Calculated from [M]$_o$/[initiator] × monomer conversion × M_M + M_{BnOH} (M_{BBL} = 86.09 g/mol, M_{BnOH} = 108.14 g/mol). [c] Determined by GPC-MLLS (gel permeation chromatography Multi-angle laser light scattering) to the polystyrene standard calibration via the Mark–Houwink equation in CH_2Cl_2 at 25 °C ([η] = KM^a while [η] = intrinsic viscosity, M = molecular weight, and K and a are Mark–Houwink parameters, K = 1.832 × 10^{-4} dl/g and a = 0.69; dn/dc = 0.067 mL/g for PHB in THF). [d] NMR molecular weight. [e] Reaction times are not optimized. [f] P_r is the probability of racemic linkages between monomer units and is determined by methane region of invers gated ^{13}C{^{1}H} NMR spectra.

4.2.4 Melt rheological and mechanical characterization of syndiotactic PHB

The thermorheological and mechanical bulk properties of high molecular weight syndio-rich PHBs, were investigated for the first time. A series of large scale (2 g) polymerizations were set up using complex (±)-**6** as the initiator and all the reactions were carried out at room temperature using dichloromethane as the solvent. Differential scanning calorimetry (DSC) was used to measure the thermal characteristics of the polymers. Representative values of melting point and the enthalpy of melting are reported in Table 4.5 (Figure B26-31). Since the maximum reachable P_r value for the large scale synthesis of PHBs using this system was 0.7, previously reported complex (**B)** with cumyl substituents on the phenolate rings was synthesized[126] and used to form

highly syndiotactic PHB (P_r = 0.83) with the maximum reachable molecular weight of 65.7 kgmol^{-1} [1] (Table 4.5, entry 1). Based on the DSC results, all of the syndio-rich PHBs (e.g. P_r = 0.64, Table 4.5 entry 6) are semicrystalline with melting points ranging from 45 to 84 °C (due to the presence of various microcrystalline regions) and the syndiotactic polymer (P_r = 0.83) is crystalline with a high melting point of 155 °C.

Table 4.5 Large scale PHB synthesis for thermorheological and mechanical characterizations.

Entry	Catalyst	$M_{W,GPC}$ g mol^{-1}	$Đ$ [a]	P_r [b]	T_{m1} (°C) [c]	ΔH_{m1} (J g^{-1}) [c]	T_{m2} (°C) [c]	ΔH_{m2} (J g^{-1}) [c]
1	**B** [126]	65690[d]	-	0.83	155	35	-	-
2	(±)-**6**	57500	1.27	0.70	48.3	1.13	61.2	2.1
3	(±)-**6**	126000	1.23	0.68	48.6	1.1	64.8	2.5
4	(±)-**6**	134000	1.30	0.64	50.1	7.3	78.2	5.1
5	(±)-**6**	190800	1.21	0.65	49.4	1.4	69.2	7.5
6	(±)-**6**	225000	1.14	0.64	45.5 (54.1) [e]	1.0 (2.9) [e]	66.4 (85.7) [e]	5.5 (1.1) [e]
7	(±)-**6**	285000	1.12	0.68	45.2	2.2	62.0	4.5
8	(±)-**6**	385000	1.14	0.64	48.9	7.4	84.4	1.5

All reactions carried out in CH_2Cl_2 at 25 °C. [a] Determined by GPC-MLLS to the polystyrene standard calibration via the Mark–Houwink equation in CH_2Cl_2 at 25 °C ($[\eta] = KM^a$ while [η] = intrinsic viscosity, M = molecular weight, and K and a are Mark–Houwink parameters, K = 1.832 × 10^{-4} dl/g and a = 0.69; dn/dc = 0.067 mL/g for PHB in THF). [b] P_r is the probability of racemic linkages between monomer units and is determined by methane region of inverse gated $^{13}C\{^1H\}$ NMR spectra. [c] Measured using DSC scanned from 25 to 100 °C with the rate of 10 °C/min (Figure S24 –S29). [d] Determined using MALDI-TOF mass spectroscopy (Figure S23). [e] Measured after Sentmanat Extensional Rheometer (SER) experiment at 80 °C (Figure S34).

Thermal stability of the PHBs was investigated using rotational parallel-plate rheometer. Dynamic time sweeps were carried out at different temperatures at the fixed frequency of 1 rad/s. Representative results for the polymer of entry 6 listed Table 4.5 are plotted in Figure 4.5 (a). The consistency of storage and loss moduli during the test up to 2000 s indicate that sample degradation

had not occurred at temperatures below 140 °C. However, these viscoelastic properties and the complex viscosity (a function of the viscoelastic moduli) drop at temperatures above 140 °C, which is due to random chain scissioning.[247] These results demonstrate that syndiotactically enriched PHBs of high molecular weight possess enough thermal stabilities for melt processing below 140 °C. However, as seen in Figure 4.5 (b) highly syndiotactic PHB suffers from dramatic thermal degradation at temperatures above melting point and undergoes isothermal crystallization at temperatures below the melting point (note the increase in G' and G'' at 150 and 157 °C). This behavior has been reported frequently in literature for highly isotactic bacterial based PHBs[209] as well and is the reason for the nearly impossible melt processing of these polymers. Therefore, the very limited processing window of the syndiotactic PHB prevents any further rheological studies.

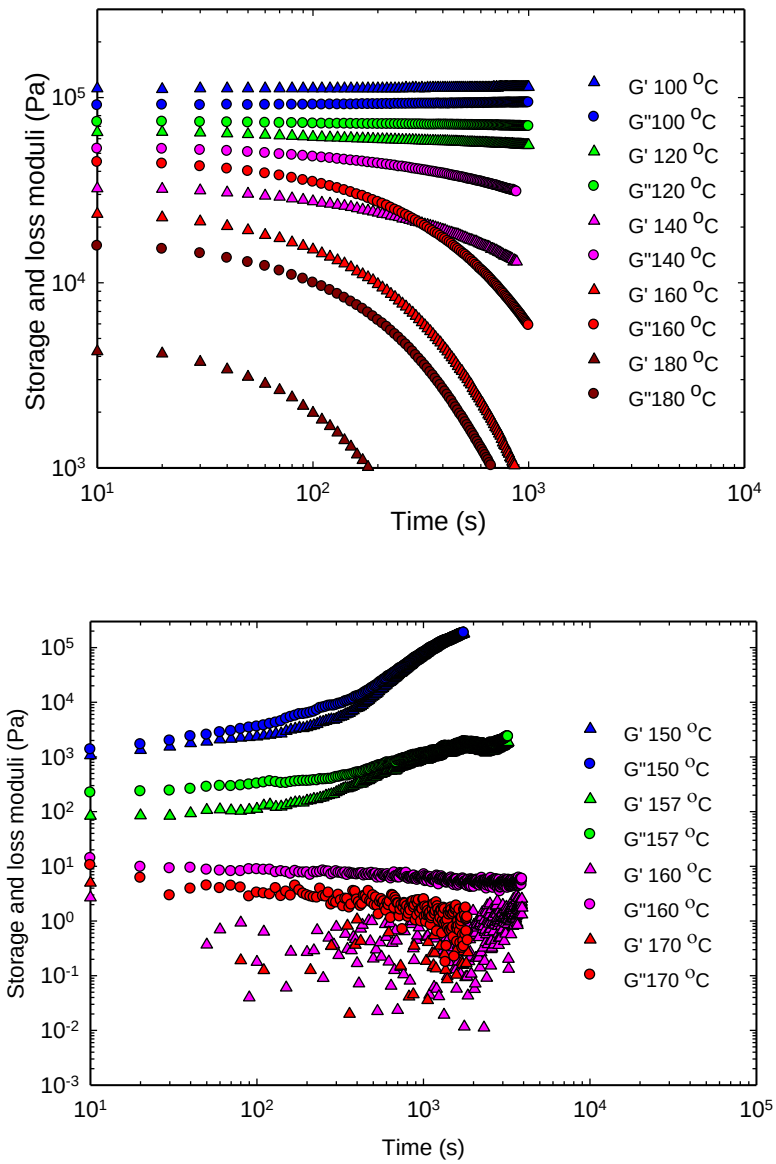

Figure 4.5 Dynamic time sweep test results at different temperatures of **(a)** top, Syndio-rich PHB Table 5 entry 6; **(b)** bottom, Syndiotactic PHB Table 5 entry 1.

Figure 4.6 shows the effect of molecular weight on the complex viscosity of the sydioenriched PHBs (Table 4.5 entries 2-8), and the values of the zero-shear viscosities versus molecular weights of syndio-rich PHBs are depicted in Figure 4.7 at the reference temperature of 80 °C. Syndio-rich PHBs reveal higher melt viscosity compared to their atactic counterparts and follow the power law

relationship with the power of around 3.4, an indication of a linear monodispersed polymer. This is consistent with our previously reported results in chapter 3, showing the effect of PHB microstructure on the melt viscosity of moderately syndiotactic star PHBs. Similar observations have been reported for other syndiotactic polymers including poly(methylmethacrylate), poly(styrene), and poly(propylene).[244,269,270]

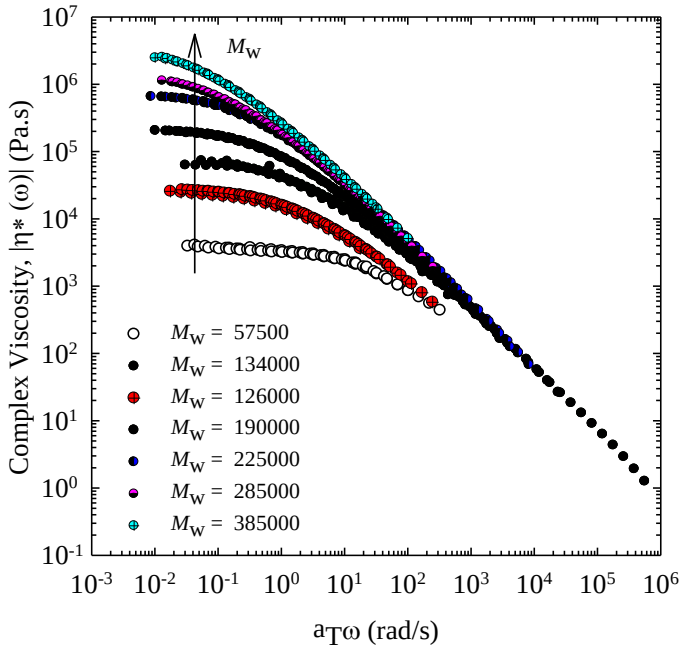

Figure 4.6 Molecular weight dependence of zero shear viscosity of Syndio-rich PHBs of different molecular weights synthesized using (±)-6 as the catalyst in CH_2Cl_2 at RT (Table 4.5, entries 2-8).

For a polymer melt to exhibit strong rubberlike behavior and high melt strength, high entanglement density is crucial. To determine this value, the entanglement molecular weight can be calculated from $M_e = \rho RT/G_N^0$ in which ρ is the density (0.90 g/cm^3), R is the gas constant, T is the reference temperature, and G_N^0 is the plateau modulus.

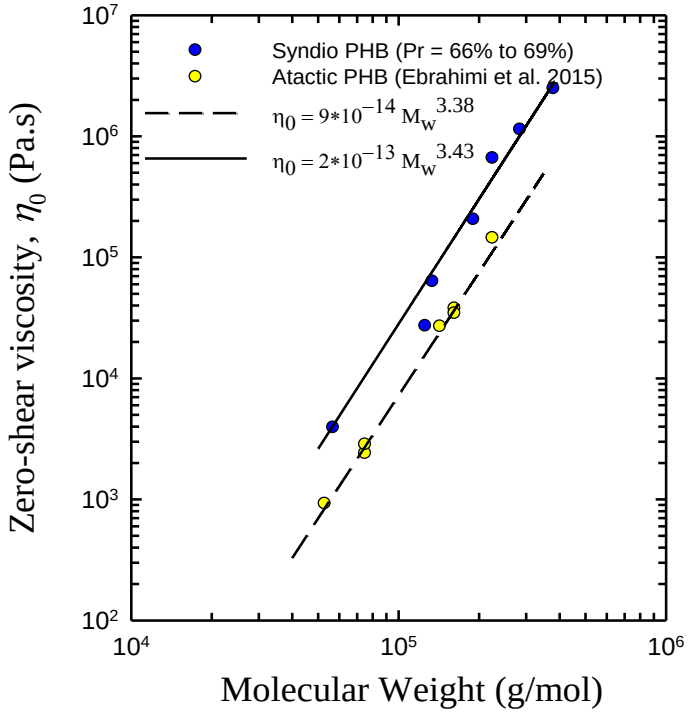

Figure 4.7 Molecular weight dependence of zero-shear viscosity for both series of atactic and syndio-rich PHBs at T_{ref} = 80 °C.

We showed the importance of entanglement molecular weight on melt viscoelastic behavior of moderately syndiotactic star PHBs in chapter 3. Herein this chapter, the entanglement molecular weights of PHBs of different microstructures including highly isotactic bacterial based will also be measured. Isotactic bacterial based PHB, with the weight average molecular weight of 225 $kgmol^{-1}$ and melting point of 185 °C, was provided by Biomer Corporation. Isothermal dynamic frequency sweeps were collected at the temperature range of 185-200 °C and the corresponding master curve produced at 195 °C as the reference temperature (Figure 4.8). The calculated values for isotactic PHBs and also moderately syndiotactic PHB (Table 4.5, entry 6) are listed in Table 4.6.

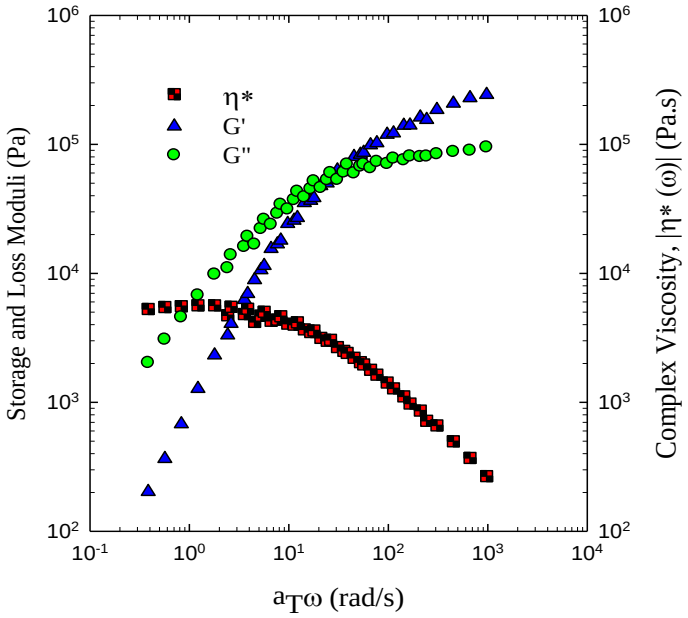

Figure 4.8 Master curve of bacterial based isotactic PHB (iPHB, provided from Biomer Corporation) at T_{ref} = 195 °C.

The data in Table 4.6 show that syndiotactically enriched PHBs have higher entanglement molecular weights (5179 $gmol^{-1}$) compared to the atactic counterpart (4833 $gmol^{-1}$). The entanglement molecular weight of highly isotactic PHB (14600 $gmol^{-1}$), however, is 3 times higher than that of atactic PHB. This result reveals that isotactic PHB has an entanglement density of 15 (225000/14600), while this value is 43 (225000/5179) for syndio-rich PHB (Table 4.6, entries 1 and 3 respectively). This suggests that the low melt strength of isotactic PHB homopolymer is due to very low entanglement densities and to extensive thermal degradations at high temperatures. Similar results have been reported by Frank *et al.* for poly (hydroxybutyrate-co-3-hydroxyhexanoate).[271] As mentioned above, since the highly syndiotactic PHB has very low melt strength and is highly crystalline, it is expected that it possesses high entanglement molecular

weights (stiffer polymer segments) and therefore suffers from lack of entanglements necessary for enhanced mechanical properties.

Table 4.6 Rheological characteristics of PHBs of different microstructures.

	Sample	T_m (°C)	T_{ref} (°C)	G_N^0 (MPa)	M_e (g mol^{-1}) [c]
1	Isotactic PHB	182.7	195	0.24 [a]	14600
2	Syndiotactic PHB Table 5, entry 1	155	-	n.d. [d]	n.d. [d]
3	Syndio-rich PHB Table 5, entry 6	45.5, 66.4	80	0.51 [b]	5179
4	Atactic PHB	-	50	0.50[100]	4833[100]

[a] Determined using $G_N^0 = \frac{2}{\pi}\int_{-\infty}^{\infty} G"(\omega) dln\omega$. [b] Determined from molecular weight independent G'. [c] Calculated using $M_e = \rho RT/G_N^0$ [d] Not determined due to instabilities in rheological measurements.

In various industrial polymer processing operations such as film blowing and blow molding, products form outside the die. For a stable operation, high melt strength is required to avoid instabilities such as sagging and curtaining.[172] Uniaxial extensional rheometry is the simplest rheological experiment that can be used to assess the melt strength of polymers under extensional deformations. The Sentmanat Extensional Rheometer (SER) is a dual wind-up fixture that can be used in conjunction with the rotational rheometer to generate uniform extensional deformation at high Hencky strain rates up to 20 s^{-1} under isothermal conditions.

Figure 4.9 plots the tensile stress growth coefficient of syndio-rich PHB (Table 4.5, entry 6) at several Hencky strain rates from 0.01 to 20 s^{-1} at 80 °C. At Hencky strain rates as low as 0.1 s^{-1} a clear strain hardening effect can be observed and at longer times the tensile stress growth coefficient clearly deviates from the linear viscoselastic behavior. Extensive strain hardening was also observed at higher strain rates up to 20 s^{-1}. Since the temperature used was well above the

melting point of the sample, the hardening effect is solely due to the dynamics of the polymer chains, indicating high melt strength of these polymers.

To understand the origin of strain hardening behavior, DSC was used to determine crystallization effects. DSC results of the stretched samples after performing SER at 1 s^{-1} are listed in Table 4.5 (Figure B.34). These values show that T_{m1} and T_{m2} are increased by 8.6 and 19.3 °C after the imposition of extensional flow. The increased melting points and slightly enhanced melting enthalpy of the crystalline regions of syndio-rich PHBs after SER experiment clearly show the presence of flow induced crystallization due to chain orientation under uniaxial extension.[272,273] Several attempts were made to run SER of bacterial based isotactic PHB and syndiotactic PHB at near their melting points. However due to dramatically low melt strength and sagging no reportable results were obtained. Extensional experiments were also run for high molecular weight atactic PHB at 80 °C and no recordable results were obtained. These observations reveal that to synthesize melt processable PHBs, a high density of entanglement and moderate stereoregularities are required to increase the entanglement density and thus the melt strength of polymers.

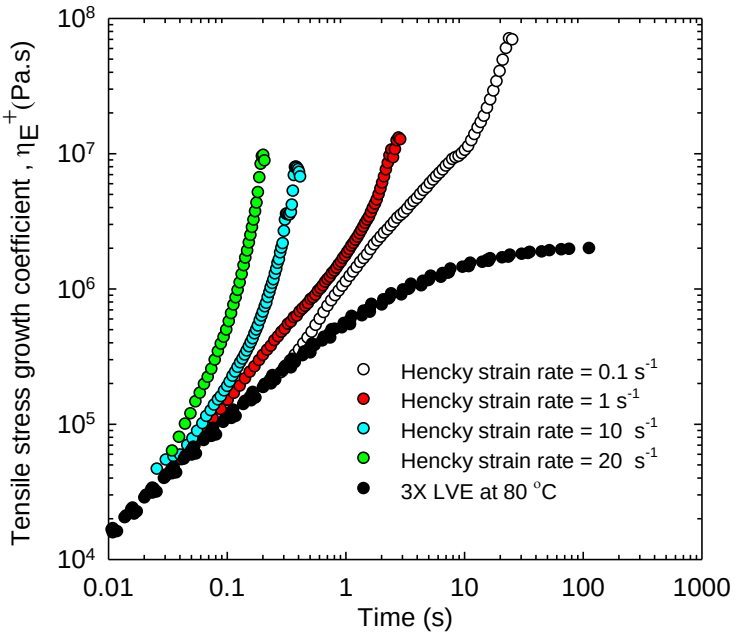

Figure 4.9 Tensile stress growth coefficient as a function of time measured at various Hencky strain rates for Table 5, entry 6 at 80 °C.

To further demonstrate the usefulness of these newly synthesized PHBs in terms of their semicrystalline microstructure and entanglement density, the mechanical behavior of PHBs with different microstructures were investigated using tensile testing (Figure 4.10). The relevant tensile test parameters for Isotactic, syndio-rich, and atactic PHB (Table 4.6 entries 1, 3-4) including tensile strength, elastic modulus, and elongation at break are presented in Table 4.7.

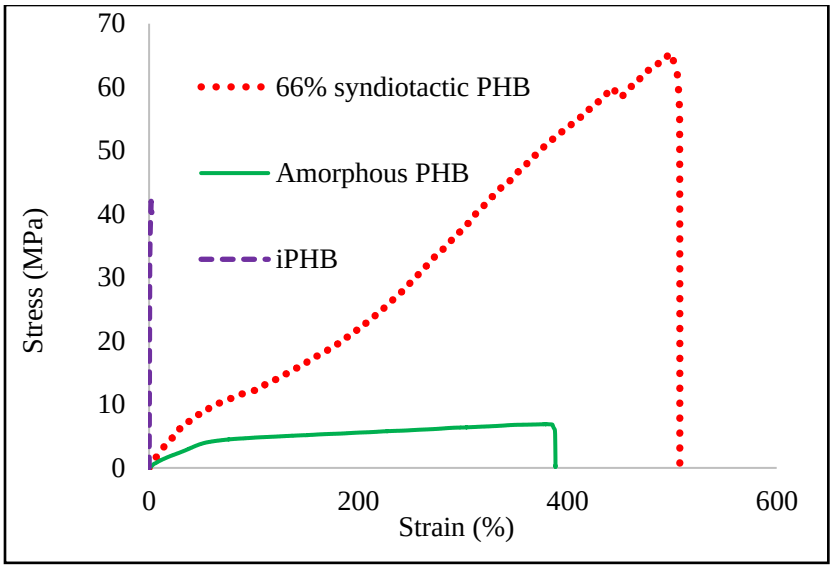

Figure 4.10 Tensile test results of Table 6 entry1 (dashed line), entry 3(dotted line), and entry 4(solid line).

As reported in literature,[58] isotactic PHB shows high tensile modulus, however with very low drawability and low strength, indicative of a brittle weak material. In contrast, atactic PHB shows very low tensile strength but good extensibility, which are characteristics of soft, weak, ductile material. The data in Table 4.7 shows that the syndio-rich PHB sample has considerable extensibility, high tensile strength, and high elastic modulus compared to its polyolefinic counterpart (66% syndiotactic polypropylene).[274] These results demonstrate that semicrystalline syndio-enriched PHBs have the potential to be used in place of their biostable analogues for manufacturing consumer products.

Table 4.7 Tensile properties of PHBs of different microstructures.

	Sample	Tensile strength (MPa)	Elastic modulus (MPa)	Elongation at break (%)
1	Isotactic PHB	43	5500	2.6
2	Atactic PHB [a]	6.5	7	380
3	Syndio-rich PHB [b]	64	25	507
4	66% syndio PP [c]	14	30	700

[a] 100. [b] Sample from Table 5, entry 6. [c] 274

4.3 Summary

In this chapter, we showed that using the right catalytic systems, it is possible to generate processable PHB. A series of zinc complexes supported by diaminophenolate ligands are introduced as excellent catalysts for the controlled living and immortal polymerization of BBL. Importantly, using these catalysts, syndio-rich PHBs of high molecular weight were obtained. These complexes revealed surprisingly high tolerance to high loadings of alcohols (up to 5000 equivalents) and to polymerization of high loadings of BBL to form high molecular weight PHB ($\leq$ 385 kgmol^{-1}). The thermorheological properties of the high molecular weight syndio-rich PHBs showed good thermal stabilities in the absence of any additives and excellent melt strength, which shows for the first time that PHB can be a processable thermoplastic.

.

Chapter 5: Air and moisture stable indium salan catalysts for living multi-block PLA formation in air

While the application based production of PLA takes place in the melt state under air, often with minimally purified monomers, the majority of highly controlled catalysts reported in the literature lose their catalytic activity and/or selectivity under these conditions. In this chapter an air and moisture stable hydroxy-bridged indium salan complex will be introduced as a highly active and controlled catalyst for the ring opening polymerization of cyclic esters in air. The reversible activation of this complex with linear and branched alcohols leads to immortal polymerization, allowing the controlled formation of block copolymers in air. This complex is the only reported moisture resistant catalyst for high molecular weight PLA production. Controlled star-block copolymerization of PLA and PHB under inert atmosphere will also be reported.

5.1 Introduction

As it was mentioned in the chapter 1, aliphatic polyesters, such as poly (lactic acid) (PLA) and other poly (hydroxyalkanoates) are increasingly important members of biodegradable and biocompatible materials.[275-279] These important polymers can be synthesized through well-explored organocatalytic,[32,33] as well as main group and transition metal-based, ring opening polymerization.[9,10,34-48] However, despite these concentrated efforts in catalyst development, tin octanoate ($Sn(Oct)_2$) remains the most common metal-based catalyst used for ring opening polymerization (ROP) in industrial applications and pharmaceutical studies.[32,33,38,39,41-44,280,281]

$Sn(Oct)_2$ allows the ROP of lactide (LA) in the melt without the use of ultrapure monomers. However, the facility of reactivity comes at a price: $Sn(Oct)_2$ lacks control over polymer molecular weight and dispersity, which prohibits formation of complex polymer morphologies such as

multiblock copolymers. Nor is it active for some lactones such as β-butyrlactone (BBL).[1,6,48-55] This limits the range of possible polymers available widely for industrial or pharmaceutical applications.

Despite the recent focus in the literature to develop air/water stable catalysts for a range of catalytic applications,[282-292] fewer efforts have been made to develop air and moisture resistant metal-based catalysts for ROP of cyclic esters that can be used under industrially-relevant conditions.[293] Zinc complexes bearing guanidine-pyridine ligands,[294] and magnesium–sodium/lithium heterobimetallic complexes[295] are active for the ring opening polymerization (ROP) of lactide under industrially relevant conditions, however the polymerizations are sluggish (high conversion is achieved after 24-48 hours) and suffer from extensive transesterification reactions which limits control over polymer macrostructure.[295,296] Indium catalysts bearing pyridine bisphinal ligands polymerize 100 equivalents of lactide in air at 80 °C over the course of 24h with 86% conversion.[297] Other air stable catalysts with Al,[298] Cu,[299] Ti,[300] Y,[301] and Mg-Na/Li,[295] metal centres have been reported; however, in these studies polymerization reactions were carried out under inert conditions. Mg[302], and Ti-based[303] catalysts for the polymerization of caprolactone in air have been reported. To our knowledge, there are no reported examples of metal-based catalysts for the highly-controlled polymerization and block copolymerization of lactide in air.

In this chapter, an air and moisture stable indium catalyst will be reported for the first time. This catalyst is supported by easy to make diaminobisphenolate (salan) ligands with secondary amine backbones for the ring opening copolymerization of lactide in air. This complex catalyzes the rapid ring opening of lactide, in solution or in the melt, to form linear and star shaped high

molecular weight PLA triblock copolymers and PLA-PHB block copolymers with an unprecedented combination of high activity and control over molecular weight and dispersity.

5.2 Results and discussion

5.2.1 Synthesis and characterization of air/moisture stable complexes 17 and 18

Asymmetrically bridged dinuclear salan indium alkoxy complexes (*RR/RR*)-[(ON_HN_HO)In]$_2$(μ-Cl)(μ-OEt) (**17**) were prepared from (*RR*)-*N,N'*-bis(3,5-di-tertbutylsalicylidene)-1,2-cyclohexanediamine (*RR*-$H_2(ON_HN_HO)$ or salan)[304-307] in two consecutive salt metathesis reactions (Scheme 1). Although the reaction is similar to the synthesis of the salen analogue, (**K**)[166,167] (Figure 5.1), there are some differences.

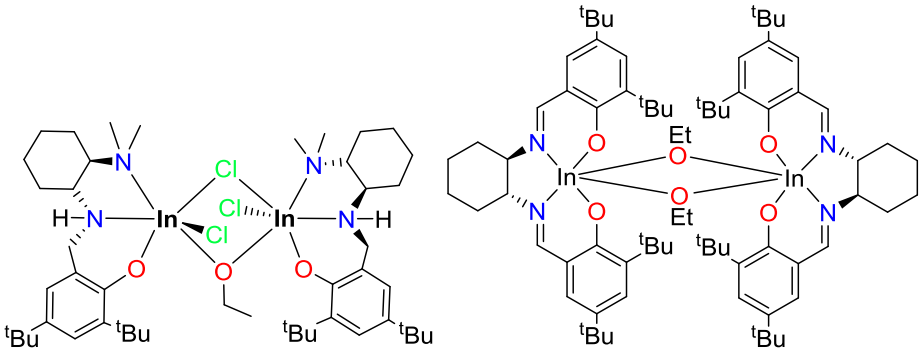

Figure 5.1 Dinuclear indium complexes for ring opening polymerization of lactide.[161,167]

Deprotonation of $H_2(ON_HN_HO)$ with KO^{t}Bu forms the resulting $K_2(ON_HN_HO)$. However, the subsequent salt metathesis reaction require greater than two equivalents of $InCl_3$ to form an indium-chloro intermediate which was not isolable. This species was reacted with excess NaOEt to form complex **17** in 55% yield based on $H_2(ON_HN_HO)$ (Scheme 5.1, Figure C.1-5).

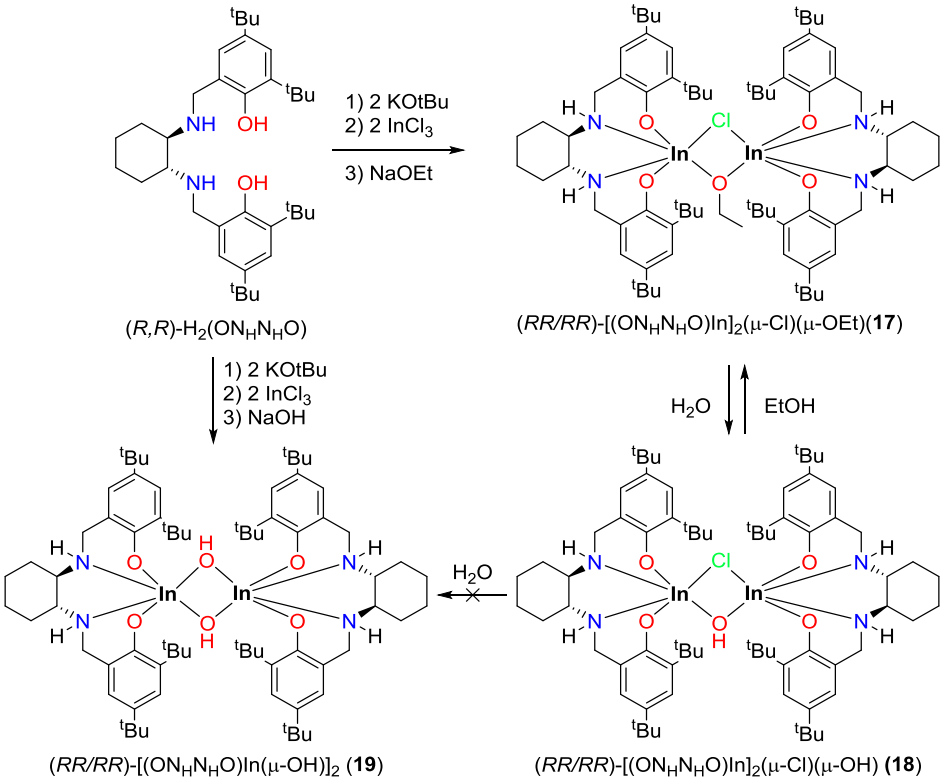

Scheme 5.1 Synthesis of dinuclear indium complexes.

Exposure of complex **17** to trace water in CH_2Cl_2 for 48 h formed asymmetrically bridged (*RR/RR*)-[(ON_HN_HO)In]$_2$(μ-Cl)(μ-OH) (**18**) (Scheme 5.1, Figure C6-7) (95% yield). Solid-state structures of **17** and **18**, derived by single-crystal X-ray diffraction, are similar to dinuclear complexes **D** and mono-hydroxy bridged analogue [(NN_HO)InCl]$_2$(μ-Cl)(μ-OH)[238] respectively, and show distorted octahedral indium centers asymmetrically bridged by chloride and ethoxy (or hydroxy) ligands (Figure 5.2, Table C1-2). The PGSE derived diffusion coefficients of complexes **17** (6.7(1) × 10^{-10} m^2s^{-1}) and **18** (6.5(6) × 10^{-10} m^2s^{-1}) are 28-30% lower than that of the proligand[267] (9.4(3)×10^{-10} m^2s^{-1}) and confirm dinuclear solution structures for both species (Figure C.16, Table C.5).[308]

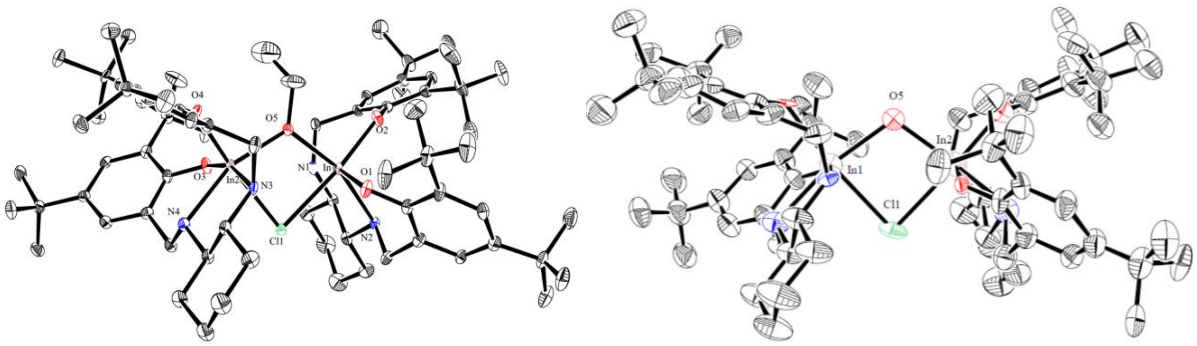

Figure 5.2 Molecular structures of (*RR/RR*)-**17** (a, top) and (*RR/RR*)-**18** (b, bottom) (depicted with thermal ellipsoids at 50% probability. H atoms as well as solvent molecules omitted for clarity).

The lack of reactivity of complex **18** with water is unexpected and contrasts with previously reported systems. While complex **D** reacts with water to form bis-hydroxylated complex $[(NN_HO)In)(\mu\text{-}OH)]_2$ [238], and **K** undergoes significant decomposition,[309] complex **18** does not convert to the bis-hydroxy bridged complex $[(ON_HN_HO)In(\mu\text{-}OH)]_2$ (**19**) in the presence of water (Scheme 1). Complex **19** can be prepared independently from $H_2(ON_HN_HO)$ after consecutive reactions with KO^{t}Bu, excess $InCl_3$, and excess NaOH and is characterized in solution and in the solid state (Figures C.8, Table C.3).

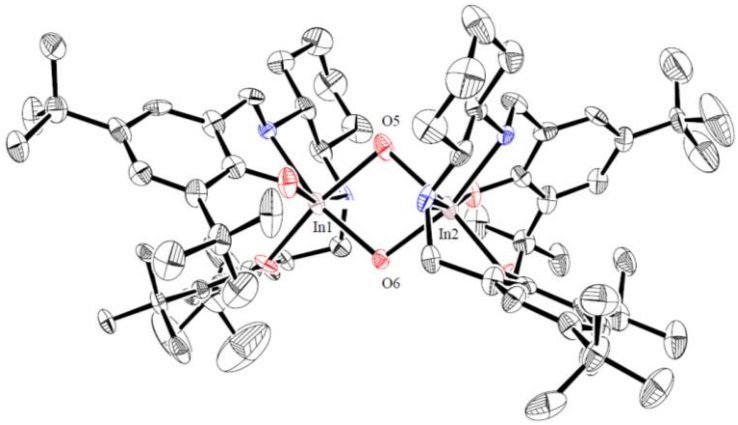

Figure 5.3 Molecular structure of complex (*RR,RR*)-**19** (depicted with thermal ellipsoids at 50% probability. H atoms as well as solvent molecules omitted for clarity).

A solid sample of complex **18** was exposed to air for over 60 days and was monitored using ^{1}H NMR spectroscopy during and after this period. These spectra show that complex **18** remains unchanged (Figure 5.4). Under more forcing conditions, for example exposure to air for more than two months or addition of 100 equivalents of water, the ^{1}H NMR spectrum of the mixture shows only the presence of **18** and traces of free ligand, with absolutely no traces of complex (**19**) (Figure 5.4).

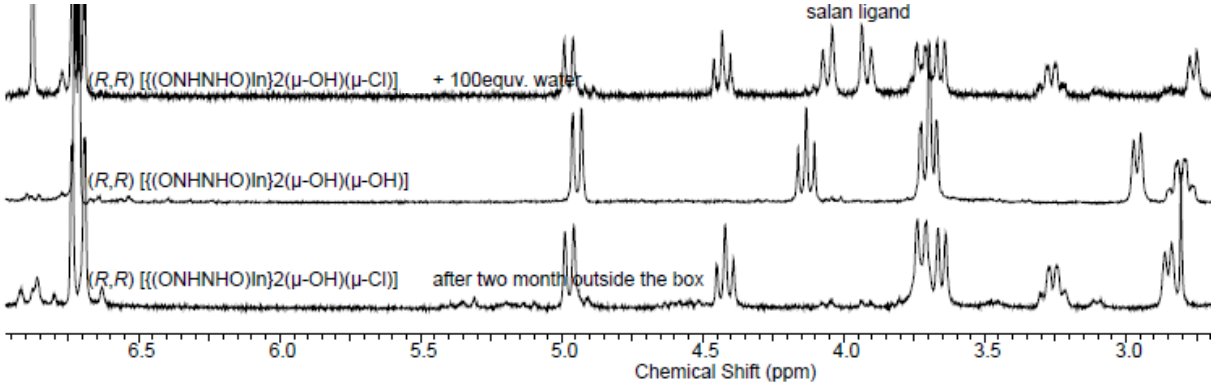

Figure 5.4 ^{1}H NMR spectrum ($CDCl_3$, 25 °C, 400MHz) of (*RR*/*RR*)-**18** (bottom) after exposure to air for over 60 days overlaid with (*RR*/*RR*)-**19** (middle), and the results after stirring (*RR*/*RR*)-**18** in DCM in the presence of 100 equivalences of water(top).

Most importantly, the hydroxylation reaction of complex **18** is reversible. The hydroxy species complex **18** can be stirred in neat ethanol to regenerate active complex **17** with more than 90% purity (Scheme 5.1, Figure C.12). Therefore, complex **18** can be used as an air stable surrogate for complex **17** which is an excellent catalyst for cyclic ester polymerization.

5.2.2 Living ring opening polymerization of LA and BBL to form homo and block copolymers

Polymerization of up to about 2000 equivalents of racemic lactide (*rac*-LA) with complex **17** shows a linear relationship between M_n and added monomer equivalence. This catalyst is capable of forming high molecular weight PLA (up to 320000 $gmol^{-1}$) with very low dispersity, which is indicative of a highly controlled and living system (Table 5.1, Figure 5.5).

Table 5.1 Ring opening polymerization of *rac*-lactide with (*RR/RR*)-**17**

Entry	Monomer	[LA] : [initiator]	Conv.[a] (%)	$M_{n,theo}$[b]/g mol^{-1}	$M_{n,GPC}$[c]/g mol^{-1}	$Đ$ [c]
1	*rac*-LA	213	> 99%	30750	43800	1.13
2	*rac*-LA	400	> 99%	57700	91300	1.10
3	*rac*-LA	650	> 99%	93730	106800	1.11
4	*rac*-LA	854	> 99%	123130	168900	1.33
5	*rac*-LA	1496	> 99%	215660	189700	1.01
6	*rac*-LA	1692	> 99 %	243900	219300	1.02
7	*rac*-LA	1950	> 99 %	282000	321000	1.03

All reaction carried out in CH_2Cl_2 at 25 °C, 16h. [a] Monomer conversion, determined by ^1H NMR spectroscopy. [b] Calculated from $[M]_o/[initiator] \times$ monomer conversion $\times M_M + M_{EtOH}$ (M_{LA} = 144.13 $gmol^{-1}$, M_{EtOH} = 46 $gmol^{-1}$). [c] Determined by GPC-MALS, dn/dc = 0.044 mL/g for PLA in DCM).

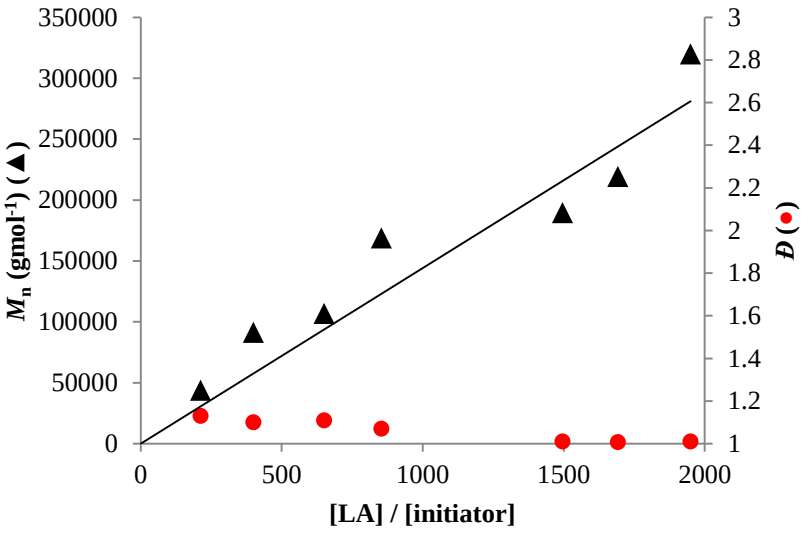

Figure 5.5 Plot of observed PLA M_n (▲) and molecular weight distribution (●) as functions of *rac*-LA/ethoxide in (*RR*/*RR*)-**17** (25 °C, CH_2Cl_2, 99% conv.) The line indicates calculated M_n values based on the *rac*-LA/ethoxide ratio (Table S6).

The MALDI–TOF spectra of PLA oligomers made with this catalyst shows peaks corresponding to $[H(C_6H_8O_2)_n(OEt)H]^+$ separated by m/z = 144, which indicates the absence of any transesterification reactions, and the fact that the polymerization proceeds through coordination-insertion mechanism (Figure 5.6).

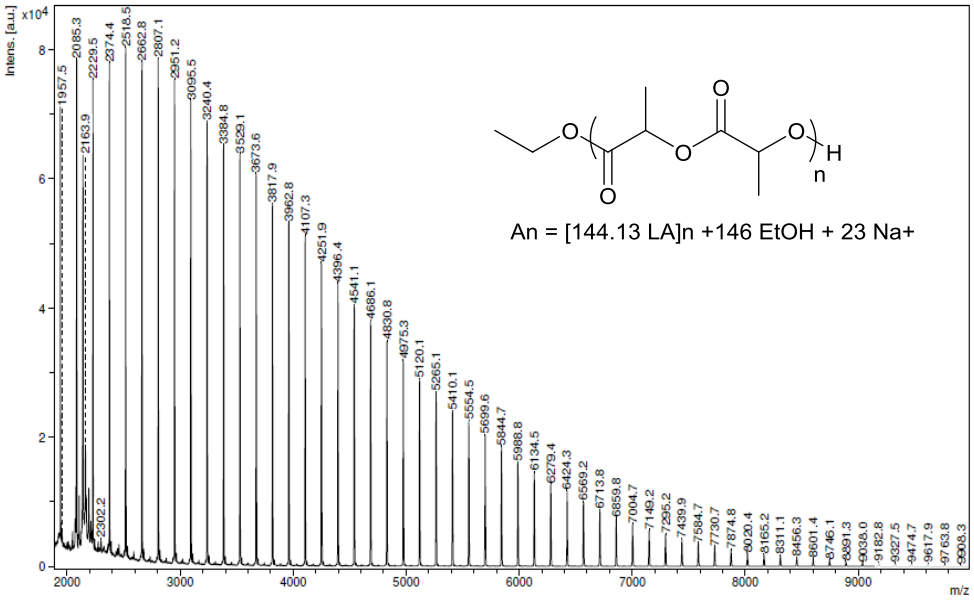

Figure 5.6 MALDI-TOF mass spectrum of PLA produced by (*R*/*R*,*R*/*R*)-**17** from ROP of 50 equivalents of *rac*-lactide. $A_n = [144.13_{LA}]_n + 46_{EtOH} + 23_{Na+}$.

The rate of polymerization is first order in LA concentration with k_{obs} values (k_{obs} = 3.1(0.8)× 10^{-4} s^{-1}) comparable to indium complexes (**D**) (k_{obs} = 6.2 (0.16) × 10^{-4} s^{-1}), and (**K**) (k_{obs} = 4.6 (0.9) × 10^{-4} s^{-1}) (Figure 5.7). The stereoselectivity of (*RR/RR*)-**1** for the polymerization of *rac*-LA differs from that of complex **D**.[165] A comparison of the ROP rates for D- and L-LA with (*RR/RR*)-**17** shows a k_L/k_D value of ~3 which is lower than the value of ~14 observed for (*RR*/*RR*)-**D** (Table 5.2).[165] In addition, polymerization of *rac*-LA with (*RR*/*RR*)-**17** yields heterotactically enriched PLA (P_r = 0.72) from the polymerization of *rac*- LA as determined by $^1H\{^1H\}$ NMR spectroscopy (Figure C.17).

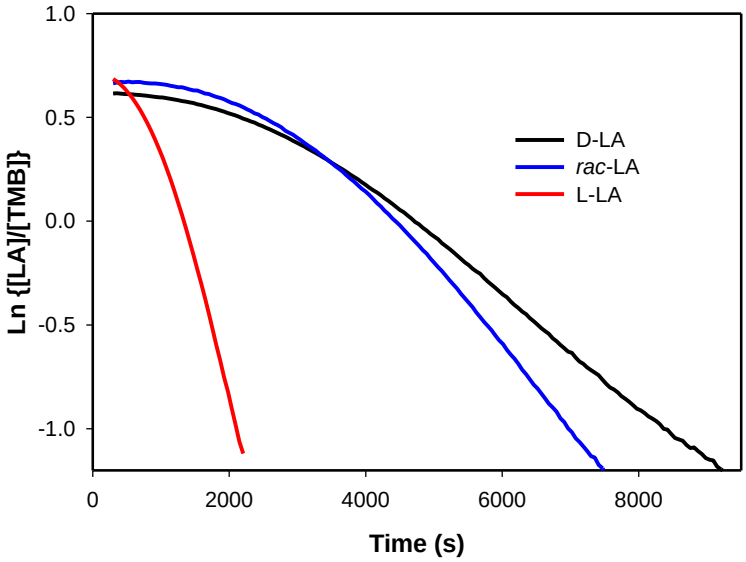

Figure 5.7 Plots for the ROP of 200 equiv L-LA, D-LA, and rac-LA vs. time for (*RR/RR*)-**17**. All reactions were carried out in CD_2Cl_2 at 25 °C and followed to 90% conversion. [Catalyst] = 0.0011 M, [LA] = 0.45 M. k_{obs} was determined from the slope of the plots of ln([LA]/[TMB]) vs. time (TMB = 1,3,5-trimethoxybenzene).

Table 5.2 Rates of the ROP of 200 equiv L-LA, D-LA, and rac-LA vs. time for (*RR/RR*)-**17**

	Monomer	$k_{obs}{}^{a} \times 10^{-4}$	k_{rel}
1	*rac*-LA	3.1(0.8)	
2	L-LA	12.5(0.3)	2.9
3	D-LA	4.2(0.5)	

All reactions were carried out in CD_2Cl_2 at 25 °C and followed to 90% conversion. [Catalyst] = 0.0011 M, [LA] = 0.45 M. k_{obs} was determined from the slope of the plots of ln([LA]/[TMB]) vs. time (TMB = 1,3,5-trimethoxybenzene). [a] Determined from the negative of the slope of the linear portions of the plots of ln([LA]) vs. time

Complex **17** also catalyzes controlled living polymerization in the presence of a chain transfer agent (immortal polymerization). Polymerizations of *rac*-LA in the presence of up to 100 equivalents of ethanol, catalyzed by (±)- or (*RR*/*RR*)-**17**, generates monodispersed PLAs with

excellent control of molecular weight (Table 5.3, entries 1-4). The decrease of the actual molecular weight of the produced PLAs with the increase of the ethanol loading, indicates that the transfer reaction proceeded efficiently and therefore the number of the produced polymer chains per molecule of catalyst is equal to the equivalence of the added ethanol, which increase the catalyst efficiency and reduces metal contamination (Figure 5.8). Also, these results confirm that this catalyst does not undergo any deactivation or dissociation in the presence of high loadings of transfer agents.

Table 5.3 Immortal ring opening polymerization of *rac*-lactide and BBL with (*RR*/*RR*)-**17**, (*RR*/*RR*)-**18**, and *in-situ* formed –OTHMB bridged complex **17***

	Cat.	**M1(M2)**	**CTA**	**Solv.**	**[M1+M2]/ [CTA]/ [initiator]**	**Conv. [b] (%)**	$M_{n,theo}$ [c]/ g mol^{-1}	$M_{n,GP}$ [d]/ g mol^{-1}	$Đ$ [d]
1	**17**	*rac*-LA	EtOH	DCM	1000/5/1	> 90	21600	15780	1.01
2	**17**	*rac*-LA	EtOH	DCM	1000/10/1	> 90	11830	9610	1.03
3	**17**	*rac*-LA	EtOH	DCM	1000/50/1	> 99	2840	2580	1.05
4	**17**	*rac*-LA	EtOH	DCM	1000/100/1	> 99	1460	1580	1.10
5	**18**	*rac*-LA	EtOH	DCM	1000/10/1	> 95	13730	12430	1.06
6	**18**	*rac*-LA	EtOH	DCM	2000/10/1	> 90	25970	27230	1.08
7	**17***	*rac*-LA	THMB	THF	2500/10/1	> 99	35800	38500	1.01
8	**17***	BBL	THMB	THF	2500/10/1	> 90	19520	16890	1.02
9[a]	**17***	BBL(*rac*-LA)	THMB	THF	2500+2500/10 /1	> 90	53200	48600	1.01

All reaction carried out at 25 °C over 16h to >90% conversion under inert dinitrogen atmosphere inside the glovebox. [a] Order of monomer BBL followed by LA, conversion BBL:L-LA 90:94. [b]Monomer conversion determined by ^{1}H NMR spectroscopy. [c] Calculated from $([M1]_o/([ROH]/[I]) \times$ monomer conversion $\times M_{M1}) + ([M2]_o/([ROH]/[I]) \times$ monomer conversion $\times M_{M2}) + M_{ROH}$ (M_{BBL} = 86.09 g/mol, $M_{L\text{-}LA}$ = 144.13 g/mol, M_{THMB} = 168.19 g/mol). [d] Determined by GPC-MALS in THF using dn/dc = 0.068 for PHB and 0.044 for PLA. ***** After stirring complex (**17**) in a THMB solution for 1 hr, the solvent and the released ethanol are removed under vacuu followed by dissolving in THF and addition of the monomer.

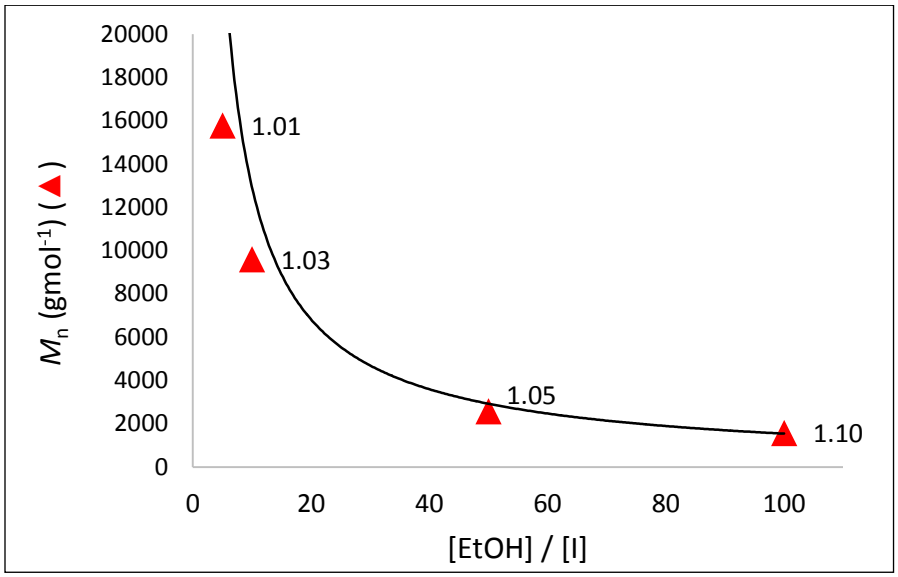

Figure 5.8 Plot of observed PLA Mn (▲) as functions of EtOH/(*RR*/*RR*)-**17** (25 °C, CH_2Cl_2, 99% conv.). Molecular weight distribution are shown in parenthesis. The line indicates calculated M_n values based on the LA/ethoxide ratio.

Chain-end analyses of the PLA oligomers (n = 25, $M_{n,theo}$ = 3646) by MALDI-TOF mass spectroscopy clearly revealed the major population of $[H(C_6H_8O_2)_n(OEt)H]^+$ separated by m/z = 144 which shows the absence of any transesterifications. The degree of polymerization resulted from this spectrum (n = 27, $M_{n,MS}$ = 3960) is in good agreement with the theoretical value, indicative of the controlled and immortal nature of the catalytic process with the (*RR*/*RR*)-**17** in the presence of EtOH (Figure 5.9). Similar reactivity is observed in the presence of the trio1,3,5-tris (hydroxymethyl)benzene (THMB) to form well-controlled star shaped (co)polymers.[100,113]

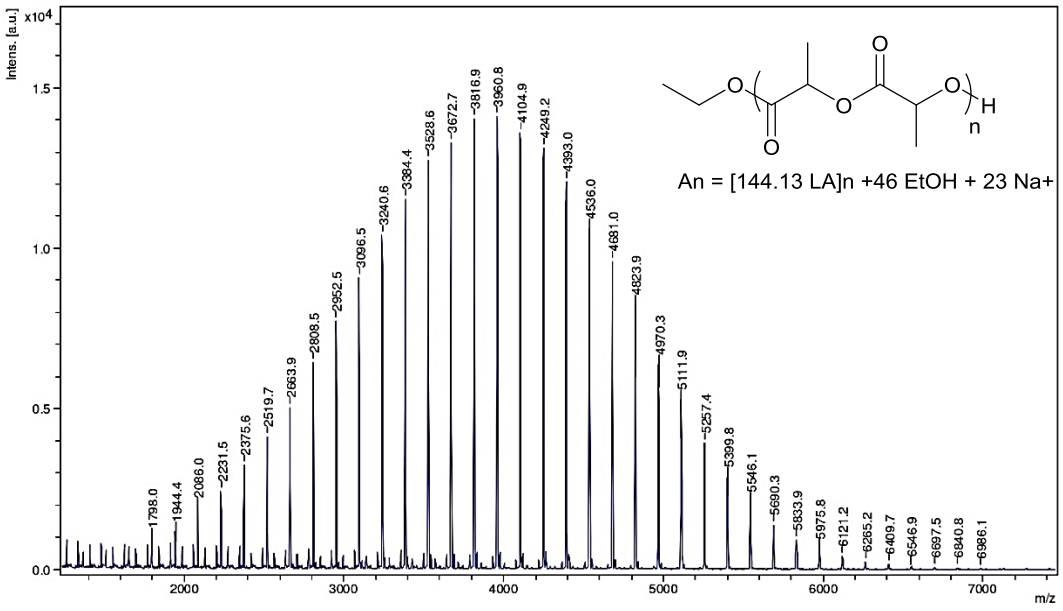

Figure 5.9 MALDI-TOF mass spectrum of PLA isolated from polymerization of [LA]:[EtOH]:[**17**] ratios of 500/20/1 in CH_2Cl_2 at 25 °C. An = $[144.13_{\ LA}]_n +46_{\ EtOH} + 23_{\ Na+}$.

Complex **17** catalyzes immortal polymerization of 2500 equiv of BBL or *rac*-LA with [THMB]:[**I**] ratios of 10 (Table 5.3, entries 7 and 8) to form star PHB and PLA. The resulting polymers have predictable molecular weights and narrow molecular weight distributions which shows that this catalyst is a robust system to form symmetric star polymers. Additionally, this system is capable of forming star block-copolymers of PHB and PLA. Sequential addition of BBL followed by *rac*-LA to *in-situ* formed –OTHMB bridged complex **17** forms star block copolymers of PHB- PLA (Table 5.3, entry 9): the first addition of 2500 equiv of BBL yields symmetric 3-arm star PHB homopolymer with M_n value of 17 $kgmol^{-1}$. Following by this, the addition of 2500 equiv *rac*-LA to the reaction mixture of 3-arm star PHB allows formation of 3-arm star copolymer PHB-PLA with predictable molecular weight (Figure 5.10). The agreement between experimental and theoretical molecular weights and the fact that the produced polymers are highly

monodispersed, implies that complexes **17** and **18** are robust systems against high loadings of alcohols and proceed the polymerization in living mode.

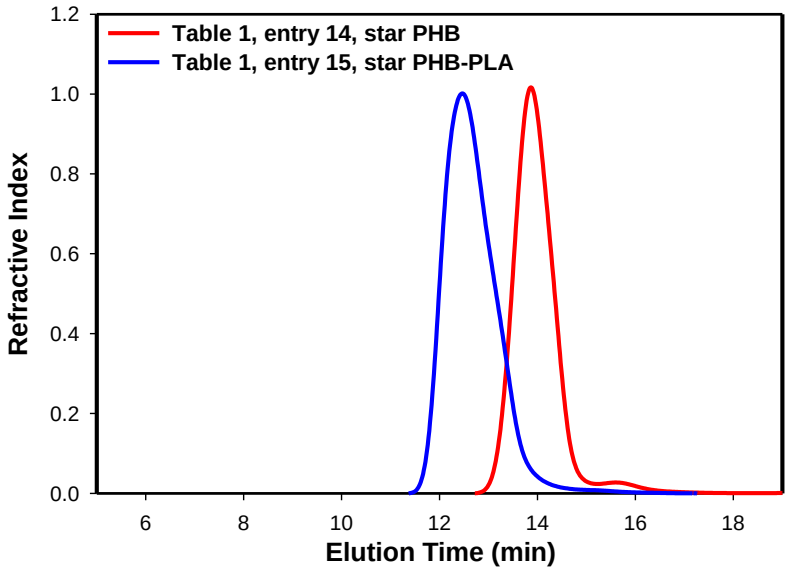

Figure 5.10 GPC overlaid chromatograms of 3-arm star PHB obtained from the polymerization with [BBL]/[THMB]/[**17**] ratios of 2500/10/1 (M_n =16890 gmol^{-1} , $Đ$= 1.02) and 3-arm star di-block copolymers of PHB-PLA obtained from the polymerization with [BBL+L-LA]/[THMB]/[**17**] = 2500/2500/10/1(M_n = 48600 gmol^{-1}, $Đ$= 1.01) in THF at 25 °C (Table 1, entries 14 and 15).

5.2.3 Polymerization and block copolymerization of as-received lactide

Complex **18** shows unprecedented control over the polymerization of unpurified *rac*-LA in air in the presence of chain transfer agents (Table 5.4). Reaction of **18** with lactide in toluene at 80 °C in the presence of up to 10 equivalents of ethanol yields polymers with predictable molecular weights and controlled dispersities (Table 5.4, entries 1-3.) We can carry out the reaction in the melt when using a high boiling alcohol such as THMB as a CTA. Reaction of complex **18** with up to 10000 equivalents of LA in the presence of up to 100 equivalents of THMB in the melt forms highly controlled star-PLAs (Table 5.4, entries 4-7).

Table 5.4 ROP of impure/wet *rac*-LA, and block copolymerization of industrially relevant recrystallized L-LA and D-LA using complex **18** in air.

	M1-M2-M3	CTA	[M] / [CTA] / [2]	Solvent	Temp (°C)	Time (min)	$M_{n,theo}$ [b] ($gmol^{-1}$)	$M_{n,GPC}$ [c] ($gmol^{-1}$)	$Đ$ [c]
1	*rac*-LA	EtOH	1500/2/1	Tol	80	240	106970	73960	1.33
2	*rac*-LA	EtOH	1500/5/1	Tol	80	240	42810	36200	1.36
3	*rac*-LA	EtOH	1500/10/1	Tol	80	240	21430	24980	1.32
4[a]	*rac*-LA	THMB	5000/10/1	-	120	120	52730	50080	1.07
5[a]	*rac*-LA	THMB	5000/50/1	-	120	120	11540	11800	1.06
6[a]	*rac*-LA	THMB	5000/100/1	-	120	120	5570	6900 [d]	-
7[a]	*rac*-LA	THMB	10000/10/1	-	120	120	100970	91200	1.34
8	LLA	THMB	520/21/1	-	130	30	3570	3510 [d]	-
9	LLA[e]	THMB	526/22/1	-	130	30	3460	3800 [d]	-
10[a]	LLA[e]-DLA[e]	THMB	526+526/22/1	-	155	60	6360	6100[d]	-
11[g]	LLA[e]-DLA[e]-LLA[e]	THMB	243+120+243/6/1	-	155	120	11220	10200	1.05
12[g]	LLA[e]-DLA[e]-LLA[e]	THMB	700+500+700/8/1	-	155	300	31000	28500	1.10
13[g]	LLA-DLA-LLA[f]	THMB	700+500+700/8/1	-	155	300	34370	30300	1.05

All reactions performed in ambient atmospheric conditions without any protection of inert gases and wet/impure lactide was used for polymerization. Monomer conversion, determined by ^{1}H NMR spectroscopy and unless indicated 90-99%. [a] Reactions stopped after 120 minutes, 70-80% conversion. [b] Calculated from $[M]_o/[initiator] \times$ monomer conversion $\times M_M + M_{CTA}$ (M_{LA} = 144.13 g/mol, M_{BBL} = 86.09 g/mol, M_{EtOH} = 46 g/mol, M_{THMB} = 168.19 g/mol). [c] Determined by GPC-MALS, dn/dc = 0.044 and 0.068 mL/g, respectively, for PLA and PHB in THF. Chloroform was used as the GPC solvent for PLLA, PLLA-PDLA, and PLLA-PDLA-PLLA, dn/dc = 0.029 mL/g). [d] NMR/MALDI-TOF molecular weight. [e] Recrystallized lactide. [f] Purified monomers, reactions carried out under nitrogen using *in-situ* formed THMB bridged complex. [g] Racemic complex **18** was used.

To our knowledge, complex **18** is the only system able to catalyze the formation of high molecular weight, monomodal star-PLAs from unpurified *rac*-LA in the melt, under air, and with high reactivity. The purity of the lactide was not a factor for reactivity: immortal polymerization reactions with THMB carried out with as-received commercial grade lactide and thrice-recrystallized lactide yielded identical results (Table 5.4, entries 8-9). Importantly complex **18** catalyzes the formation of di-block and triblock star shaped PLA in the melt in air (Table 5.4, entries 10 and 11). The monomodal molecular weight distribution of the prepared di- and tri-block copolymers confirms the absence of any homopolymerizations, even after the third monomer addition (Figure 5.11). As a general polymerization procedure, after weighting out the required amounts of (*RR/RR*)-**18** and THMB in a Schlenk flask outside the dinitrogen glovebox, L-LA was added and the reaction started by immersing the flask in oil bath at 130 ^{o}C. After full conversion, D-LA was added and the temperature raised to 155 ^{o}C along with the addition of few drops of toluene to ease stirring. After full conversion of the monomer, another batch of L-LA was fed to the reaction to form tri-block copolymer of PLLA-PDLA-PLLA in 2 hours. Both ^{1}H NMR and MALDI-TOF results confirm the presence of –OH and –OTHMB chain ends, indicating that the polymerization proceeds via a coordination-insertion mechanism under these conditions (Figure 5.12 and C.20). However, leaving the reaction for longer times after monomer depletion, causes minor intermolecular transesterification side reactions evidencing by the appearance of a lactyl unit with the molar mass of 72 at the chain end (Figure 5.12).

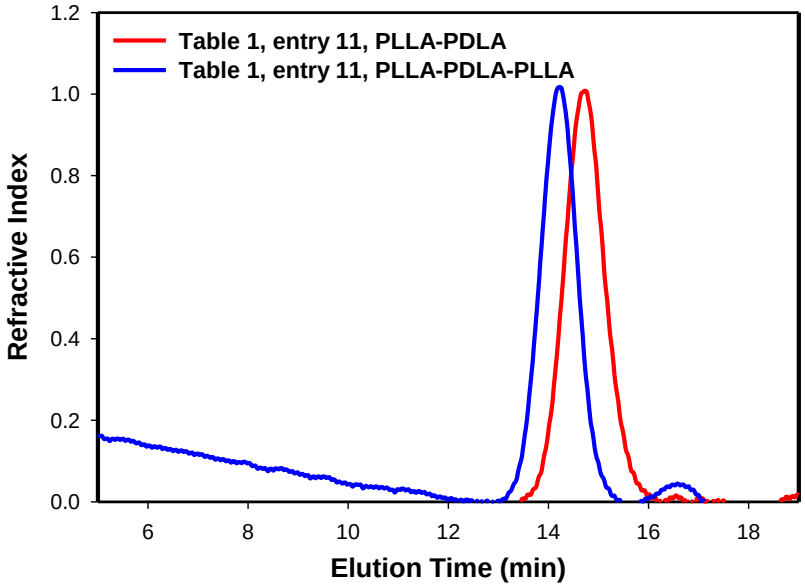

Figure 5.11 GPC overlaid chromatograms of 3-arm star di-block copolymers of PLLA-PDLA obtained from the polymerization with [L-LA+D-LA]/[THMB]/[**18**] ratios of 243+120/6/1(M_n =85960 gmol^{-1}, $Đ$= 1.03), and 3-arm star tri-block copolymers of PLLA-PDLA-PLLA obtained from the polymerization with [L-LA+D-LA+L-LA]/[THMB]/[1] ratios of 243+120+243/6/1 (M_n = 10200 gmol^{-1}, $Đ$= 1.05) in melt state at 155 °C in air (Table 5.4, entry 11).

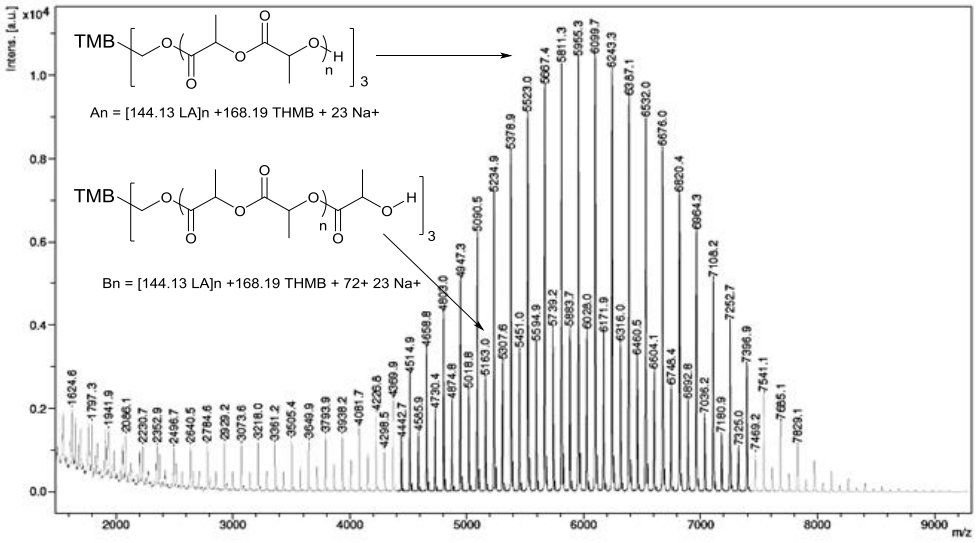

Figure 5.12 MALDI-TOF mass spectrum of Table 5.4, entry 10 after monomer deplition in melt state in air (sample was collected after 60 mins. Time of the experiment is not optimized). An = [144.13 $_{LA}$]$_n$ +168.19 $_{THMB}$ + 23 $_{Na+}$ and Bn = [144.13 $_{LA}$]$_n$ +168.19 $_{THMB}$ + 72+ 23 $_{Na+}$.

The agreement between experimental and theoretical molecular weights of the resulting block copolymers, along with very narrow molecular weight distributions, and the fact that sequential monomer addition leads to complete conversion of the monomer and increase of the molecular weight (Table 5.4, entries 9 and 10) imply excellent control in these systems and the living characteristic of the polymerization.

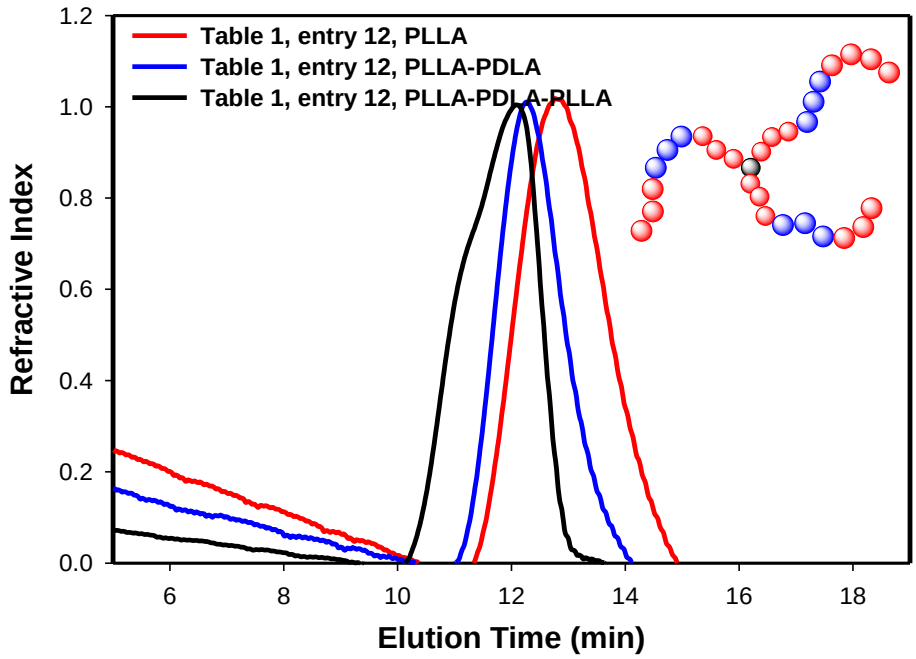

Figure 5.13 GPC overlaid chromatograms of 3-arm star PLLA obtained from the polymerization with [L-LA]//[THMB]/[**18**] ratios of 700/8/1 (M_n =16500 gmol^{-1}, $Đ$= 1.06), 3-arm star di-block copolymers of PLLA-PDLA obtained from the polymerization with [L-LA+D-LA]/[THMB]/[**18**] ratios of 700+500/8/1(M_n = 24160 gmol^{-1}, $Đ$= 1.07), and 3-arm star tri-block copolymers of PLLA-PDLA-PLLA obtained from the polymerization with [L-LA+D-LA+L-LA]/[THMB]/[**18**] ratios of 700+500+700/8/1 (M_n = 28500 gmol^{-1}, $Đ$= 1.10) in neat at 155 °C (Table 5.4, entry 12). The slight broadening of the chromatogram is due to the lack of homogeneous stirring at higher molecular weights.

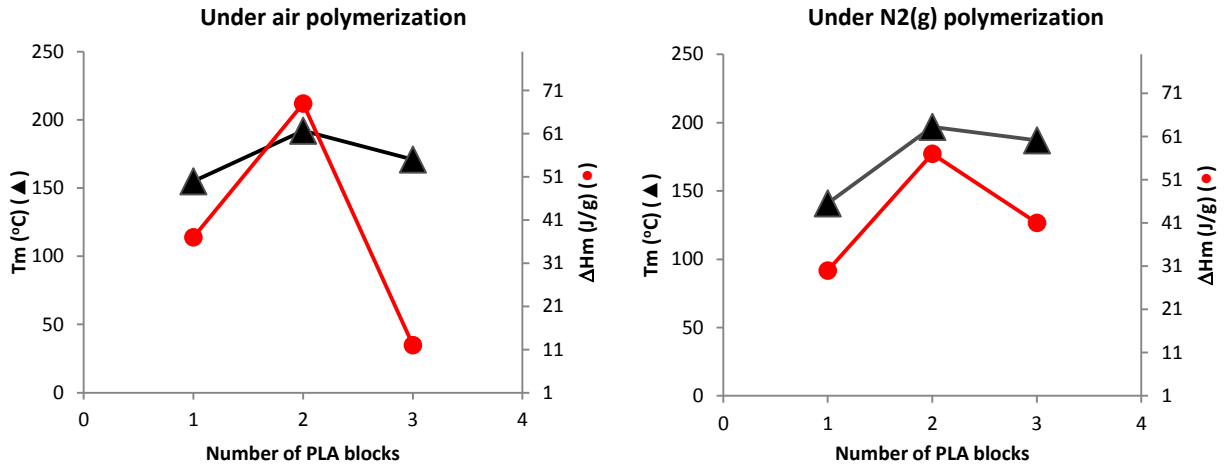

Figure 5.14 The effect of PLA blocks on the melting point and the enthalpy of melting of PLA bock copolymers prepared in air (left), and in inert atmosphere (right)

In air, complex **18** forms high molecular weight triblock copolymers of PLLA-PDLA-PLLA with narrow molecular weight distribution (Table 5.4 entry 12, Figure 5.13) in one pot after 5 hours. In contrast, similar high molecular weight PLLA-PDLA block copolymers can be synthesized with $Sn(Oct)_2$ through two step synthesis under inert atmosphere after 7 days.[310] Importantly, based on DSC results, the abrupt increase in the melting point of the PLLA block upon introduction of the PDLA block confirms the formation of stereocomplexed crystalline regions, as the melting point of the PLLA-PDLA diblock copolymer reaches the value of 197 °C. This T_m value is slightly lower than expected for the reported analogues systems (T_m = 206 °C).[311] The source of this disparity is the fact that these polymers are star shaped and the presence of branch points can interfere with the crystal growth. However, it is expected that under annealing process, branch points can actually act as nucleating agents and increase the melting point.

DSC analysis of the triblock enantiomers (Figure 5.14, Figure C27-31) shows lower T_m and ΔH_m values than those of the diblock copolymers. This behavior is due to the crystallization of

unpaired enantiomeric blocks in triblock copolymers which causes defects in the stereocomplex formation.[312]

The polymerization results for complex **18** carried out under N_2 atmosphere (Table 5.4, entry 13) shows close results, to the batch prepared under air, however with narrower molecular weight distribution. Comparing the homodecoupled ^{1}H NMR results of the triblock copolymers prepared under air with does prepared under N_2, shows identical results, which rules out any possible racemization (Figure C. 21-26). Therefore, the only explanation for the broader molecular weight distribution is the actual difference in the method of polymerizations. For polymerizations carried out under air, for every batch of monomer addition, the vessel was exposed to air at high temperature, causing an extensive toluene evaporation. This resulted in an increase in the melt viscosity and hence improper mixing. However, for the batches that were prepared under N_2 gas, the reactor recharge took place inside the glovebox, while the mixture was in solid state, with much lower amount of solvent loss and hence better mixing conditions in the melt state. Nonetheless, complex **18**, forms high molecular weight monodispersed star-stereoblock copolymers of PLA with as received monomers under ambient atmospheric conditions and to the best of our knowledge this is the only reported example of a living catalyst that remains controlled after multiple exposures to air at high temperatures.[114,311]

5.3 Summary

Salan-supported dinuclear indium complex **2** is an air and water stable, highly active, and highly controlled catalyst for the polymerization of lactide in air. We show that salan ligand support for indium favors the formation of a mixed hydroxyl/chloro bridged indium complex **18** which can convert to an active alkoxy/chloro bridged complex **17** to allow reactivity. Complex **17** is

synthesized in 3 steps from a simple salan ligand and can be converted to **18** quantitatively by exposure to moist air. Industrial production of PLA takes place in melt state. Most of the isoselective catalysts reported in the literature (including complexes **D** and **K**), lose their selectivity towards polymerization of *rac*-LA in melt state. Hence, in order to achieve highly crystalline PLA, development of catalytic systems which do not cause transesterification/racemization in melt state is vital. Complex **18** can be a real solution to the need for a stable catalyst, capable of high activity and strict macrostructure control, to form high molecular weight block copolymers in industrial environments without inert atmosphere facilities.

Chapter 6: Conclusions, contribution to knowledge and recommendations

6.1 Conclusions

Although PHB has great potential in a wide range of commodity and medical applications, no reports existed on the synthesis and rheological properties of PHBs with different topologies and microstructures. Also, to the best of our knowledge, none of the existing highly active/selective catalysts reported in the literature are capable of polymerizing lactide in industrially relevant setups to form high molecular weight monodispersed polymers. The main goal of this interdisciplinary PhD thesis, was to design a new catalytic system to form star-shaped PHBs in a single pot and develop highly efficient catalytic systems for the formation of high molecular weight high melt strength processable PHBs. Also, in an attempt, it was shown that multiblock copolyesters can be formed in melt state under ambient atmospheric conditions using indium-salan complexes.

In chapter 3, the previously reported dinuclear indium complex (**D**) was modified with tris(hydroxymethyl)benzene (THMB) to form a new catalyst (**3**) as an intermediate to polymerize cyclic esters in the presence of THMB for the formation of symmetric 3-armed star homo and block copolyesters in one pot. Zinc based catalyst (NN_iO_{tBu})Zn(CH_2CH_3) (**2**),was prepared to produce monodispersed six-armed star PHB homopolymers using dipentaerythritol (DPET) as the chain transfer agent. Reactions catalyzed by (**2**), and (**3**) formed highly symmetric well-defined, 3-armed and 6-armed PHBs for the first time. Solution viscometric properties of the synthesized star and linear PHBs with different molecular weights were examined to confirm their self-similarity as a results of the reduced compactness factor. Thermorheological characterization of these polymers revealed that the zero-shear viscosity of linear PHBs have a power law relationship with the span molecular weight, while it scales exponentially for star polymers with slightly higher

values for the 6-armed star PHBs. This was attributed to the moderately syndiotactic microstructure of these polymers. Our non-linear rheological measurements confirmed that the stars are more shear thinning compared to their linear counterparts, which makes them potential candidates to be used as processing aids for PHB processing.

A series of racemic and enantiopure zinc catalysts were introduced in chapter 4 to form processable PHBs with syndiotactically enriched microstructures (up to 75%) and high molecular weights and melt strengths. These catalysts are supported by variously substituted diaminophenolate ancillary ligands. These complexes are surprisingly active towards the controlled polymerization of BBL; some can polymerize 4000 equivalents of BBL in less than 30 minutes to form syndioenriched PHBs with molecular weights up to 340 $kgmol^{-1}$. Turnover frequency reached up to about 23000 h^{-1} exceeding by far any other value reported in the literature. These are highly robust systems capable of polymerizing an unprecedented 20000 equivalents of BBL in the presence of 5000 equivalents of benzyl alcohol. This system for the controlled ROP of BBL has industrial potential, and to our knowledge no comparably effective catalyst has been reported for BBL polymerization to this date. Having a highly active and robust catalytic system in hand, the synthesis of syndio-enriched PHBs was scaled up to gram scale in order to examine the thermorheological and mechanical properties of high molecular weight syndio-enrich PHBs. The consistency of storage and loss moduli during the isothermal time sweep tests to up to 2000 s indicated that sample degradation had not occurred at temperatures below 140 °C. These results demonstrate that these polymers possesses enough thermal stability for melt processing below 140 °C. Highly syndiotactic PHBs (85% syndiotactic) were also prepared using the land mark yttrium complex (**B**). Results clearly showed that the highly syndio PHB suffers from dramatic thermal degradation and isothermal crystallization at temperatures around the melting point. This

observation disclosed the fact that highly syndiotactic PHBs, just like bacterial based PHBs, are not processable. The extensional rheometry results revealed a profound melt strength due to high entanglement density and the presence of flow induced crystallization in syndioenriched PHBs. Our tensile test results also demonstrated that high molecular weight syndioenriched PHB has considerable extensibility and high tensile strength comparable to its polyolefinic counterpart (70% syndiotactic polypropylene).

In chapter 5, asymmetrically bridged dinuclear indium alkoxy complex (**17**) was prepared from salan ligand in two consecutive salt metathesis reactions. Exposure of (**17**) to trace water in as-received organic solvents for 48 h forms asymmetrically bridged complex (**18**). Complex (**18**) showed air and water stability as it stays unchanged outside the N_2 (g) glovebox, in ambient atmospheric conditions, for more than 1 month. Reaction of complex **18** with up to 10000 equivalents of as-received lactide in the presence of THMB in the melt forms monodispersed star-PLAs. Importantly, complex (**18**) catalyzes the formation of di-block and tri-block star shaped PLAs in the melt in air through sequential addition of lactide different isomers (L and D lactide) to forms high molecular weight stereotriblock copolymers of PLA in one pot.

6.2 Contributions to knowledge

1. Preparation of monodispersed linear and star shaped PHBs are reported along with monodispersed star shaped diblock copolymers of PHB-PLLA for the first time using modified –OTHMB bridged dinuclear indium complex and zinc-ethyl complex.

2. Throughout solution and melt rheological characterization of the star PHBs are reported for the first time. Our results confirmed the presence of branching on the polymer backbone, and the fact that the prepared star polymers are highly self-similar and symmetric.

3. The first example of a processable PHB, with no need for additives or processing aids, and good thermal stability and high melt strength above the melting point is reported. It is shown that for processable PHBs, the density of entanglements should be high, while the melting point/stereoregularity must be kept low. These polymers can be prepared in gram scale using a series of zinc-based complexes in both living and immortal fashions. These complexes are by far more robust and tolerant against high loadings of chain transfer agents than the existing catalysts in the literature, making them potential candidates for the polymerization of PHB in industrial scales.

4. An easy to make, indium based catalyst is introduced with an exceptional functionality under ambient atmospheric conditions for the formation of star-shaped multiblock copolyesters. This system forms monodispersed PLAs with as-received lactide, which facilitates PLA preparation without any need for monomer purification through several steps of recrystallizations from solution.

6.3 Recommendations for future work

1. Post polymerization reactions of the tri-OH and hexa-OH terminated star PHBs can be carried out to form functionalized PHBs. These polymers can be used as initiators for radical polymerization of methyl methacrylate (MMA) to form star block copolymers of PHB-PMMA. These copolymers can then be used for the preparation of nano- or mesoporous PMMA monoliths using selective hydrolysis of PHB segments in PMMA-PHB matrix.

2. Functionalized monomers including functionalized-malolactonates and propiolactones can be used for the preparation of functionalized polyhydroxyalkanoates using the introduced zinc complexes. Throughout rheological, thermal and mechanical characterization of these polymers can be carried out to develop a structure-property relationship for a range of PHAs with different functionalities.

3. Detailed studies can be carried out on the mechanism of crystallization and crystallization kinetic of star-shaped stereotriblock copolymers of PLA using *in-situ* crystallization techniques (e.g. isothermal time-sweeps and wide-angle X-ray scattering (WAXS)) to investigate the effect of branching on the crystallization kinetics of these polymers.

4. Salan indium complexes can be used for facile open-air homo and block copolymerization of caprolactone with other cyclic esters including lactide. These star-shaped block copolymers can then be used as compatibilizers in the preparation of homogenous PLA/PCL binary blends. These complexes can also be used for the *in-situ* grafting of PLA on the surface of nanofillers such as Cellulose Nanocrystals (CNC) to form hydrophobically modified CNC from as-received lactide. These fillers may be used as macroinitiators for PHB grafting on the surface, or as compatible fillers to enhance the mechanical properties of aliphatic polyesters.

Bibliography

(1) Mecking, S. *Angew. Chem. Int. Ed.* **2004**, *43*, 1078.

(2) Bernhard Rieger, A. K., Geoffrey W. Coates, Robert Reichardt, Eckhard Dinjus, Thomas A. Zevaco *Synthetic Biodegradable Polymers*; Springer, 2012; Vol. 245

(3) http://plastic-pollution.org/.Accessed on September 1th, 2017

(4) Andrew J. Peacock, A. R. C. *Polymer Chemistry - Properties and Applications*; Hanser Gardner, 2006.

(5) Brydson, J. A. *Plastics Materials*; Elsevier 2017.

(6) Okada, M. *Prog. Polym. Sci.* **2002**, *27*, 87.

(7) Sabu Thomas, N. N., Sneha Mohan, Elizabeth Francis *Natural Polymers, Biopolymers, Biomaterials, and Their Composites, Blends, and IPNs*; CRC press, 2012

(8) Doi, Y.; Kitamura, S.; Abe, H. *Macromolecules* **1995**, *28*, 4822.

(9) Carpentier, J. F. *Macromol. Rapid Commun.* **2010**, *31*, 1696.

(10) Ajellal, N.; Carpentier, J.-F.; Guillaume, C.; Guillaume, S. M.; Helou, M.; Poirier, V.; Sarazin, Y.; Trifonov, A. *Dalton Trans.* **2010**, *39*, 8363.

(11) Dealy, J. M.; Larson, R. G. In *Structure and Rheology of Molten Polymers*; Carl Hanser Verlag GmbH & Co. KG: 2006, p 7.

(12) Dealy, J. M.; Larson, R. G. In *Structure and Rheology of Molten Polymers*; Carl Hanser Verlag GmbH & Co. KG: 2006, p 233.

(13) Ren, J.; Zhang, Z.; Feng, Y.; Li, J.; Yuan, W. *J. Appl. Polym. Sci.* **2010**, *118*, 2650.

(14) Perry, M. R.; Shaver, M. P. *Can. J. Chem.* **2011**, *89*, 499.

(15) Zhao, W.; Cui, D.; Liu, X.; Chen, X. *Macromolecules* **2010**, *43*, 6678.

(16) Målberg, S.; Basalp, D.; Finne-Wistrand, A.; Albertsson, A.-C. *J. Polym. Sci. A* **2010**, *48*, 1214.

(17) George, K. A.; Schué, F.; Chirila, T. V.; Wentrup-Byrne, E. *J. Polym. Sci. A* **2009**, *47*, 4736.

(18) Moravek, S. J.; Messman, J. M.; Storey, R. F. *J. Polym. Sci. A* **2009**, *47*, 797.

(19) Biela, T.; Duda, A.; Pasch, H.; Rode, K. *J. Polym. Sci. A* **2005**, *43*, 6116.

(20) Mehta, R.; Kumar, V.; Bhunia, H.; Upadhyay, S. N. *J Macromol. Sci Polym. Rev.* **2005**, *45*, 325.

(21) Cameron, D. J. A.; Shaver, M. P. *Chem. Soc. Rev.* **2011**, *40*, 1761.

(22) Huskić, M.; Pulko, I. *Eur. Polym. J.* **2015**, *70*, 384.

(23) Mya, K. Y.; Gose, H. B.; Pretsch, T.; Bothe, M.; He, C. *J. Mater. Chem.* **2011**, *21*, 4827.

(24) Teng, C. P.; Mya, K. Y.; Win, K. Y.; Yeo, C. C.; Low, M.; He, C.; Han, M.-Y. *NPG Asia Mater* **2014**, *6*, e142.

(25) Shadi, L.; Karimi, M.; Entezami, A. A. *Colloid Polym. Sci.* **2015**, *293*, 481.

(26) Shadi, L.; Karimi, M.; Ramazani, S.; Entezami, A. A. *J. Mater. Sci.* **2014**, *49*, 4844.

(27) Dong, C.-M.; Qiu, K.-Y.; Gu, Z.-W.; Feng, X.-D. *Macromolecules* **2001**, *34*, 4691.

(28) Wang, T.-L.; Huang, F.-J.; Lee, S.-W. *Polym. Int.* **2002**, *51*, 1348.

(29) Ajellal, N.; Bouyahyi, M.; Amgoune, A.; Thomas, C. M.; Bondon, A.; Pillin, I.; Grohens, Y.; Carpentier, J.-F. *Macromolecules* **2009**, *42*, 987.

(30) Zintl, M.; Molnar, F.; Urban, T.; Bernhart, V.; Preishuber-Pfugl, P.; Rieger, B. *Angew. Chem. Int. Ed.* **2008**, *47*, 3458.
(31) Reichardt, R.; Vagin, S.; Reithmeier, R.; Ott, A. K.; Rieger, B. *Macromolecules* **2010**, *43*, 9311.
(32) Brown, H. A.; Waymouth, R. M. *Acc. Chem. Res.* **2013**, *46*, 2585.
(33) Kamber, N. E.; Jeong, W.; Waymouth, R. M.; Pratt, R. C.; Lohmeijer, B. G. G.; Hedrick, J. L. *Chem. Rev.* **2007**, *107*, 5813.
(34) Sarazin, Y.; Carpentier, J. F. *Chem. Rev.* **2015**, *115*, 3564.
(35) Guillaume, S. M.; Kirillov, E.; Sarazin, Y.; Carpentier, J. F. *Chem. Eur. J.* **2015**, *21*, 7988.
(36) Yao, K. J.; Tang, C. B. *Macromolecules* **2013**, *46*, 1689.
(37) Vieira, I. D.; Herres-Pawlis, S. *Eur. J. Inorg. Chem.* **2012**, 765.
(38) Dijkstra, P. J.; Du, H. Z.; Feijen, J. *Polym. Chem.* **2011**, *2*, 520.
(39) Buffet, J. C.; Okuda, J. *Polym. Chem.* **2011**, *2*, 2758.
(40) Brule, E.; Guo, J.; Coates, G. W.; Thomas, C. M. *Macromol. Rapid Commun.* **2011**, *32*, 169.
(41) Thomas, C. M. *Chem. Soc. Rev.* **2010**, *39*, 165.
(42) Sutar, A. K.; Maharana, T.; Dutta, S.; Chen, C. T.; Lin, C. C. *Chem. Soc. Rev.* **2010**, *39*, 1724.
(43) Stanford, M. J.; Dove, A. P. *Chem. Soc. Rev.* **2010**, *39*, 486.
(44) Wheaton, C. A.; Hayes, P. G.; Ireland, B. J. *Dalton Trans.* **2009**, *25*, 4832.
(45) Wu, J. C.; Yu, T. L.; Chen, C. T.; Lin, C. C. *Coord. Chem. Rev.* **2006**, *250*, 602.
(46) Wu, J. C.; Huang, B. H.; Hsueh, M. L.; Lai, S. L.; Lin, C. C. *Polymer* **2005**, *46*, 9784.
(47) Bourissou, D.; Martin-Vaca, B.; Dumitrescu, A.; Graullier, M.; Lacombe, F. *Macromolecules* **2005**, *38*, 9993.
(48) Dechy-Cabaret, O.; Martin-Vaca, B.; Bourissou, D. *Chem. Rev.* **2004**, *104*, 6147.
(49) Pouton, C. W.; Akhtar, S. *Adv. Drug Delivery Rev.* **1996**, *18*, 133.
(50) Drumright, R. E.; Gruber, P. R.; Henton, D. E. *Adv. Mater.* **2000**, *12*, 1841.
(51) O'Keefe, B. J.; Hillmyer, M. A.; Tolman, W. B. *J. Chem. Soc. Dalton Trans.* **2001**, 2215.
(52) Chisholm, M. H.; Zhou, Z. P. *J. Mater. Chem.* **2004**, *14*, 3081.
(53) Dove, A. P.; Gibson, V. C.; Marshall, E. L.; Rzepa, H. S.; White, A. J. P.; Williams, D. J. *J. Am. Chem. Soc.* **2006**, *128*, 9834.
(54) Schwach, G.; Coudane, J.; Engel, R.; Vert, M. *Biomaterials* **2002**, *23*, 993.
(55) Schwach, G.; Coudane, J.; Engel, R.; Vert, M. *J. Polym. Sci. A* **1997**, *35*, 3431.
(56) Chen, G.-Q. *Chem. Soc. Rev.* **2009**, *38*, 2434.
(57) Bugnicourt, E. C., P.; Lazzeri, A.; Alvarez, V *Express Polym. Let.* **2014**, *8*, 791.
(58) Chen, G. Q.; Patel, M. K. *Chem. Rev.* **2012**, *112*, 2082.
(59) Chen, G. Q. *Chem. Soc. Rev.* **2009**, *38*, 2434.
(60) Hopewell, J.; Dvorak, R.; Kosior, E. *Philos Trans R Soc Lond B Biol Sci.* **2009**, *364*, 2115.
(61) Hrabak, O. *FEMS Microbiol Lett* **1992**, *103*, 251.
(62) Verlinden, R. A. J.; Hill, D. J.; Kenward, M. A.; Williams, C. D.; Radecka, I. *Appl. Microbiol.* **2007**, *102*, 1437.

(63) Lendlein, A. *Chemie in unserer Zeit* **1999**, *33*, 279.
(64) Zhang, L.; Deng, X.; Zhao, S.; Huang, Z. *Polymer* **1997**, *38*, 6001.
(65) Ahmed, T.; Marçal, H.; Lawless, M.; Wanandy, N. S.; Chiu, A.; Foster, L. J. R. *Biomacromolecules* **2010**, *11*, 2707.
(66) Caballero, K. P.; Karel, S. F.; Register, R. A. *Int. J. Biol. Macromol.* **1995**, *17*, 86.
(67) Zhao, K.; Deng, Y.; Chun Chen, J.; Chen, G.-Q. *Biomaterials* **2003**, *24*, 1041.
(68) Dubois, P.; Narayan, R. *Macromol Symp.* **2003**, *198*, 233.
(69) Avella, M.; Martuscelli, E.; Raimo, M. *J. Mater. Sci.* **2000**, *35*, 523.
(70) Scaffaro, R.; Dintcheva, N. T.; Marino, R.; La Mantia, F. P. *J Polym. Environ.* **2012**, *20*, 267.
(71) Madhavan Nampoothiri, K.; Nair, N. R.; John, R. P. *Bioresour Technol.* **2010**, *101*, 8493.
(72) Auras, R.; Harte, B.; Selke, S. *Macromol. Biosci* **2004**, *4*, 835.
(73) Steve, V. E. T. H. a. D. *Ind Biotechnol.* **2015**.
(74) Ajellal, N.; Durieux, G.; Delevoye, L.; Tricot, G.; Dujardin, C.; Thomas, C. M.; Gauvin, R. M. *Chem. Commun.* **2010**, *46*, 1032.
(75) Ajellal, N.; Lyubov, D. M.; Sinenkov, M. A.; Fukin, G. K.; Cherkasov, A. V.; Thomas, C. M.; Carpentier, J. F.; Trifonov, A. A. *Chem. Eur. J.* **2008**, *14*, 5440.
(76) Ajellal, N.; Thomas, C. M.; Carpentier, J. F. *J. Polym. Sci., Part A: Polym. Chem.* **2009**, *47*, 3177.
(77) Amsden, B. *Soft Matter* **2007**, *3*, 1335.
(78) Tanahashi, N.; Doi, Y. *Macromolecules* **1991**, *24*, 5732.
(79) Kricheldorf, H. R.; Eggerstedt, S. *Macromolecules* **1997**, *30*, 5693.
(80) Jendrossek, D.; Schirmer, A.; Schlegel, H. G. *Appl. Microbiol. Biotechnol.* **1996**, *46*, 451.
(81) Jaimes, C.; Dobreva-Schué, R.; Giani-Beaune, O.; Schué, F.; Amass, W.; Amass, A. *Polym. Int.* **1999**, *48*, 23.
(82) Kemnitzer, J. E.; McCarthy, S. P.; Gross, R. A. *Macromolecules* **1992**, *25*, 5927.
(83) Scandola, M.; Focarete, M. L.; Gazzano, M.; Matuszowicz, A.; Sikorska, W.; Adamus, G.; Kurcok, P.; Kowalczuk, M.; Jedlinski, Z. *Macromolecules* **1997**, *30*, 7743.
(84) He, Y.; Shuai, X.; Kasuya, K.-i.; Doi, Y.; Inoue, Y. *Biomacromolecules* **2001**, *2*, 1045.
(85) Scandola, M.; Focarete, M. L.; Adamus, G.; Sikorska, W.; Baranowska, I.; Świerczek, S.; Gnatowski, M.; Kowalczuk, M.; Jedliński, Z. *Macromolecules* **1997**, *30*, 2568.
(86) Focarete, M. L.; Ceccorulli, G.; Scandola, M.; Kowalczuk, M. *Macromolecules* **1998**, *31*, 8485.
(87) Dove, A. P. *Chem. Commun.* **2008**, 6446.
(88) Fukushima, K.; Kimura, Y. *Polym. Int.* **2006**, *55*, 626.
(89) Thakur, K. A. M.; Kean, R. T.; Hall, E. S.; Kolstad, J. J.; Lindgren, T. A.; Doscotch, M. A.; Siepmann, J. I.; Munson, E. J. *Macromolecules* **1997**, *30*, 2422.
(90) Zell, M. T.; Padden, B. E.; Paterick, A. J.; Thakur, K. A. M.; Kean, R. T.; Hillmyer, M. A.; Munson, E. J. *Macromolecules* **2002**, *35*, 7700.
(91) Lee, J. T.; Alper, H. *Macromolecules* **2004**, *37*, 2417.
(92) Allmendinger, M.; Molnar, F.; Zintl, M.; Luinstra, G. A.; Preishuber-Pflügl, P.; Rieger, B. *Chem. Eur. J* **2005**, *11*, 5327.

(93) Getzler, Y. D. Y. L.; Mahadevan, V.; Lobkovsky, E. B.; Coates, G. W. *J. Am. Chem. Soc.* **2002**, *124*, 1174.

(94) Mulzer, M.; Whiting, B. T.; Coates, G. W. *J. Am. Chem. Soc.* **2013**, *135*, 10930.

(95) Kricheldorf, H. R.; Eggerstedt, S. *Macromolecules* **1994**, *30*, 5693.

(96) Fang, J.; Yu, I.; Mehrkhodavandi, P.; Maron, L. *Organometallics* **2013**, *32*, 6950.

(97) Ryner, M.; Stridsberg, K.; Albertsson, A.-C.; von Schenck, H.; Svensson, M. *Macromolecules* **2001**, *34*, 3877.

(98) Wang, H. B.; Guo, J.; Yang, Y.; Ma, H. Y. *Dalton Trans.* **2016**, *45*, 10942.

(99) Kronast, A.; Reiter, M.; Altenbuchner, P. T.; Jandl, C.; Pothig, A.; Rieger, B. *Organometallics* **2016**, *35*, 681.

(100) Ebrahimi, T.; Hatzikiriakos, S. G.; Mehrkhodavandi, P. *Macromolecules* **2015**, *48*, 6672.

(101) Chuang, H. J.; Chen, H. L.; Huang, B. H.; Tsai, T. E.; Huang, P. L.; Liao, T. T.; Lin, C. C. *J. Polym. Sci., Part A: Polym. Chem.* **2013**, *51*, 1185.

(102) Schnee, G.; Fliedel, C.; Aviles, T.; Dagorne, S. *Eur. J. Inorg. Chem.* **2013**, *2013*, 3699.

(103) Guillaume, C.; Ajellal, N.; Carpentier, J. F.; Guillaume, S. M. *J. Polym. Sci., Part A: Polym. Chem.* **2011**, *49*, 907.

(104) Liu, Y. C.; Lin, C. H.; Ko, B. T.; Ho, R. M. *J. Polym. Sci., Part A: Polym. Chem.* **2010**, *48*, 5339.

(105) Garces, A.; Sanchez-Barba, L. F.; Alonso-Moreno, C.; Fajardo, M.; Fernandez-Baeza, J.; Otero, A.; Lara-Sanchez, A.; Lopez-Solera, I.; Rodriguez, A. M. *Inorg. Chem.* **2010**, *49*, 2859.

(106) Dunn, E. W.; Coates, G. W. *J. Am. Chem. Soc.* **2010**, *132*, 11412.

(107) Rieth, L. R.; Moore, D. R.; Lobkovsky, E. B.; Coates, G. W. *J. Am. Chem. Soc.* **2002**, *124*, 15239.

(108) MacDonald, J. P.; Sidera, M.; Fletcher, S. P.; Shaver, M. P. *Eur. Polym. J.* **2016**, *74*, 287.

(109) Leborgne, A.; Spassky, N. *Polymer* **1989**, *30*, 2312.

(110) Bloembergen, S.; Holden, D. A.; Bluhm, T. L.; Hamer, G. K.; Marchessault, R. H. *Macromolecules* **1989**, *22*, 1656.

(111) Agatemor, C.; Arnold, A. E.; Cross, E. D.; Decken, A.; Shaver, M. P. *J. Organomet. Chem.* **2013**, *745*, 335.

(112) Xu, C.; Yu, I.; Mehrkhodavandi, P. *Chem. Commun.* **2012**, *48*, 6806.

(113) Yu, I.; Ebrahimi, T.; Hatzikiriakos, S. G.; Mehrkhodavandi, P. *Dalton Trans.* **2015**, *44*, 14248.

(114) Aluthge, D. C.; Xu, C. L.; Othman, N.; Noroozi, N.; Hatzikiriakos, S. G.; Mehrkhodavandi, P. *Macromolecules* **2013**, *46*, 3965.

(115) Quan, S. M.; Diaconescu, P. L. *Chem. Commun.* **2015**, *51*, 9643.

(116) Briand, G. G.; Cairns, S. A.; Decken, A.; Dickie, C. M.; Kostelnik, T. I.; Shaver, M. P. *J. Organomet. Chem.* **2016**, *806*, 22.

(117) Kremer, A. B.; Osten, K. M.; Yu, I.; Ebrahimi, T.; Aluthge, D. C.; Mehrkhodavandi, P. *Inorg. Chem.* **2016**, *55*, 5365.

(118) Hori, Y.; Suzuki, M.; Yamaguchi, A.; Nishishita, T. *Macromolecules* **1993**, *26*, 5533.

(119) Hori, Y.; Takahashi, Y.; Yamaguchi, A.; Nishishita, T. *Macromolecules* **1993**, *26*, 4388.

(120) Nie, K.; Fang, L.; Yao, Y. M.; Zhang, Y.; Shen, Q.; Wang, Y. R. *Inorg. Chem.* **2012**, *51*, 11133.

(121) D'Auria, I.; Mazzeo, M.; Pappalardo, D.; Lamberti, M.; Pellecchia, C. *J. Polym. Sci., Part A: Polym. Chem.* **2011**, *49*, 403.

(122) Ajellal, N.; Thomas, C. M.; Aubry, T.; Grohens, Y.; Carpentier, J. F. *New J. Chem.* **2011**, *35*, 876.

(123) Carpentier, J. F. *Angew. Chem. Int. Ed.* **2010**, *49*, 2662.

(124) Grunova, E.; Kirillov, E.; Roisnel, T.; Carpentier, J. F. *Dalton Trans.* **2010**, *39*, 6739.

(125) Amgoune, A.; Thomas, C. M.; Ilinca, S.; Roisnel, T.; Carpentier, J. F. *Angew. Chem. Int. Ed.* **2006**, *45*, 2782.

(126) Ajellal, N.; Bouyahyi, M.; Amgoune, A.; Thomas, C. M.; Bondon, A.; Pillin, I.; Grohens, Y.; Carpentier, J. F. *Macromolecules* **2009**, *42*, 987.

(127) Brule, E.; Gaillard, S.; Rager, M. N.; Roisnel, T.; Guerineau, V.; Nolan, S. P.; Thomas, C. M. *Organometallics* **2011**, *30*, 2650.

(128) Wolfle, H.; Kopacka, H.; Wurst, K.; Preishuber-Pflugl, P.; Bildstein, B. *J. Organomet. Chem.* **2009**, *694*, 2493.

(129) Kramer, J. W.; Coates, G. W. *Tetrahedron* **2008**, *64*, 6973.

(130) Coulembier, O.; Moins, S.; Dubois, P. *Macromolecules* **2011**, *44*, 7493.

(131) Brestaz, M.; Desilles, N.; Le, G.; Bunel, C. *J. Polym. Sci., Part A: Polym. Chem.* **2011**, *49*, 4129.

(132) Kawalec, M.; Smiga-Matuszowicz, M.; Kurcok, P. *Eur. Polym. J.* **2008**, *44*, 3556.

(133) Adamus, G.; Kowalczuk, M. *Biomacromolecules* **2008**, *9*, 696.

(134) Coulembier, O.; Delva, X.; Hedrick, J. L.; Waymouth, R. M.; Dubois, P. *Macromolecules* **2007**, *40*, 8560.

(135) Church, T. L.; Getzler, Y.; Byrne, C. M.; Coates, G. W. *Chem. Commun.* **2007**, 657.

(136) Le Borgne, A.; Spassky, N. *Polymer* **1989**, *30*, 2312.

(137) Kemnitzer, J. E.; McCarthy, S. P.; Gross, R. A. *Macromolecules* **1993**, *26*, 6143.

(138) Hori, Y.; Suzuki, M.; Yamaguchi, A.; Nishishita, T. *Macromolecules* **1993**, *26*, 5533.

(139) Amgoune, A.; Thomas, C. M.; Carpentier, J. F. *Macromol. Rapid Commun.* **2007**, *28*, 693.

(140) Kricheldorf, H. R.; Soo-Ran Lee, S.-R. *Macromolecules* **1996**, *29*, 8689.

(141) Kricheldorf, H. R.; Lee, S.-R.; Scharnagl, N. *Macromolecules* **1997**, *27*, 3139.

(142) Kramer, J. W.; Treitler, D. S.; Dunn, E. W.; Castro, P. M.; Roisnel, T.; Thomas, C. M.; Coates, G. W. *J. Am. Chem. Soc.* **2009**, *131*, 16042.

(143) Pappalardo, D.; Bruno, M.; Lamberti, M.; Pellecchia, C. *Macromol. Chem. Phys.* **2013**, *214*, 1965.

(144) Fang, J.; Tschan, M. J. L.; Roisnel, T.; Trivelli, X.; Gauvin, R. M.; Thomas, C. M.; Maron, L. *Polym. Chem.* **2013**, *4*, 360.

(145) Xu, C.; Yu, I.; Mehrkhodavandi, P. *Chem. Commun.* **2012**, *48*, 6806.
(146) Inoue, S. *J. Polym. Sci. A* **2000**, *38*, 2861.
(147) Guillaume, C.; Carpentier, J. F.; Guillaume, S. M. *Polymer* **2009**, *50*, 5909.
(148) Grunova, E.; Roisnel, T.; Carpentier, J. F. *Dalton Trans.* **2009**, 9010.
(149) Poirier, V.; Roisnel, T.; Carpentier, J. F.; Sarazin, Y. *Dalton Trans.* **2009**, 9820.
(150) Poirier, V.; Roisnel, T.; Carpentier, J. F.; Sarazin, Y. *Dalton Trans.* **2011**, *40*, 523.
(151) Rafler, G.; Dahlmann, J. *Act. Polym.* **1992**, *43*, 91.
(152) Nijenhuis, A. J.; Grijpma, D. W.; Pennings, A. J. *Macromolecules* **1992**, *25*, 6419.
(153) Ovitt, T. M.; Coates, G. W. *J. Polym. Sci. A* **2000**, *38*, 4686.
(154) Chamberlain, B. M.; Cheng, M.; Moore, D. R.; Ovitt, T. M.; Lobkovsky, E. B.; Coates, G. W. *J. Am. Chem. Soc.* **2001**, *123*, 3229.
(155) Spassky, N.; Wisniewski, M.; Pluta, C.; Le Borgne, A. *Macromol. Chem. Phys.* **1996**, *197*, 2627.
(156) Cheng, M.; Attygalle, A. B.; Lobkovsky, E. B.; Coates, G. W. *J. Am. Chem. Soc.* **1999**, *121*, 11583.
(157) Williams, C. K.; Brooks, N. R.; Hillmyer, M. A.; Tolman, W. B. *Chem. Commun.* **2002**, 2132.
(158) Knight, P. D.; White, A. J. P.; Williams, C. K. *Inorg. Chem.* **2008**, *47*, 11711.
(159) Zhong, Z.; Dijkstra, P. J.; Feijen, J. *Angew. Chem. Int. Ed.* **2002**, *41*, 4510.
(160) Nomura, N.; Ishii, R.; Yamamoto, Y.; Kondo, T. *Chem. Eur. J* **2007**, *13*, 4433.
(161) Douglas, A. F.; Patrick, B. O.; Mehrkhodavandi, P. *Angew. Chem. Int. Ed.* **2008**, *120*, 2322.
(162) Osten, K. M.; Aluthge, D. C.; Mehrkhodavandi, P. *Dalton Trans.* **2015**, *44*, 6126.
(163) Osten, K. M.; Aluthge, D. C.; Patrick, B. O.; Mehrkhodavandi, P. *Inorg. Chem.* **2014**, *53*, 9897.
(164) Osten, K. M.; Yu, I.; Duffy, I. R.; Lagaditis, P. O.; Yu, J. C. C.; Wallis, C. J.; Mehrkhodavandi, P. *Dalton Trans.* **2012**, *41*, 8123.
(165) Yu, I.; Acosta-Ramirez, A.; Mehrkhodavandi, P. *J. Am. Chem. Soc.* **2012**, *134*, 12758.
(166) Aluthge, D. C.; Ahn, J. M.; Mehrkhodavandi, P. *Chem. Sci.* **2015**, *6*, 5284.
(167) Aluthge, D. C.; Patrick, B. O.; Mehrkhodavandi, P. *Chem. Commun.* **2013**, *49*, 4295.
(168) Carpentier, J.-F. *Organometallics* **2015**, *34*, 4175.
(169) Amgoune, A.; Thomas, C. M.; Roisnel, T.; Carpentier, J.-F. *Chem. Eur. J* **2006**, *12*, 169.
(170) Williams, C. K.; Breyfogle, L. E.; Choi, S. K.; Nam, W.; Young, V. G.; Hillmyer, M. A.; Tolman, W. B. *J. Am. Chem. Soc.* **2003**, *125*, 11350.
(171) Astarita, G. *Principles of Non-Newtonian Fluid Mechanics*; McGraw-Hill Education - Europe, 1974.
(172) Dealy, J. M.; Wissbrun, K. F. *Melt Rheology and Its Role in Plastics Processing, 2nd ed.*; Van Nostrand Reinhold New York, 1990.
(173) Ferry, J. D. *Viscoelastic Properties of Polymers*
1980.
(174) Aho, J.; Boetker, J. P.; Baldursdottir, S.; Rantanen, J. *Int. J. Pharm.* **2015**, *494*, 623.
(175) Sentmanat, M.; Wang, B. N.; McKinley, G. H. *J. Rheol.* **2005**, *49*, 585.

(176) Sentmanat, M. L. *Rheol. Acta* **2004**, *43*, 657.
(177) Mitsoulis, E.; Hatzikiriakos, S. G. *Food Bioprod. Process.*, *87*, 124.
(178) Fetters, L. J.; Kiss, A. D.; Pearson, D. S.; Quack, G. F.; Vitus, F. J. *Macromolecules* **1993**, *26*, 647.
(179) Hatada, K. *Macromolecular Design of Polymeric Materials*; CRC Press, 1997
(180) Inoue, K. *Prog. Polym. Sci.* **2000**, *25*, 453.
(181) Corneillie, S.; Smet, M. *Polym. Chem.* **2015**, *6*, 850.
(182) Normand, M.; Kirillov, E.; Carpentier, J.-F.; Guillaume, S. M. *Macromolecules* **2012**, *45*, 1122.
(183) Ren, J. M.; McKenzie, T. G.; Fu, Q.; Wong, E. H. H.; Xu, J.; An, Z.; Shanmugam, S.; Davis, T. P.; Boyer, C.; Qiao, G. G. *Chem. Rev.* **2016**, *116*, 6743.
(184) Park, S. Y.; Han, B. R.; Na, K. M.; Han, D. K.; Kim, S. C. *Macromolecules* **2003**, *36*, 4115.
(185) Hao, Q.; Li, F.; Li, Q.; Li, Y.; Jia, L.; Yang, J.; Fang, Q.; Cao, A. *Biomacromolecules* **2005**, *6*, 2236.
(186) George, K. A.; Chirila, T. V.; Wentrup-Byrne, E. *Polymer* **2010**, *51*, 1670.
(187) Kricheldorf, H. R.; Rost, S. *Macromol. Chem. Phys.* **2004**, *205*, 1031.
(188) Biela, T.; Duda, A.; Rode, K.; Pasch, H. *Polymer* **2003**, *44*, 1851.
(189) Lee, S.-H.; Hyun Kim, S.; Han, Y.-K.; Kim, Y. H. *J. Polym. Sci. A* **2001**, *39*, 973.
(190) Shaver, M. P.; Cameron, D. J. A. *Biomacromolecules* **2010**, *11*, 3673.
(191) Isono, T.; Kondo, Y.; Otsuka, I.; Nishiyama, Y.; Borsali, R.; Kakuchi, T.; Satoh, T. *Macromolecules* **2013**, *46*, 8509.
(192) Chen, J.; Gorczynski, J. L.; Zhang, G.; Fraser, C. L. *Macromolecules* **2010**, *43*, 4909.
(193) Zhao, W.; Li, C.; Liu, B.; Wang, X.; Li, P.; Wang, Y.; Wu, C.; Yao, C.; Tang, T.; Liu, X.; Cui, D. *Macromolecules* **2014**, *47*, 5586.
(194) Pitet, L. M.; Hait, S. B.; Lanyk, T. J.; Knauss, D. M. *Macromolecules* **2007**, *40*, 2327.
(195) Kricheldorf, H. R.; Fechner, B. *J. Polym. Sci. A* **2002**, *40*, 1047.
(196) Zhao, W.; Li, C. Y.; Liu, B.; Wang, X.; Li, P.; Wang, Y.; Wu, C. J.; Yao, C. G.; Tang, T.; Liu, X. L.; Cui, D. M. *Macromolecules* **2014**, *47*, 5586.
(197) Doi, M.; Edwards, S. *The Theory of Polymer Dynamics*; OXFORD University Press, 1999.
(198) Graessley, W. W.; Roovers, J. *Macromolecules* **1979**, *12*, 959.
(199) Milner, S. T.; McLeish, T. C. B. *Macromolecules* **1997**, *30*, 2159.
(200) McLeish, T. C. B. *Adv. Phys.* **2002**, *51*, 1379.
(201) Kraus, G.; Gruver, J. T. *J. Polym. Sci. A* **1965**, *3*, 105.
(202) Kraus, G.; Gruver, J. T. *J. Polym. Sci. A-2* **1970**, *8*, 305.
(203) Pearson, D. S.; Helfand, E. *Macromolecules* **1984**, *17*, 888.
(204) Watanabe, H.; Matsumiya, Y.; Ishida, S.; Takigawa, T.; Yamamoto, T.; Vlassopoulos, D.; Roovers, J. *Macromolecules* **2005**, *38*, 7404.
(205) Tezel, A. K.; Oberhauser, J. P.; Graham, R. S.; Jagannathan, K.; McLeish, T. C. B.; Leal, L. G. *J. Rheol.* **2009**, *53*, 1193.
(206) Koga, T.; Tanaka, F.; Kaneda, I.; Winnik, F. M. *Langmuir* **2009**, *25*, 8626.
(207) Dorgan, J. R.; Williams, J. S.; Lewis, D. N. *J. Rheol.* **1999**, *43*, 1141.

(208) Nouri, S.; Dubois, C.; Lafleur, P. G. *J. Polym. Sci. B* **2015**, *53*, 522.
(209) Yamaguchi, M.; Arakawa, K. *Eur. Polym. J.* **2006**, *42*, 1479.
(210) Chen, C.; Dong, L.; Yu, P. H. F. *Eur. Polym. J.* **2006**, *42*, 2838.
(211) Chen, C.; Fei, B.; Peng, S.; Zhuang, Y.; Dong, L.; Feng, Z. *J. Appl. Polym. Sci.* **2002**, *84*, 1789.
(212) Mousavioun, P.; Doherty, W. O. S.; George, G. *Ind Crops Prod.* **2010**, *32*, 656.
(213) Persico, P.; Ambrogi, V.; Baroni, A.; Santagata, G.; Carfagna, C.; Malinconico, M.; Cerruti, P. *Int. J. Biol. Macromol.* **2012**, *51*, 1151.
(214) Jellinek, H. H. G. *J. Polym. Sci. C* **1982**, *20*, 599.
(215) Lee, S. N.; Lee, M. Y.; Park, W. H. *J. Appl. Polym. Sci.* **2002**, *83*, 2945.
(216) Arza, C. R.; Jannasch, P.; Johansson, P.; Magnusson, P.; Werker, A.; Maurer, F. H. J. *J. Appl. Polym. Sci.* **2015**, *132*, n/a.
(217) Osten, K. M.; Aluthge, D. C.; Mehrkhodavandi, P. *Dalton Transactions* **2015**, *44*, 6126.
(218) Labourdette, G.; Lee, D. J.; Patrick, B. O.; Ezhova, M. B.; Mehrkhodavandi, P. *Organometallics* **2009**, *28*, 1309.
(219) Ebrahimi, T. E., Mamleeva; Yu, Insun ; Hatzikiriakos, Savvas ;Mehrkhodavandi,Parisa **2016**.
(220) Holmberg, A. L.; Reno, K. H.; Wool, R. P.; Epps, T. H. *Soft Matter* **2014**, *10*, 7405.
(221) Hillmyer, M. A.; Tolman, W. B. *Acc. Chem. Res.* **2014**, *47*, 2390.
(222) Roux, R.; Ladaviere, C.; Montembault, A.; Delair, T. *Mater. Sci. Eng., C* **2013**, *33*, 997.
(223) Chen, G. Q.; Wu, Q. *Biomaterials* **2005**, *26*, 6565.
(224) Lenz, R. W.; Marchessault, R. H. *Biomacromolecules* **2005**, *6*, 1.
(225) Reddy, C. S. K.; Ghai, R.; Rashmi; Kalia, V. C. *Bioresour Technol.* **2003**, *87*, 137.
(226) Duda, A.; Kowalski, A. In *Handbook of Ring-Opening Polymerization*; Dubois, P., Coulembier, O., Raquez, J. M., Eds.; Wiley-VCH Verlag GmbH & Co.: 2009, p 1.
(227) Grunova, E.; Kirillov, E.; Roisnel, T.; Carpentier, J. F. *Organometallics* **2008**, *27*, 5691.
(228) Mahrova, T. V.; Fukin, G. K.; Cherkasov, A. V.; Trifonov, A. A.; Ajellal, N.; Carpentier, J. F. *Inorg. Chem.* **2009**, *48*, 4258.
(229) Hiki, S.; Miyamoto, M.; Kimura, Y. *Polymer* **2000**, *41*, 7369.
(230) Kricheldorf, H. R.; Lee, S. R. *Macromolecules* **1995**, *28*, 6718.
(231) Oh, J. K. *Soft Matter* **2011**, *7*, 5096.
(232) Cross, E. D.; Allan, L. E. N.; Decken, A.; Shaver, M. P. *J. Polym. Sci., Part A: Polym. Chem.* **2013**, *51*, 1137.
(233) Kricheldorf, H. R.; Lee, S.-R. *Macromolecules* **1996**, *29*, 8689.
(234) Seebach, D.; Herrmann, G. F.; Lengweiler, U. D.; Bachmann, B. M.; Amrein, W. *Angew. Chem. Int. Ed.* **1996**, *35*, 2795.
(235) Zhu, J. L.; Liu, K. L.; Zhang, Z. X.; Zhang, X. Z.; Li, J. *Chem. Commun.* **2011**, *47*, 12849.
(236) Douglas, A. F.; Patrick, B. O.; Mehrkhodavandi, P. *Angew. Chem. Int. Ed.* **2008**, *47*, 2290.
(237) Fang, J.; Yu, I.; Mehrkhodavandi, P.; Maron, L. *Organometallics* **2013**, *32*, 6950.

(238) Acosta-Ramirez, A.; Douglas, A. F.; Yu, I.; Patrick, B. O.; Diaconescu, P. L.; Mehrkhodavandi, P. *Inorg. Chem.* **2010**, *49*, 5444.

(239) Mamleeva, E., University of British Columbia, 2015.

(240) Trinkle, S.; Friedrich, C. *Rheol. Acta* **2001**, *40*, 322.

(241) Vega, D. A.; Sebastian, J. M.; Russel, W. B.; Register, R. A. *Macromolecules* **2001**, *35*, 169.

(242) Das, C.; Inkson, N. J.; Read, D. J.; Kelmanson, M. A.; McLeish, T. C. B. *J. Rheol.* **2006**, *50*, 207.

(243) Kainthan, R. K.; Muliawan, E. B.; Hatzikiriakos, S. G.; Brooks, D. E. *Macromolecules* **2006**, *39*, 7708.

(244) Huang, C.-L.; Chen, Y.-C.; Hsiao, T.-J.; Tsai, J.-C.; Wang, C. *Macromolecules* **2011**, *44*, 6155.

(245) Snijkers, F.; Ratkanthwar, K.; Vlassopoulos, D.; Hadjichristidis, N. *Macromolecules* **2013**, *46*, 5702.

(246) Kim, E. S.; Kim, B. C.; Kim, S. H. *J. Polym. Sci. B* **2004**, *42*, 939.

(247) Kunioka, M.; Doi, Y. *Macromolecules* **1990**, *23*, 1933.

(248) Arza, C. R.; Jannasch, P.; Johansson, P.; Magnusson, P.; Werker, A.; Maurer, F. H. J. *J. Appl. Polym. Sci.* **2015**, *132*, 41836.

(249) Park, S. H.; Lim, S. T.; Shin, T. K.; Choi, H. J.; Jhon, M. S. *Polymer* **2001**, *42*, 5737.

(250) Chee, M. J. K.; Ismail, J.; Kummerlöwe, C.; Kammer, H. W. *Polymer* **2002**, *43*, 1235.

(251) Xing, P.; Dong, L.; An, Y.; Feng, Z.; Avella, M.; Martuscelli, E. *Macromolecules* **1997**, *30*, 2726.

(252) Ariffin, H.; Nishida, H.; Shirai, Y.; Hassan, M. A. *Polym. Degrad. Stab.* **2010**, *95*, 1375.

(253) Hablot, E.; Bordes, P.; Pollet, E.; Avérous, L. *Polym. Degrad. Stab.* **2008**, *93*, 413.

(254) Csomorová, K.; Rychlý, J.; Bakoš, D.; Janigová, I. *Polym. Degrad. Stab.* **1994**, *43*, 441.

(255) Doi, Y.; Kunioka, M.; Nakamura, Y.; Soga, K. *Macromolecules* **1986**, *19*, 2860.

(256) Rieth, L. R.; Moore, D. R.; Lobkovsky, E. B.; Coates, G. W. *J. Am. Chem. Soc.* **2002**, *124*, 15239.

(257) Guillaume, C.; Carpentier, J.-F.; Guillaume, S. M. *Polymer* **2009**, *50*, 5909.

(258) Poirier, V.; Roisnel, T.; Carpentier, J.-F.; Sarazin, Y. *Dalton Trans.* **2009**, 9820.

(259) Poirier, V.; Roisnel, T.; Carpentier, J.-F.; Sarazin, Y. *Dalton Trans.* **2011**, *40*, 523.

(260) Zhang, X. M.; Emge, T. J.; Hultzsch, K. C. *Organometallics* **2010**, *29*, 5871.

(261) Ebrahimi, T.; Mamleeva, E.; Yu, I.; Haztzikiriakos, S. G.; Mehrkhodavandi, P. *Inorg. Chem.* **2016**, *55*, 9445−9453.

(262) Chen, H. Y.; Tang, H. Y.; Lin, C. C. *Macromolecules* **2006**, *39*, 3745.

(263) Chamberlain, B. M.; Cheng, M.; Moore, D. R.; Ovitt, T. M.; Lobkovsky, E. B.; Coates, G. W. *J. Am. Chem. Soc.* **2001**, *123*, 3229.

(264) Chuang, H. J.; Weng, S. F.; Chang, C. C.; Lin, C. C.; Chen, H. Y. *Dalton Trans.* **2011**, *40*, 9601.

(265) Valentini, M.; Ruegger, H.; Pregosin, P. S. *Helv. Chim. Acta* **2001**, *84*, 2833.

(266) Silvernail, C. M.; Yao, L. J.; Hill, L. M. R.; Hillmyer, M. A.; Tolman, W. B. *Inorg. Chem.* **2007**, *46*, 6565.

(267) Macchioni, A.; Ciancaleoni, G.; Zuccaccia, C.; Zuccaccia, D. *Chem. Soc. Rev.* **2008**, *37*, 479.

(268) footnote 5 min rxn.

(269) Fuchs, K.; Friedrich, C.; Weese, J. *Macromolecules* **1996**, *29*, 5893.

(270) Rojo, E.; Muñoz, M. E.; Santamaría, A.; Peña, B. *Macromol. Rapid Commun.* **2004**, *25*, 1314.

(271) Liao, Q.; Noda, I.; Frank, C. W. *Polymer* **2009**, *50*, 6139.

(272) Derakhshandeh, M.; Doufas, A. K.; Hatzikiriakos, S. G. *Rheol. Acta* **2014**, *53*, 519.

(273) Derakhshandeh, M.; Hatzikiriakos, S. G. *Rheol. Acta* **2012**, *51*, 315.

(274) De Rosa, C.; Auriemma, F. *Prog. Polym. Sci.* **2006**, *31*, 145.

(275) Iwata, T. *Angew. Chem. Int. Ed.* **2015**, *54*, 3210.

(276) Liu, J. Y.; Liu, W. E.; Weitzhandler, I.; Bhattacharyya, J.; Li, X. H.; Wang, J.; Qi, Y. Z.; Bhattacharjee, S.; Chilkoti, A. *Angew. Chem. Int. Ed.* **2015**, *54*, 1002.

(277) Thomas, C. M.; Lutz, J. F. *Angew. Chem. Int. Ed.* **2011**, *50*, 9244.

(278) Green, J. J.; Elisseeff, J. H. *Nature* **2016**, *540*, 386.

(279) Lendlein, A.; Langer, R. *Science* **2002**, *296*, 1673.

(280) Pretula, J.; Slomkowski, S.; Penczek, S. *Adv. Drug Delivery Rev.* **2016**, *107*, 3.

(281) Kricheldorf, H. R. *Chem. Rev.* **2009**, *109*, 5579.

(282) Obligacion, J. V.; Bezdek, M. J.; Chirik, P. J. *J. Am. Chem. Soc.* **2017**, *139*, 2825.

(283) Bagh, B.; Broere, D. L. J.; Sinha, V.; Kuijpers, P. F.; van Leest, N. P.; de Bruin, B.; Demeshko, S.; Siegler, M. A.; van der Vlugt, J. I. *J. Am. Chem. Soc.* **2017**, *139*, 5117.

(284) Inagaki, F.; Matsumoto, C.; Okada, Y.; Maruyama, N.; Mukai, C. *Angew. Chem. Int. Ed.* **2015**, *54*, 818.

(285) Hu, X. B.; Soleilhavoup, M.; Melaimi, M.; Chu, J. X.; Bertrand, G. *Angew. Chem. Int. Ed.* **2015**, *54*, 6008.

(286) Zeng, M. S.; Li, L.; Herzon, S. B. *J. Am. Chem. Soc.* **2014**, *136*, 7058.

(287) Xue, Y. X.; Zhu, Y. Y.; Gao, L. M.; He, X. Y.; Liu, N.; Zhang, W. Y.; Yin, J.; Ding, Y. S.; Zhou, H. P.; Wu, Z. Q. *J. Am. Chem. Soc.* **2014**, *136*, 4706.

(288) Scott, D. J.; Fuchter, M. J.; Ashley, A. E. *Angew. Chem. Int. Ed.* **2014**, *53*, 10218.

(289) Pan, B. F.; Gabbai, F. P. *J. Am. Chem. Soc.* **2014**, *136*, 9564.

(290) Standley, E. A.; Jamison, T. F. *J. Am. Chem. Soc.* **2013**, *135*, 1585.

(291) Tu, T.; Assenmacher, W.; Peterlik, H.; Weisbarth, R.; Nieger, M.; Dotz, K. H. *Angew. Chem. Int. Ed.* **2007**, *46*, 6368.

(292) Ackermann, L.; Born, R.; Spatz, J. H.; Meyer, D. *Angew. Chem. Int. Ed.* **2005**, *44*, 7216.

(293) Kunioka, M.; Wang, Y.; Onozawa, S. Y. *Macromol Symp.* **2005**, *224*, 167.

(294) Borner, J.; Herres-Pawlis, S.; Floke, U.; Huber, K. *Eur. J. Inorg. Chem.* **2007**, 5645.

(295) Wang, L.; Zhang, J. F.; Yao, L. H.; Tang, N.; Wu, J. C. *Inorg. Chem. Commun.* **2011**, *14*, 859.

(296) Borner, J.; Florke, U.; Huber, K.; Doring, A.; Kuckling, D.; Herres-Pawlis, S. *Chem. Eur. J.* **2009**, *15*, 2362.

(297) Hu, M. G.; Wang, M.; Zhang, P. L.; Wang, L.; Zhu, F. J.; Sun, L. C. *Inorg. Chem. Commun.* **2010**, *13*, 968.

(298) Li, C. Y.; Tsai, C. Y.; Lin, C. H.; Ko, B. T. *Dalton Trans.* **2011**, *40*, 1880.
(299) Li, C.-Y.; Hsu, S.-J.; Lin, C.-l.; Tsai, C.-Y.; Wang, J.-H.; Ko, B.-T.; Lin, C.-H.; Huang, H.-Y. *J. Polym. Sci. A* **2013**, *51*, 3840.
(300) Chuck, C. J.; Davidson, M. G.; Jones, M. D.; Kociok-Köhn, G.; Lunn, M. D.; Wu, S. *Inorg. Chem.* **2006**, *45*, 6595.
(301) Lee, K.-C.; Chuang, H.-J.; Huang, B.-H.; Ko, B.-T.; Lin, P.-H. *Inorg. Chim. Acta* **2016**, *450*, 411.
(302) Fang, H.-J.; Lai, P.-S.; Chen, J.-Y.; Hsu, S. C. N.; Peng, W.-D.; Ou, S.-W.; Lai, Y.-C.; Chen, Y.-J.; Chung, H.; Chen, Y.; Huang, T.-C.; Wu, B.-S.; Chen, H.-Y. *J. Polym. Sci. A* **2012**, *50*, 2697.
(303) Parssinen, A.; Kohlmayr, M.; Leskela, M.; Lahcini, M.; Repo, T. *Polym. Chem.* **2010**, *1*, 834.
(304) Pratt, R. C.; Lyons, C. T.; Wasinger, E. C.; Stack, T. D. P. *J. Am. Chem. Soc.* **2012**, *134*, 7367.
(305) Bryliakov, K. P.; Talsi, E. P. *Eur. J. Org. Chem.* **2008**, 3369.
(306) Sun, J. T.; Zhu, C. J.; Dai, Z. Y.; Yang, M. H.; Pan, Y.; Hu, H. W. *J. Org. Chem.* **2004**, *69*, 8500.
(307) Balsells, J.; Carroll, P. J.; Walsh, P. J. *Inorg. Chem.* **2001**, *40*, 5568.
(308) Liang, L. C.; Tsai, T. L.; Li, C. W.; Hsu, Y. L.; Lee, T. Y. *Eur. J. Inorg. Chem.* **2011**, 2948.
(309) Ebrahimi, T.; Aluthge, D. C.; Patrick, B. O.; Hatzikiriakos, S. G.; Mehrkhodavandi, P. *ACS Catal.* **2017**, 6413.
(310) Tsuji, H.; Matsumura, N.; Arakawa, Y. *J. Phys. Chem. B* **2016**, *120*, 1183.
(311) Rosen, T.; Goldberg, I.; Venditto, V.; Kol, M. *J. Am. Chem. Soc.* **2016**, *138*, 12041.
(312) Masutani, K.; Lee, C. W.; Kimura, Y. *Polym J* **2013**, *45*, 427.
(313) Hatzikiriakos, S. G.; Kapnistos, M.; Vlassopoulos, D.; Chevillard, C.; Winter, H. H.; Roovers, J. *Rheol. Acta* **2000**, *39*, 38.
(314) Chen, H. C.; Chen, S. H. *J. Phys. Chem.* **1984**, *88*, 5118.

Appendices

Appendix A

A.1 Characterization of complexes 1-2 by ^{1}H NMR, and $^{13}C\{^{1}H\}$ NMR spectroscopy

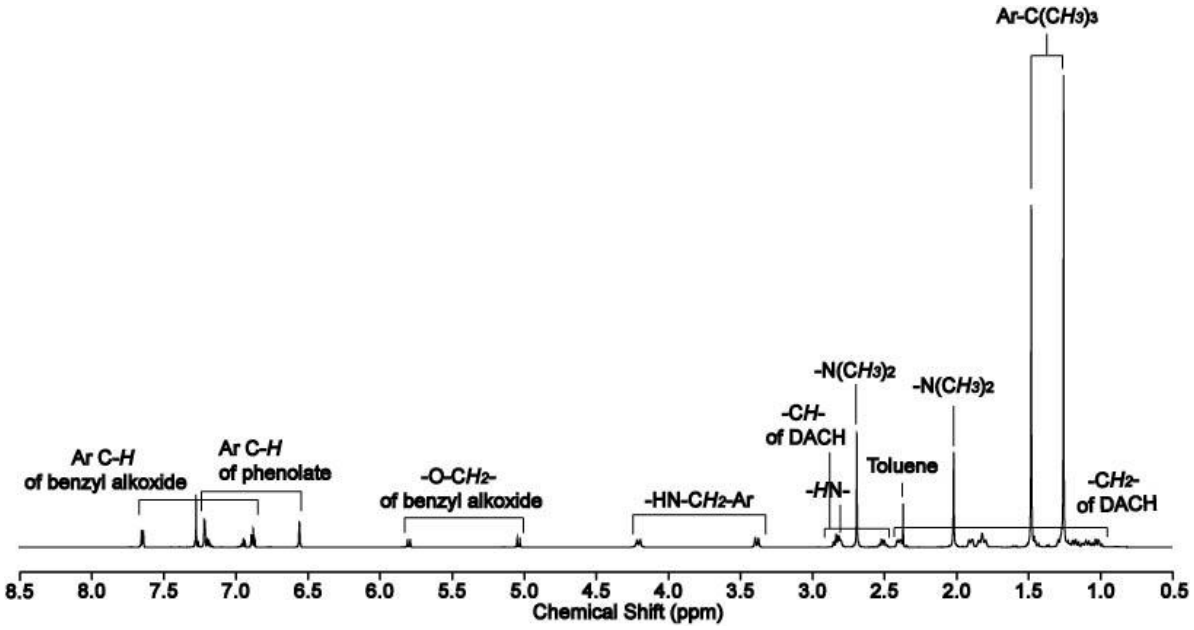

Figure A.1 ^{1}H NMR spectrum ($CDCl_3$, 25 °C) of $[(NNO_{tBu})InCl]_2(\mu\text{-}Cl)(\mu\text{-}OBn)$ (**1**).

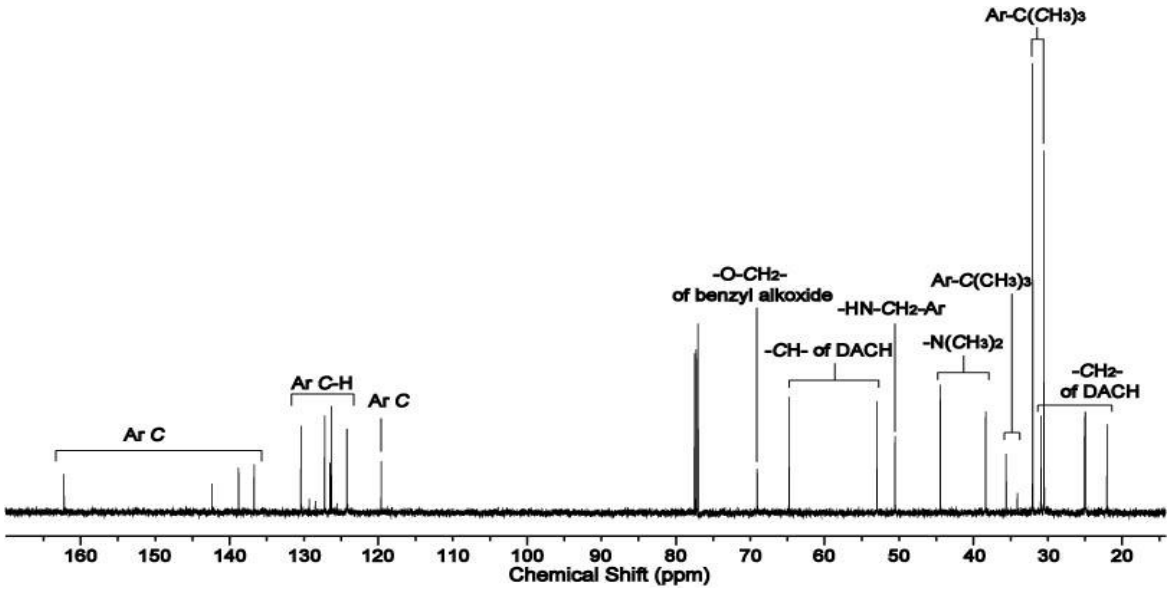

Figure A.2 $^{13}C\{^{1}H\}$ NMR spectrum ($CDCl_3$, 25 °C) of $[(NNO_{tBu})InCl]_2(\mu\text{-}Cl)(\mu\text{-}OBn)$ (**1**).

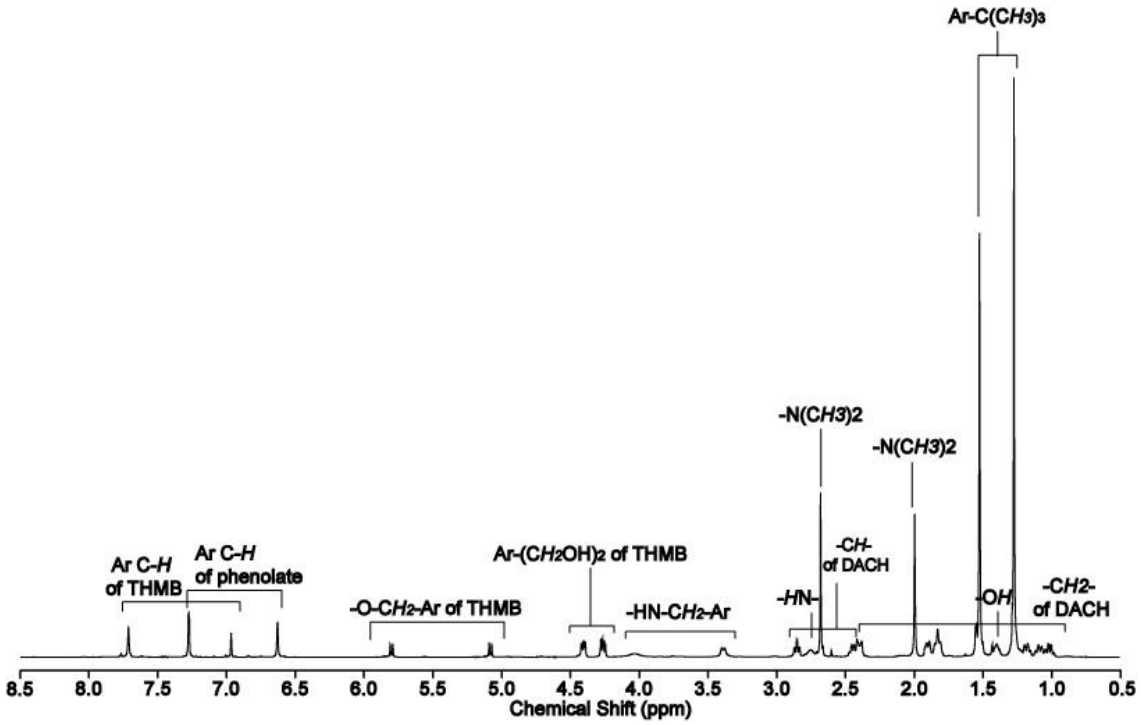

Figure A.3 ^{1}H NMR spectrum ($CDCl_3$, 25 °C) of $[(NNO_{tBu})InCl]_2(\mu\text{-Cl})(\mu\text{-OTHMB})$ (**2**).

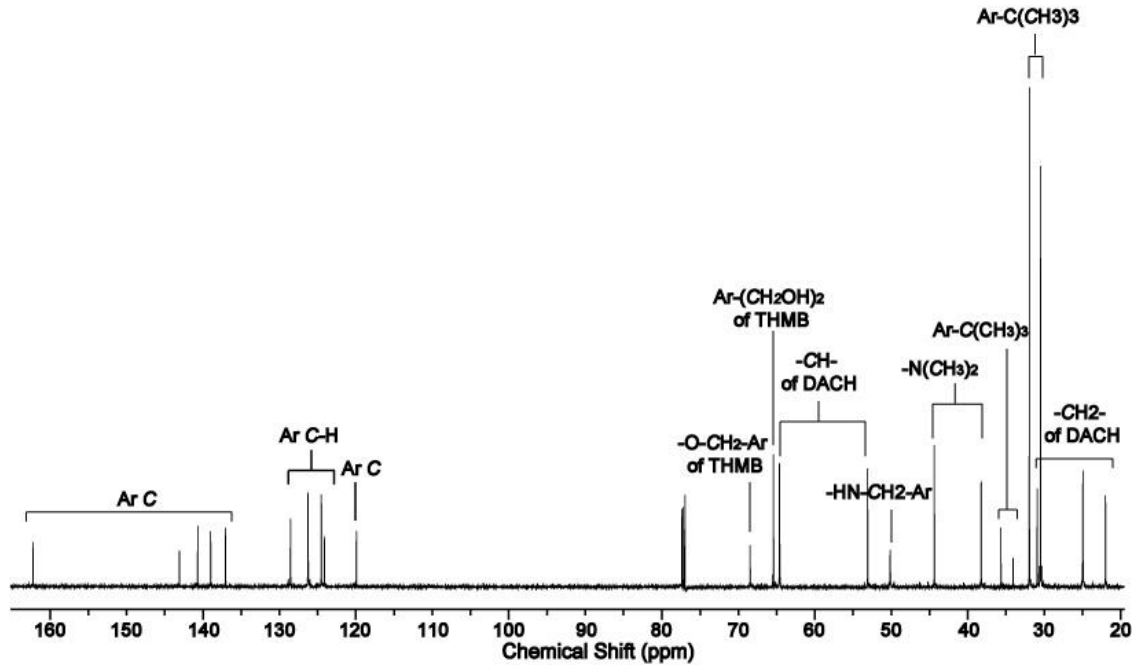

Figure A.4 $^{13}C\{^{1}H\}$ NMR spectrum ($CDCl_3$, 25 °C) of $[(NNO_{tBu})InCl]_2(\mu\text{-Cl})(\mu\text{-OTHMB})$ (**2**).

A.2 Crystallographic data for the solid state structure of complex 2

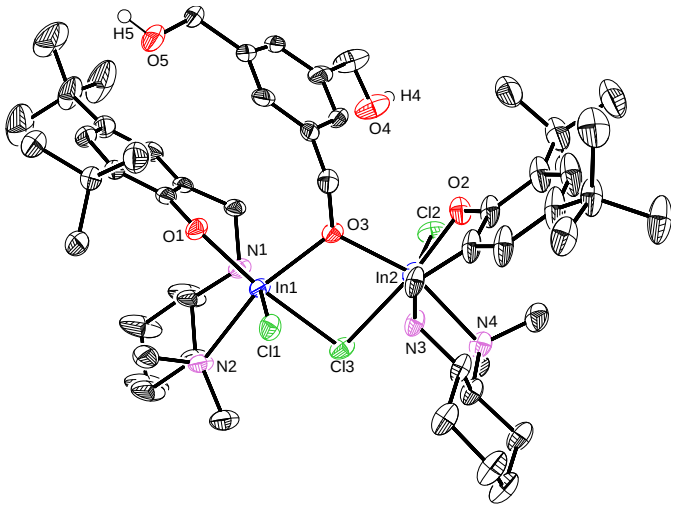

Figure A.5 Molecular structure of (*SS/SS*)-**2** (depicted with thermal ellipsoids at 50% probability and most H atoms omitted for clarity). Selected bond lengths (Å) and angles (deg): N1-In1 2.205(4), N2-In1 2.378(3), O1-In1 2.089(3), O3-In1 2.164(3), Cl1-In1 2.4165(12), Cl3-In1 2.6613(12), N3-In2 2.257(3), N4-In2 2.366(3), O2-In2 2.078(3), O3-In2 2.168(2), Cl2-In2 2.4297(13), Cl3-In2 2.6066(12), In1-O3-In2 114.89(11), In2-Cl3-In1 87.77(3), N1-In1-N2 77.22(12), N1-In1-O1 86.15(12), N1-In1-O3 97.50(12), N1-In1-Cl3 85.19(10), N1-In1-Cl1 168.51(9), N2-In1-Cl1 91.31(9), N2-In1-Cl3 85.54(9), O1-In1-O3 98.18(10), O1-In1-N2 98.56(11), O1-In1-Cl1 95.02(8), O1-In1-Cl3 169.36(8), O3-In1-N2 162.05(11), O3-In1-Cl1 93.65(7), O3-In1-Cl3 76.87(7), Cl1-In1-Cl3 94.70(3), N3-In2-N4 76.90(11), N3-In2-O2 86.63(13), N3-In2-O3 94.36(11), N3-In2-Cl2 166.72(9), N3-In2-Cl3 86.29(10), N4-In2-O3 160.80(11), N4-In2-Cl2 90.94(9), N4-In2-Cl3 84.30(9), O2-In2-N4 102.93(11), O2-In2-O3 93.45(10), O2-In2-Cl2 91.01(9), O2-In2-Cl3 168.47(8), O3-In2-Cl2 98.82(7), O3-In2-Cl3 78.03(7), Cl2-In2-Cl3 97.92.

Table A.1 X-ray results of complex **2**

Crystal characteristics	**2**
empirical formula	$C_{62}H_{97}Cl_3In_2N_4O_5$
fw	1314.42
T (K)	90(2)
a (Å)	12.169(3)
b (Å)	15.269(4)
c (Å)	18.288(5)
α (deg)	81.554(7)
β (deg)	80.349(6)
γ (deg)	74.877(6)
volume (Å^3)	3215.0(15)
Z	2

cryst syst	triclinic
space group	P -1
d_{calc} (g/cm^3)	1.358
μ (Mo K α) (cm^{-1})	8.9
2 θ_{max} (deg)	55.2
absor corr (T_{min}, T_{max})	0.8570, 0.9396
total no. of reflns	68 410
no. of indep reflns (R_{int})	14 748 (0.0464)
residuals (refined on F^2): R_1; wR_2	0.0708, 0.1065
GOF	1.049
no. obsrvns [$I > 2\sigma(I)$]	9921
residuals (refined on F^2: $R_1{}^a$; $wR_2{}^b$)	0.0460, 0.0938

A.3 ^{1}H NMR, ^{13}C NMR and MALDI-TOF analysis of PHB oligomers

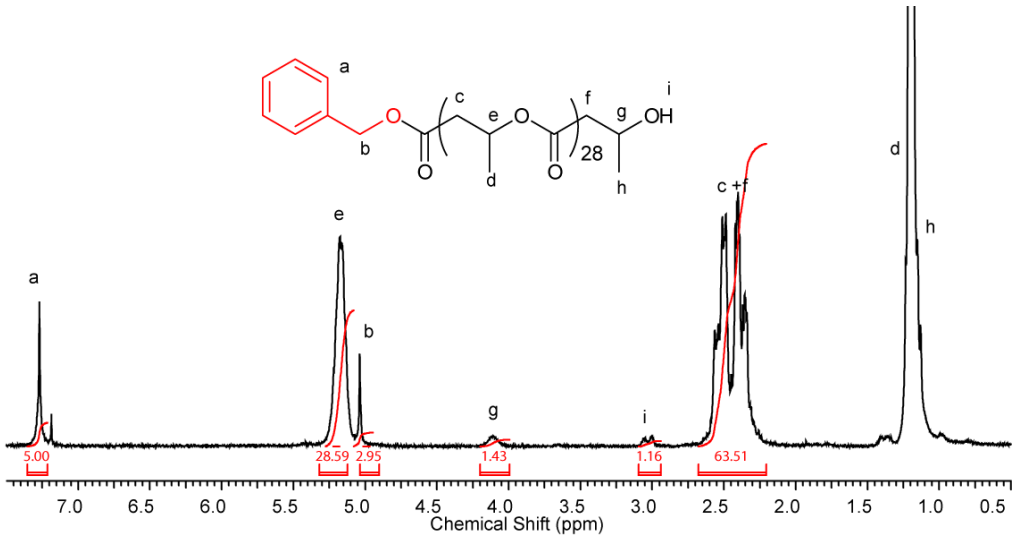

Figure A.6 ^{1}H NMR ($CDCl_3$, 25 °C) spectra of the isolated linear PHB, [BBL]:[BnOH]:[1] ratios of 5000:190:1 (Table 3.1, entry 1)

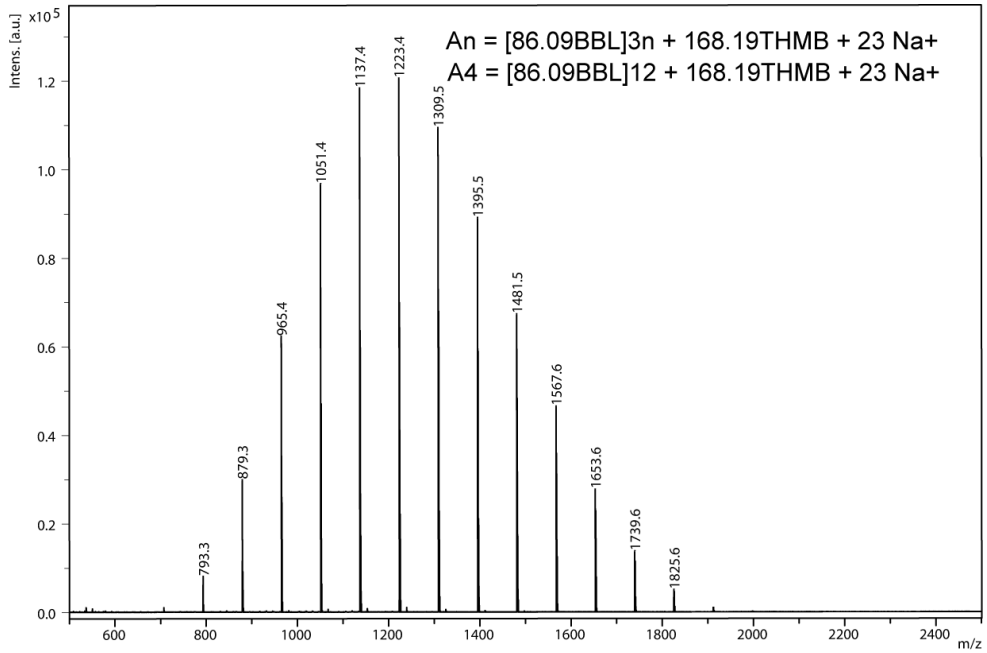

Figure A.7 MALDI-TOF spectrum of 3-arm star PHB isolated from polymerization of [BBL]:[THMB]:[1] ratios of 7400:590:1 (Table 3.1, entry 9. Reaction stopped after 87% conversion and the monomer left overs where removed under high vacuum overnight.

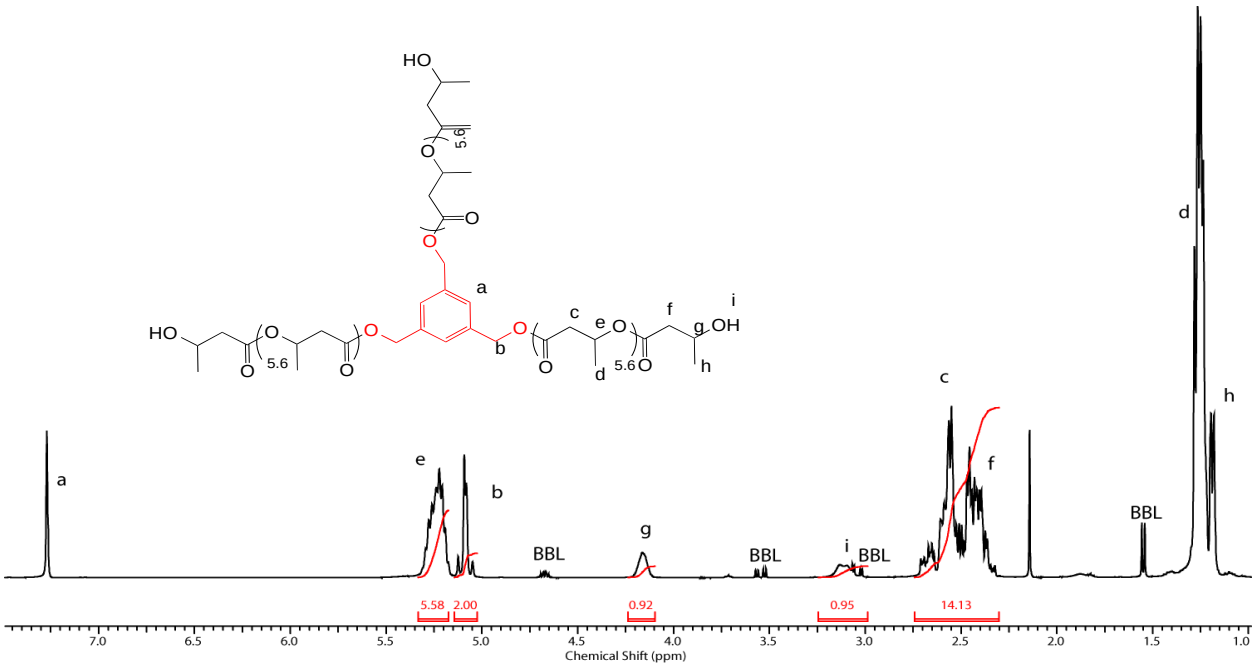

Figure A.8 ^{1}H NMR ($CDCl_3$, 25 °C) spectra of the isolated star PHB, [BBL]:[THMB]:[1] ratios of 5000:300:1 (Table 3.1, entry 10)

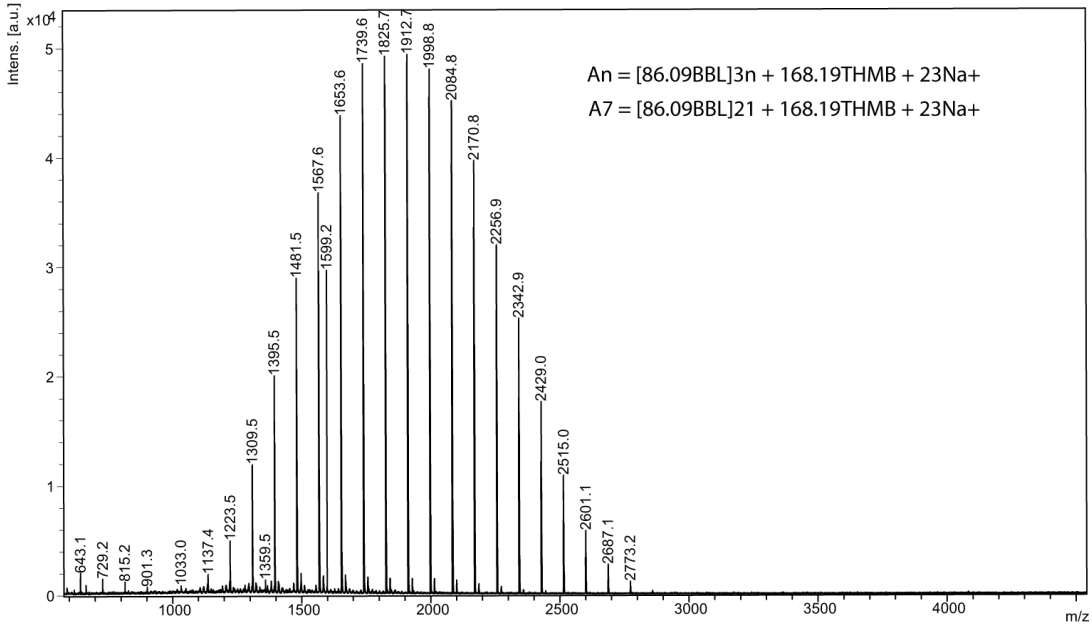

Figure A.9 MALDI-TOF spectrum of 3-arm star PHB isolated from polymerization of [BBL]:[THMB]:[1] ratios of 5000:300:1 (Table 3.1, entry 10)

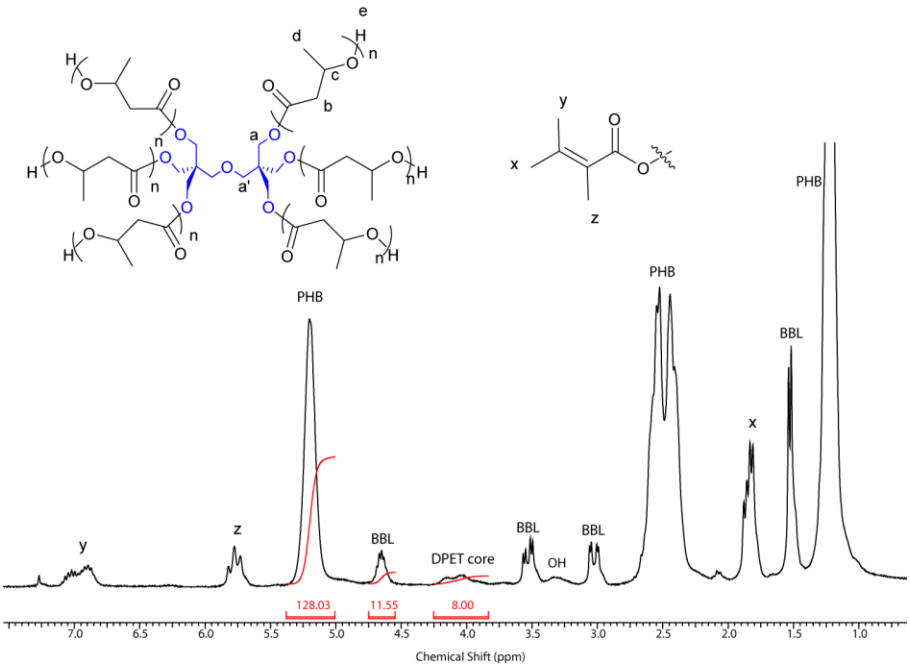

Figure A.10 ^{1}H NMR ($CDCl_3$, 25 °C) spectra of the isolated star PHB, [BBL]:[DPET] ratios of 250:1.

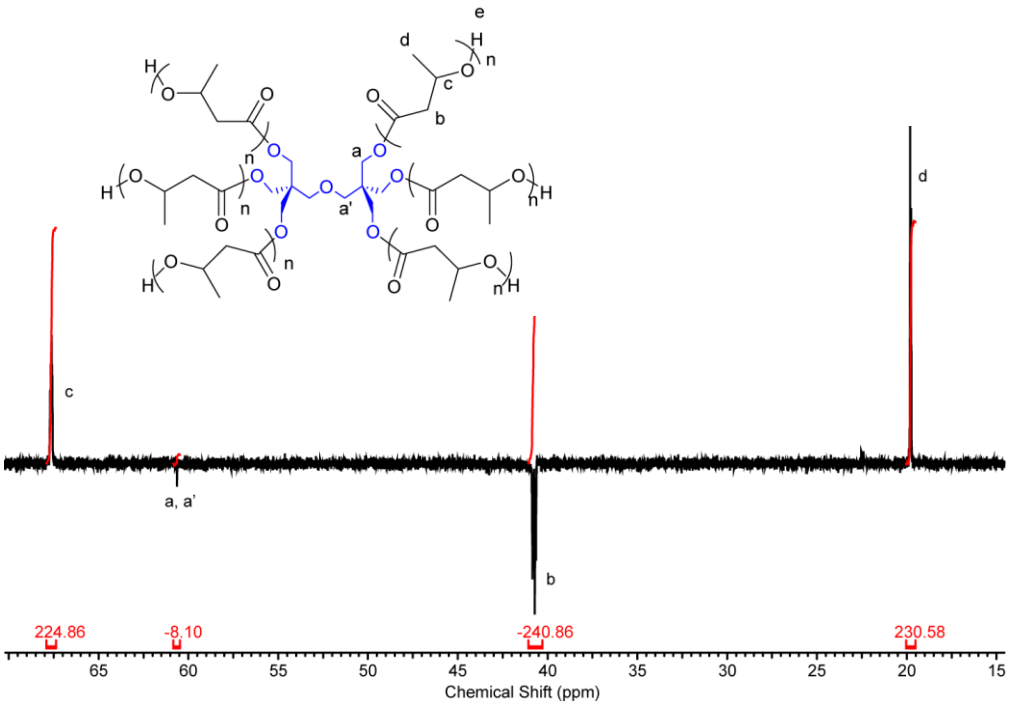

Figure A.11 ^{13}C DEPT NMR ($CDCl_3$, 100 MHz, 25 °C) of isolated star PHB [BBL]:[DPET]:[**3**] ratios of 294:1:1(Table 3.3, entry 1).

A.4 DSC thermograms of moderately syndiotactic star PHBs

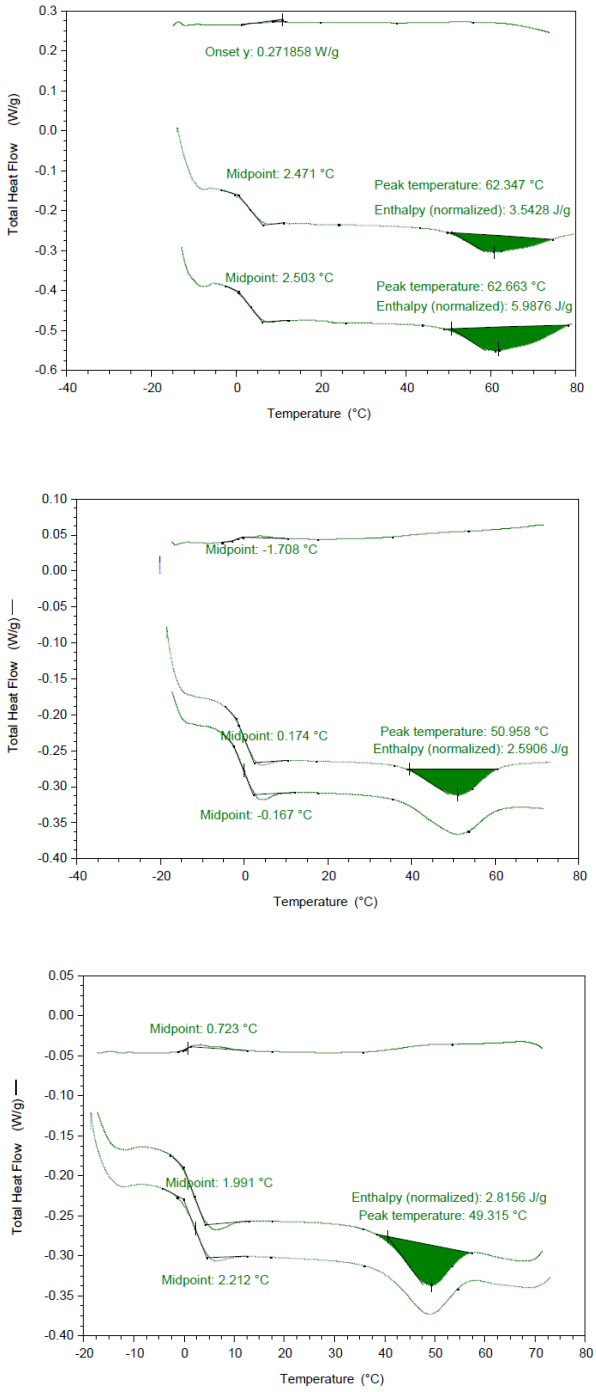

Figure A.12 DSC curves of 6armed star PHBs. Top (Table 3.3 entry 7), bottom left (Table 3.3 entry 6), and bottom right (Table 3.3 entry 5).

A.5 Molecular weight dependence of the linear viscoelastic behavior of linear, 3-armed, and 6-armed star PHBs

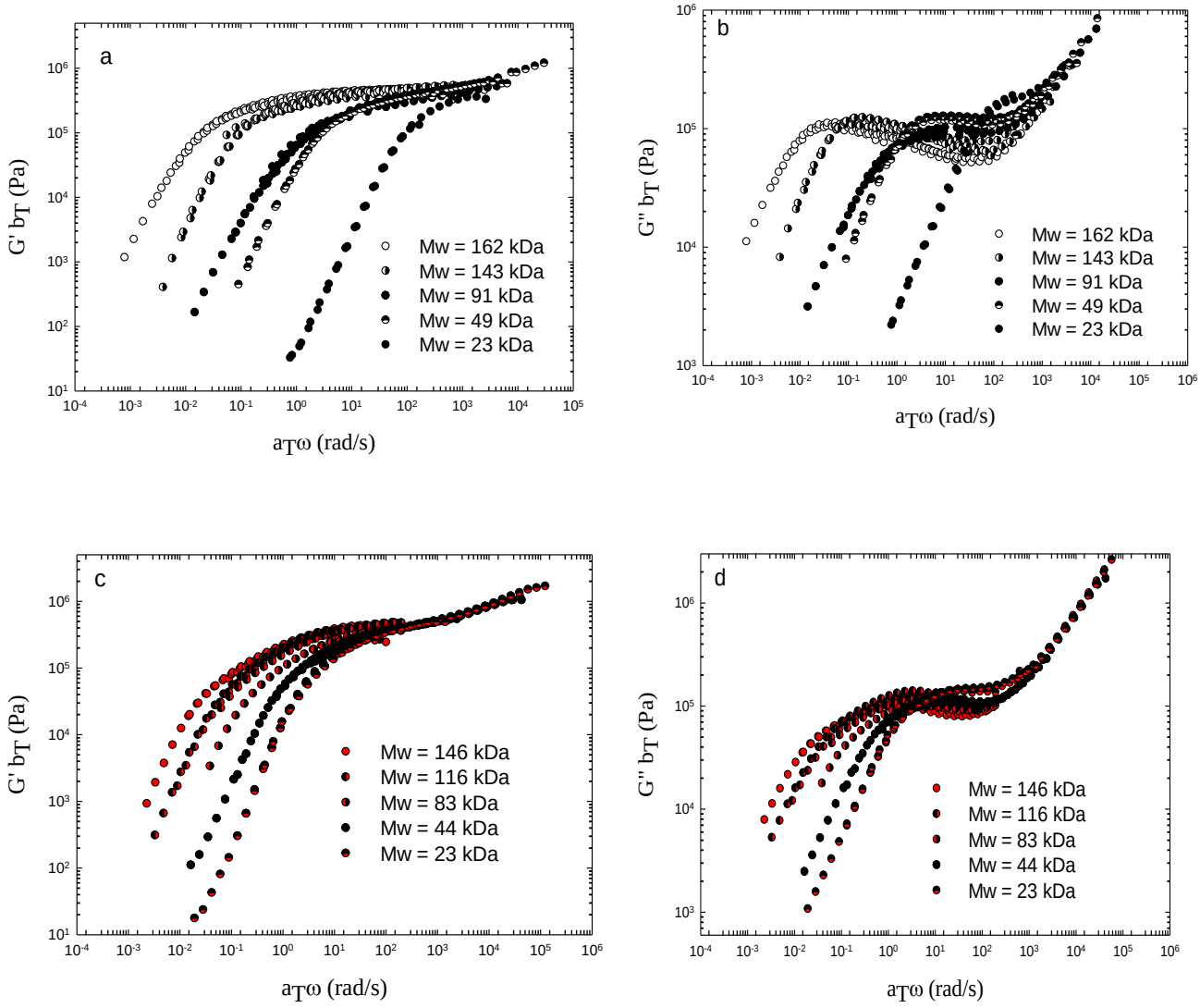

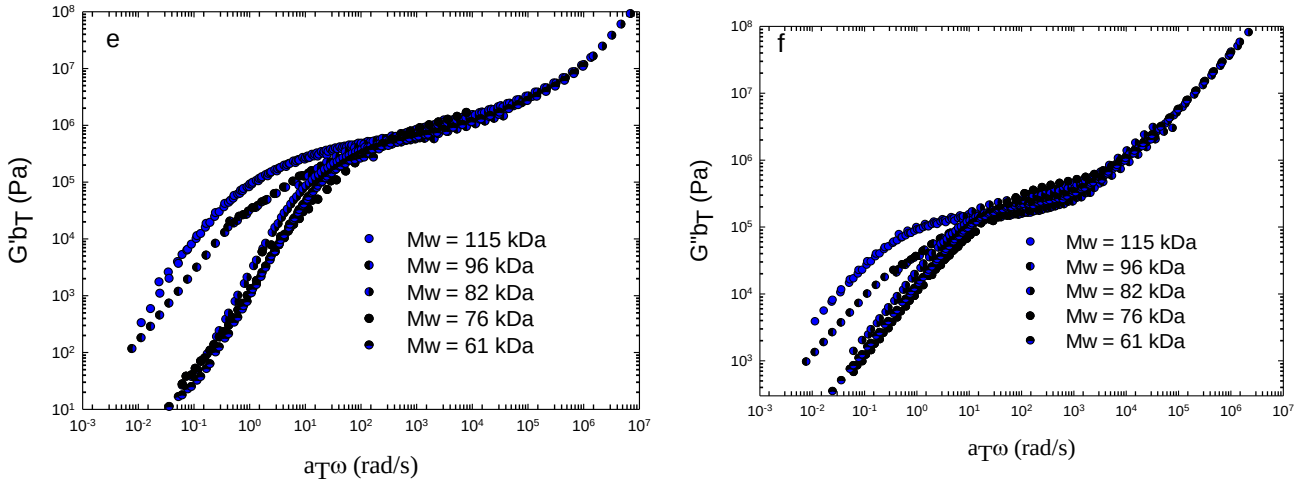

Figure A.13 (a), (b) storage and loss modulus of the linear sample series, **(c), (d)** storage and loss modulus of the 3-armed sample series, and **(e), (f)** storage and loss modulus of the 6-armed sample series at 50 °C as reference temperature.

A.6 Parsimonious relaxation spectrum (g_i, λ_i)

Parsimonious relaxation spectrum calculated from Equations 1 and 2:

$$G'(\omega) = \sum_{i=1}^{n} g_i \frac{(\omega\lambda_i)^2}{1+(\omega\lambda_i)^2} \qquad (A.1)$$

$$G''(\omega) = \sum_{i=1}^{n} g_i \frac{(\omega\lambda_i)}{1+(\omega\lambda_i)^2} \qquad (A.2)$$

Where g_i and λ_i are the relaxation moduli and relaxation times of the generalized Maxwell model and *n* is the number of relaxation modes.

Plotting the g_i values versus λ_i, PM relaxation spectrum, along with curve fitting to the BSW equation (Eqn. 3), showed good agreement between the PM spectrum for linear and star polymers with the BSW model to obtain continues relaxation spectrums (Figure S5).

$$H(\lambda) = \left[H_g \left(\frac{\lambda}{\lambda_c}\right)^{-n_g} + n_e G_N^o \left(\frac{\lambda}{\lambda_{max}}\right)^{n_e}\right] \exp\left(-(\lambda/\lambda_{max})^{\beta}\right)$$

$$H_g = n_e G_N^o \left(\frac{\lambda_1}{\lambda_c}\right)^{n_g} \left(\frac{\lambda_1}{\lambda_{max}}\right)^{n_e} \qquad \text{(A.3)}$$

Where G_N^o is the plateau modulus and λmax is the longest relaxation time. n_e and n_g are the slopes of the spectrum in the entanglement and glass transition zones respectively, and λc is the crossover time to the glass transition.[313]

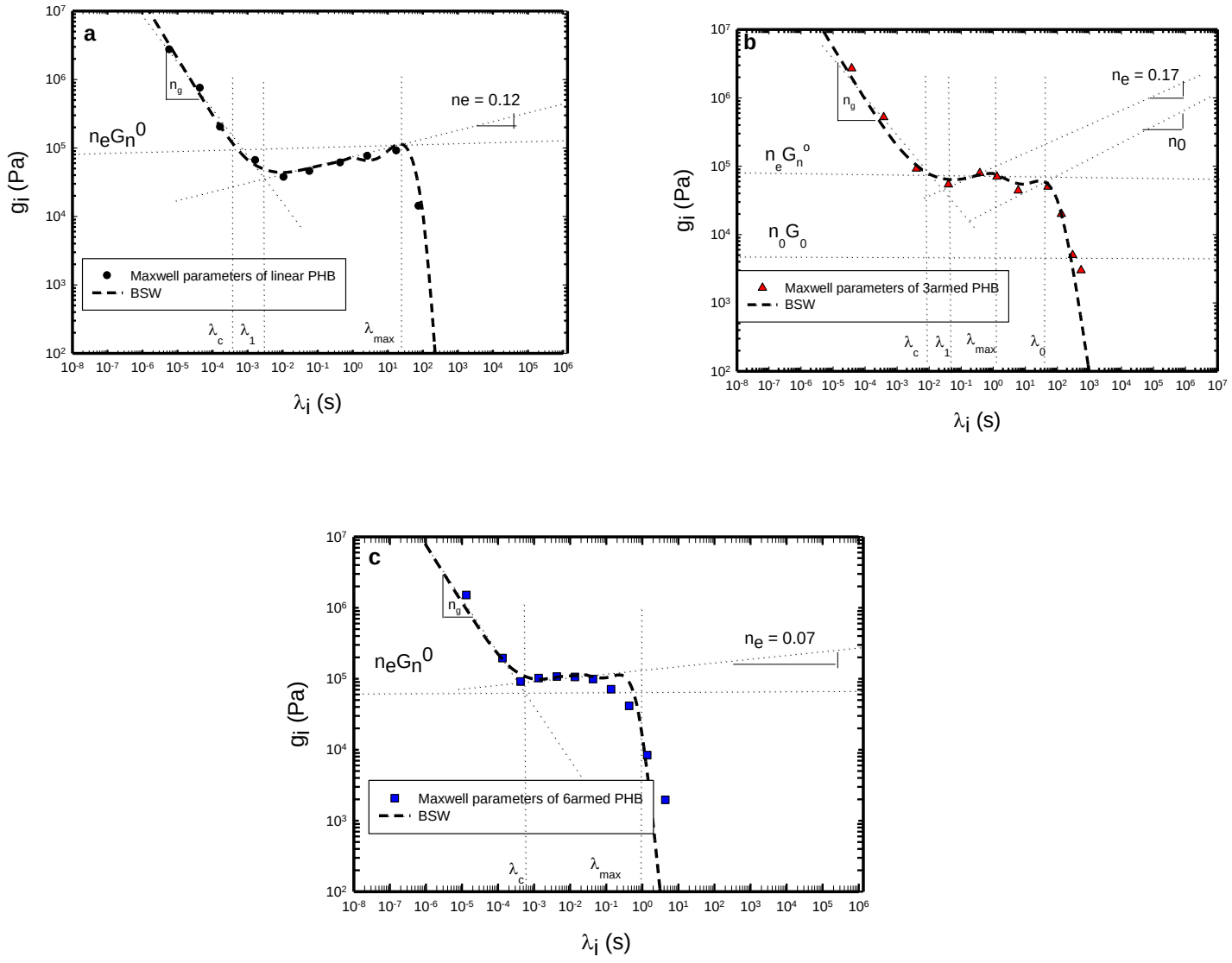

Figure A.14 The PM along with the relaxation spectrum of **(a)** entry 7 of Table 3.1 (Linear PHB, M_w = 162 kgmol^{-1}, $Đ$ = 1.03), **(b)** entry 16 of Table 3.1 (3-armed star PHB, M_w = 146 kgmol^{-1}, $Đ$ = 1.06), **(c)** entry 7 of Table 3.3 (6-armed star PHB, M_w = 114 kgmol^{-1}, $Đ$ = 1.14).

A.7 Shear relaxation modulus plots at different strain rates

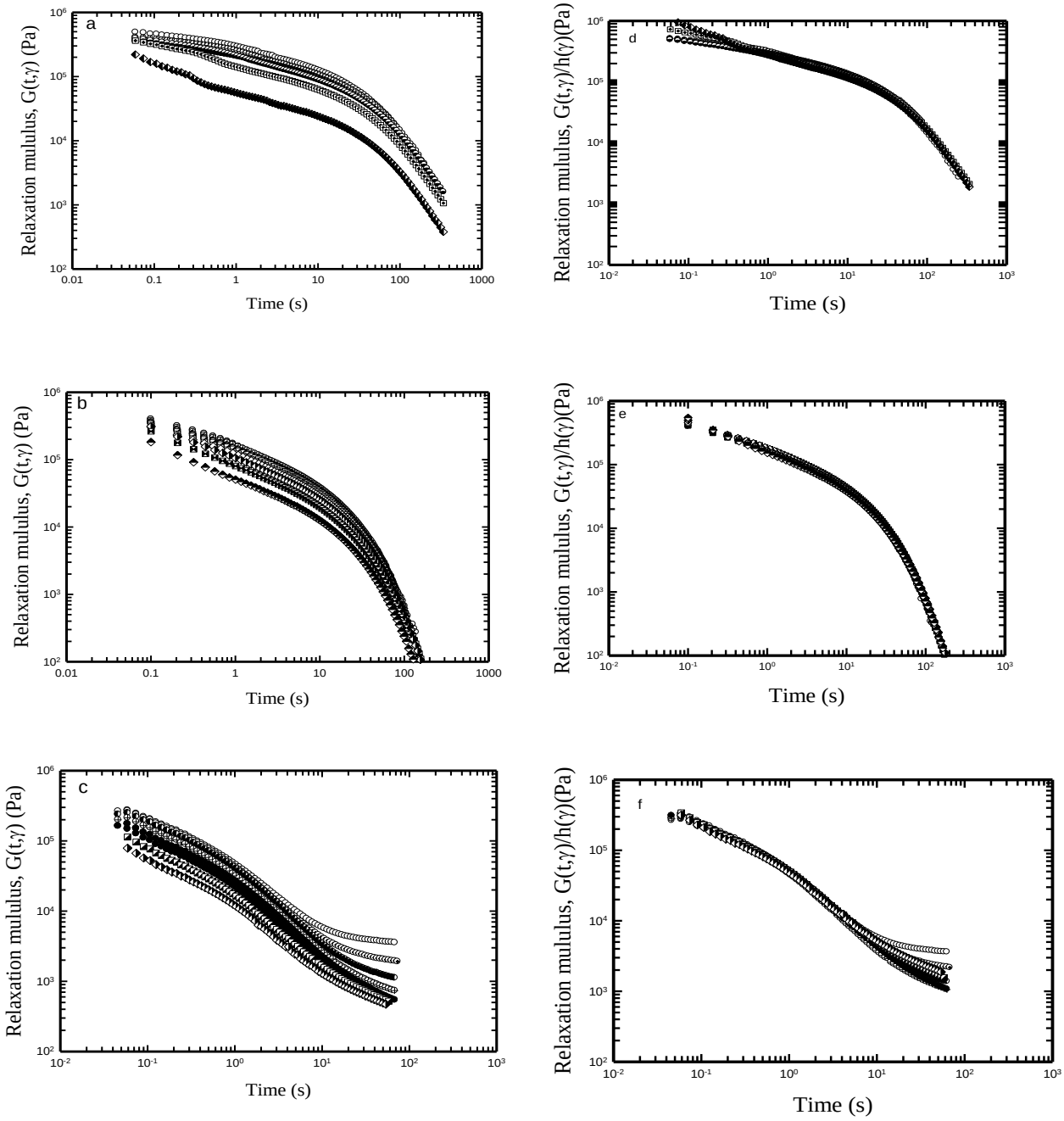

Figure A.15 (a),(b),(c) The shear relaxation modulus $\boldsymbol{G(t,\gamma)}$of entries 7, 16 and of Table 3.1 and entry 7 of Table 3.2 after the imposition of sudden strain values, $\boldsymbol{\gamma}$, at 50 °C; **(d),(e),(f)** Superposition of the stress relaxation modulus data of parts **(a),(b),(c)** to determine the damping function.

A.8 Intrinsic viscosity measurements using Cannon-Fenske viscometer

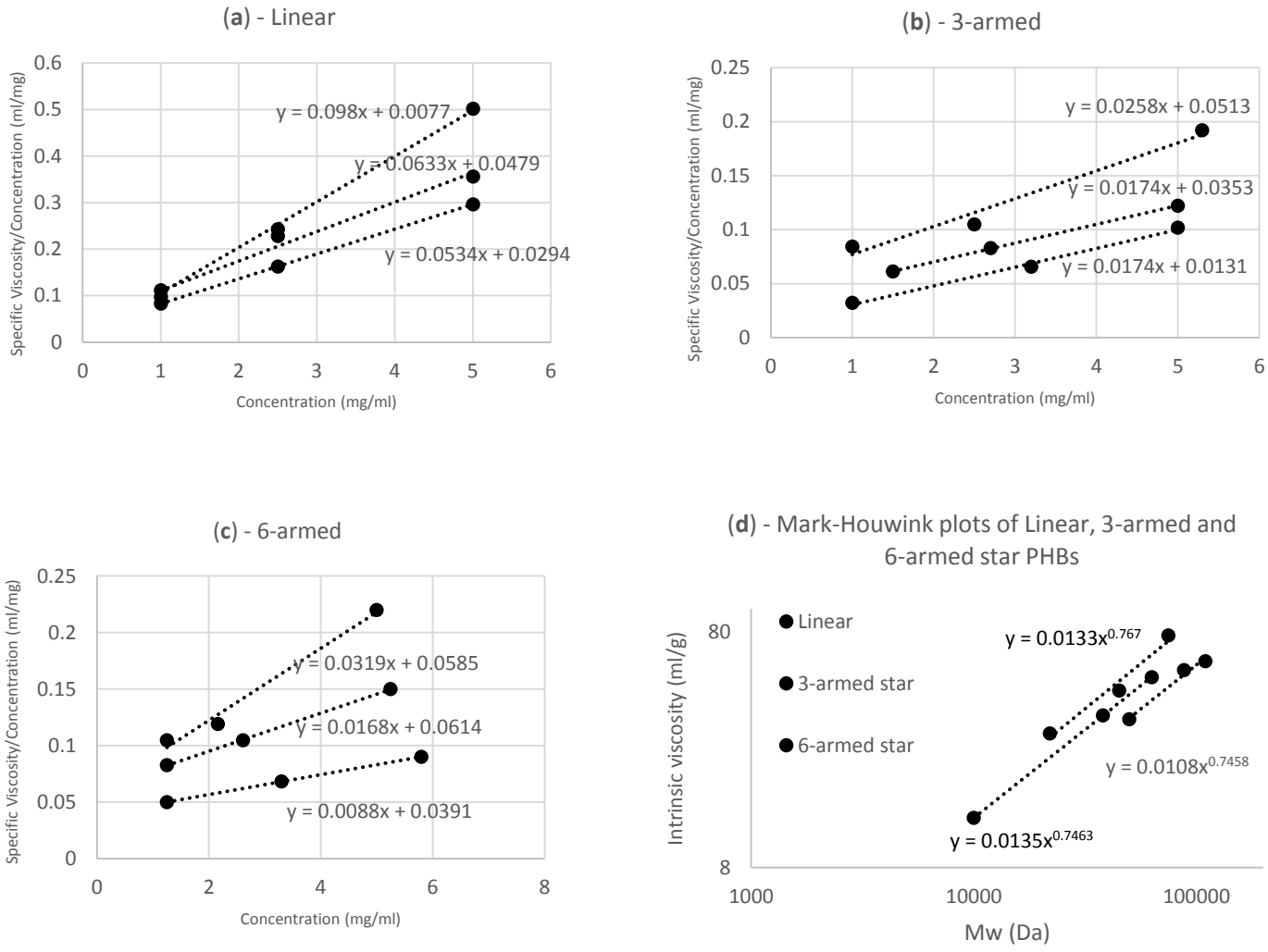

Figure A.16 (a), (b), (c) $(\frac{\eta_{sp}}{C})$ versus concentration of linear, 3-armed and 6 armed star PHBs respectively. **(d)** Mark-Houwink plots of Linear, 3-armed and 6-armed star PHBs

Appendix B

B.1 Characterization of complexes 6-16 by ^{1}H and $^{13}C\{^{1}H\}$ NMR spectroscopy

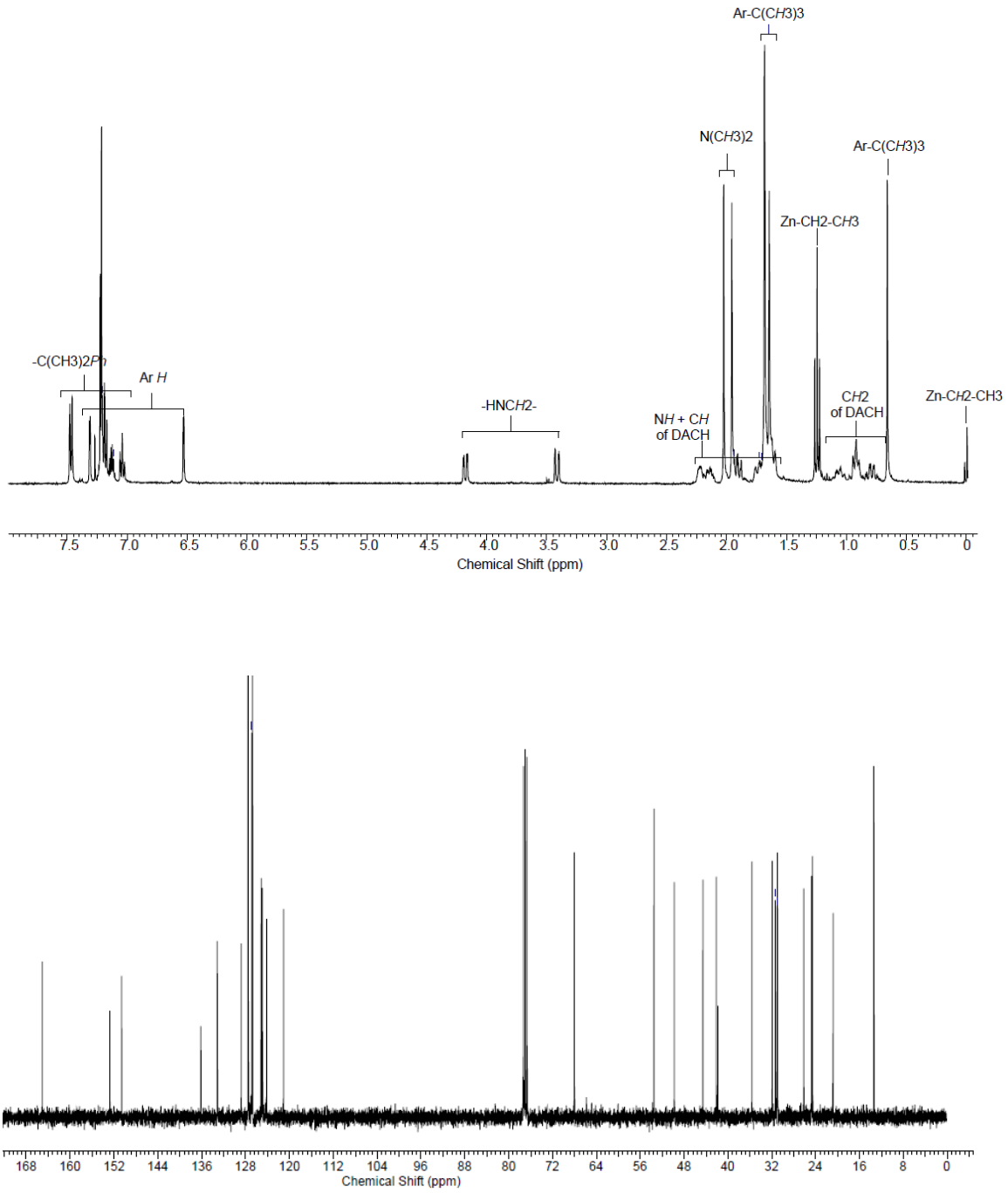

Figure B.1 (top)^{1}H NMR spectrum (bottom) $^{13}C\{^{1}H\}$ NMR ($CDCl_3$, 600 MHz, 25 °C) of complex (±)-**6**

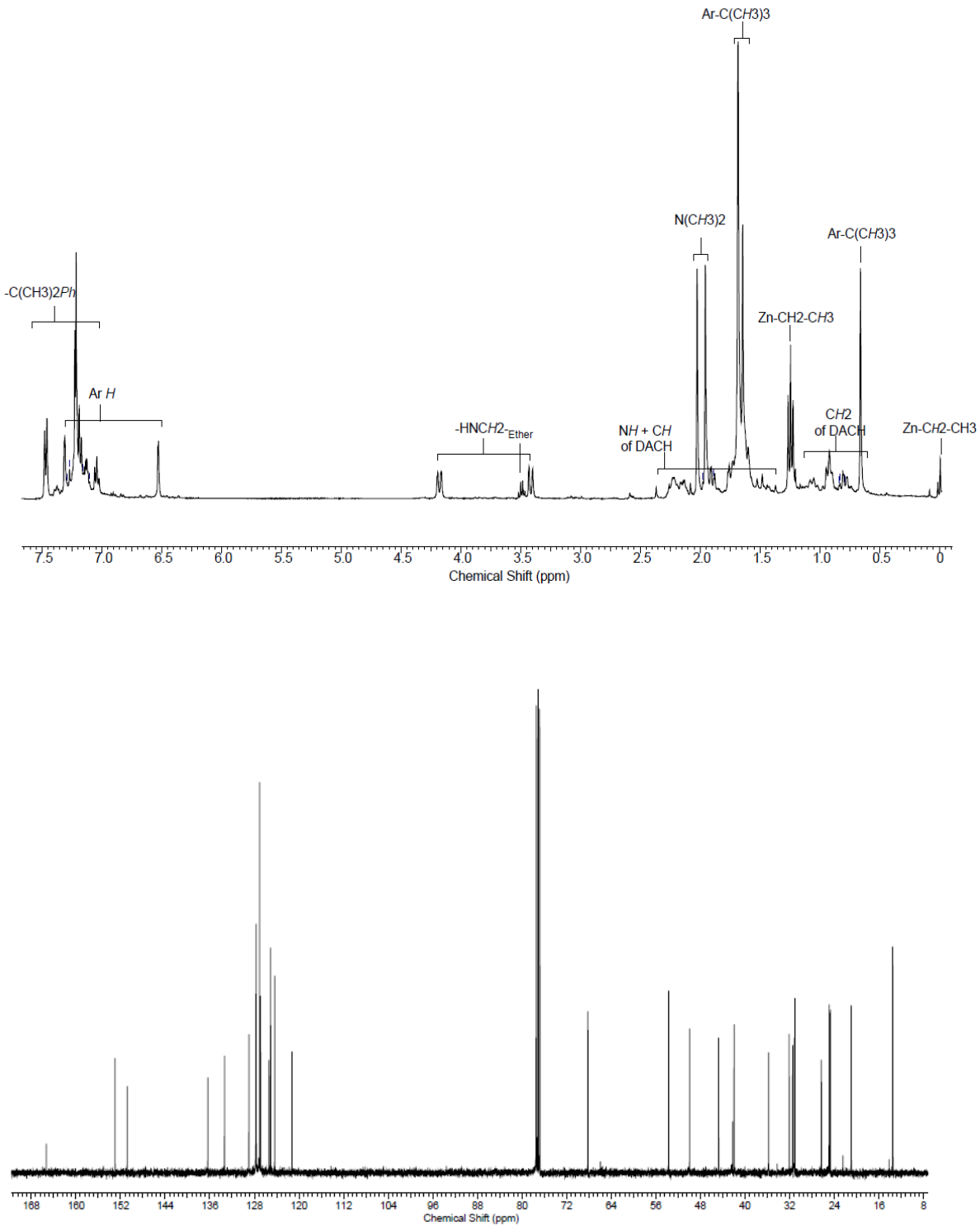

Figure B.2 (top)^{1}H NMR spectrum (bottom) $^{13}C\{^{1}H\}$ NMR ($CDCl_3$, 600 MHz, 25 °C) of complex (*R,R*)-**6**

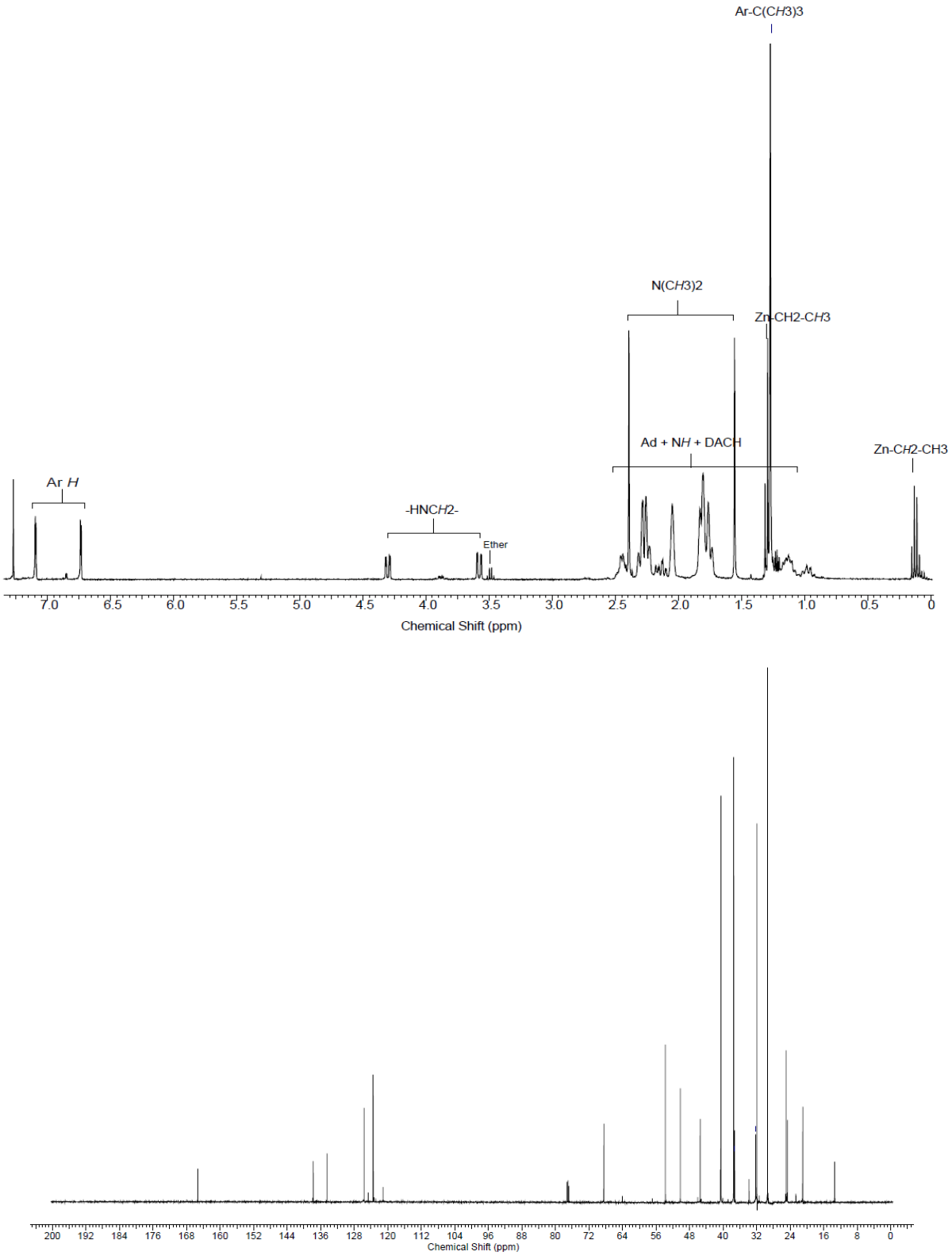

Figure B.3 (top)^{1}H NMR spectrum (bottom) $^{13}C\{^{1}H\}$ NMR ($CDCl_3$, 600 MHz, 25 °C) of complex (±)-**7**

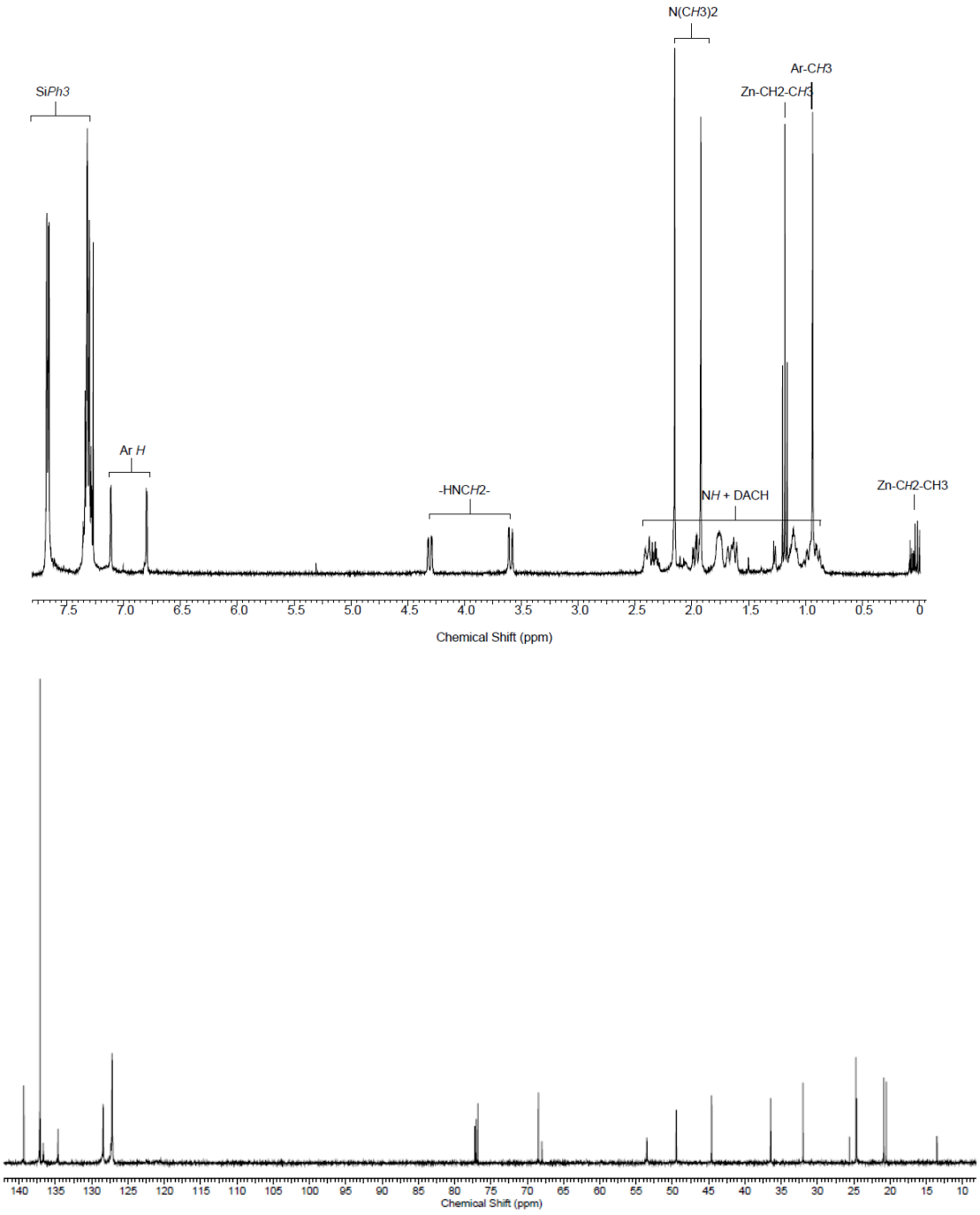

Figure B.4 (top)^{1}H NMR spectrum (bottom) $^{13}C\{^{1}H\}$ NMR ($CDCl_3$, 600 MHz, 25 °C) of complex (*R*,*R*)-**8**

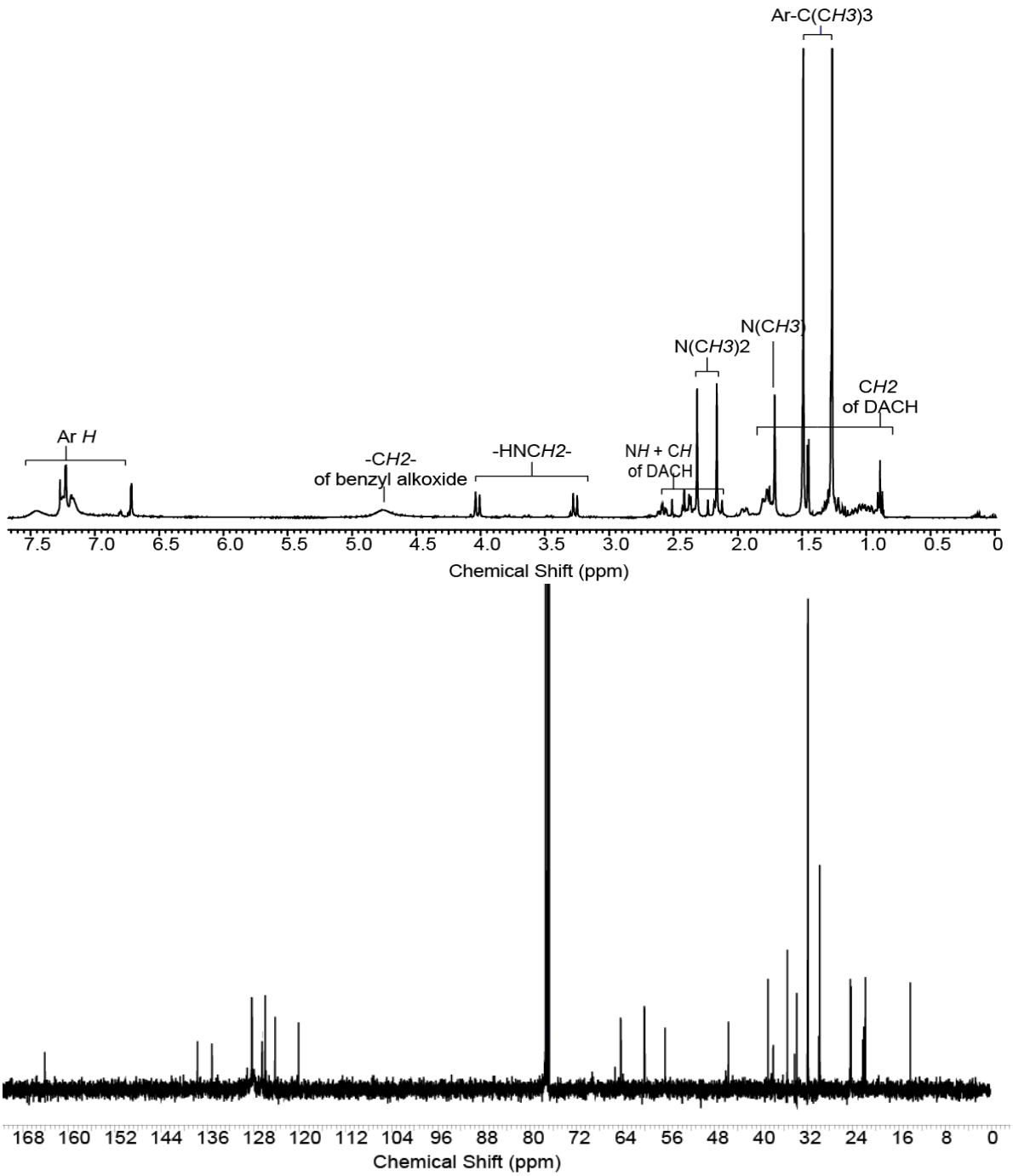

Figure B.5 (top)^{1}H NMR spectrum (bottom) $^{13}C\{^{1}H\}$ NMR ($CDCl_3$, 600 MHz, 25 °C) of complex (*R*,*R*)-**10**

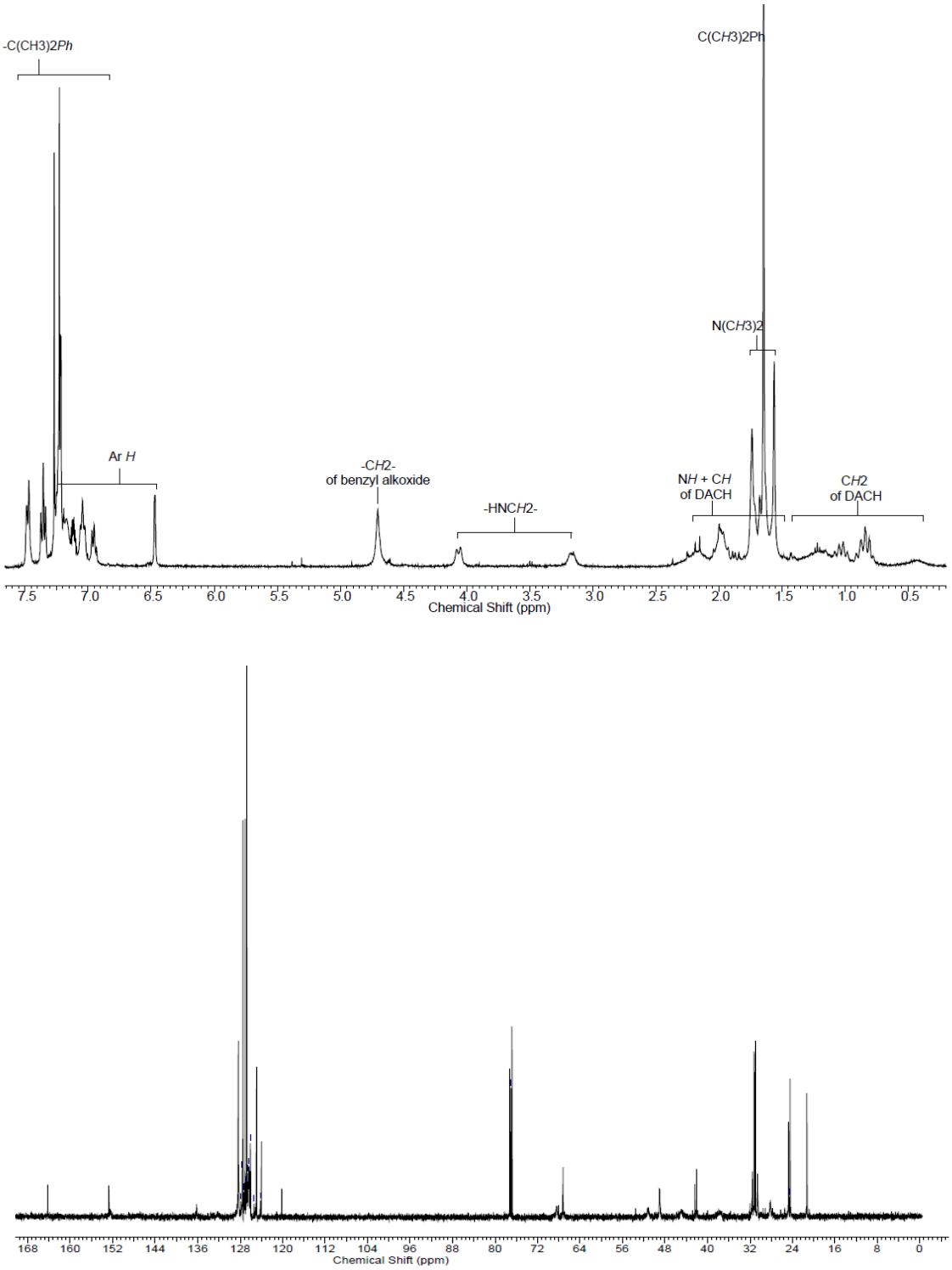

Figure B.6 (top)^{1}H NMR spectrum (bottom) $^{13}C\{^{1}H\}$ NMR ($CDCl_3$, 600 MHz, 25 °C) of complex (±)-**11**

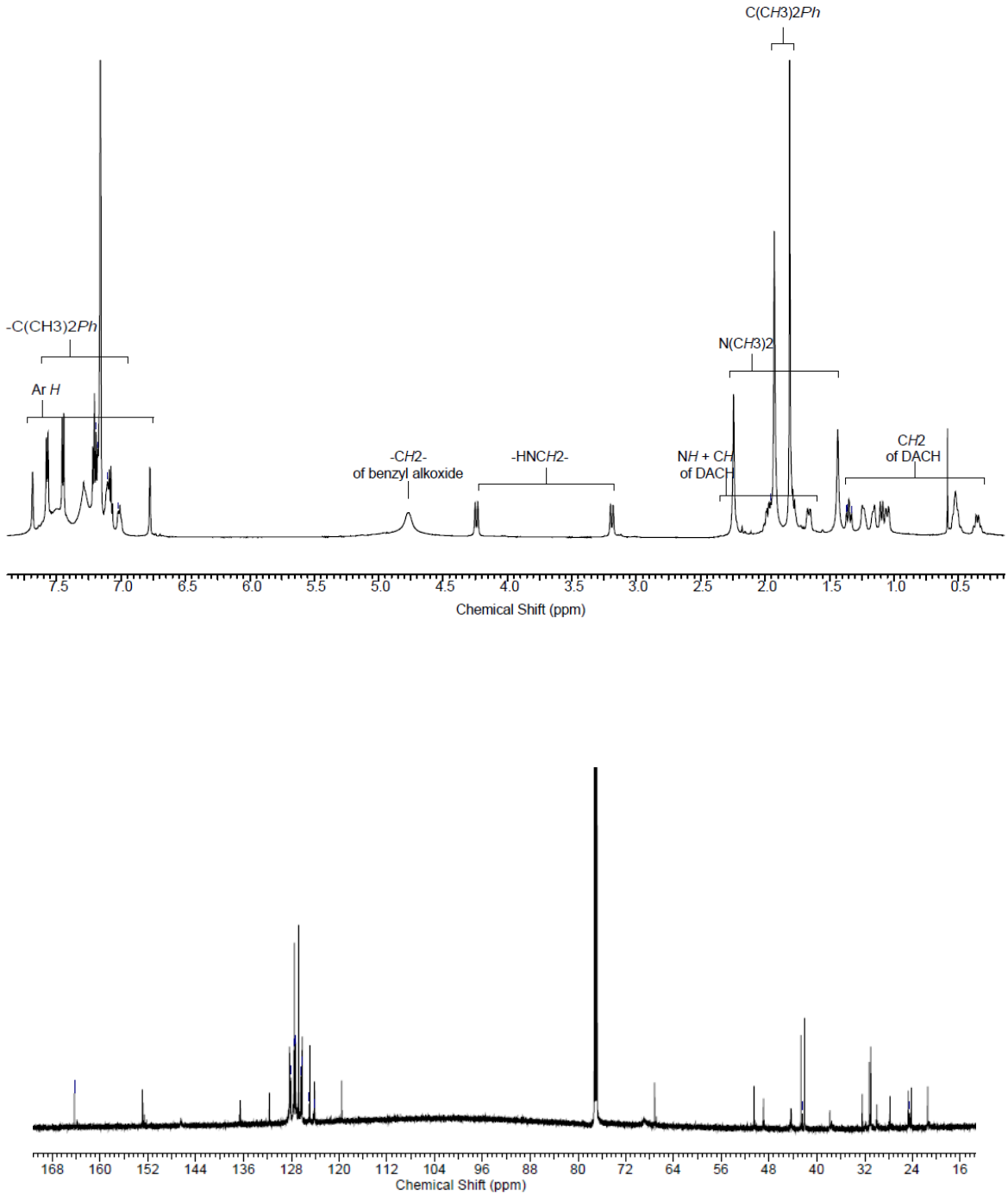

Figure B.7 (top)^{1}H NMR spectrum (bottom) $^{13}C\{^{1}H\}$ NMR ($CDCl_3$, 600 MHz, 25 °C) of complex (*R*,*R*)-**11**

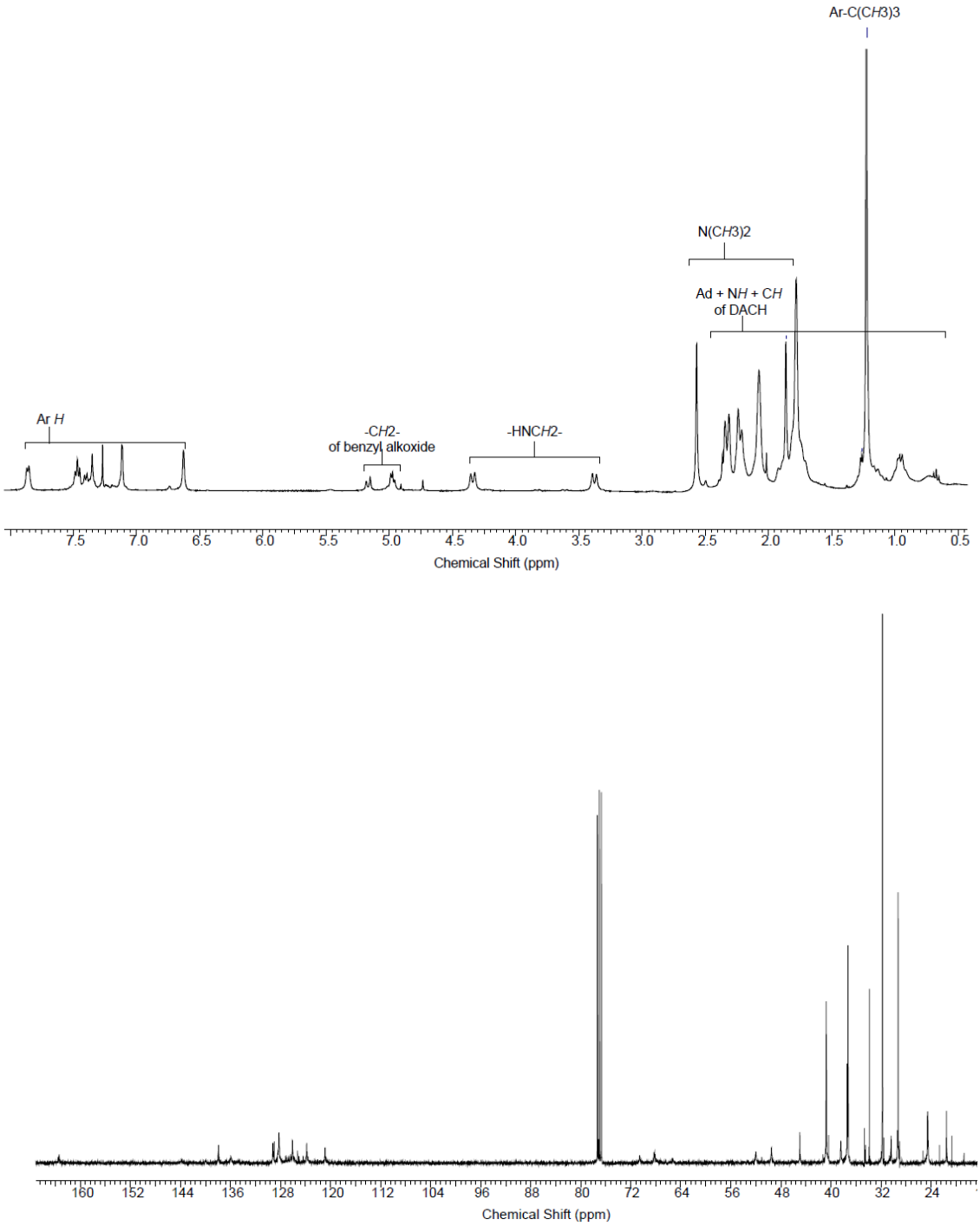

Figure B.8 (top)^{1}H NMR spectrum (bottom) $^{13}C\{^{1}H\}$ NMR ($CDCl_3$, 600 MHz, 25 °C) of complex (±)-**12**

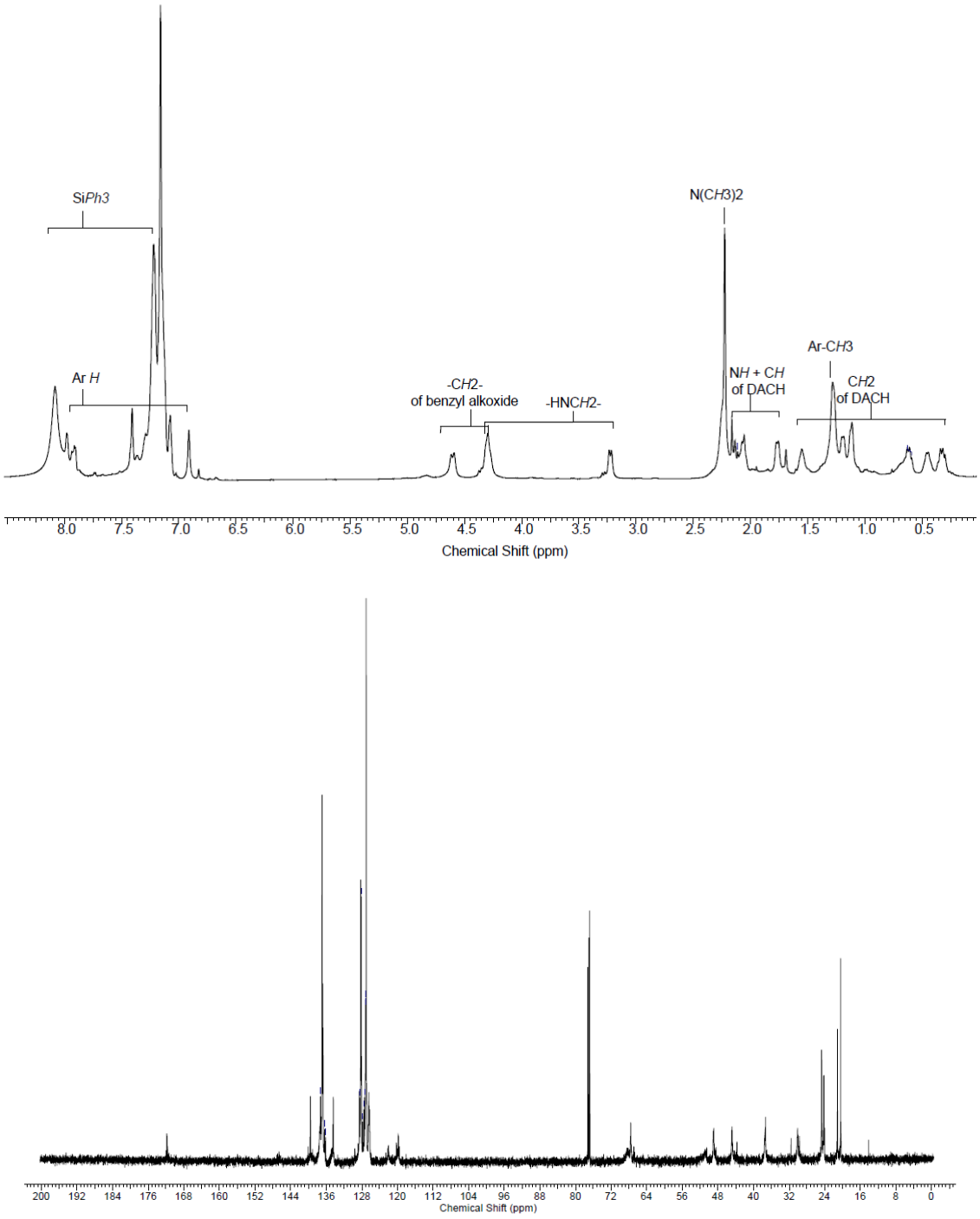

Figure B.9 (top)^{1}H NMR spectrum (bottom) $^{13}C\{^{1}H\}$ NMR ($CDCl_3$, 600 MHz, 25 °C) of complex (*R*,*R*)-**13**

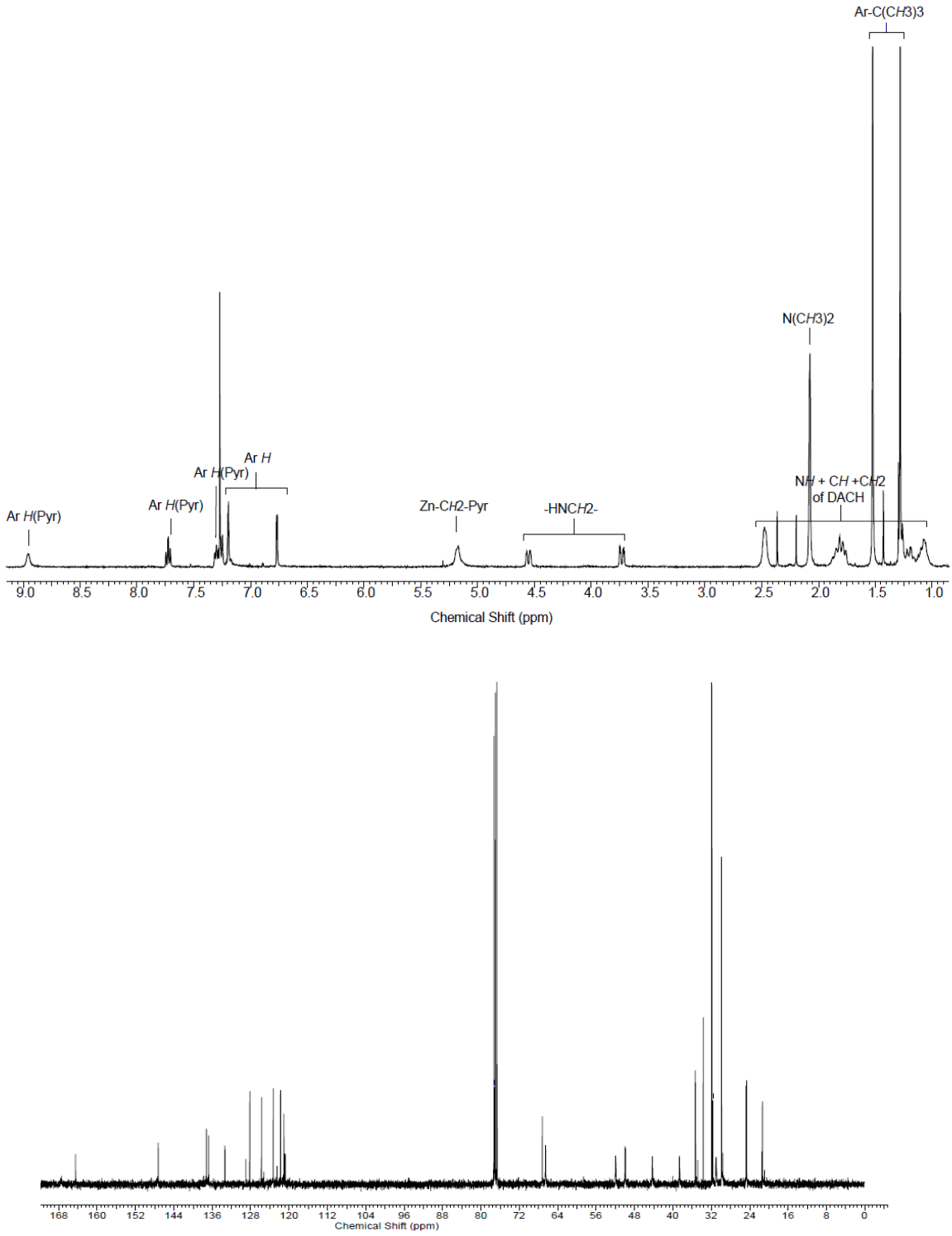

Figure B.10 (top)^{1}H NMR spectrum (bottom) $^{13}C\{^{1}H\}$ NMR ($CDCl_3$, 600 MHz, 25 °C) of complex (±)-**14**

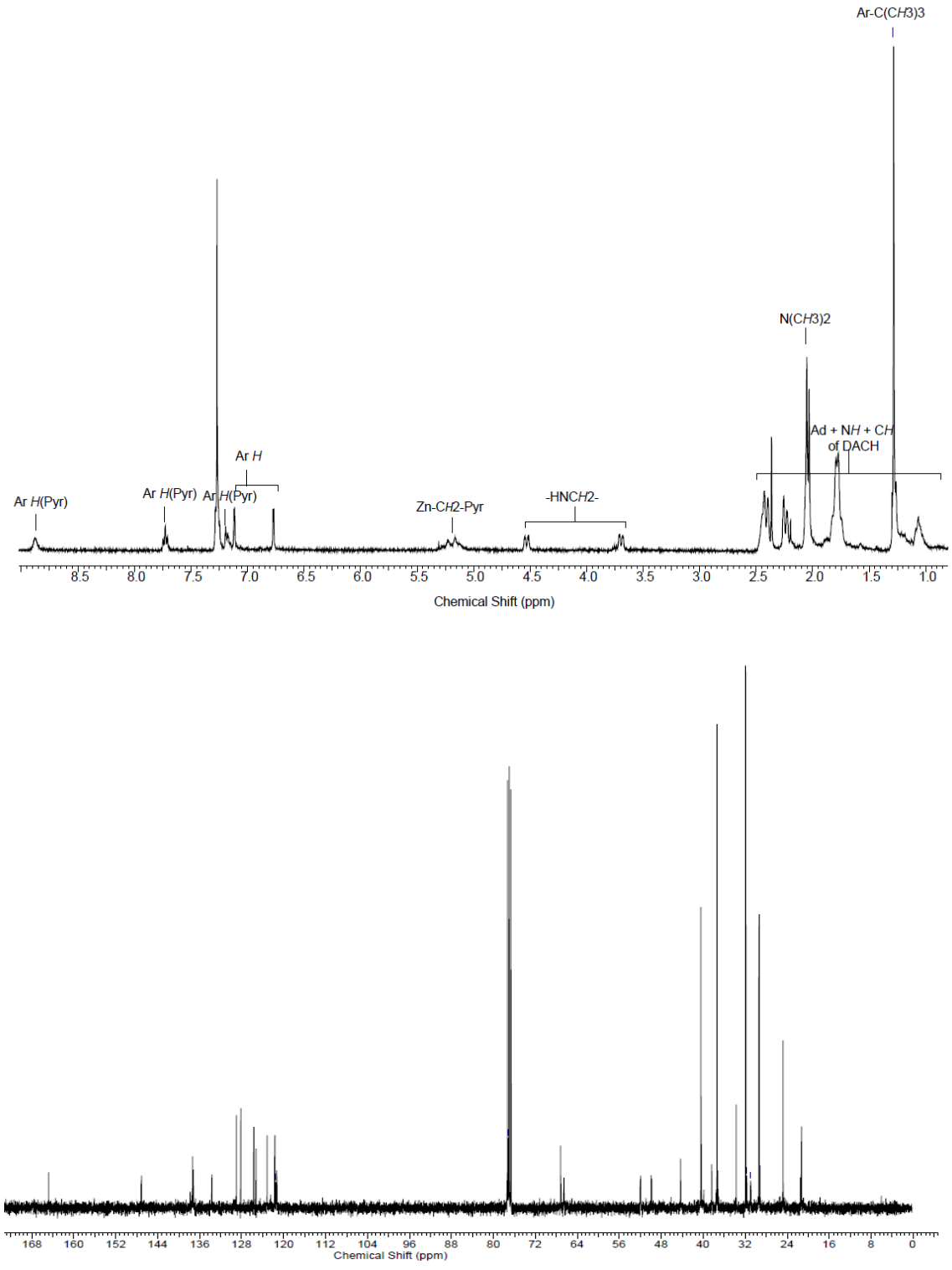

Figure B.11 (top)^{1}H NMR spectrum (bottom) $^{13}C\{^{1}H\}$ NMR ($CDCl_3$, 600 MHz, 25 °C) of (±)-**15**

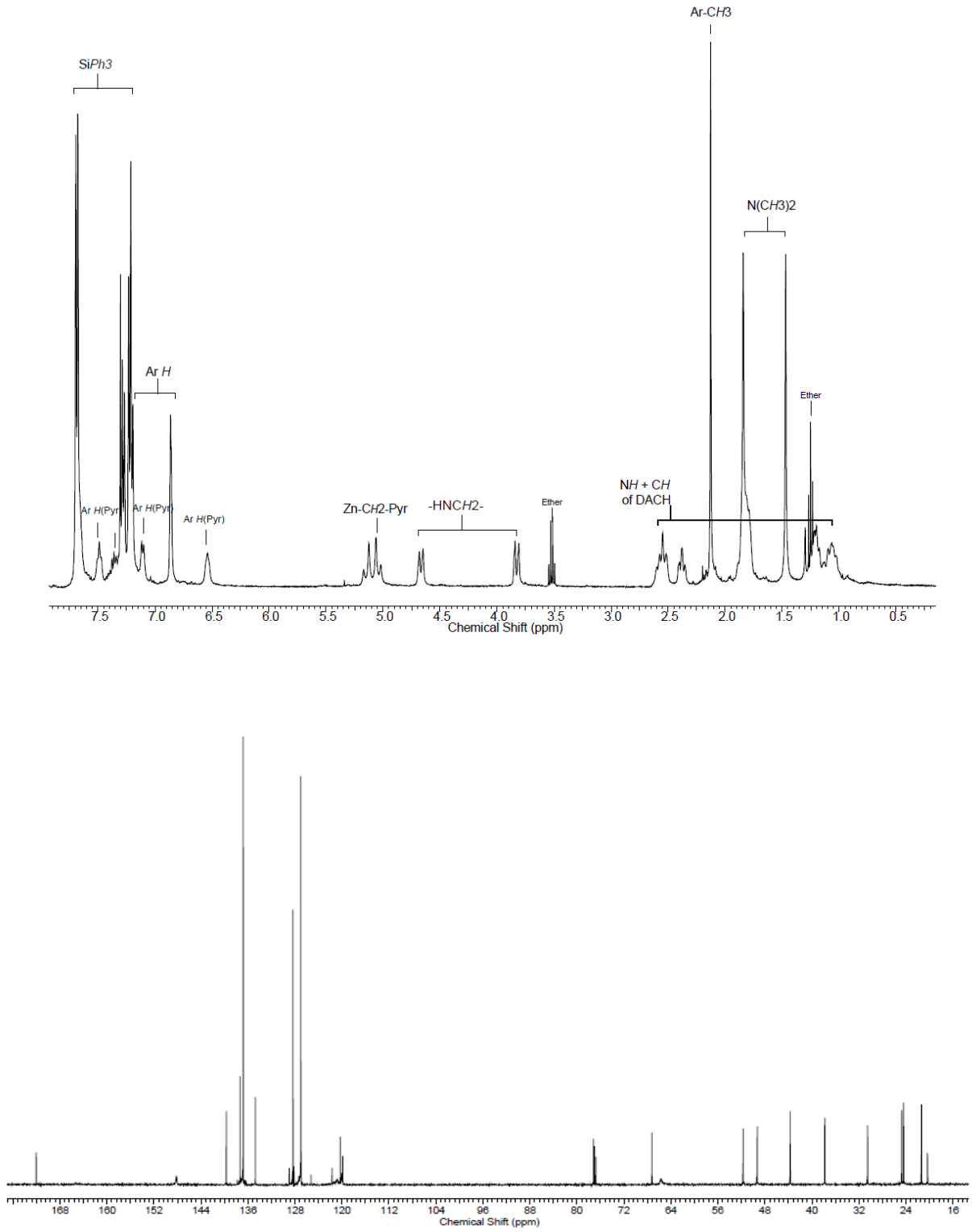

Figure B.12 (top)^{1}H NMR spectrum (bottom) $^{13}C\{^{1}H\}$ NMR ($CDCl_3$, 600 MHz, 25 °C) of complex (±)-**16**

B.2 Characterization of compounds by PGSE NMR spectroscopy

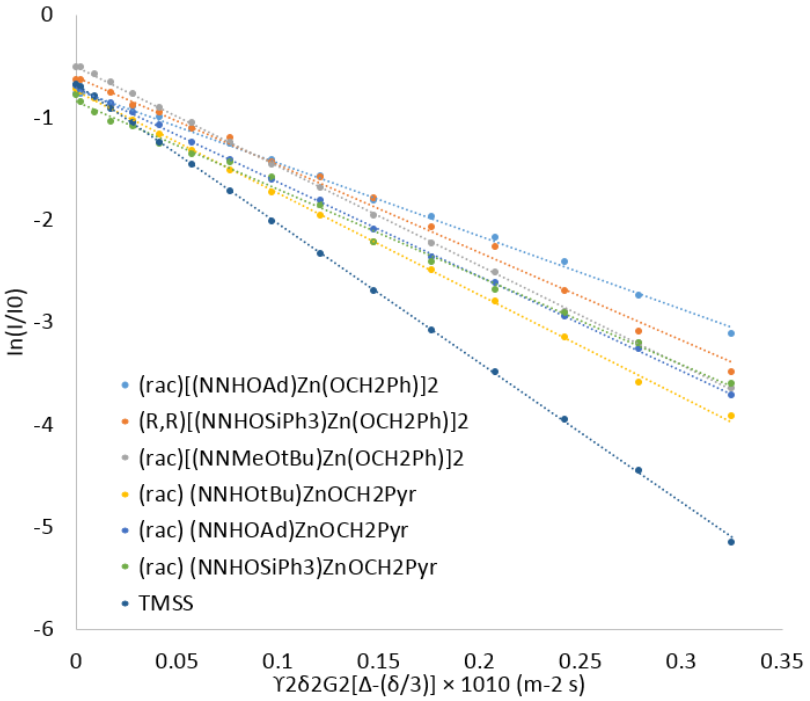

Figure B.13 Plot of $\ln(I/I_0)$ vs $\Upsilon^2\delta^2G^2[\Delta-(\delta/3)] \times 10^{10}$ (m^{-2} s) from PGSE experiments (400 MHz, CD_2Cl_2, 25 °C, Δ = 80 ms, δ = 1.1 ms). The hydrodynamic radius (r_H) of each compound was calculated by using the slopes (D_t) of the linear fits. I = intensity of the observed spin-echo, I_0 = intensity of the spin-echo in the absence of gradients, G = varied gradient strength, ϒ = gyromagnetic ratio (2.675×10^8 rad s^{-1} T^{-1}), δ = length of the gradient pulse, Δ = delay between the midpoints of the gradients.

Self-diffusion translational coefficients (D_t) were calculated graphically from the slopes of the linear best-fit lines. [267] The $c^{sa}r_H^{sa}$ value of each diffusing sample was estimated by the equation **1** which was derived from the advanced Stokes-Einstein equation **2**. r_H^{sa} was taken from the trend line of a plot, $c^{sa}\, r_H^{sa}$ vs. r_H^{sa}, based on the equation **4** reported by Chen and coworkers.[314]

$$c^{sa}r_H^{sa} = \frac{D_t^{st}c^{st}f_s^{st}r_H^{st}}{D_t^{sa}f_s^{sa}} \qquad \textbf{(1)}$$

D_t^{st} = translational diffusion coefficient of internal standard (TMSS, $D_t^{st} \approx 14.2 \times 10^{-10}$ m^2 S^{-1}, CD_2Cl_2, 25 °C)
c^{st} = internal standard size correction factor (TMSS, c^{st} = 5.1)
f_s^{st} = internal standard size and shape correction factor (TMSS, f_s^{st} = 1)
r_H^{st} = internal standard hydrodynamic radius (TMSS, 4.51 Å)
D_t^{sa} = translational diffusion coefficient of sample (CD_2Cl_2, 25 °C)
c^{sa} = sample size correction factor
f_s^{sa} = sample size and shape correction factor calculated from eq (3)

r_H^{sa} = sample hydrodynamic radius

$$D_t = \frac{kT}{cf_s \rho h r_H} \qquad \textbf{(2)}$$

k = Boltzmann constant ($k = 1.38 \times 10^{-23}$ m^2 kg s^{-1} K^{-1})
T = absolute temperature (K)
η = fluid viscosity (CH_2Cl_2, η = 0.0004 kg s^{-1} m^{-1})

$$f_s = \frac{\sqrt{1-\left(\frac{b}{a}\right)^2}}{\left(\frac{b}{a}\right)^{\frac{2}{3}} \ln \frac{1+\sqrt{1-\left(\frac{b}{a}\right)^2}}{\left(\frac{b}{a}\right)}} \qquad \textbf{(3)}$$

a = major semiaxes of a prolate ellipsoid estimated from X-ray crystal structure
b = minor semiaxes of a prolate ellipsoid estimated from X-ray crystal structure

$$cr_H = \frac{6r_H}{1+0.695\left(\frac{r_{solv}}{r_H}\right)^{2.234}} \qquad \textbf{(4)}$$

r_{solv} = hydrodynamic radius of the solvent (CH_2Cl_2 = 2.49 Å)

B.3 Characterization of compounds in the solid state

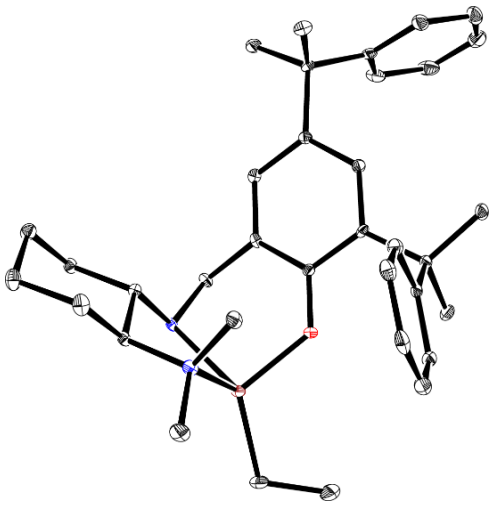

Figure B.14 Molecular structures of complex **(±)-6** (depicted with thermal ellipsoids at 50% probability and most H atoms omitted for clarity). Selected distances (Å) and angles (deg) for **6**: Zn1- N2 2.171(3), Zn1- N1 2.116(3), Zn1- N1 2.116(3), Zn1-C34 1.982(3), O1-Zn1-N2 106.98(10), O1-Zn1-N1 93.74(10), O1-Zn1-C34 113.77(13), N1-Zn1-N2 82.54(10), C34-Zn1-N2 119.10(14), C34-Zn1-N1 134.68(13).

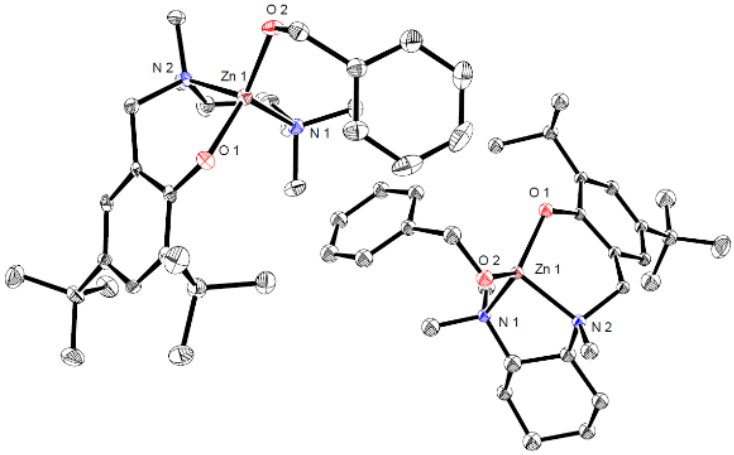

Figure B.15 Molecular structure of complex ***rac*-10** (depicted with thermal ellipsoids at 50% probability and most H atoms as well as solvent molecules omitted for clarity). Selected distances (Å) and angles (deg): Zn1 O2 1.8757(17) Zn1 O1 1.9211(19), Zn1 N2 2.125(2), Zn1 N1 2.080(2). O2 Zn1 O1 124.44(8), O2 Zn1 N2 114.27(8), O2 Zn1 N1 111.34(9), O1 Zn1 N2 112.01(9), O1 Zn1 N1 100.75(8), N1 Zn1 N2 86.02(9), Zn1 O2 C23 116.84(4), O2 C23 C24 112.19(8).

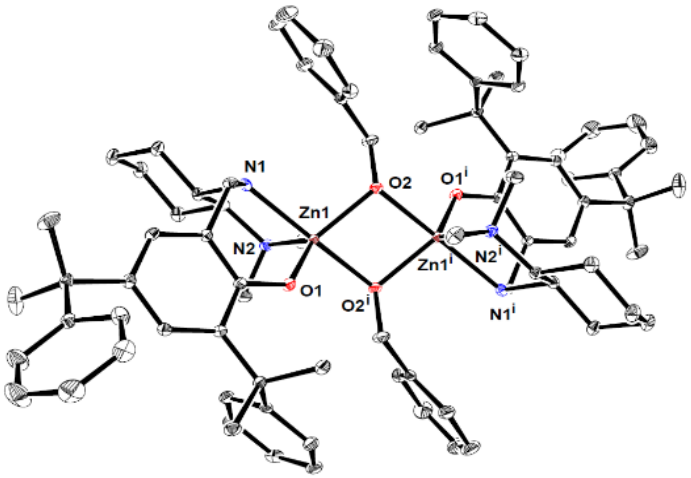

Figure B.16 Molecular structure of complex **(±)-11** (depicted with thermal ellipsoids at 50% probability and H atoms as well as solvent molecules omitted for clarity). Selected distances (Å) and angles (deg): Zn1 $Zn1^{i}$ 3.0515(4), Zn1 O1 1.9659(10), Zn1 $O2^{i}$ 2.0568(9), Zn1 O2 2.0045(10), Zn1 N1 2.1613(11), Zn1 N2 2.1976(12), O2 $Zn1^{1}$ 2.0568(9). O1 Zn1 $O2^{1}$ 95.32(4), O1 Zn1 O2 128.93(4), O1 Zn1 N1 91.12(4), O1 Zn1 N2 117.83(4), O2 Zn1 $Zn1^{1}$ 97.40(3), O2 Zn1 $O2^{1}$ 82.59(4) $O2^{1}$ Zn1 N1 172.42(4), O2 Zn1 N1 96.46(4), O2 Zn1 N2 113.24(4), $O2^{1}$ Zn1 N2 93.24(4), N1 Zn1 N2 80.19(4), Zn1 O2 $Zn1^{1}$ 97.41(4), C34 O2 $Zn1^{1}$ 118.37(8), O2 C34 C35 114.48 (11).

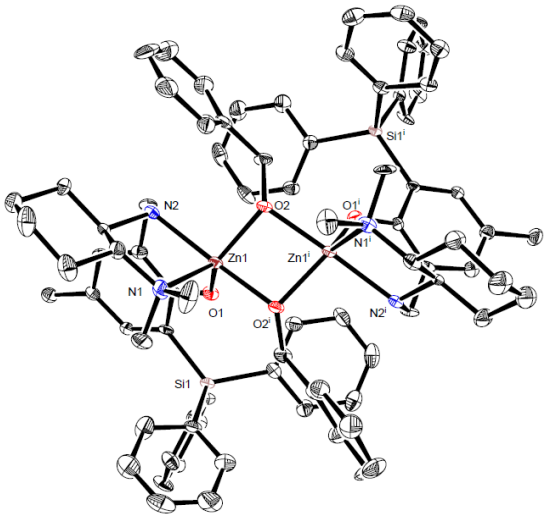

Figure B.17 Molecular structure of complex (***RR***)**-13** (depicted with thermal ellipsoids at 50% probability and most H atoms as well as solvent molecules omitted for clarity). Selected distances (Å) and angles (deg): Selected distances (Å) and angles (deg): Zn1 $Zn1^{i}$ 2.9989(3), Zn1 O1 1.968(6), Zn1 $O2^{i}$ 2.034(6), Zn1 O2 2.021(6), Zn1 N1 2.170(7), Zn1 N2 2.173(8), O2 $Zn1^{1}$ 1.988(6). O1 Zn1 $O2^{1}$ 128.0(2), O1 Zn1 O2 94.24(5), O1 Zn1 N1 92.0(2), O1 Zn1 N2 117.3(3), O2 Zn1 $Zn1^{1}$ 96.4(2), O2 Zn1 $O2^{1}$ 80.7(2) $O2^{1}$ Zn1 N1 95.6(4), O2 Zn1 N1 173.8(4), O2 Zn1 N2 96.6(4), $O2^{1}$ Zn1 N2 114.6(4), N1 Zn1 N2 80.34(4), Zn1 O2 $Zn1^{1}$ 96.41(4), C35 O2 $Zn1^{1}$ 119.5(8), O2 C35 C36 112.8 (11).

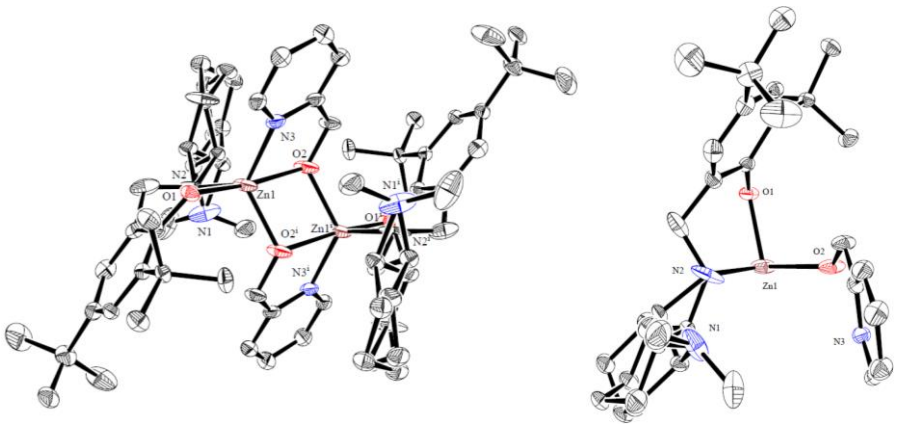

Figure B.18 Molecular structure of complex **(±)-14** (right: half structure depicted with thermal ellipsoids at 50% probability and most H atoms as well as solvent molecules omitted for clarity). Selected distances (Å) and angles (deg): Selected distances (Å) and angles (deg): Zn1 $Zn1^{i}$ 3.1189(8), Zn1 O1 2.0117(19), Zn1 $O2^{i}$ 2.105(2), Zn1 O2 1.998(2), Zn1 N3 2.115(3), Zn1 N2 2.115(4), O2 $Zn1^{1}$ 2.105(2). O1 Zn1 $O2^{1}$ 167.81(9), O1 Zn1 O2 103.34(8), O1 Zn1 N2 93.35(10), O2 Zn1 $Zn1^{1}$ 41.82(6), O2 Zn1 $O2^{1}$ 81.07(0), O2 Zn1 N1 173.8(4), O2 Zn1 $N3^{1}$ 122.01(11), $O2^{1}$ Zn1 N2 106.26(11), Zn1 O2 $Zn1^{1}$ 41.82(6), C24 O2 $Zn1^{1}$ 124.1(2), O2 C24 C25 112.0 (2).

Table B.1 Selected crystallographic data for compounds **6**, **11**, **13**, and **14**.

	(±)-6	**(±)-10**	**(±)-11**	**(*R*,*R*)-13**	**(±)-14**
empirical formula	$C_{35}H_{48}N_2OZn$	$C_{62}H_{96}N_4O_4Zn_2$	$C_{80}H_{100}N_4O_4Zn_2$	$C_{80}H_{88}N_4O_4Si_2Zn_2$	$C_{29}H_{45}N_3O_2Zn$
fw	578.12	1092.16	1312.37	1356.46	533.05
T (K)	90	90	90	296.15	296.15
a/Å	8.4530(14)	11.8172(5)	12.0439(15)	10.894(2)	11.1804(11)
b/Å	18.142(3)	15.9905(9)	12.0523(15)	33.799(7)	13.0247(13)
c/Å	10.3805(15)	16.8567(9)	13.1052(16)	21.937(5)	19.4626(19)
α/°	90	89.9930(10)	91.335(3)	90	90
β/°	97.637(4)	82.361(2)	107.129(3)	101.820(4)	95.724(2)
γ/°	90	72.8900(10)	109.096(3)	90	90
Volume/Å^3	1577.8(4)	3014.7(3)	1702.7(4)	7906(3)	2820.0(5)
Z	2	2	1	4	4
cryst syst	monoclinic	triclinic	triclinic	monoclinic	monoclinic
space group	*P 2$_1$*	*P*-1	*P-1*	*P 2$_1$*	*P 2$_1$/c*
d_{calc} (g/cm^3)	1.231	1.203	1.280	1.140	1.256
μ (Mo Kα) (cm^{-1})	0.807	8.43	0.758	0.684	0.900
$2\theta_{max}$ (deg)	61.204	60.128	61.208	55.468	57.15
total no. of reflns	25006	10665	48808	128764	53818
no. of indep reflns (R_{int})	9676	10637	10305	36757	7170
residuals (refined on F^2): R_1; wR_2	0.0653, 0.0946	0.0396,0.0826	0.0463, 0.0422	0.0631,0.1514	0.0560, 0.1291
GOF	0.963	0.916	1.022	1.013	1.134
residuals (refined on F^2: R_1^a; wR_2^b)	0.0444, 0.0730	0.0612, 0.0878	0.0334, 0.0732	0.0783, 0.1595	0.0689, 0.1369
	$^aR_1 = \Sigma \lvert\lvert F_o\rvert - \lvert F_c\rvert\rvert / \Sigma \lvert F_o\rvert$. $^b wR_2 = [\ \Sigma\ (\ w\ (F_o^2 - F_c^2)^2\ ) / \Sigma\ w(F_o^2)_2]^{1/2}$				

B.4 Kinetic studies of the polymerization of BBL

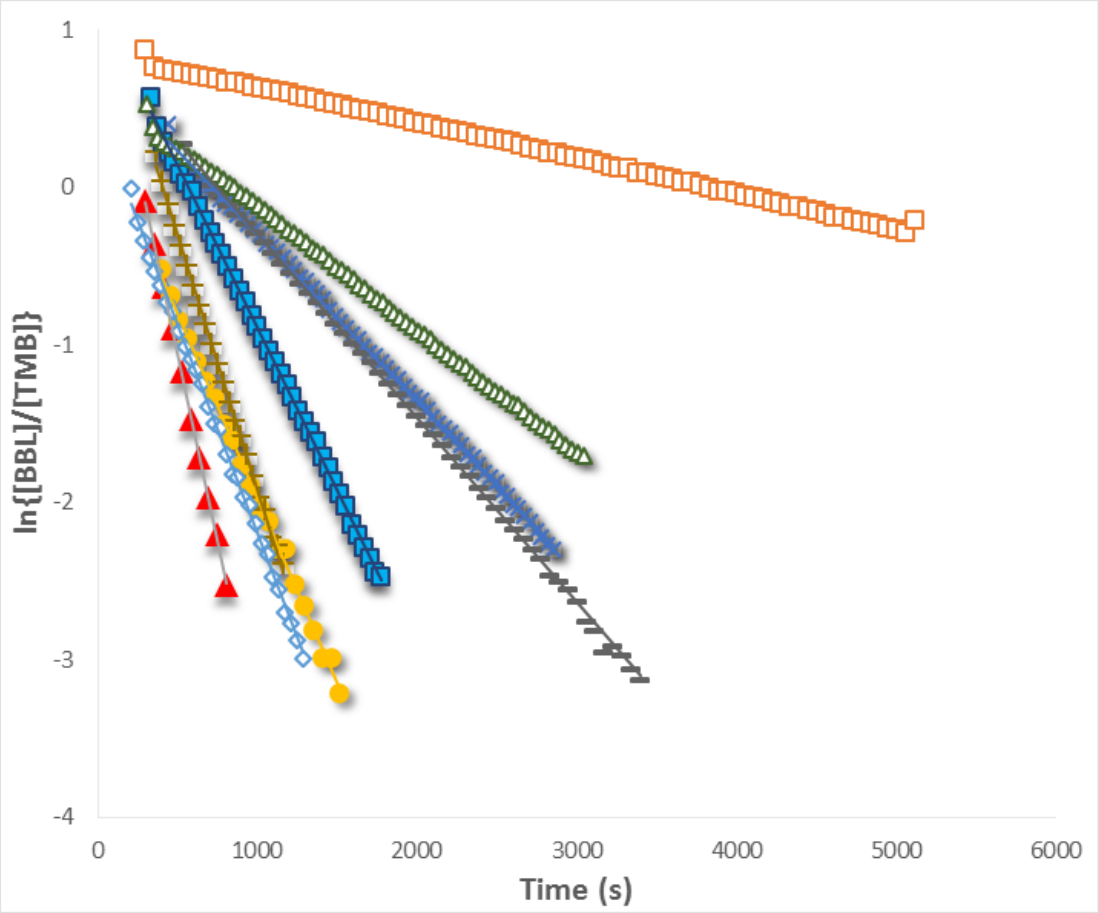

Figure B.19 The ROP plots of 400 equiv of [BBL] vs. [Catalyst] ((±)-**9** (red triangle), (±)-**10** (empty square), (±)-**11**(orange cycle), (*R*,*R*)-**11**(cross), (±)-**12**(empty dimonds), (*R*,*R*)-**13**(empty triangle), (±)-**14**(plus), (±)-**15**(blue square), (±)-**16**(dash)) at 25 °C and followed to 95% conversion. [BBL] = 0.16 M. [catalyst] = 0.40 mM in CD_2Cl_2.1,3,5-trimethoxybenzene (TMB) was used as internal standard.

B.5 Inverse gated $^{13}C\{^{1}H\}$ NMR spectra of selected Table 3.3 entries

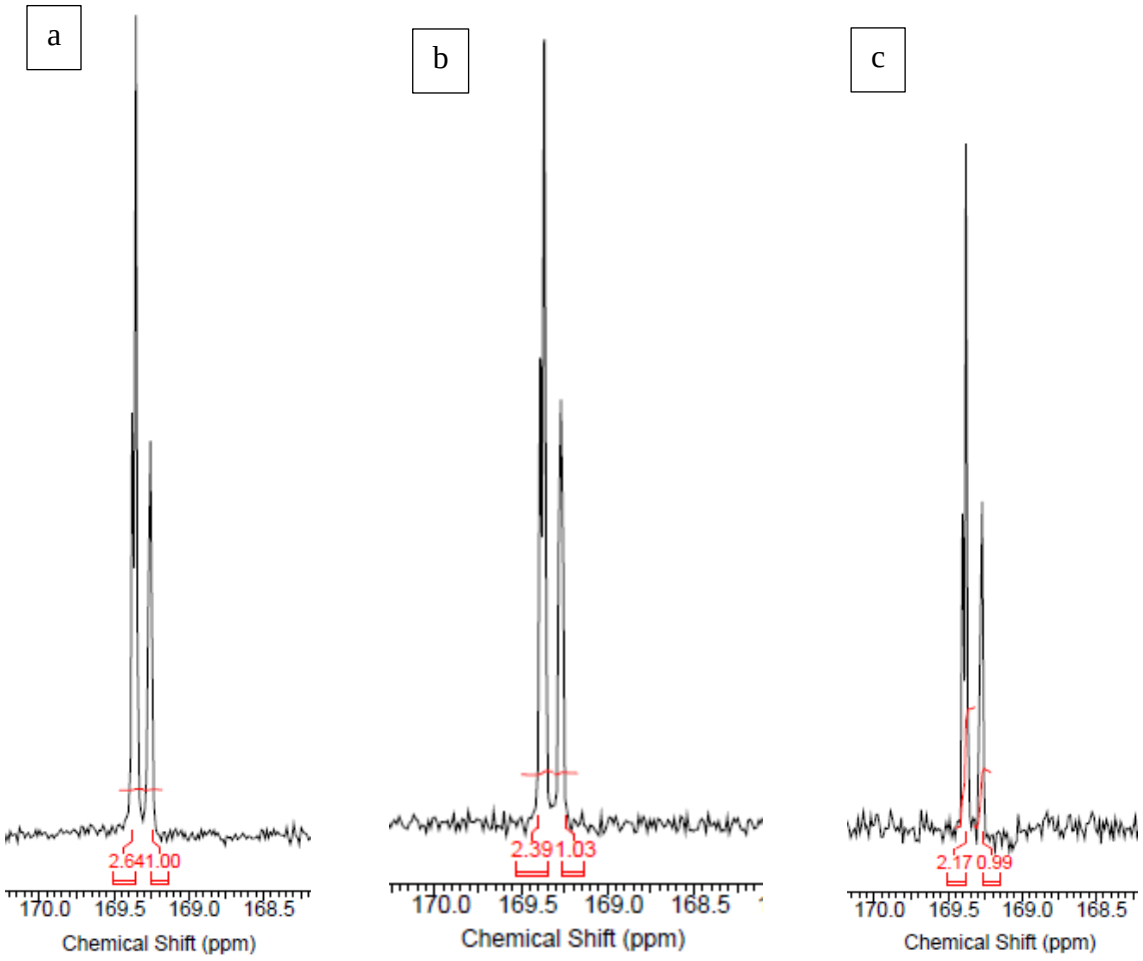

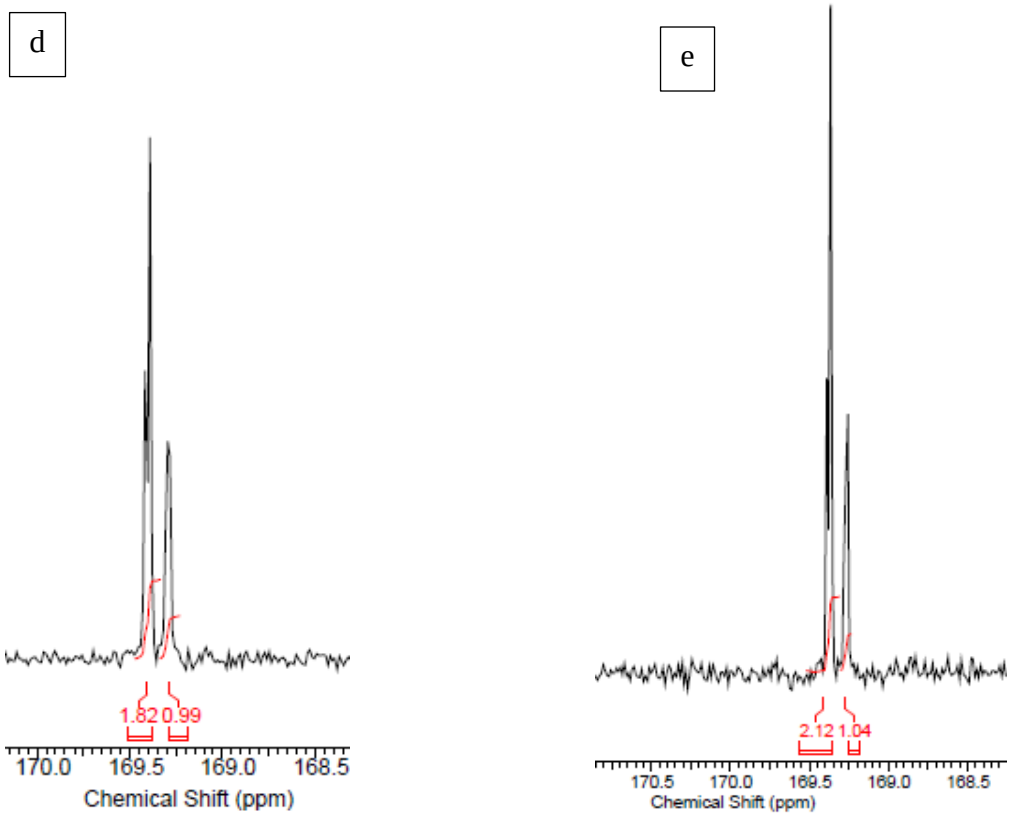

Figure B.20 Carbonyl region of inverse gated $^{13}C\{^{1}H\}$ (125 MHz, $CDCl_3$, 12 °C)of Table 2 entries (a) 1, (b) 3, (c) 6, (d) 9, (e) 11. P_r values (probability of racemic linkages between monomer units) were calculated using the below equation, were "r" and "m" represents *racemic* and *meso* linkages respectively and *I*r and *I*m are the integrations of corresponding inverse gated $^{13}C\{^{1}H\}$peaks:

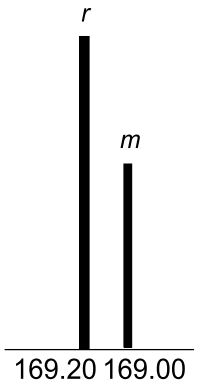

$$P_r = I_r / (I_m + I_r)$$
$$P_m = I_m / (I_m + I_r)$$

B.6 Depolymerization studies using complex 9

In the glovebox, a 100 mg sample of isolated, dry PHB (synthesized using previously reported indium ethoxide complex **D**)[145] was dissolved in 1 mL of CH_2Cl_2. To this stirring solution, (±)-**9** (3 mg, 0.0028 mmol) dissolved in 1 mL CH_2Cl_2 was added. After 1 and 16 h, reactions were quenched with a drop of HCl (1.5 M in Et_2O) and the polymer samples were isolated through the addition of cold methanol. The polymers were dried under vacuum for 8 h prior to GPC analysis.

Table B.2 GPC data for depolymerization experiments

Entry	Description	$M_{n,\,exp}$[a] (g/mol)	$Đ$[a]
1	PHB prior to reaction	160200	1.02
2	PHB isolated after reaction with (±)-**6** (1 h)	65100	1.50
3	PHB isolated after reaction with (±)-**6** (16 h)	38400	1.50

aDetermined by GPC-LLS (gel permeation chromatography-low angle laser light scattering) (dn/dc = 0.037 for PHB). Reactions carried out in 5 min with rac-lactide and [Zn] = 0.7 mM.

B.7 Chain end analysis using MALDI-TOF and ^{1}H NMR

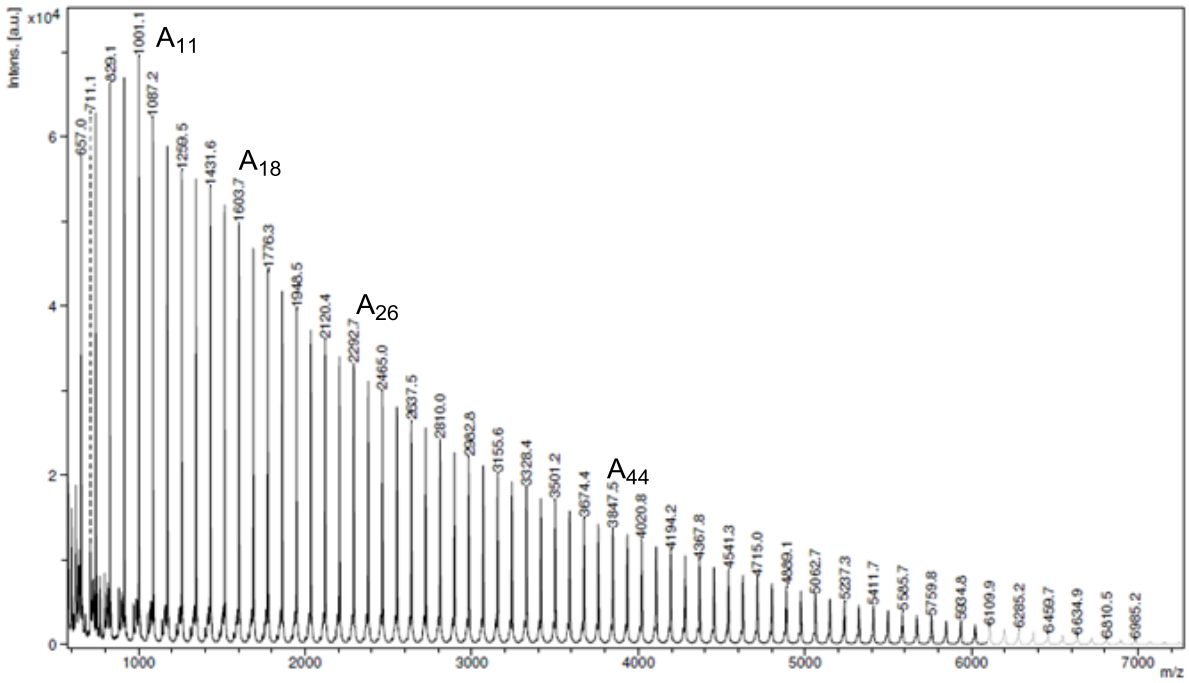

Figure B.21 MALDI-TOF mass spectrum of PHB produced by (±)-**9** from ROP of 50 equiv. of *rac*-BBL after quenching with MeOH (2,5-dihydroxybenzoic acid with NaTFA). A_n = $[86.09\ BBL]_n$ +32 MeOH + 23 Na^+ (A_{11} = $[86.09BBL]_{11}$ +32 MeOH + 23 Na^+ =1001.99).

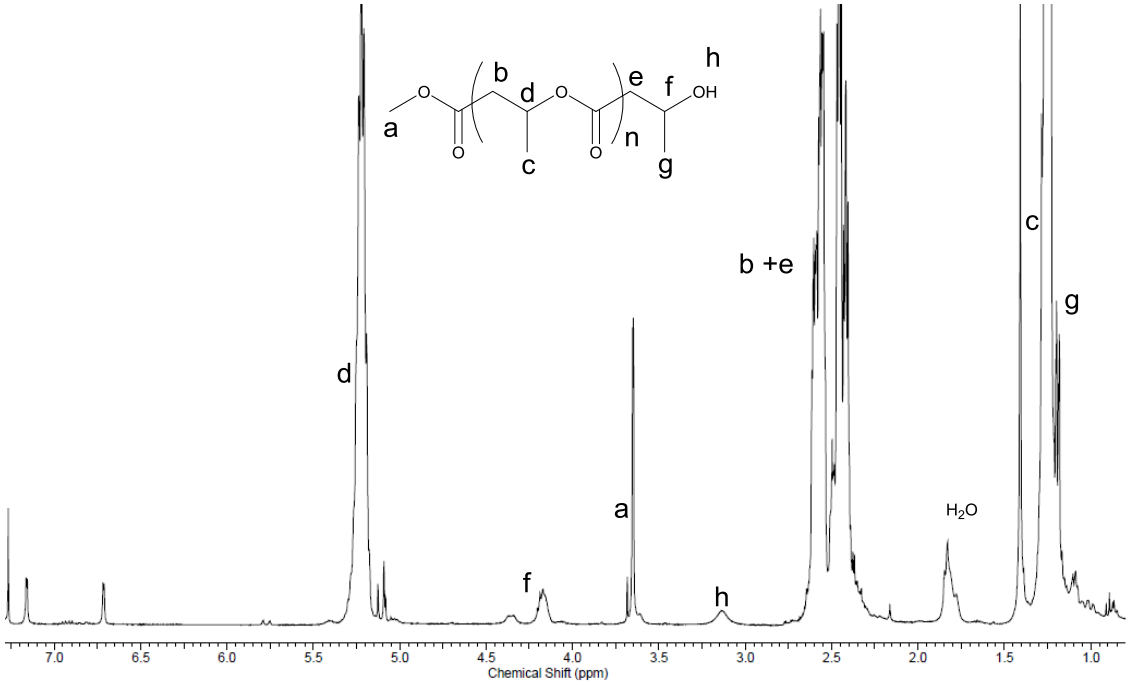

Figure B.22 ^{1}H NMR spectrum of PHB produced by (±)-**9** from ROP of 50 equivalents of *rac*-BBL

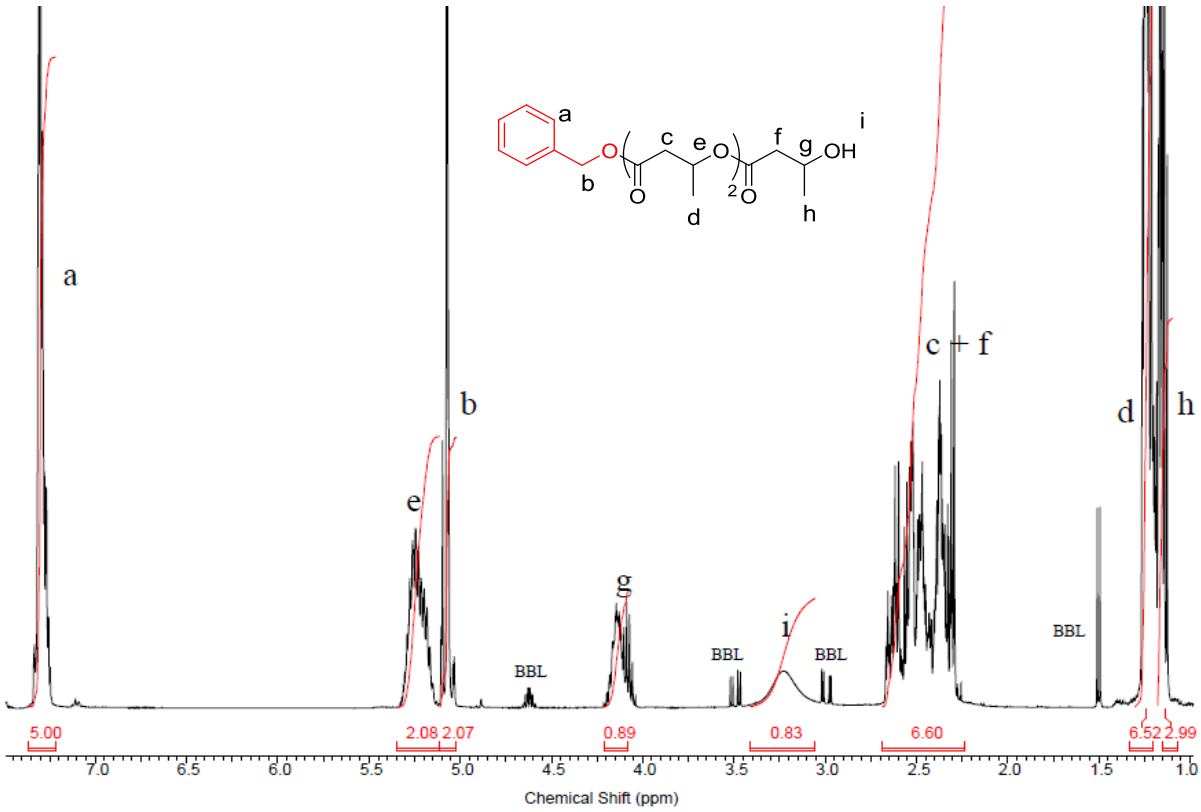

Figure B.23 ^{1}H NMR spectrum ($CDCl_3$, 25 °C) of PHB isolated from polymerization of [BBL]:[BnOH]:[**9**] ratios of 20000:5000:1 (Table 4.4, entry 7).

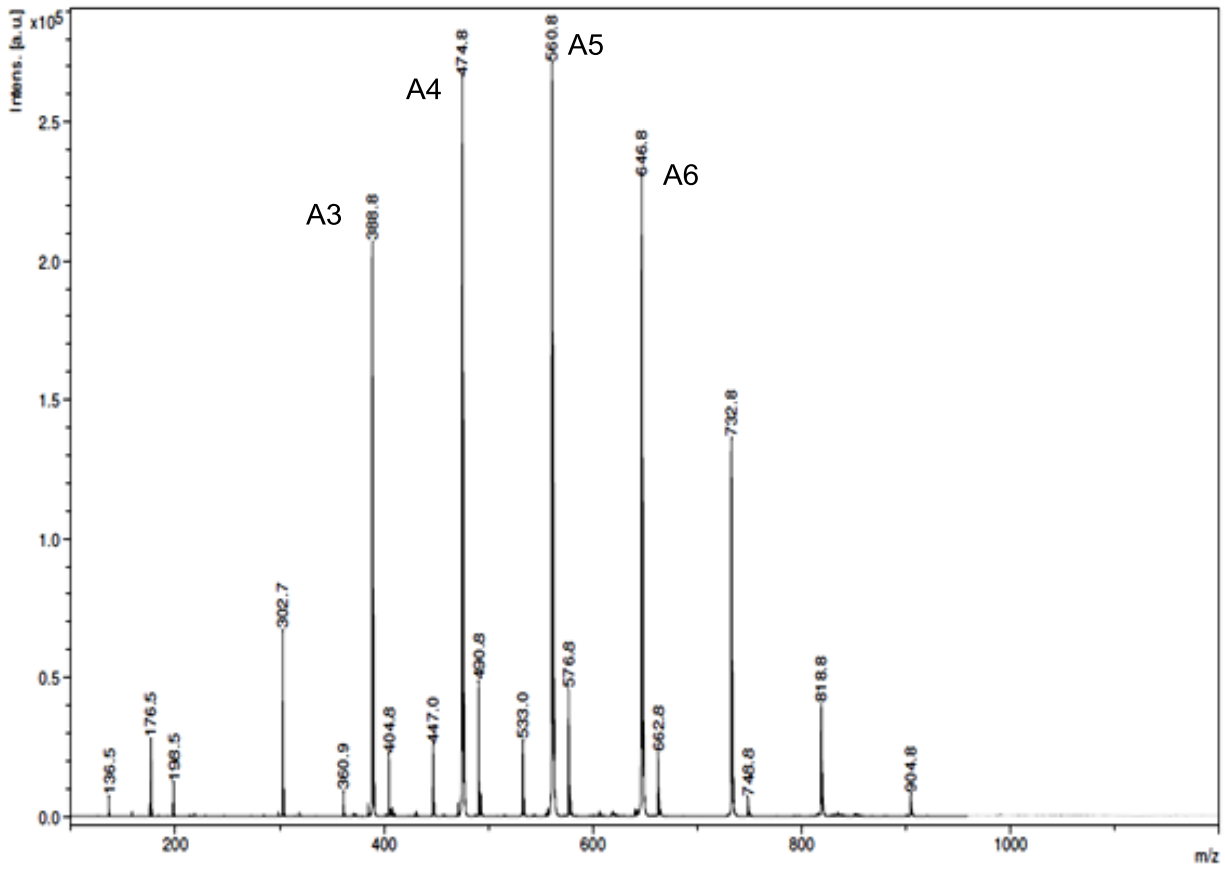

Figure B.24 MALDI-ToF of PHB isolated from polymerization of [BBL]:[BnOH]:[**9**] ratios of 20000:5000:1 (A_n = [86.09 BBL]$_n$ +108.14 BnOH + 23 Na^+, A4 = [86.09BBL]$_4$ +108.14 BnOH + 23 Na^+ =475.5) (Table 4.4, entry 7).

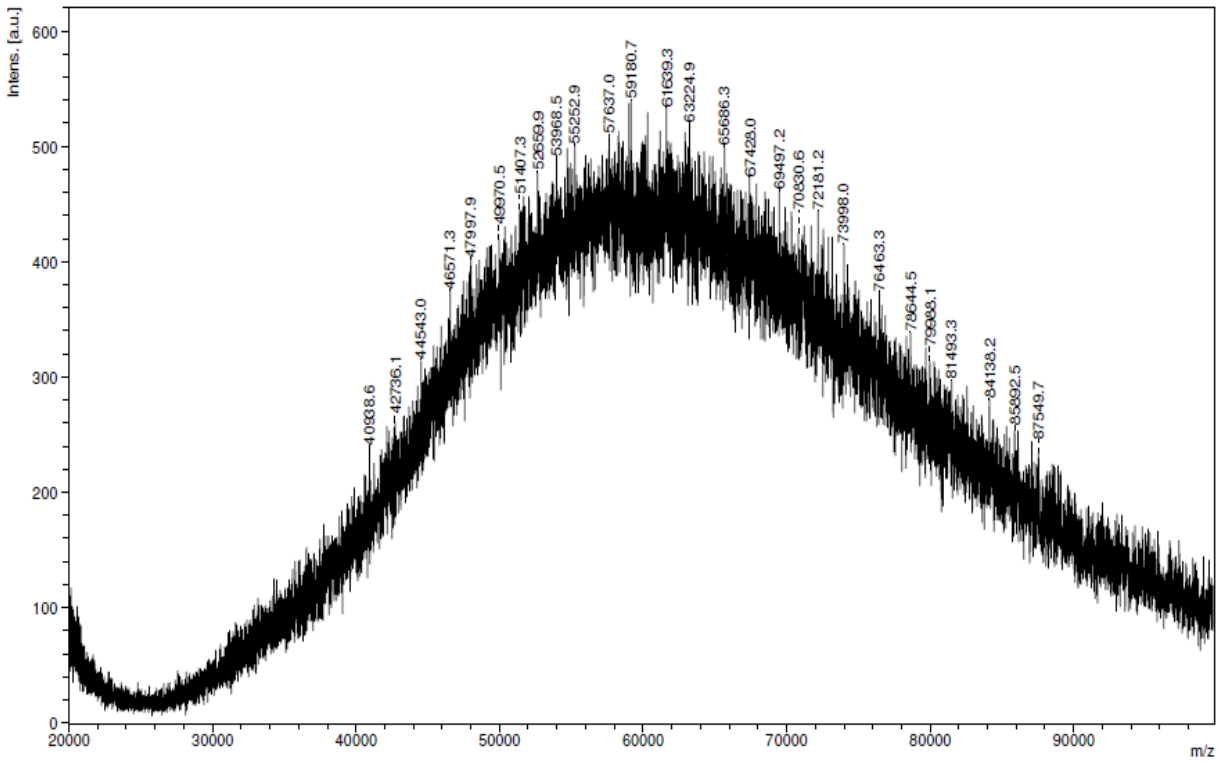

Figure B.25 Highly syndiotactic PHB (P_r = 0.83) is prepared using Complex **B** in THF with isopropanol as the initiator. Since the polymer is highly crystalline and is not soluble in THF, MALDI-ToF was used to estimate the molecular weight of the polymer. (entry 1, Table 4.5).

B.8 DSC Thermograms of selected Table 4.5 entries

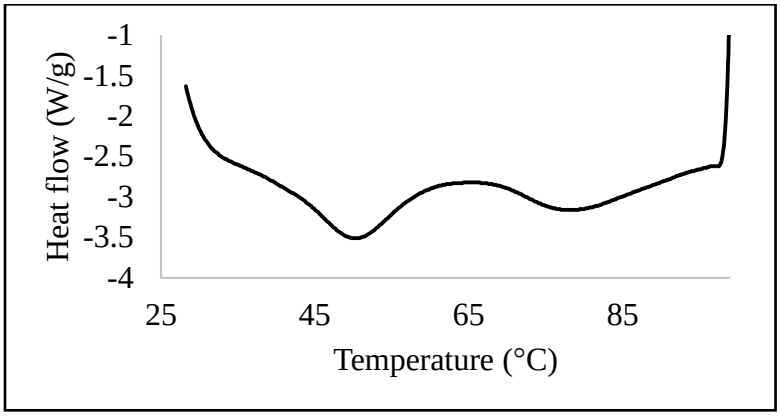

Figure B.26 DSC thermogram of Syndio-rich PHB synthesized using (±)-**9** as the catalyst in CH_2Cl_2 at RT (Table 4.5 entry 3, M_w = 126000 , P_r = 0.68).

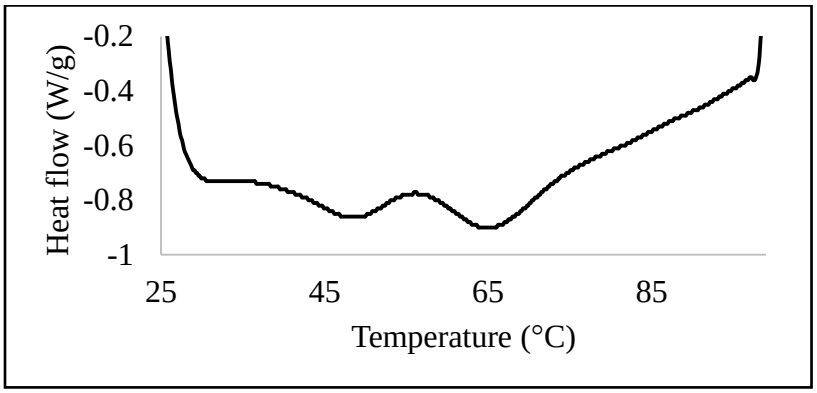

Figure B.27 DSC thermogram of Syndio-rich PHB synthesized using (±)-**9** as the catalyst in CH_2Cl_2 at RT (Table 4.5 entry 4, M_w = 134000, P_r = 0.64).

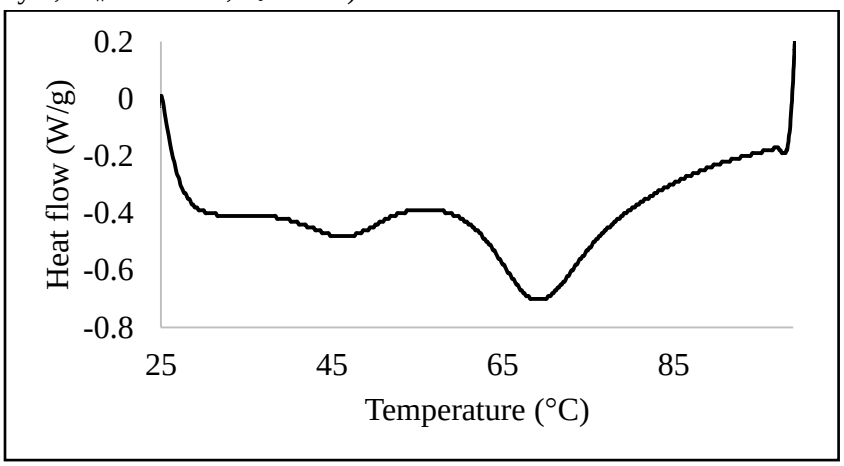

Figure B.28 DSC thermogram of Syndio-rich PHB synthesized using (±)-**9** as the catalyst in CH_2Cl_2 at RT (Table 4.5 entry 5, M_w = 190800, P_r = 0.65).

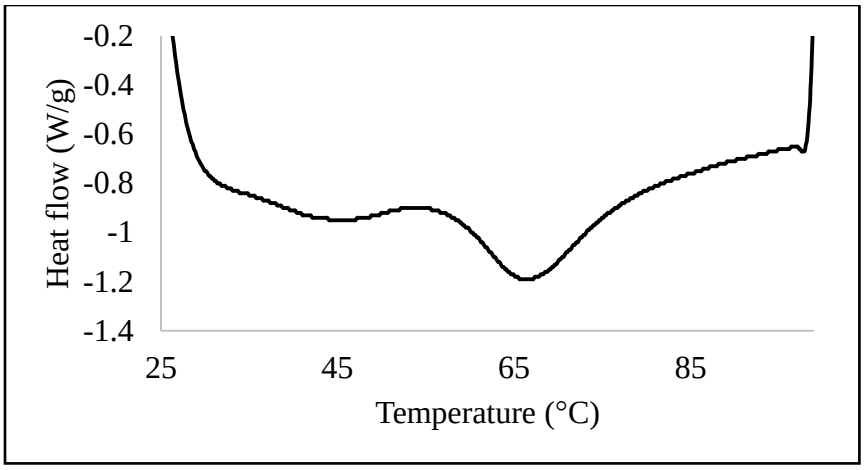

Figure B.29 DSC thermogram of Syndio-rich PHB synthesized using (±)-**9** as the catalyst in CH_2Cl_2 at RT (Table 4.5 entry 6, M_w =225000 , P_r = 0.64).

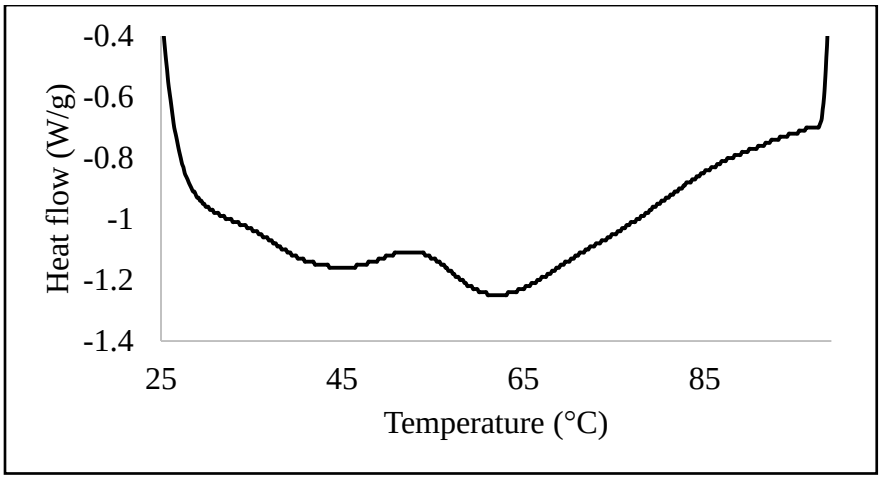

Figure B.30 DSC thermogram of Syndio-rich PHB synthesized using (±)-**9** as the catalyst in CH_2Cl_2 at RT (Table 4.5 entry 7, M_w = 285000, P_r = 0.68).

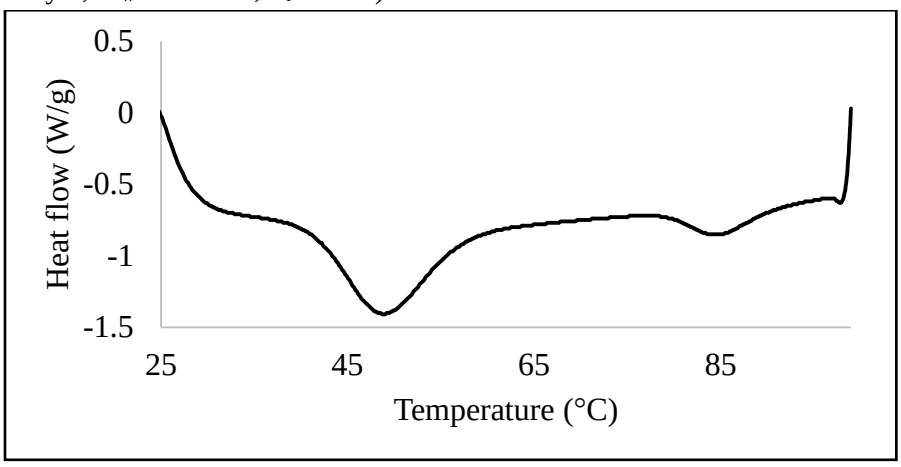

Figure B.31 DSC thermogram of Syndio-rich PHB synthesized using (±)-**9** as the catalyst in CH_2Cl_2 at RT (Table 4.5 entry 8, M_w =385000 , P_r = 0.64).

B.9 Isothermal frequency sweep test results of syndio-rich PHB

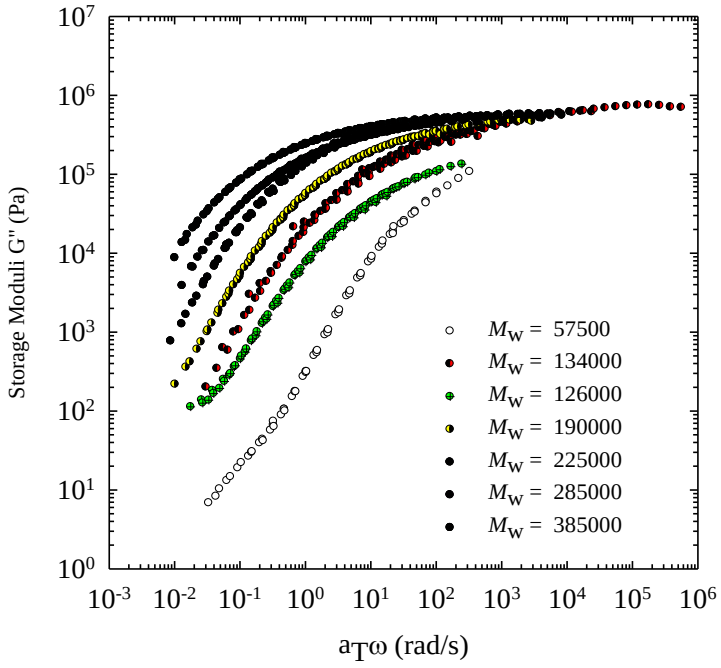

Figure B.32 Molecular weight dependence of storage modulus of of Syndio-rich PHBs of different molecular weights synthesized using (±)-**9** as the catalyst in CH_2Cl_2 at RT (Table 4.5, entries 2-8).

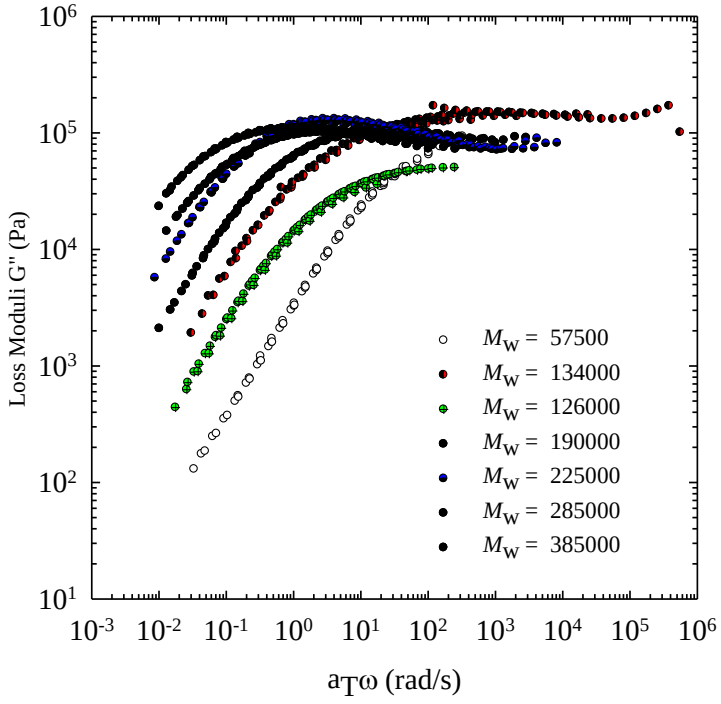

Figure B.33 Molecular weight dependence of loss modulus of Syndio-rich PHBs of different molecular weights synthesized using (±)-**9** as the catalyst in CH_2Cl_2 at RT (Table 4.5, entries 2-8)

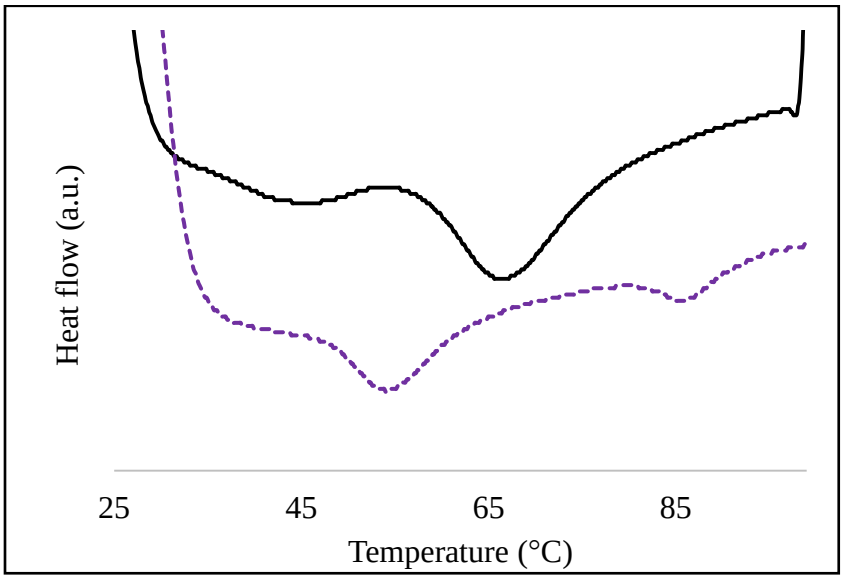

Figure B.34 DSC results of Syndio-rich PHB synthesized using (±)-**9** as the catalyst in CH_2Cl_2 at RT (M_w =225000 , P_r = 0.64) before (solid line) and after (dashed line) extensional rheometery (SER) at the strain rate of 1 s^{-1}(Table 4.5 entry 6).

Appendix C

C.1 Characterization of complexes 17-19 by ^{1}H NMR, and ^{13} C{^{1}H} NMR spectroscopy

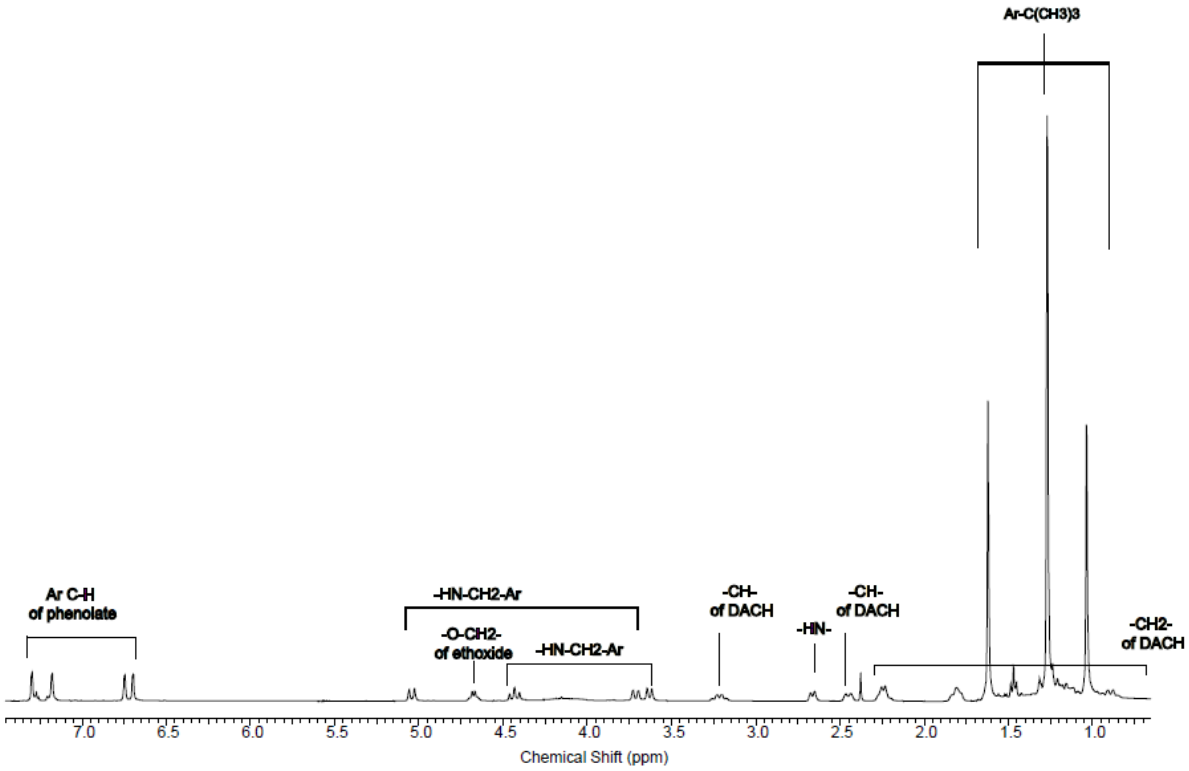

Figure C.1 ^{1}H NMR spectrum ($CDCl_3$, 25 °C, 400 MHz) of (*RR/RR*)-**1**7

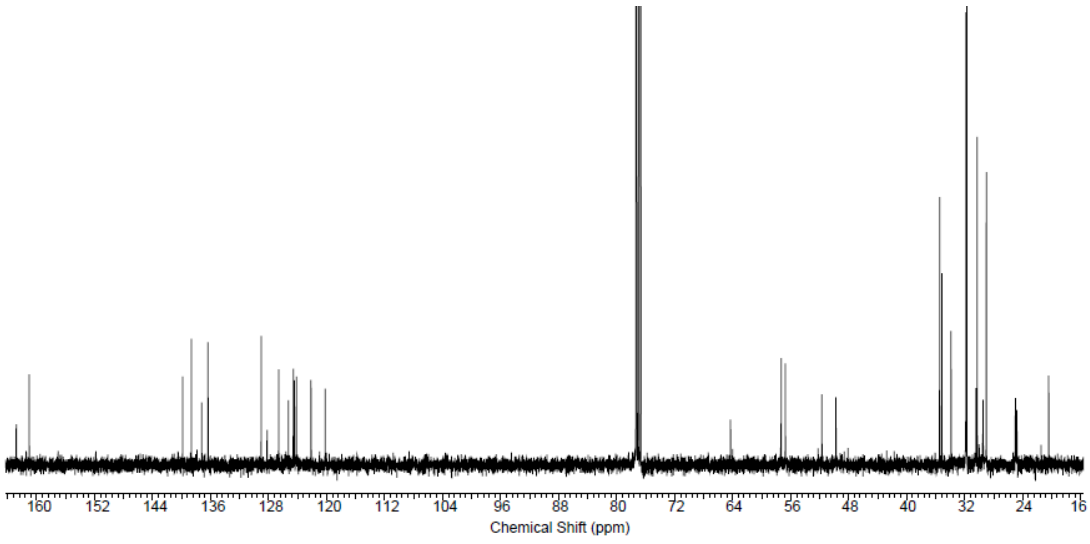

Figure C.2 ^{13}C{^{1}H} NMR spectrum ($CDCl_3$, 25 °C, 151 MHz) of (*RR/RR*)-**17**

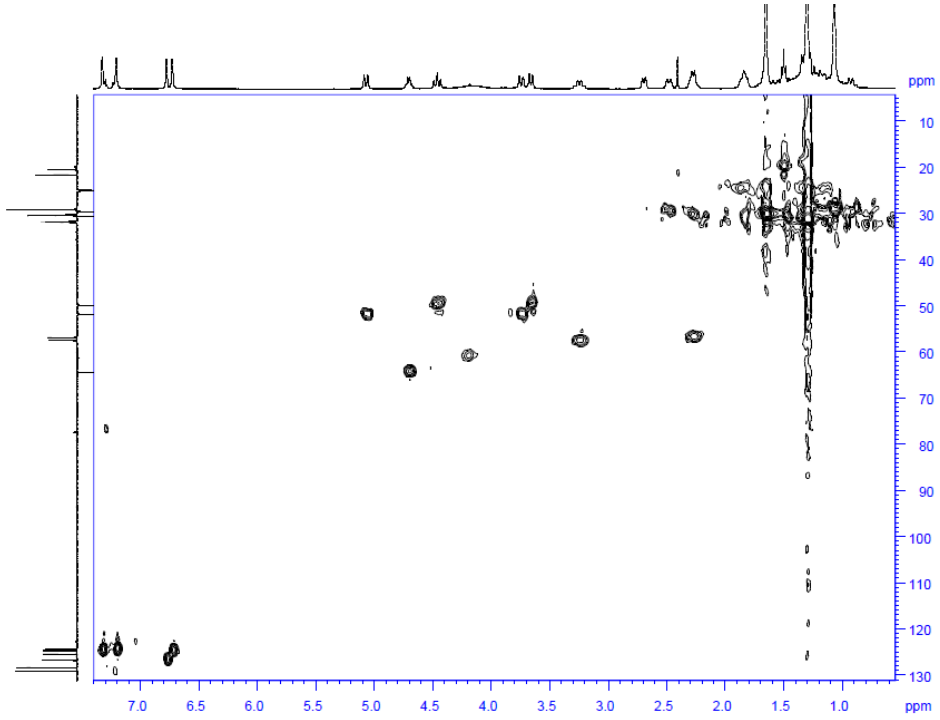

Figure C.3 ^{1}H-^{13}C HSQC spectrum ($CDCl_3$, 25 °C) of (*RR/RR*)-**17**

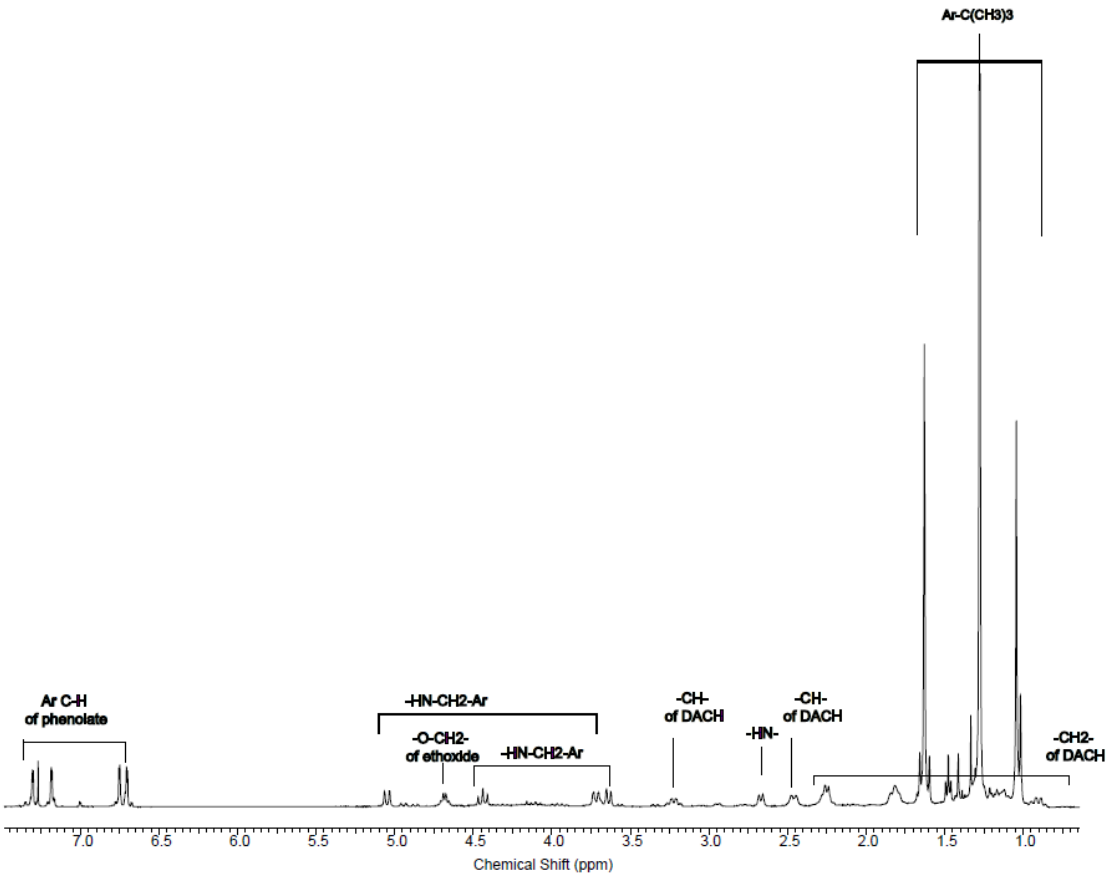

Figure C.4 ^{1}H NMR spectrum ($CDCl_3$, 25 °C, 400 MHz) of (±)-**17**

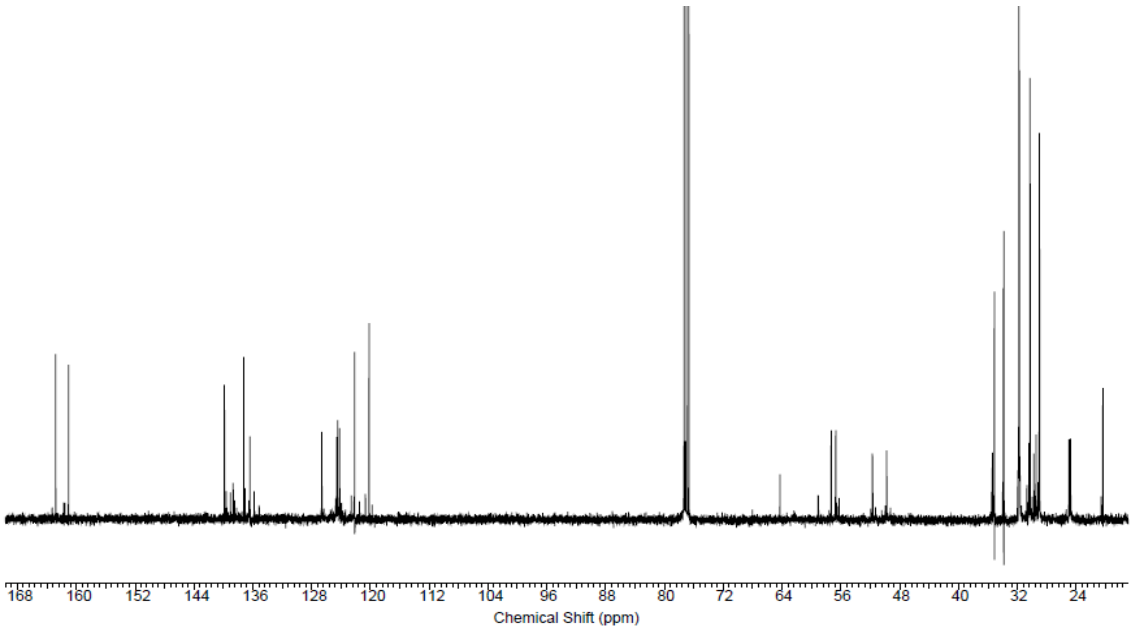

Figure C.5 $^{13}C\{^{1}H\}$ NMR spectrum ($CDCl_3$, 25 °C, 151 MHz) of (±)-**17**

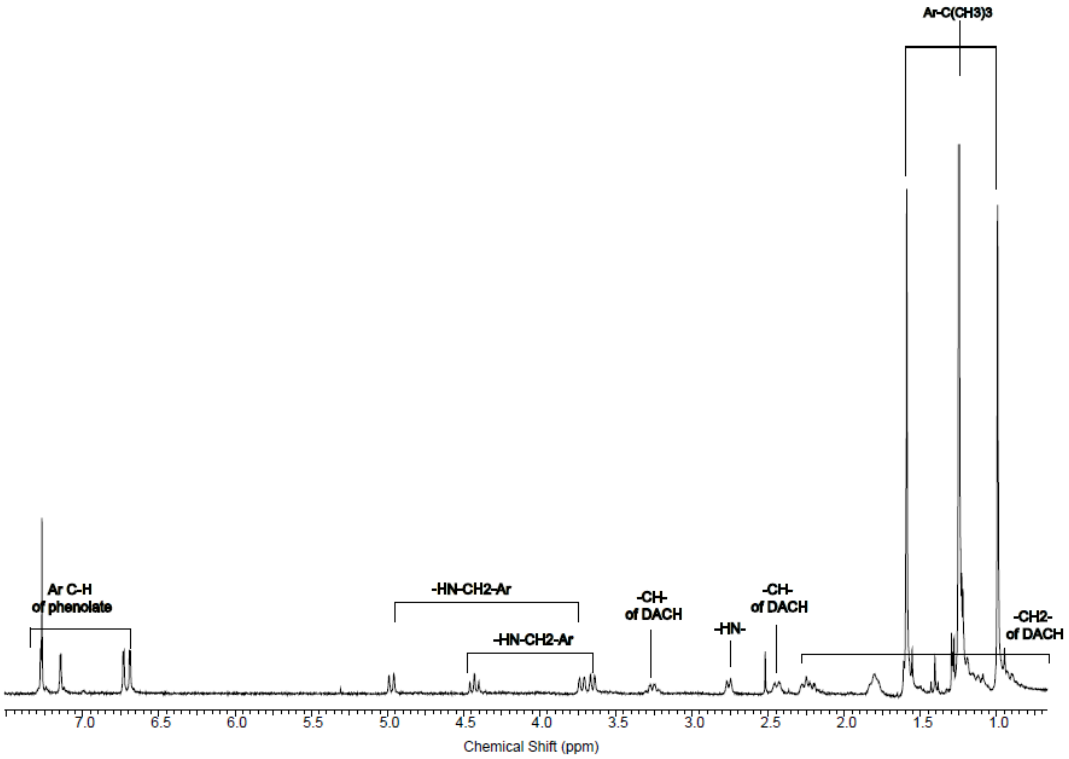

Figure C.6 ^{1}H NMR spectrum ($CDCl_3$, 25 °C, 400 MHz) of (*RR/RR*)-**18** ((±)-**18** shows similar spectrum)

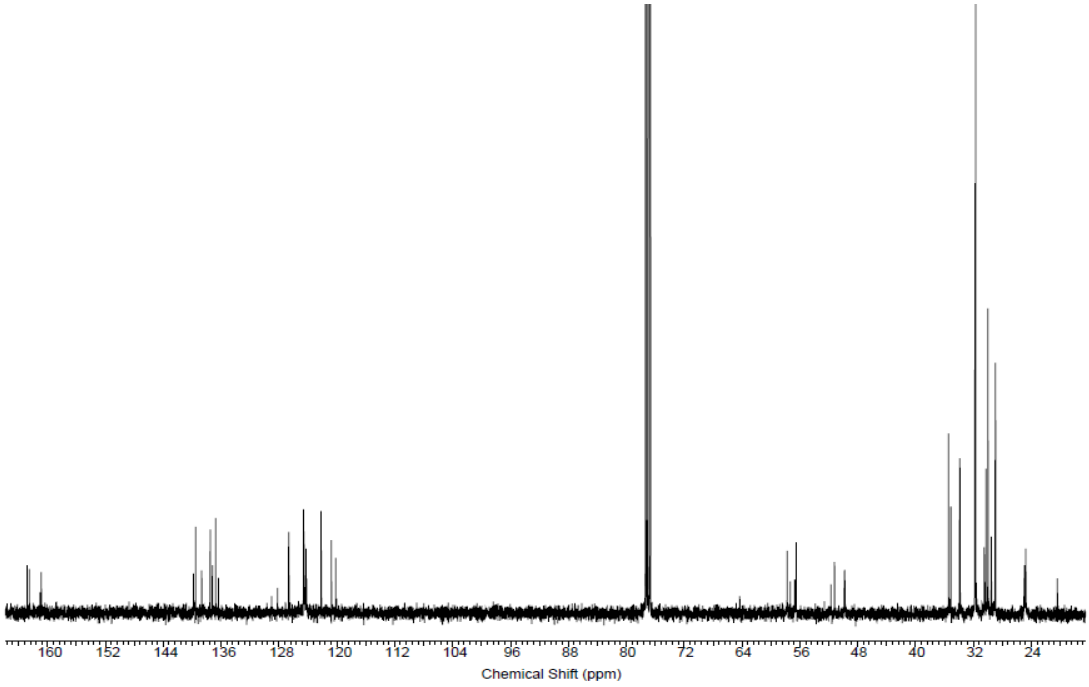

Figure C.7 $^{13}C\{^{1}H\}$ NMR spectrum ($CDCl_3$, 25 °C, 151 MHz) of (*RR/RR*)-**18** ((±)-**18** shows similar spectrum)

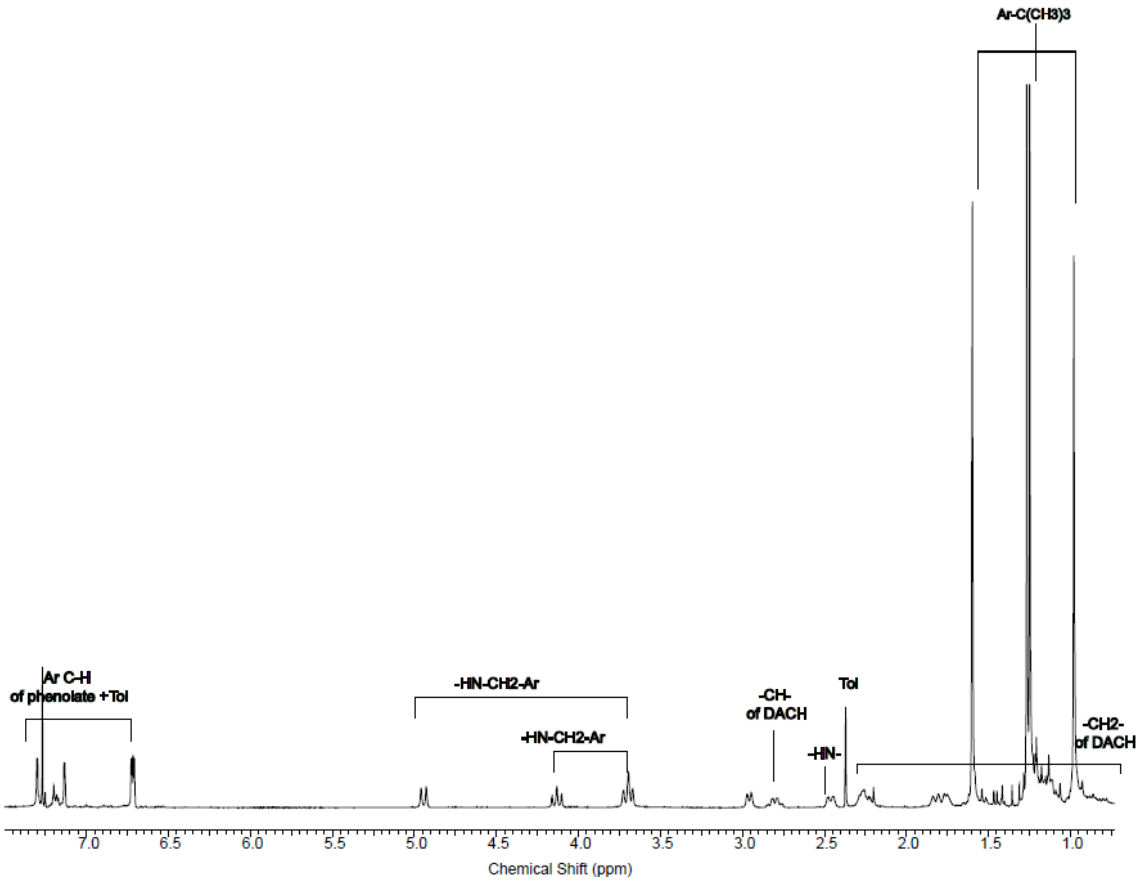

Figure C.8 ^{1}H NMR spectrum ($CDCl_3$, 25 °C, 400 MHz) of (*RR/RR*)-**19**

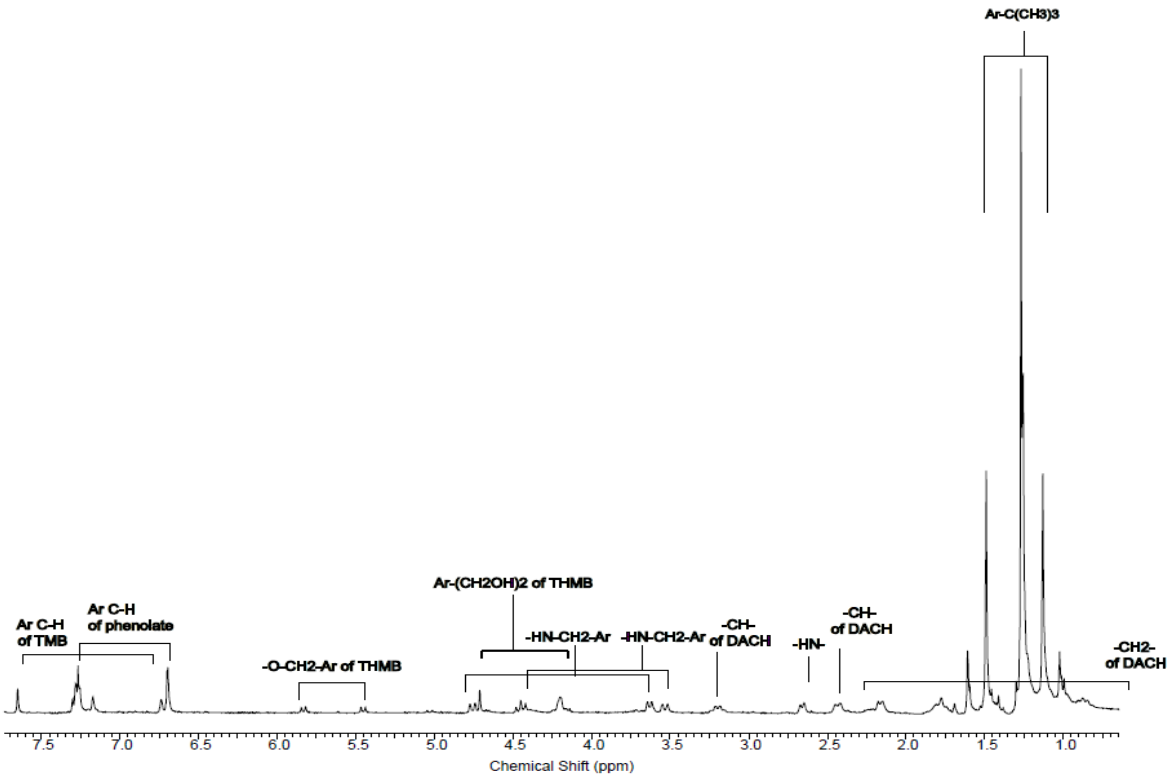

Figure C.9 ^{1}H NMR spectrum ($CDCl_3$, 25 °C, 400 MHz) of (*RR/RR*)–OTHMB bridge complex **17**

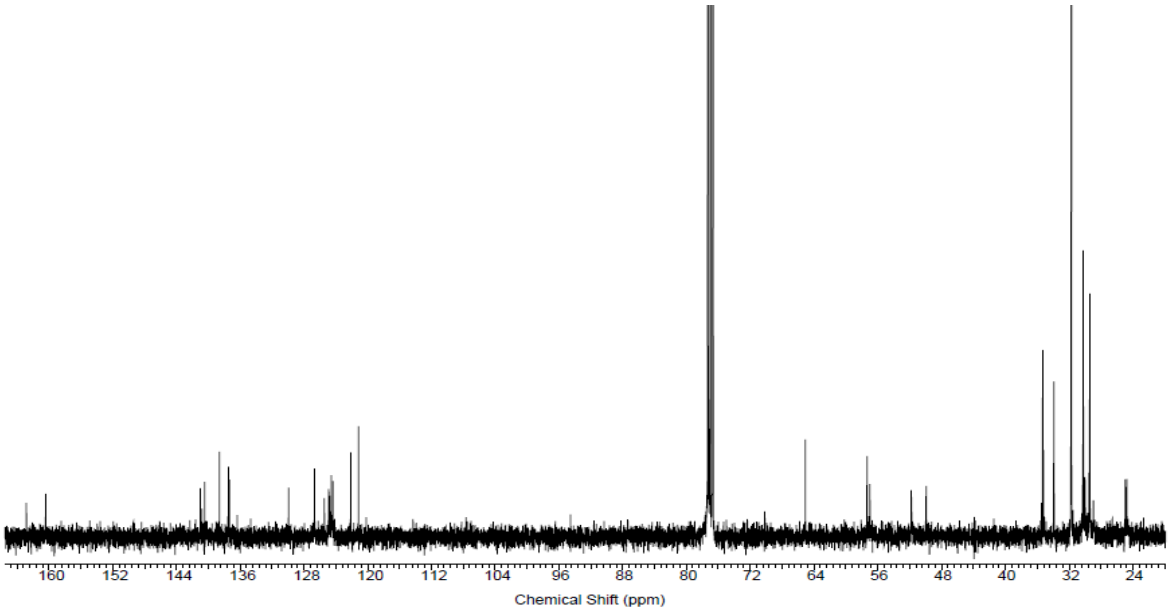

Figure C.10 13C{1H} NMR spectrum (CDCl3, 25 °C, 151 MHz) of (*RR/RR*)–OTHMB bridged complex **17**

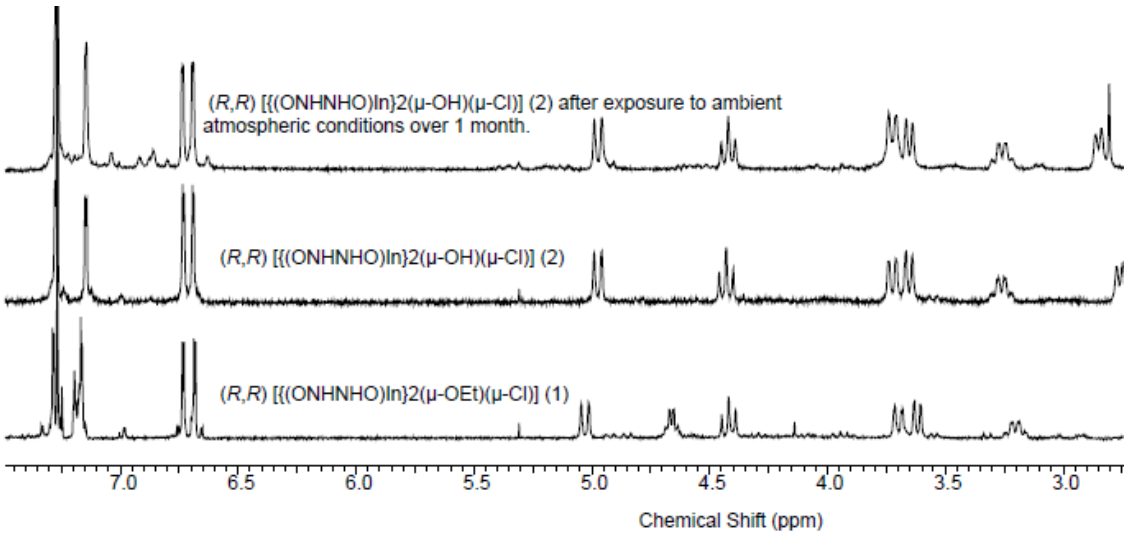

Figure C.11 ^{1}H NMR spectrum ($CDCl_3$, 25 °C, 400MHz) of (*RR*/*RR*)-**18** after exposure to air for 32 days overlaid with original spectrum of (*R*,*R*)-**17**.

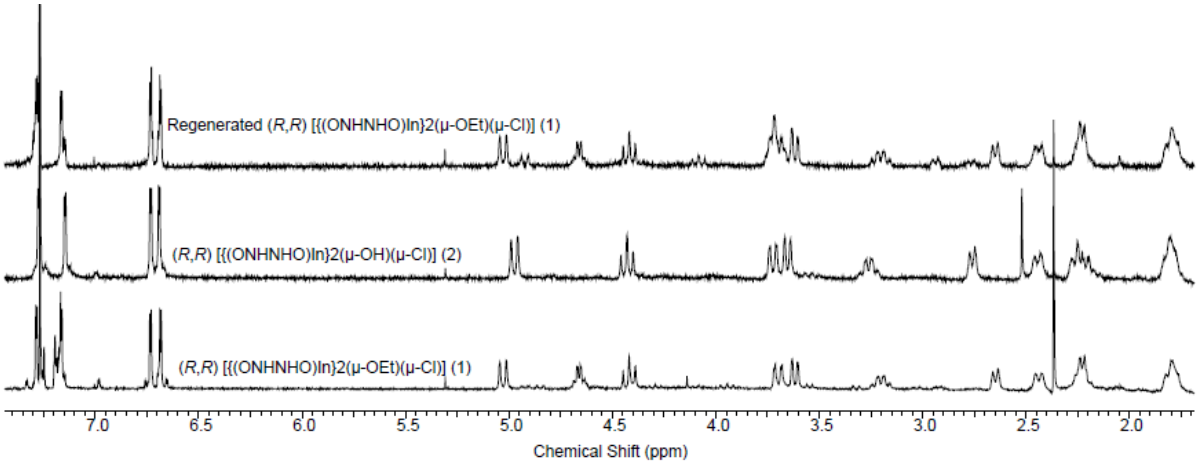

Figure C.12 ^{1}H NMR spectrum of (*RR*/*RR*)-**17** regenerated by stirring (*RR*/*RR*)-**18** (resulted from stirring in wet solvent) in neat ethanol

C.2 Crystallographic data for the solid state structure of (*RR*/*RR*)-17, 18, and 19

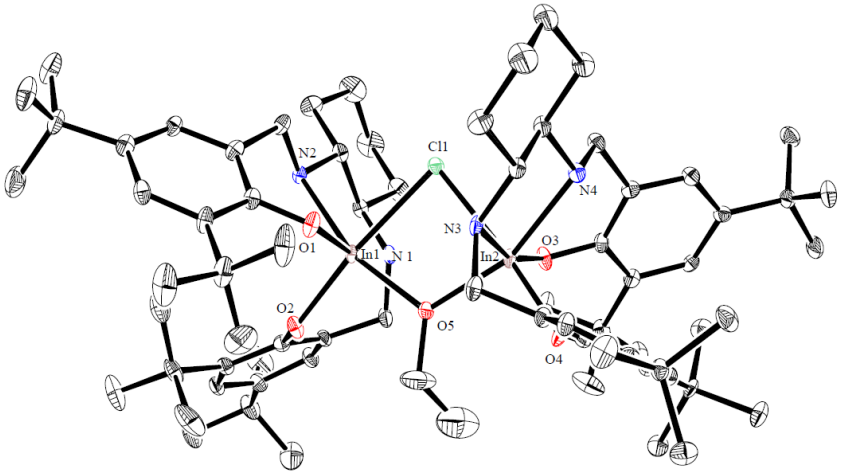

Figure C.13 Molecular structure of complex (*RR*/*RR*)-**17**. (Depicted with thermal ellipsoids at 50% probability. H atoms as well as Toluene molecules omitted for clarity).

Table C.1 Selected bond lengths (Å) and angles (°) for compound (*RR*/*RR*)-**17**.

In2-Cl1	2.6327(8)	O3-In2-Cl1	170.98(7)
In2-O3	2.087(2)	O3-In2-O5	98.62(8)
In2-O4	2.073(2)	O3-In2-N4	87.19(19)
In2-O5	2.1378(18)	O3-In2-N3	97.63(10)
In2-N4	2.285(3)	O4-In2-Cl1	86.10(6)
In2-N3	2.302(3)	O4-In2-O3	102.72(9)
In1-Cl1	2.6198(7)	O4-In2-O5	97.29(7)
In1-O1	2.082(2)	O4-In2-N4	163.35(8)
In1-O2	2.073(2)	O4-In2-N3	89.14(9)
In1-O5	2.1413(19)	O5-In2-Cl1	78.15(6)

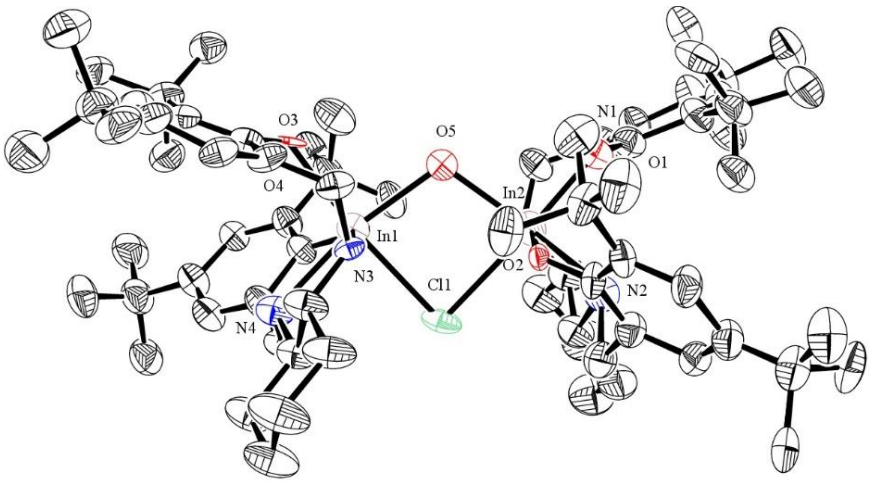

Figure C.14 Molecular structure of complex (*RR*/*RR*)-**18** (depicted with thermal ellipsoids at 50% probability. H atoms as well as Toluene molecules omitted for clarity).

Table C.2 Selected bond lengths (Å) and angles (°) for compound (*RR*/*RR*)-**18**.

In1-Cl1	2.674(6)	O1-In1-Cl1	172.5(5)
In1-O1	2.119(18)	O1-In1-O2	101.8(6)
In1-O2	2.075(13)	O1-In1-O5	96.5(7)
In1-O5	2.259(15)	O1-In1-N1	88.7(7)
In1-N1	2.28(2)	O1-In1-N2	94.2(9)
In1-N2	2.27(2)	O2-In1-Cl1	85.7(4)
In2-Cl1	2.623(6)	O2-In1-N1	164.8(6)
In2-O3	2.147(16)	O5-In1-Cl1	81.5(5)
In2-O4	2.058(14)	O5-In1-O2	98.8(5)
In2-O5	2.261(16)	O5-In1-N1	90.9(6)
In2-N3	2.274(19)	N1-In1-Cl1	84.2(5)

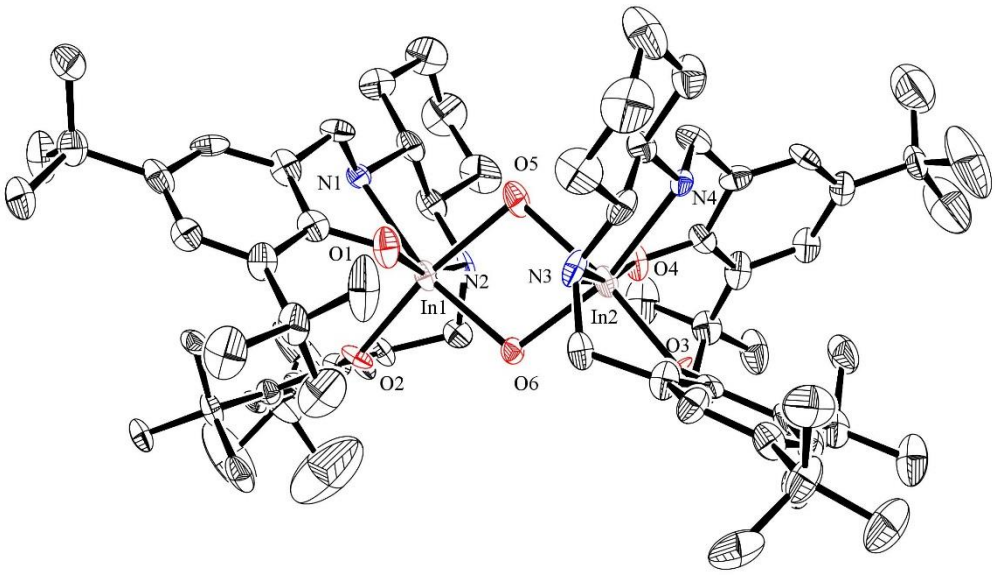

Figure C.15. Molecular structure of complex (*RR*/*RR*)-**19** (depicted with thermal ellipsoids at 50% probability. H atoms as well as Toluene molecules omitted for clarity).

Table C.3 Selected bond lengths (Å) and angles (°) for compound (*RR*/*RR*)-**19**.

In1-In2	3.3789(8)	O1-In1-In2	92.5(2)
In1-O1	2.091(7)	O1-In1-O5	83.0(3)
In1-O2	2.072(8)	O1-In1-O6	98.7(3)
In1-O5	2.244(9)	O1-In1-N1	87.9(3)
In1-O6	2.145(9)	O1-In1-N2	161.1(3)
In1-N1	2.337(10)	O2-In1-In2	131.2(2)
In1-N2	2.249(9)	O2-In1-O1	104.7(3)
In2-O3	2.084(8)	O2-In1-O5	169.9(4)
In2-O4	2.094(7)	O2-In1-O6	94.6(3)
In2-O5	2.215(10)	O2-In1-N1	98.4(3)
In2-O6	2.109(8)	O2-In1-N2	88.8(3)

Table C.4 Selected crystallographic parameters for (*RR*/*RR*)-**17**, (*RR*/*RR*)-**18**, (*RR*/*RR*)-**19**.

	(*RR*/*RR*)-**17**	(*RR*/*RR*)-**18**	(*RR*/*RR*)-**19**
empirical formula	$C_{102}H_{149}N_4O_5ClIn_2$	$C_{96.9}H_{139.5}ClIn_2N_4O_5$	$C_{86}H_{128}In_2N_4O_6$
Fw	1776.33	1705.60	1543.56
T (K)	100(2)	100(2)	100(2)
a (Å)	12.1349(8)	12.196(4)	12.0666(5)
b (Å)	12.2766(8)	12.295(4)	12.3213(6)
c (Å)	18.6225(12)	18.618(6)	18.3525(8)
α (deg)	85.3880(10)	86.040(10)	74.0920(10)
β (deg)	74.1760(10)	73.489(9)	87.9700(10)
γ (deg)	65.3920(10)	64.932(10)	65.2360(10)
volume ($Å^3$)	2425.0(3)	2420.5(13)	2372.91(18)
Z	1	1	1
crystal system	triclinic	triclinic	triclinic
space group	*P*1	*P*1	*P*1
Unique reflections/parameters	21442/1133	11685/955	14821/939
d_{calc} (g/cm^3)	1.216	1.170	1.080
μ (MoKα) (mm^{-1})	0.554	0.553	0.531
absor corr (*T*min, *T*max)	0.855,0.942	0.759,0.962	0.892,0.979
residuals (refined on F^2): R_1($I > 2\sigma(I)$); *w*R_2 (all data)	0.023, 0.047	0.085, 0.243	0.052, 0.127
Flack parameter	-0.005(5)	0.064(19)	-0.07(2)
GOF	1.01	1.11	0.830

C.3 Pulsed gradient spin-echo (PGSE) spectroscopy data of the pro-ligand, and complexes (*RR*/*RR*)-17, 18, and 19

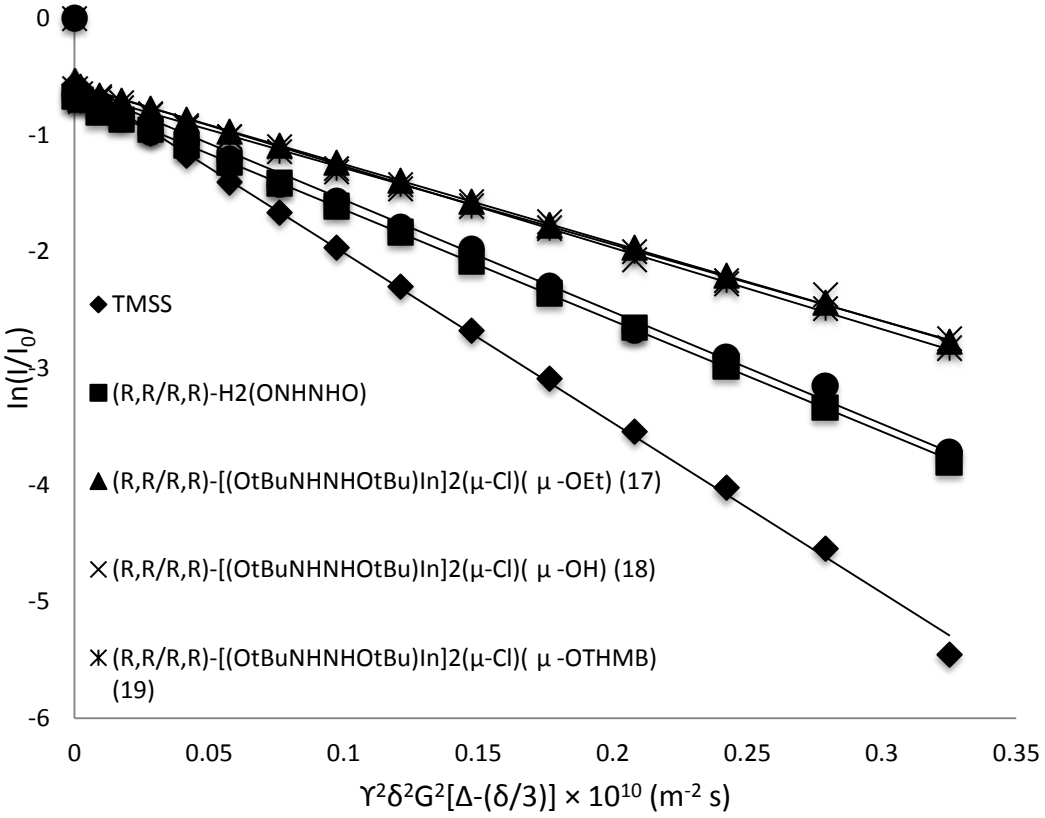

Figure C.16 Plot of $\ln(I/I_0)$ vs $\Upsilon^2\delta^2G^2[\Delta-(\delta/3)] \times 10^{10}$ (m^{-2} s) from PGSE experiments (400 MHz, CD_2Cl_2, 25 °C, Δ = 80 ms, δ = 1.1 ms). The hydrodynamic radius (r_H) of each compound was calculated by using the slopes (D_t) of the linear fits. I = intensity of the observed spin-echo, I_0 = intensity of the spin-echo in the absence of gradients, G = varied gradient strength, Υ = gyromagnetic ratio (2.675×10^8 rad s^{-1} T^{-1}), δ = length of the gradient pulse, Δ = delay between the midpoints of the gradients.

Table C.5 Diffusion coefficient and hydrodynamic radii of the complexes measured through PGSE measurements and solid state x-ray crystallography.

	Complexes	D_t [a] ($\times 10^{-10}$ m^2s^{-1})	r_H (Å) [a]	$r_{x\text{-}ray}$ (Å)[b]
1	(*R,R*)-Salan ligand	9.4(0.3)	6.5	nd[c]
2	**A**	7.8(0.31)	7.53[165]	7.30[165]
3	**B**	6.5(0.5)	8.5[166]	8.3[166]
4	(*RR*/*RR*)-[(ON_HN_HO)In]$_2$(μ-Cl)(μ-OEt) (**17**)	6.7(0.1)	8.7	8.33
5	(*RR*/*RR*)- [(ON_HN_HO)In]$_2$(μ-Cl)(μ-OH) (**18**)	6.5(0.6)	8.51	8.32
6	(*RR*/*RR*)- [(ON_HN_HO)In]$_2$(μ-OH)(μ-OH) (**19**)	6.5(0.2)	8.51	8.27

[a] Calculated hydrodynamic Radii (r_H) from translational diffusion coefficients (D_t) (0.9 mM TMSS used as internal standard; 4.5 mM in CD_2Cl_2). [b] X-ray crystallographic data was used to calculate $r_{x\text{-}ray}$ using the equation $r_{x\text{-}ray} = (3V/ 4\pi n)^{⅓}$ where V is the volume of unit cell and n is the number of the compounds of interest occupying the unit cell assuming spherical shape . [c] Not determined.

C.4 Extra polymer characterizations

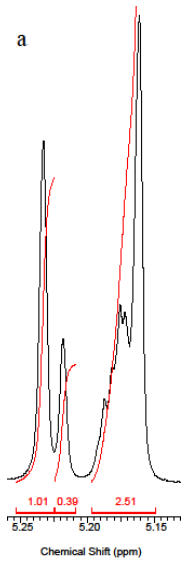

Figure C.17 Heterotactic (P_r = 0.72) PLA produced from polymerization of *rac*-Lactide with (*RR*/*RR*)-**17** ($CDCl_3$, 25 °C, 600 MHz).

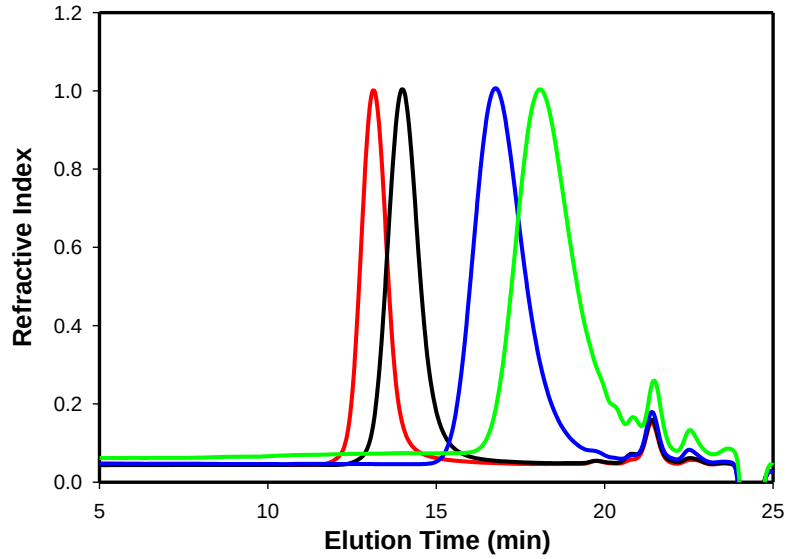

Figure C.18 GPC traces of PLA obtained from the polymerization of rac-LA in the presence of different equivalences of EtOH (Table 5.3, entries 1-4). (red) LA/EtOH/(**17**):1000/5/1, (black) LA/EtOH/(**1**):1000/10/1, (blue) LA/EtOH/(**1**):1000/50/1, (green) LA/EtOH/(**17**):1000/100/1 (25 °C, CH_2Cl_2, 99% conv.)

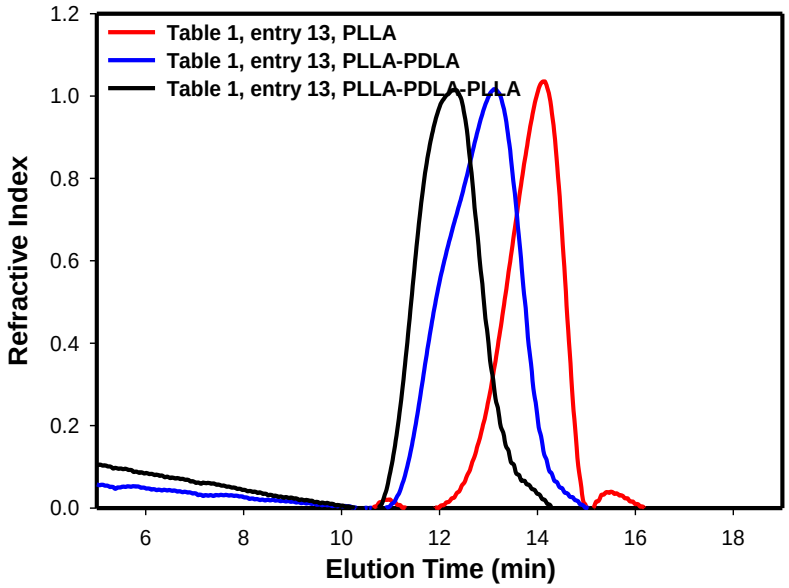

Figure C.19 GPC overlaid chromatograms 3-arm star PLLA obtained from the polymerization with [L-LA]//[THMB]/[**18**] ratios of 700/8/1 (M_n =11430 , *Đ*= 1.06), 3-arm star di-block copolymers of PLLA-PDLA obtained from the polymerization with [L-LA+D-LA]/[THMB]/[**18**] ratios of 700+500/8/1(M_n = 20600, *Đ*= 1.07), and 3-arm star tri-block copolymers of PLLA-PDLA-PLLA obtained from the

polymerization with [L-LA+D-LA+L-LA]/[THMB]/[**18**] ratios of 700+500+700/8/1(M_n = 30300, $Đ$= 1.05) in melt state at 155 °C under N_2 (Table 5.4, entry 13).

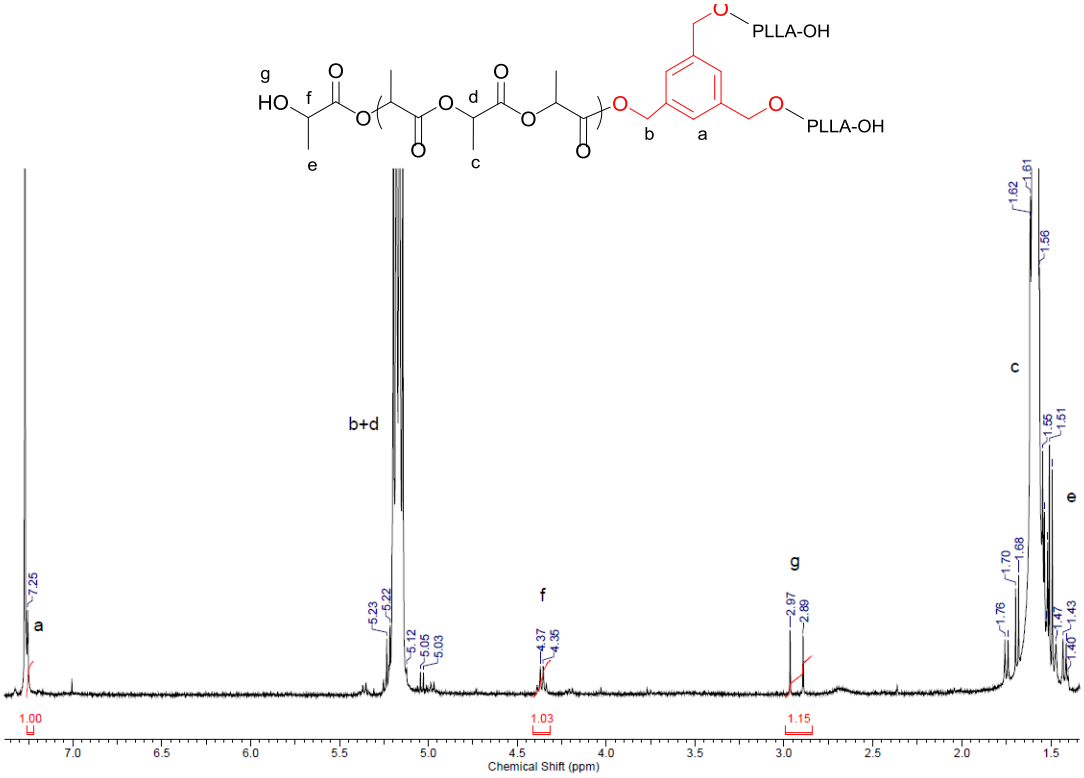

Figure C.20 ^{1}H NMR spectra of Table 5.4, entry 10 ($CDCl_3$, 25 °C) after monomer depletion in melt state in air (sample was collected after 60 mins. Time of the experiment is not optimized).

C.5 $^{1}H\{^{1}H\}$ NMR and ^{1}H NMR spectra of the methine region of PLA obtained with complex 18 in melt state under air and dinitrogen atmosphere

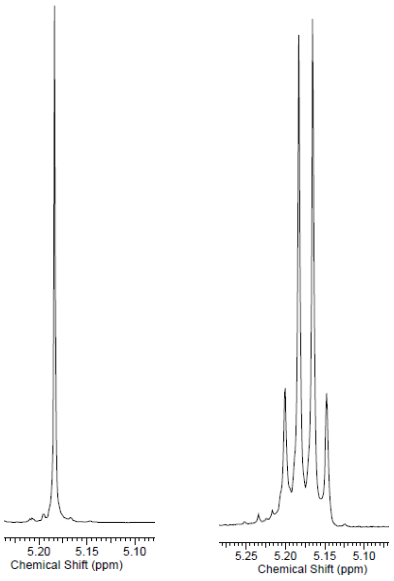

Figure C.21 (left) $^{1}H\{^{1}H\}$ and (right) regular ^{1}H NMR spectrum of the methine region of Table 5.4, entry 12, first block (PLLA) ($CDCl_3$, 25 °C, 600 MHz).

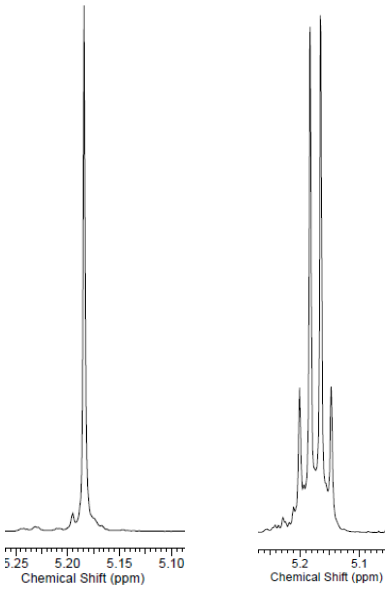

Figure C.22 (left) $^{1}H\{^{1}H\}$ and (right) regular ^{1}H NMR spectrum of the methine region of Table 5.4 entry 12, second block (PLLA-PDLA) ($CDCl_3$, 25 °C, 600 MHz).

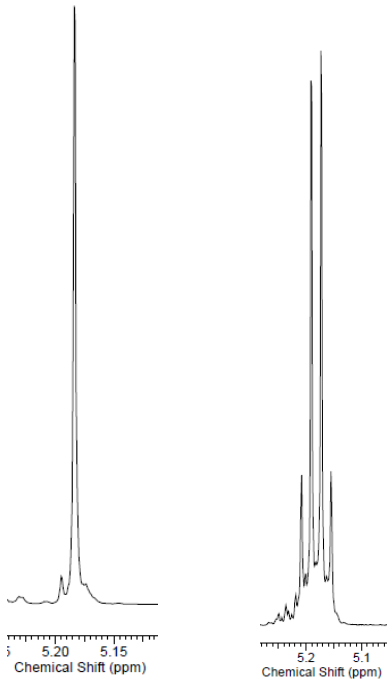

Figure C.23 (left) $^{1}H\{^{1}H\}$ and (right) regular ^{1}H NMR spectrum of the methine region of Table 5.4 entry 12, third block (PLLA-PDLA-PLLA) ($CDCl_3$, 25 °C, 600 MHz).

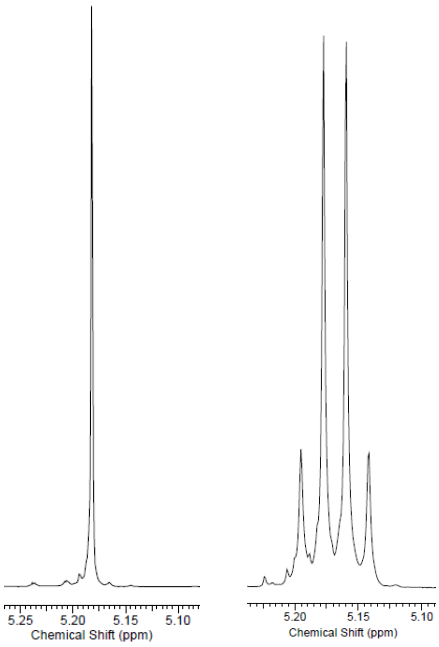

Figure C.24 (left) $^{1}H\{^{1}H\}$ and (right) regular ^{1}H NMR spectrum of the methine region of Table 5.4 entry 13, first block (PLLA) ($CDCl_3$, 25 °C, 600 MHz).

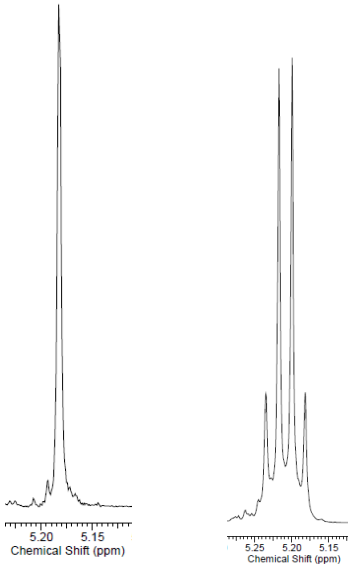

Figure C.25 (left) $^{1}H\{^{1}H\}$ and (right) regular ^{1}H NMR spectrum of the methine region of Table 5.4 entry 13, second block (PLLA-PDLA) ($CDCl_3$, 25 °C, 600 MHz).

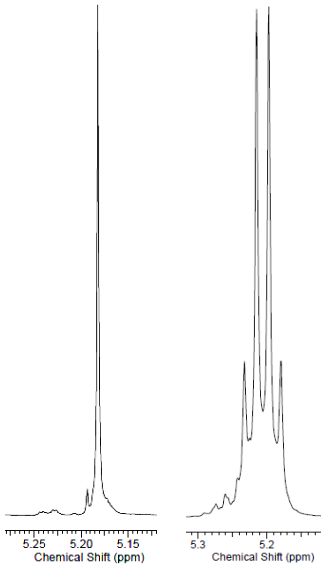

Figure C.26 (left) Homonuclear-decoupled and (right) regular ^{1}H NMR spectrum of the methine region of Table 5.4, entry 13, third block (PLLA-PDLA-PLLA) ($CDCl_3$, 25 °C, 600 MHz).

C.6 DSC results of PLA triblock copolymers of Table 5.4 entries 12 and 13

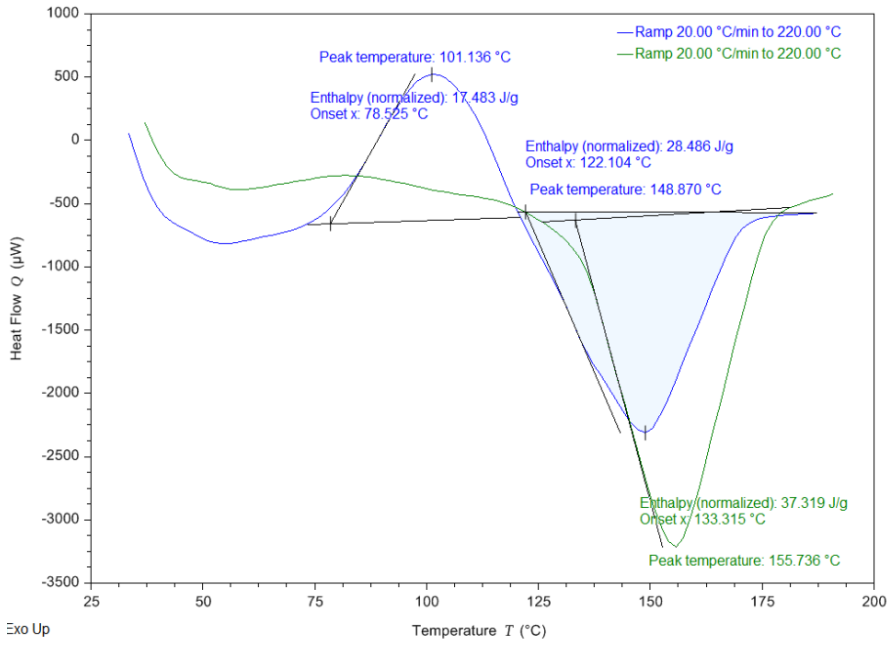

Figure C.27 DSC results of entry 12, PLLA

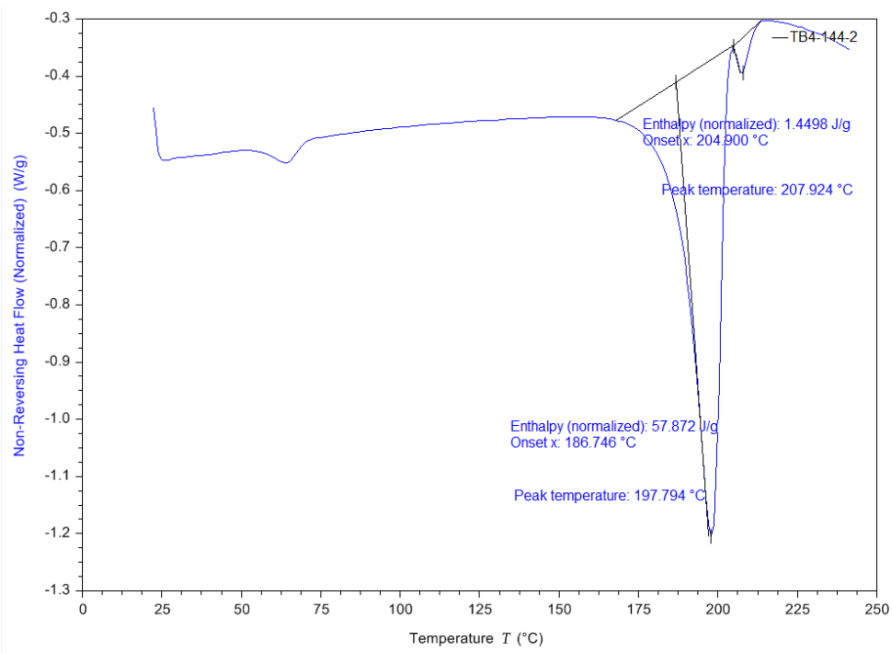

Figure C.28 DSC results of entry 12, PLLA-PDLA

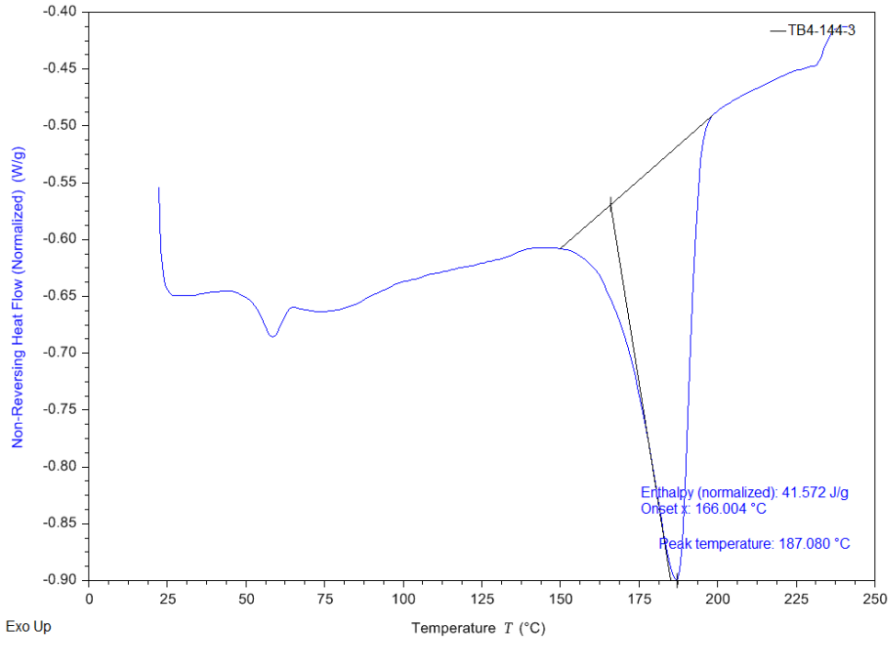

Figure C.29 DSC results of entry 12, PLLA-PDLA-PLLA

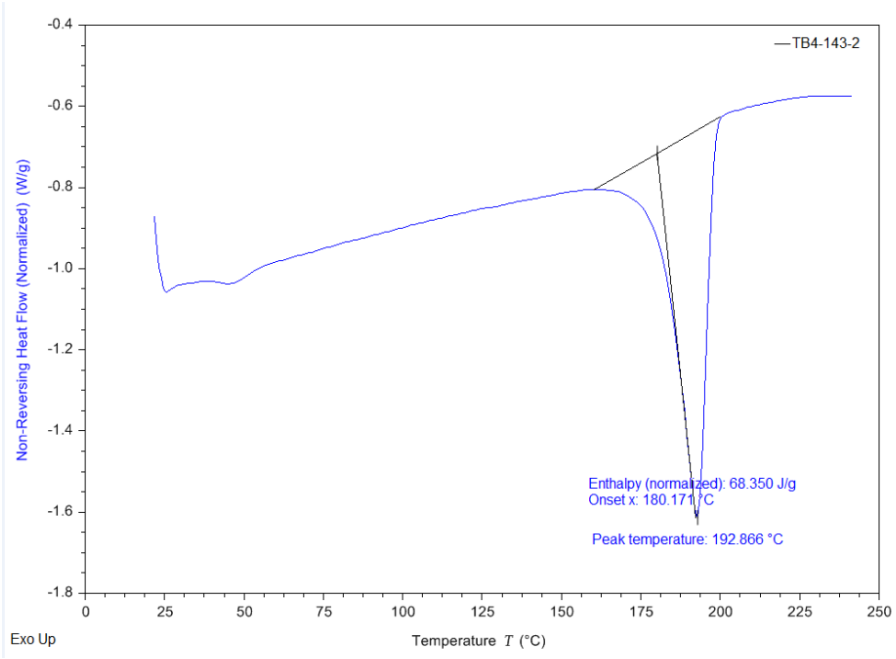

Figure C.30 DSC results of entry 13, PLLA-PDLA

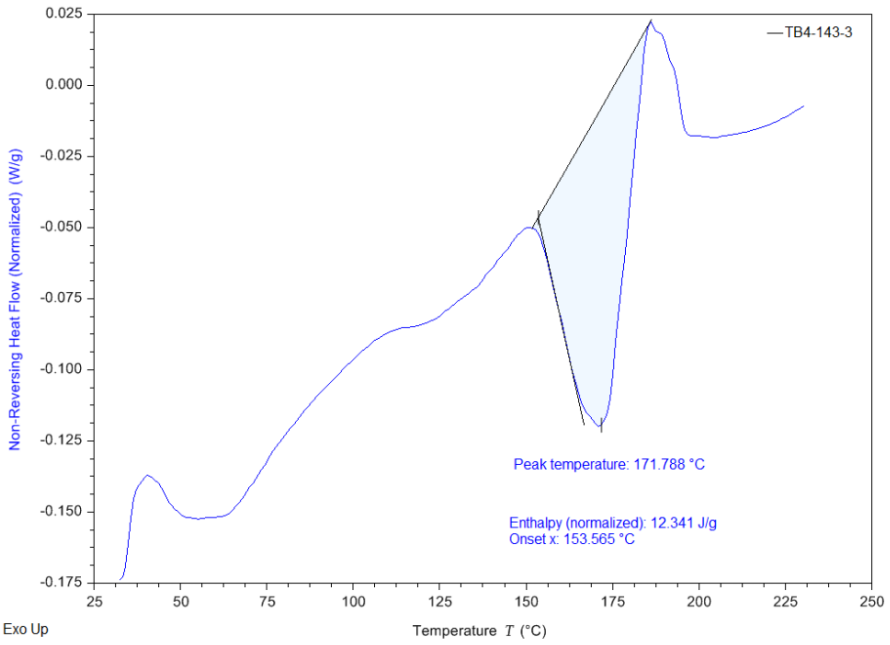

Figure C.31 DSC results of entry 13, PLLA-PDLA-PLLA